AN ABSTRACT OF THE DISSERTATION OF

Juliana M. Huizenga for the degree of Doctor of Philosophy in Environmental Engineering presented on October 19, 2023.

Title: Aromatic Hydrocarbon Contaminants: Investigations of Detection Methods, Bioremediation Strategies, and Toxicity Impacts.

Abstract approved:

_____

Lewis Semprini

Aromatic hydrocarbons represent a large class of environmental contaminants that have a broad range of structures, physicochemical properties, and toxicities. Arising from the burning of organic matter, particularly fossil fuels, they are both widespread and abundant in all environmental compartments. Both monoaromatic hydrocarbons (BTEX) and polycyclic aromatic hydrocarbons (PAHs) are toxic to ecosystems and humans, with some exhibiting carcinogenic and mutagenic properties. As such, they are regulated by the EPA with maximum contaminant levels (MCLs) that reflect their toxicity and are often the target for remediation efforts at contaminated sites. This dissertation focuses on bioremediation, using bacteria to break down contaminants, as the primary remediation strategy. Although a valuable remediation method in terms of cost and required resources, bioremediation of aromatic hydrocarbons is not without its own unique set of challenges.

Aromatic hydrocarbons exist as complex mixtures in the environment that can be difficult to biologically treat in their entirety. Finding microorganisms that can transform a wide range of aromatic hydrocarbon structures can be a bottleneck for bioremediation technology development. Furthermore, these mixtures are difficult to

monitor analytically, particularly in a rapid manner. The ability to monitor treatment progress in real time is of great value for novel bioremediation strategy development, however this is not possible with traditional analytical techniques. Finally, aromatic hydrocarbon contaminants, particularly PAHs, present an interesting challenge where their transformation products can be more toxic that the parent compounds. This is a troublesome factor to consider in remediation studies, as it is typically only the parent compounds that are considered and regulated. The work presented in this dissertation was motivated by these challenges to support the progress of aromatic hydrocarbon bioremediation strategies and tools needed for their continued development.

Chapter II presents an initial investigation of the ability of a bacterial pure culture, *Rhodococcus rhodochrous* ATCC 21198, to transform aromatic hydrocarbon contaminants using BTEX as model contaminants. Methyl-tertiary-butyl ether (MTBE) was studied as well, as it is a common co-contaminant of BTEX that can hinder biodegradation of the mixture. It was found that 21198 was able to degrade BTEX, and MTBE both individually and as a mixture, and that isobutane, 1-butanol, and 2-butanol all supported this activity. Furthermore, MTBE's primary transformation product, tertiary-butyl alcohol (TBA), was also transformed by 21198, but at a slower rate compared to MTBE. This degradation was a combination of metabolic and cometabolic activity, as 21198 was observed to grow on benzene and toluene. This work supported further investigations of aromatic hydrocarbon treatment with 21198 and was the first demonstration of 21198's ability to degrade and grow on aromatic hydrocarbon contaminants.

Chapter III details the development of a rapid bioremediation monitoring tool using fluorescent spectroscopy and parallel factor analysis (PARAFAC). A microorganism previously studied for phenanthrene transformation, *Mycobacterium* Sp. Strain ELW1, was used to develop an experimental data set where phenanthrene was transformed to the primary transformation product *trans*-9,10-dihydroxy-9,10-dihydrophenanthrene (P1). The transformation of phenanthrene and the formation of P1 were monitored and quantified with the novel fluorescent spectroscopy/PARAFAC method. Results were validated with an established GC-MS method, demonstrating comparable results in a fraction of the time. This was the first

use of a fluorescent spectroscopy/PARAFAC method to monitor, identify, and quantify PAH biotransformation and product formation.

Chapter IV adapts the method presented in Chapter III to a new biological system, embryonic zebrafish, with the same motivation: reduce time and resources required for monitoring aqueous PAH concentrations. Embryonic zebrafish have been used extensively for screening chemicals for toxicity and can be used in a high-throughput system established at the Sinnhuber Aquatic Research Laboratory at Oregon State University. A fluorescent spectroscopy method was developed to accommodate a 96-well plate and measure PAH concentrations in embryo media over a 5-day incubation period. It was observed that measurements with a fluorescent plate reader did not impact embryo development, nor did normal embryo development significantly impact background fluorescence in the microwells. Chemical dose, uptake rate, and abiotic loss rates were all derived from fluorescent measurements for acridine and 2-hydroxynaphthalene, demonstrating the ability to use the fluorescent plate reader for rapid, non-destructive analysis of PAHs in high-throughput toxicity assays with embryonic zebrafish.

Chapter V combined aspects from the previous three chapters to investigate 21198's ability to transform a mixture of phenanthrene, anthracene, fluorene, and pyrene on its own and in combination with the surfactant Tween ® 80 and cell immobilization techniques. Transformation of PAHs was observed in all batch tests, with cell immobilization in PVA/alginate beads generally improving the rate and extent of PAH transformation, especially when combined with the surfactant. However, toxicity to zebrafish embryos increased after bioremediation, indicating that transformation products contributed to toxicity more so than the parent PAHs. A complex mixture of hydroxylated products, ring fission products, and quinones, were putatively identified using UPLC-MS, many of which have been demonstrated to elicit toxic responses in embryonic zebrafish. Despite this, 21198's ability to rapidly transform such a broad range of environmentally relevant aromatic hydrocarbon contaminants suggests that it is a valuable bacterium in treating these contaminants and is amenable to use in combined treatment strategies that can improve treatment outcomes.

Aromatic Hydrocarbon Contaminants: Investigations of Detection Methods, Bioremediation Strategies, and Toxicity Impacts

by
Juliana M. Huizenga

A DISSERTATION

submitted to

Oregon State University

in partial fulfillment of
the requirements for the
degree of

Doctor of Philosophy

Presented October 19, 2023
Commencement June 2024

Doctor of Philosophy dissertation of Juliana M. Huizenga presented on October 19, 2023.

APPROVED:

Major Professor, representing Environmental Engineering

Head of the School of Chemical, Biological, and Environmental Engineering

Dean of the Graduate School

I understand that my dissertation will become part of the permanent collection of Oregon State University libraries. My signature below authorizes release of my dissertation to any reader upon request.

Juliana M. Huizenga, Author

ACKNOWLEDGEMENTS

The collection of experiences, challenges, triumphs, and relationships manifesting from my four years in Corvallis has filled me with such gratitude I can only begin to express in the following acknowledgements. Thank you to my advisor, Dr. Lewis Semprini, for your guidance and trust. Your support in every decision, whether it be as small as a conference abstract or as big as changing from a master's to a PhD program, has allowed me to learn and accomplish far more than I thought was possible when I began this journey. Thank you to my committee members; Drs. Stacey Harper, Tyler Radniecki, Sarah Rothenberg, and Susan Tilton for your support in my research and career development. Along with Dr. Harper, I would like to thank Dr. Craig Marcus for their stewardship of the many Superfund Research Program trainee resources that have enriched my experience here. This work would not have been possible without the one and only Dr. Mohammad Azizian, who provides the Semprini lab with endless support on analytical equipment and fills the lab with his calm, jovial energy. There was more than one occasion that Mohammad dropped everything he was doing to work his so-called Mohammad Magic on an instrument that my research depended on. Similarly, thank you to Jason Schindler and Dr. Manuel García-Jaramillo for your analytical support, and enduring my many questions over the years – you were both instrumental (pun intended) in this research. Thank you to Drs. Lisa Truong, Mike Simonich, and Robyn Tanguay for your support with all things zebrafish.

Outside of research, there are many people and organizations that significantly contributed to my graduate school experience. The Coalition of Graduate Employees and the CBEE graduate student association are invaluable to us graduate students, and I am proud to be a part of our resilient community. Thank you to Amy Thompson and Dr. Jeff Nason for your care and dedication to improving our graduate student experience, especially during the pandemic. Thank you to previous Semprinites, Hannah, Alisa, Jacob, Sean, and Kestrel for your advice and collegiality across the years. It has been a bittersweet part of my experience to see you all graduate and move on to bigger and better things. Thank you to the Katherine Sanders and the

Downtown Dance community for warmly accepting me into your creative space and keeping the performer in me alive.

To family and friends who became like family: John, Emily, Jared, and Jesse, you filled my graduate school experience with so much laughter, fun, and love. Every bad scary movie night, jam session, and Oregon adventure is among my most cherished memories from this chapter of my life. Of all the challenges this PhD program presented, the grandest of all was being separated from my family by the three time zones, two thousand miles, and one pandemic. Thank you to my incredible parents, Jim, and Kathy, for your unwavering support in everything I do. Thank you, Mom, for instilling in me the "Groll women grit" that has served me well in my life but especially in pursuing my PhD. Thank you, Dad, the original Dr. Huizenga, for sharing with me your passion of using science for good. It is my ultimate goal to have as great of a positive impact on the world as you have as "Dr. Huizenga". Thank you, Liz, for cheering me on through the many catch up calls and facetimes, every one of which gave me a vital confidence boost. Lastly, thank you to my wonderful partner, Conor, for being everything good in this world wrapped up into one person.

Finally, I would like to acknowledge the contributions of the bacteria and zebrafish used in this research. While I may not be able to express gratitude to them directly, it should be acknowledged that it took billions of bacterial cells and thousands of zebrafish embryos to complete the work presented in this dissertation. Although my collaborators and I designed and carried out the experiments, it was the bacteria that transformed the contaminants, and it was the zebrafish that revealed toxicity, not us. I feel that I am an interpreter of their work which I, myself, am unable to do. It was a privilege to learn from such resilient wee beasties and tiny creatures.

CONTRIBUTION OF AUTHORS

The CRediT model (https://www.elsevier.com/authors/policies-and-guidelines/credit-author-statement) was used to describe the contribution of authors for the manuscripts included in this dissertation. Juliana M. Huizenga is first author on all manuscripts, contributing to conceptualization, methodology, formal analysis, investigation, data curation, visualization, and writing of the original draft. Dr. Lewis Semprini is the final author on all manuscripts, contributing to funding acquisition, conceptualization, visualization, supervision, project administration, and review and editing of the manuscripts.

Manuscript 1: No additional authors

Manuscript 2: No additional authors

Manuscript 3: Dr. Lisa Truong contributed to conceptualization and review and editing of the manuscript.

Manuscript 4: Dr. Lisa Truong, Dr. Mike Simonich, and Dr. Robyn Tanguay contributed to methodology, data curation, and validation of the embryonic zebrafish work. Dr. Manuel Garcia-Jaramillo and Jason Schindler contributed to methodology, data curation, and formal analysis of the UPLC-MS work. All authors contributed to review and editing of the manuscript.

TABLE OF CONTENTS

Page

TABLE OF CONTENTS (CONTINUED)

TABLE OF CONTENTS (CONTINUED)

TABLE OF CONTENTS (CONTINUED)

LIST OF FIGURES

Figure Page

LIST OF FIGURES (CONTINUED)

Figure Page

LIST OF FIGURES (CONTINUED)

Figure Page

LIST OF TABLES

Table Page

LIST OF APPENDICES

LIST OF APPENDIX FIGURES

Figure Page

LIST OF APPENDIX FIGURES (CONTINUED)

Figure Page

LIST OF APPENDIX FIGURES (CONTINUED)

Figure Page

LIST OF APPENDIX FIGURES (CONTINUED)

Figure Page

LIST OF APPENDIX TABLES

Table Page

LIST OF APPENDIX TABLES (CONTINUED)

Table Page

LIST OF APPENDIX TABLES (CONTINUED)

Table Page

Chapter I: Introduction

1.0 Aromatic Hydrocarbons

Aromatic hydrocarbons are a broad class of compounds that are produced from both abiotic and biotic sources. Aromatic in chemistry terminology means a compound with a ring-shaped structure with pi bonds in resonance, where electrons of the pi bonds are delocalized. Therefore, an aromatic compound can exist as one of many structures called resonance structures. Aromatic compounds are very stable compared to aliphatic compounds (non-aromatics) and thus are useful for molecules that are essential for life, including nucleotides in DNA and amino acids in proteins. In the environment, aromatic hydrocarbons are most associated with petroleum products (petrogenic) or the burning of organic material (pyrogenic) (Lawal, 2017). The extensive use of petroleum products in the industrial world has led to aromatic hydrocarbons becoming abundant and ubiquitous in the environment, prompting action on their regulation and removal (remediation) to deter their associated adverse ecological and health effects. Challenges related to their detection, remediation, and toxicity that informed the research direction for this dissertation are presented in the following sections.

1.1 BTEX

Benzene, toluene, ethylbenzene, and xylenes (BTEX) are monoaromatic hydrocarbons often found together in the environment from gasoline spills or fires (Barboni and Chiaramonti, 2010; Latif et al., 2019). The US Environmental Protection Agency (EPA) has listed priority pollutants (US EPA 2014) due to associated adverse health effects including carcinogenicity, neurotoxicity, and reproductive toxicity (Hazrati et al., 2016; Masih et al., 2016; Sairat et al., 2015). Due to their moderate volatility and water solubility, BTEX compounds can exist in the environment as vapors in the atmosphere and dissolved in surface and groundwaters, although they do not sorb strongly to soil and sediment and are not prone to bioaccumulation. Exposure to BTEX can occur through ingestion, dermal absorption, and inhalation (Li et al. 2020; Dobaradaran et al. 2021; Alfoldy et al. 2019). Maximum contaminant levels (MCLs) set by the EPA for BTEX in drinking water

are inversely proportional to their toxicity and range from 5 parts per billion (ppb) for benzene to 10 parts per million (ppm) for total xylenes (US EPA 2009).

Methyl tertiary butyl ether (MTBE), although not an aromatic hydrocarbon, is a common co-contaminant of BTEX that also of concern for human and ecological health. In the late 20th century, MTBE replaced lead as a gasoline additive to increase the octane level of gasoline (Steffan et al. 1997; Hernandez-Perez et al. 2001). MTBE quickly became dispersed in the environment due to its extensive use before it was found to be a regrettable substitution for lead. Despite its elimination from gasoline, MTBE continues to be a common surface water and groundwater pollutant in the US (Fiorenza and Rifai, 2003; Carter et al. 2006). MTBE is a suspected human carcinogen, and although no MCL has been established, an action level range of 20 ppb to 40 ppb has been proposed by the EPA (US EPA 1997).

1.2 PAHs

Polycyclic aromatic hydrocarbons (PAHs) first gained interest in the 18th century as one of the first examples of an occupational exposure hazard. A high incidence of cancer was observed in chimney sweeps, who were typically young boys. This has since been linked to PAH exposure from the soot in chimneys (Hogstedt et al., 2013). PAHs are made up of fused benzene rings, and are generally categorized as petrogenic, originating from petroleum, or pyrogenic, originating from combustion processes (Abdel-Shafy and Mansour, 2016).

PAHs vary widely in their molecular structures and weights, and trends of their physicochemical properties are closely related to these characteristics. Because PAHs encompass a broad range of molecular structures and sizes, they have varying physicochemical properties. Compared to BTEX, PAHs have low water solubilities and low volatility. As a result, PAHs sorb strongly to soil and sediment in the environment, and are prone to bioaccumulation (Abdel-Shafy and Mansour, 2016; Cachada et al., 2012).

Sixteen PAHs are listed as priority pollutants by the EPA (US EPA 2014) and although PAH exposure is more commonly associated with inhalation or food ingestion (Bansal and Kim, 2015; Patel et al., 2020; Phillips, 1999), the EPA has set an MCL of 0.2 ppb of benzo(a)pyrene, a model PAH, in drinking water (US EPA

2009). This order of magnitude difference in MCL compared to the lowest MCL for monoaromatic hydrocarbons (5 ppb for benzene) reflects the additional toxicity and persistence of PAHs. PAHs are associated with carcinogenic, mutagenic, and teratogenic health effects and have demonstrable bioaccumulative effects that can severely disrupt ecosystems (Ghosal et al., 2016; Krzyszczak and Czech, 2021; Tu et al., 2018).

1.3 PAH Transformation Products

Aromatic hydrocarbons can be degraded in the environment by a variety of chemical and biological means. Atmospheric transformation of these contaminants can be achieved with the UV radiation and oxidative species present in the atmosphere or surface waters, producing photodegradation products (Fasnacht and Blough, 2002; Perraudin et al., 2006). A significant amount of degradation can be attributed to biological degradation. Biodegradation of aromatic hydrocarbons can produce innumerable transformation products. Most aerobic processes will produce oxygenated intermediates that may be further degraded and even cleaved to form aliphatic products (Alegbeleye et al., 2017; Ghosal et al., 2016). Although complete oxidation of aromatic hydrocarbons would yield carbon dioxide and water, degradation to this extent is difficult to achieve, particularly for PAHs. Instead, the incomplete degradation products, also called dead-end products, can accumulate in environmental systems (Ghosal et al., 2016). This is of concern, as several studies have reported increases in toxicity after chemical or biological PAH treatment (Andersson et al., 2009; Chibwe et al., 2015; Schrlau et al., 2017), due to the formation of transformation products that are more bioavailable and more toxic that their parent compounds.

2.0 Detection Technologies

Because aromatic hydrocarbons typically exist as mixtures in relatively low concentrations in the environment, chemical analysis of environmental samples often require extraction and separation techniques before their identification and quantification (Gitipour et al., 2018). Common extraction methods for liquid matrices

are liquid-liquid extraction (LLE), and solid phase extraction (SPE) (Brum et al. 2008; Marcé and Borrull 2000), while those for solid matrices are Soxhlet extraction and ultrasonic assisted extraction (UAE) (Song et al. 2007). Chromatography using gas (GC) or liquid (LC) as the mobile phase allows for the separation of compounds based on their general physicochemical properties. Detection of aromatic hydrocarbons primarily relies on flame ionization detectors (FID), mass-selective detectors (MS), ultraviolet absorbance (UV), or fluorescent emission.

Standard EPA methods have been developed for PAHs analysis in aqueous matrices such as methods 610, 625, 525, and 8310 (Gitipour et al., 2018) that use combinations of the aforementioned extraction, chromatography, and detection methods. PAHs are notoriously difficult to identify and quantify due to their physicochemical properties, and generally require more extensive analytical procedures than BTEX (Gitipour et al., 2018). Thus, the resources and time required to analyze environmental samples for aromatic hydrocarbons are often a bottleneck for research progress.

3.0 Bioremediation of Aromatic Hydrocarbons

The remediation methods investigated in this dissertation focus on bioremediation, as it is generally less expensive and less invasive than physical and chemical removal strategies (Farhadian et al., 2008; Juwarkar et al., 2010). Microorganisms can transform BTEX and PAHs through metabolism, where the contaminants are used as carbon and energy sources, or cometabolism, where the contaminants are transformed fortuitously without any carbon or energy gain (Hazen 2010.). Although many microorganisms have been isolated that degrade BTEX and PAHs via metabolic processes (Lu et al. 2011; Farhadian et al. 2008), the application of these microorganisms is limited, as they are dependent on the aromatic contaminants for their survival and are unable to degrade the contaminants to very low concentrations (Hazen 2010). Microorganisms that cometabolize contaminants are not limited in this way and are therefore better equipped to achieve remediation goal concentrations. Two bacterial pure cultures, introduced below, were used extensively in this dissertation research.

3.1 *Rhodococcus rhodochrous* ATCC 21198

Rhodococcus rhodochrous ATCC 21198 (21198) is a gram-positive bacterium that has been deposited in the American Type Culture Collections as part of a patent for gaseous hydrocarbon utilizing bacteria (*Rhodococcus rhodochrous* (Zopf) Tsukamura emend. Rainey et al. (ATCC 21198); (MacMichael and Brown, 1987). 21198 has been studied for its effective energy storage and ability to degrade environmental contaminants, such as chlorinated solvents and 1,4-dioxane, via cometabolism (Murnane et al., 2021; Rasmussen et al., 2020; Rolston et al., 2019; Shields-Menard et al., 2015). 21198 expresses a short-chain alkane monooxygenase (SCAM) that is believed to catalyze the transformation of these contaminants, and it can be stimulated by growth on gaseous substrates such as propane and isobutane as well as alcohols such as 2-butanol (Murnane et al., 2021). Although other studies of *Rhodococcus* strains have demonstrated degradation of BTEX and MTBE (Deeb et al. 2001; Kim et al. 2002; Deeb and Alvarez-Cohen 1999) and PAHs (Wang et al., 2021a; Zampolli et al., 2019), activity towards these contaminants has been shown to be highly variable at the genus level.

3.2 *Mycobacterium* Sp. Strain ELW1

Mycobacterium Sp. Strain ELW1 (ELW1) is a gram-positive aerobic bacterium that has been used in bioremediation studies for the cometabolism of chlorinated aliphatic hydrocarbons, and the low molecular weight PAH phenanthrene (Krippaehne 2018, Rich 2015, Schrlau et al., 2017). ELW1 was isolated from stream sediment in North Carolina using isobutene as the sole carbon and energy source (Kottegoda et al., 2015a). Analogous to the SCAM 21198 expresses when grown on isobutane, ELW1 expresses an alkene monooxygenase when grown on the gaseous substrate isobutene that putatively transforms contaminants (Kottegoda et al., 2015a). Previous work with ELW1 and phenanthrene demonstrated the accumulation of hydroxylated transformation products that were more toxic than phenanthrene alone (Schrlau et al., 2017).

3.3 Bioremediation Challenges

Both BTEX and PAHs predominantly exist as complex mixtures in the environment (Abdel-Shafy and Mansour, 2016; Latif et al., 2019). These mixtures can be difficult for microorganisms to treat in their entirety due to competition and inhibition mechanisms (Bielefeldt and Stensel, 1999a; Deeb and Alvarez-Cohen, 1999). One of the biggest challenges of PAH bioremediation specifically is the bioavailability of PAHs. Sorbed PAHs are not accessible to microorganisms, therefore treatment is typically limited by the desorption rate of PAHs from the soil or sediment to the surrounding water (Mohan et al. 2006; Lamichhane et al. 2016).

To reduce the desorption rate limitation, surfactants can be used to solubilize sorbed PAHs through a process known as “soil washing”. Surfactants at concentrations above their critical micelle concentration exist as micelles in solution that have a hydrophilic shell but a hydrophobic core that is capable of accumulating PAHs (Mulligan et al. 2001; Peng et al. 2011). Because soil washing creates a PAH-rich effluent that must be treated further, many studies have investigated the treatment of this effluent with microorganisms (Jin et al., 2007; Pantsyrnaya et al., 2011). However, all surfactants are toxic to microorganisms at high enough concentrations via cellular membrane disruption (Gharibzadeh et al., 2016).

Because of the inherent toxicity of surfactants, protecting cells from the surfactants while still allowing them access to the PAH containing micelles is of interest. One method used to protect cells from surfactant toxicity is immobilizing cells in hydrogels matrices consisting of polymers such as sodium alginate, polyvinyl alcohol, chitosan, or gellan gum (Mehrotra et al., 2021). Cell immobilization not only protects cells from the outside environment, but can also increase biomass activity, improve mass transfer of contaminants, and retain biomass to extend treatment times (Mehrotra et al., 2021; Partovinia and Naeimpoor, 2013; Patel et al., 2020). Several studies have immobilized PAH degraders in hydrogel beads for the treatment of PAH contaminated soil washing effluent and have reported improved treatment with immobilized cells (Chen et al., 2021; Wen et al., 2021; Xu et al., 2019).

4.0 Toxicity Considerations

Remediation goals typically take the form of a permissible concentration of the contaminants of interest, in accordance with state or federal regulations. However, inherent in these goals is the assumption that any transformation products produced from the remediation process are not as toxic as the parent compound(s). This assumption, while true for many contaminants, is not necessarily true for PAHs (Titaley et al., 2020). In the case of combined remediation strategies with surfactants and biological treatment, toxicity measurements become even more important, as surfactants can contribute to overall toxicity (Huguenot et al. 2015; Mousset et al. 2013).

Despite these findings, it is still uncommon for transformation products or toxicity to be monitored in remediation studies (Titaley et al., 2016). The complexity of identifying and quantifying PAH transformation products exceeds that of parent PAHs, therefore including toxicity assessments can aid in assessing the importance of the transformation products without the analytical chemistry undertaking. Although animal studies remain the gold standard for quantifying and reporting toxicity in regulatory environments (Ashton et al. 2013), cell-based assays are more attractive in research for which advising regulation is not the intent (Shukla et al., 2010).

Cell-based assays require significantly less time and preparation and are more ethical (Shukla et al., 2010). Cell-based assays can be as simple as reporting cell death in terms of a live/dead ratio (Gan et al., 2018; Sun et al., 2018). Non-lethal endpoints such as mutagenicity with the Ames assay (Kim Oanh et al., 2002; Titaley et al., 2016) or the Comet Assay (Cotelle and Farard 1999), and respiration interference with the MicroTox assay (Brakstad et al., 2018; Kim Oanh et al., 2002) can been used as well. More sophisticated methods using genetically modified eukaryotic cells such as chemically activated luciferase expression (CALUX) assays have taken cell-based assays closer to being representative of complex organisms (Beitel et al., 2020; Filipkowska et al., 2018). However, extrapolation between organisms remains a significant barrier to confidently translating toxicity in single cells to toxicity in humans.

4.1 Zebrafish Toxicity Model

A more complex system that has similar high-throughput capability to cell-based assays is the embryonic zebrafish assay. Zebrafish have approximately 80% genetic homology to humans, making extrapolation of results to humans more direct than aforementioned cell-based assays (Truong et al., 2011). Furthermore, toxicity testing in the embryonic phase allows for the study of nearly all potential cell types and expression of gene products, with toxicity manifesting as distinct phenotypes such as abnormalities of the heart, spine, and brain (Geier et al., 2018; Shankar et al., 2019). Embryonic zebrafish assays can be conducted in high-throughput 96-well microplates over the course of 5-days, during which embryos develop into zebrafish larva (Truong et al., 2016).

However, studies in this format are limited analytically by the small amounts of material used. Another major limitation of the embryonic zebrafish assay is quantifying how much of the chemicals they are exposed to are taken up by the embryos. In other words, the dose of the chemical is not the same as the amount of chemical they are exposed to, and determining the uptake and dose of toxins often relies on sacrificing embryos and using significant sample preparation techniques to quantify toxins with sensitive instruments (Wang et al., 2020, 2018).

5.0 Dissertation Contents and Objectives

This dissertation is composed of four manuscripts that investigate the detection, bioremediation, and toxicity of aromatic hydrocarbon contaminants. Each manuscript was motivated by addressing the aforementioned challenges in aromatic hydrocarbon bioremediation. The objectives of this research are summarized as the following:

1) Determine suitability of a bacterial pure culture for aromatic hydrocarbon bioremediation using BTEX as model aromatic hydrocarbons
   Hypothesis: *21198 is an excellent candidate for aromatic hydrocarbon bioremediation due to its expression of enzymes with broad substrate ranges and previous demonstrations of aromatic hydrocarbon remediation within the Rhodococcus genera.*

2) Develop rapid detection methods for monitoring aqueous PAH concentrations changing in response to biological activity
   Hypothesis: *Fluorescent spectroscopy techniques can be adapted to various experimental designs to monitor aqueous PAHs without significant interference from biologically derived background fluorescence.*
3) Expand investigations in (1) to PAH remediation strategies using treatment and toxicity metrics to assess remediation success
   Hypothesis: The transformation of PAHs by 21198 can occur but is aided by combined methods to protect cells and solubilize PAHs. Using multiple analytical techniques to monitor parent PAHs, PAH-TPs, and toxicity provides a better assessment of remediation success than monitoring parent PAHs alone.

Chapter II demonstrated the bioremediation of BTEX and MTBE by the bacterial culture 21198 as individual contaminants and contaminant mixtures in both high and low biomass batch experiments. Investigation of 21198 growth substrates and metabolic pathways were also included in this work. Chapter III reports the development of a novel analytical technique to monitor and quantify PAHs and PAH transformation products in controlled laboratory conditions using ELW1 as the model organism and phenanthrene as the model PAH. Measured concentrations and kinetic parameters derived from this method were compared to those derived from an established GC-MS method. Chapter IV adapts the methods developed in Chapter III to high-throughput embryonic zebrafish toxicity assays, where a fluorescent plate reader was used to quantify PAH concentrations in the embryo media and relate changes in aqueous PAH concentrations to PAH uptake by the zebrafish with kinetic models. Chapter V combines the knowledge gained in Chapter II and the techniques developed in Chapter III to study the bioremediation of a PAH mixture with 21198. This study compares the impact of cell immobilization and surfactants on overall treatment of PAHs, production of PAH transformation products, and the toxicity of remediated material. Chapter VI summarizes the conclusions of the preceding chapters and provides recommendations for future work.

CHAPTER II

Influence of Growth Substrate and Contaminant Mixtures on the Degradation of BTEX and MTBE by *Rhodococcus rhodochrous* ATCC Strain 21198

Juliana Huizenga[a] (ORCID: 0000-0002-1242-0948) huizengj@oregonstate.edu
Lewis Semprini[a] (ORCID: 0000-0002-9174-4464) lewis.semprini@oregonstate.edu
[a] Oregon State University, School of Chemical, Biological, and Environmental Engineering
Corresponding Author: lewis.semprini@oregonstate.edu

Appears in:
Biodegradation
2023
https://doi.org/10.1007/s10532-023-10037-2

Chapter II: Influence of Growth Substrate and Contaminant Mixtures on the Degradation of BTEX and MTBE by *Rhodococcus rhodochrous* ATCC Strain 21198

Abstract

The degradation of the prevalent environmental contaminants benzene, toluene, ethylbenzene, and xylenes (BTEX) along with a common co-contaminant methyl tert-butyl ether (MTBE) by *Rhodococcus rhodochrous* ATCC Strain 21198 was investigated. The ability of 21198 to degrade these contaminants individually and in mixtures was evaluated with resting cells grown on isobutane, 1-butanol, and 2-butanol. Growth of 21198 in the presence of BTEX and MTBE was also studied to determine the growth substrate that best supports simultaneous microbial growth and contaminants degradation. Cells grown on isobutane, 1-butanol, and 2-butanol were all capable of degrading the contaminants, with isobutane grown cells exhibiting the most rapid degradation rates and 1-butanol grown cells exhibiting the slowest. However, in conditions where BTEX and MTBE were present during microbial growth, 1-butanol was determined to be an effective substrate for supporting concurrent growth and contaminant degradation. Contaminant degradation was found to be a combination of metabolic and cometabolic processes. Evidence for growth of 21198 on benzene and toluene is presented along with a possible transformation pathway. MTBE was cometabolically transformed to tertiary butyl alcohol, which was also observed to be transformed by 21198. This work demonstrates the possible utility of primary and secondary alcohols to support biodegradation of monoaromatic hydrocarbons and MTBE. Furthermore, the utility of 21198 for bioremediation applications has been expanded to include BTEX and MTBE.

1.0 Introduction

Benzene, toluene, ethylbenzene, and xylenes (BTEX) are ubiquitous environmental contaminants introduced to the environment from both natural and anthropogenic sources such as forest fires, the combustion and spills of petroleum products, and manufacturing industries including solvent, paint, and rubber industries (Latif et al. 2019; Shim et al. 2002; Barboni and Chiaramonti 2010). The US

Environmental Protection Agency (EPA) recognizes BTEX as priority pollutants (US EPA 2014), as they are associated with a multitude of adverse health effects including carcinogenicity, neurotoxicity, and reproductive toxicity (Hazrati et al., 2016; Masih et al., 2016; Sairat et al., 2015). Despite their known toxicity, BTEX continue to have a significant presence in atmospheric and aquatic environments leading to regular human exposures (Y. Li et al. 2020; Dobaradaran et al. 2021; Alfoldy et al. 2019). Of particular concern is drinking water BTEX contamination, as even trace levels of BTEX in drinking water are considered hazardous. Maximum contaminant levels (MCLs) for benzene, toluene, ethylbenzene, and total xylenes are 0.005, 1, 0.7, and 10 mg/L, respectively (US EPA 2009).

Methyl tert-butyl ether (MTBE) was a common gasoline additive in the late 20th century used to increase the octane level of gasoline and thus promote more complete fuel combustion in automobiles (Steffan et al. 1997; Hernandez-Perez et al. 2001). MTBE quickly became dispersed in the environment due to its extensive use, and despite its replacement in gasoline by ethanol in the 2000s, it continues to be a common surface water and groundwater contaminant in the US (Fiorenza and Rifai 2003.; Carter et al. 2006). Furthermore, MTBE is still used as a gasoline additive in many countries, such as China and Mexico (González et al., 2018; Li et al., 2019a). MTBE is a suspected human carcinogen, and although no MCL has been established for it, an action level range of 20 µg/L to 40 µg/L has been proposed by the EPA (US EPA 1997).

Although BTEX is suitable for physical removal strategies such as air stripping or adsorption for treatment of contaminated water, a less invasive and inexpensive method of BTEX remediation is bioremediation (Farhadian et al. 2008; Juwarkar et al. 2010). Many microorganisms are capable of degrading BTEX as carbon and energy sources via metabolism, or in conjunction with an alternative carbon and energy source via cometabolism. Despite initially being considered recalcitrant to microorganisms, MTBE has also been demonstrated to be biodegradable by many microorganisms (Chen et al., 2011; Hristova et al., 2003; Mahmoodsaleh and Roayaei Ardakani, 2021). However, MTBE is most often found in the environment with

hydrocarbon co-contaminants such as BTEX, and BTEX contamination itself typically occurs as a mixture.

Thus, bioremediation efforts for BTEX and MTBE (BTEXM) must account for mixture interactions that occur within BTEX and between BTEX and MTBE. Contaminant mixtures often introduce complexities such as competition and inhibition that can reduce the success of bioremediation efforts (Bielefeldt and Stensel, 1999b; Deeb and Alvarez-Cohen, 1999). To overcome the negative impacts of mixtures on biodegradation, microorganisms have been isolated using BTEX mixtures as enrichment substrates in pursuit of microbes that can degrade, or at minimum tolerate, all components of BTEX (Benedek et al., 2021; Hocinat et al., 2020; Kasi et al., 2013; Wongbunmak et al., 2020).

Similar methods have also been used for enriching BTEXM degrading microorganisms using MTBE as the enrichment substrate (Lin et al. 2007; Raynal and Pruden 2008; Pruden and Suidan 2004). In doing so, isolates usually require BTEX or MTBE to sustain growth and activity, limiting their ability to degrade contaminants to remediation goal concentrations. Cometabolic processes avoid this issue, as microorganisms that cometabolize BTEXM are not dependent on the contaminants for their survival. Additionally, enzymes involved in MTBE oxidation typically have a low affinity for MTBE (high K_s), thus increasing the difficulty of achieving low concentrations in the environment (House and Hyman, 2010; Smith and Hyman, 2004).

Rhodococcus rhodochrous ATCC 21198 (21198) is a gram-positive bacterium with many qualities attractive for bioremediation applications such as planktonic growth, metabolic diversity, and expression of a short chain alkane monooxygenase (SCAM) that can transform chlorinated aliphatic hydrocarbons (CAHs) as well the cyclic ether 1,4-dioxane (1,4-D) (Rasmussen et al. 2020; Rolston et al., 2022). High expression of SCAM has been observed when 21198 is grown on alkanes such as propane and isobutane, however SCAM expression has also been shown to be supported by alcohols such as 2-butanol (Chen 2016). The Rhodococcus genera has an established relevance in bioremediation for n-alkanes and aromatic hydrocarbons (Brzeszcz and Kaszycki, 2018). Although other studies of *Rhodococcus* strains with

BTEXM have been conducted (Deeb et al. 2001; Jung and Park 2004; Kim et al. 2002; Deeb and Alvarez-Cohen 1999), including studies using aliphatic hydrocarbons as growth substrates (Auffret et al., 2009; Lee and Cho, 2009), alcohols have not been investigated as potential growth substrates to support degradation of BTEXM.

The objectives of this research were to establish the ability of 21198 to degrade BTEX and MTBE both individually and in mixtures, distinguish between metabolic and cometabolic processes involved in BTEXM degradation, and demonstrate the utility of alcohol growth substrates to support the degradation of BTEXM in settings of resting cell biomass and proliferating cell biomass.

2.0 Materials and Methods

2.1 Chemicals

All chemicals used were analytical grade purity: benzene (99%, Beantown Chemical, New Hampshire), toluene (99.8%, Sigma Aldrich, Missouri), ethylbenzene (99.8%, Acros Organics, Massachusetts), o-xylene, m-xylene, p-xylene (99%, Alfa Aesar, Massachusetts), MTBE, TBA (99%, TCI America, Oregon), isobutane (99.99%, Gas Innovations, Texas), 1-butanol (99.4%, Acros Organics, Massachusetts), 2-butanol (99%, Sigma Aldrich, Missouri).

2.2 *Rhodococcus rhodochrous* ATCC 21198 Culture Methods

The pure culture *Rhodococcus rhodochrous* ATCC 21198 (21198) was provided by Dr. Michael Hyman from North Carolina State University. 21198 was maintained as a pure culture on minimal salt media (MSM) agar plates in a sterile airtight jar with isobutane supplied as the sole carbon and energy source. Growth reactors were prepared as described in Rolston et al. (2019). Briefly, an inoculum scraped from a minimal plate was added to a 500 mL Wheaton glass media bottle containing 300 mL of sterile MSM (Kottegoda et al. 2015) amended with either isobutane, 1-butanol, or 2-butanol in excess based on the oxygen content of a sealed bottle. Growth reactors were incubated in the dark at 30 ºC on a 150 RPM shaker table.

Microbial growth was monitored via optical density absorption at 600 nm (OD_{600}) using a Thermo Scientific Orion Aquamate 8000 UV–Vis Spectrophotometer. When an OD_{600} of approximately 0.3 was reached, growth reactors were refreshed to enhance biomass growth. During refreshment, reactors were opened in a laminar flow hood to equilibrate with atmospheric oxygen and streaked on a tryptic soy glucose agar (TSGA) plate to confirm culture purity. A second addition of growth substrate was added to growth reactors before reclosing them. Cells in late exponential growth phase were concentrated into a 50 mM sodium phosphate buffer via centrifugation the day after refreshing as described in Murnane et al. (2021). TSS analysis on the cell concentrate was performed according to AWWA standard protocol (Baird et al. 2017) to determine the biomass concentration. Concentrated cell solutions were stored at 4 ^{o}C and used within 2 days of harvesting.

2.3 Analytical Methods

2.3.1 Headspace Analysis

Volatile compounds were analyzed using gas chromatography (GC). For all headspace GC analyses, a Hamilton 1710 Series gas-tight syringe was used to inject 100 μL of headspace sample from the batch reactors into the gas chromatograph. BTEX and isobutane were measured using a Series 6890 Hewlett Packard Gas Chromatograph equipped with a flame ionization detector (FID). Helium flowed through the capillary column (Agilent DB-624 UI 30m x 0.53mm) at 15 mL/minute. The detector temperature and oven temperature were held constant at 250 ^{o}C and 220 ^{o}C, respectively. Chromatographic separation of all volatile hydrocarbons was achieved with the exception of m-X and p-X, which coeluted.

Oxygen was measured using a Hewlet Packard 5890 Series Gas Chromatograph equipped with thermal conductivity detector (GC-TCD) and capillary column (Supelco 60/80 Caroboxen 1000). Helium flowing at 30 mL/minute was used as the carrier gas, with the oven temperature held constant at 40 ^{o}C. All headspace methods were calibrated using external standards, with good linear fit ($R^2 > 0.99$) achieved for all calibration curves. Henry's coefficients for each compound were used

to calculate the total mass of contaminants in bottles based on the headspace measurements. A list of Henry's coefficients used is reported in Table A4.

2.3.2 Liquid Sample Analysis

Non-volatile compounds, namely MTBE, tert-butyl alcohol (TBA), 1-butanol, and 2-butanol, were analyzed in liquid samples from batch reactors. 1 mL liquid samples were taken throughout the course of batch experiments through the cap septa using a sterile syringe. These samples were filtered through 0.2 µm polyvinylidene difluoride (PVDF) filters to remove cells and stored at 4 ^{o}C until analysis. MTBE, TBA, 1-butanol, and 2-butanol were analyzed using a Hewlet Packard 6890 Series Gas Chromatograph equipped with a Hewlet Packard 5873 mass selective detector (GC-MS) and capillary column (Restk Rtx-VMS). Filtered liquid samples were diluted in 40 mL VOA vials filled with 25 mL deionized water to concentrations below 20 µg/L. 5 mL of diluted sample was taken from each VOA via a Teledyne Tekmar AQUATek100 autosampler and run through a Teledyne Tekmar Lumin PTC purge and trap. Details on the heated purge and trap method are provided in Rolston et al. (2019). The mass detector was operated in selective ion monitoring mode to quantify ion fragments associated with MTBE (*m/z* 73), TBA (*m/z* 59), 1-butanol (*m/z* 56), and 2-butanol (*m/z* 45). This method was calibrated with external standards and standards were included in sample analyses runs to monitor instrument sensitivity fluctuations.

2.4 Batch Reactor Experiment Design

2.4.1 Resting Cell Experiments

Resting cell batch reactor tests with single contaminants and contaminant mixtures were conducted in 125 mL Wheaton serum bottles with butyl septa caps. Each bottle contained 100 mL of MSM and approximately 1 mg of the contaminant(s) added as neat liquids. Actual masses of contaminants added in each experiment are reported in Table A5. Bottles were allowed to reach liquid-gas phase

equilibrium at 30 ºC on a 150 RPM shaker table, and these conditions were maintained for the duration of the experiments.

Initial headspace measurements were taken before 5 mg of cells were added to bottles through the septa using a sterile syringe. Headspace and liquid samples were taken periodically to monitor contaminant concentrations. Control bottles were prepared without cells to monitor abiotic losses of analytes. Active bottles were prepared in triplicates, while control bottles were prepared in duplicates.

Zero-order rates were derived from the calculated total contaminant mass using the linear regression model "fitlm" in MATLAB. The linear regions used to calculate rates and goodness of fit are reported in Figure S2. Initial periods of minimal transformation, referred to hereafter as lag periods, were estimated by the length of time between the first measurement and the beginning of the defined linear region. On occasion, the initial timepoint was omitted from the linear portion to improve goodness of fit. Such situations were not considered to be part of the lag period if this was the only data point omitted.

2.4.2 Growth Batch Reactor Experiments

Four sets of batch reactors were prepared to investigate 21198 growth in the presence of BTEXM. Each set was prepared in 125 mL sterilized Wheaton serum bottles with butyl septa caps with 100 mL MSM, ~1 mg of each contaminant, and a low initial biomass, 0.05 mg of isobutane grown cells, compared to the resting cell tests. Batch reactors were amended with approximately 1 mg of growth substrate, with the exception of set 1, which did not receive any additional growth substrate. Isobutane, 1-butanol, and 2-butanol were added to sets 2, 3, and 4, respectively as growth substrates. As oxygen was depleted from the headspace air, pure gaseous oxygen was added to the headspace through the cap septa. Control bottles were prepared without cells to monitor abiotic losses of analytes. Batch reactors were prepared in triplicates, while control bottles were prepared in duplicates. All bottles were incubated in the dark on a 100 RPM shaker table at 20 ºC for the duration of the experiments.

2.4.3 Growth Substrate Experiments

To explore the range of growth substrates for 21198, growth substrate experiments were conducted in 125 mL Wheaton serum bottles (nominal volume 155 mL) with butyl septa caps and 25 mL MSM. Potential growth substrates were added to from neat stocks in excess based on the amount of available oxygen in the air headspace. Specific volumes of each substrate added are reported in Table S1. Growth bottles were inoculated with ~0.1 mg isobutane grown cells from a cell concentrate, and cell growth was monitored periodically using OD_{600} measurements. Bottles were incubated in the dark at 30 ^{o}C on a 150 RPM shaker table for the duration of the experiments.

3.0 Results and Discussion

3.1 Individual Contaminant Batch Experiments

3.1.1 BTEX Compounds

The influence of growth substrate on 21198's BTEXM degradative capability was investigated using resting 21198 cells grown on either isobutane, 1-butanol, or 2-butanol. Degradation was first studied in individual contaminant tests shown in Figure II-1.

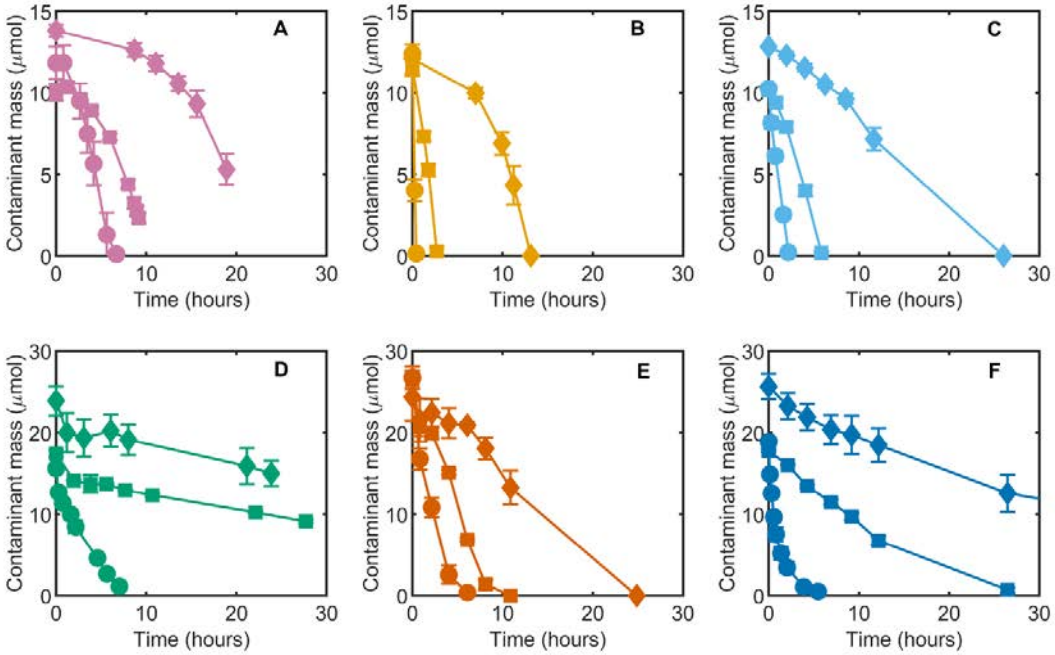

Fig. II-1 Degradation of benzene (A), toluene (B), ethylbenzene(C), o-Xylene (D), m-Xylene (E), and p-Xylene (F) in individual contaminant tests by 21198 grown on isobutane (circles), 1-butanol (diamonds), or 2-butanol (squares). Error bars represent standard deviation between triplicates

Isobutane grown cells consistently exhibited the most rapid transformation rates for all contaminants tested, followed by 2-butanol grown cells and 1-butanol grown cells. Lag periods were only observed with alcohol grown cells, as reported in Table II-1. A lag period for benzene transformation was observed with 1- and 2-butanol grown 21198, while a lag period for toluene was only observed with 1-butanol grown cells. The incidence of lag periods with alcohol grown cells indicated a potential induction period, during which the cells produced the enzyme required to transform the contaminants.

Table II-1. Zero-order transformation rates and lag periods associated with batch experiments. Error associated with transformation rates is the standard deviation among triplicates.

Contaminant	Batch Experiment	Isobutane Grown Cells		1-Butanol Grown Cells		2-Butanol Grown Cells	
		Rate (µmol/hour/mg biomass)	Lag Time (hours)	Rate (µmol/hour/mg biomass)	Lag Time (hours)	Rate (µmol/hour/mg biomass)	Lag Time (hours)
Benzene	**Individual**	0.43 ± 0.04	0	0.16 ± 0.02	11	0.25 ± 0.01	3.9
	BTEX	0.48 ± 0.06	1.3	0.10 ± 0.01	10	0.24 ± 0.06	4.6
	BTEXM	0.50 ± 0.05	0	0.11 ± 0.01	23	0.25 ± 0.04	6.5
Toluene	**Individual**	5.83 ± 0.04	0	0.31 ± 0.001	7	0.84 ± 0.04	0
	BTEX	1.35 ± 0.06	0	0.25 ± 0.02	5.9	0.30 ± 0.01	0
	BTEXM	2.17 ± 0.14	0	0.13 ± 0.01	6.4	0.29 ± 0.01	0
Ethylbenzene	**Individual**	0.86 ± 0.02	0	0.10 ± 0.01	0	0.34 ± 0.004	0
	BTEX	0.73 ± 0.04	0	0.10 ± 0.02	5.9	0.18 ± 0.01	0
	BTEXM	1.11 ± 0.05	0	0.08 ± 0.01	6.4	0.20 ± 0.01	0
o-Xylene	**Individual**	0.33 ± 0.02	0	0.04 ± 0.01	0	0.34 ± 0.004	0
	BTEX	0.29 ± 0.01	0	0.12 ± 0.01	10	0.18 ± 0.01	3.0
	BTEXM	0.47 ± 0.04	0	0.08 ± 0.01	10	0.20 ± 0.01	2.0
m-Xylene	**Individual**	7.17 ± 0.16	0	0.17 ± 0.01	0	0.58 ± 0.04	0
p-Xylene	**Individual**	1.56 ± 0.11	0	0.07 ± 0.003	0	0.18 ± 0.01	0
MTBE	**Individual**	0.16 ± 0.02	0	0.03 ± 0.01	0	0.16 ± 0.03	0
	BTEXM	0.25 ± 0.04	0	0.03 ± 0.008	26	0.08 ± 0.01	0

Because transformation of these contaminants commenced following this period, enzyme(s) required for these transformations are potentially inducible by the presence of BTEX. Among the aromatic compounds, T and m-X were transformed most rapidly, while o-X was transformed slowly. Based on the significant differences in transformation rates reported in Table II-1 among the BTEX components, it appears that a single methyl or ethyl substitution on the ring makes the compound more susceptible to enzymatic attack by 21198. However, as demonstrated by the range of degradation rates between xylene isomers, a second methyl substitution on the ring can have negative impacts on degradability. Of the three xylene isomers, o-X is commonly observed to be the most difficult to degrade microbially (Auffret et al. 2009; Taki et al. 2006; Jeong et al. 2008). Because of this, o-X has been used as an enrichment substrate to isolate o-X degrading *Rhodococcus* strains. *Rhodococcus* isolates that preferentially degrade o-X over the other isomers have been

characterized (Jeong et al. 2008; You et al. 2018). The same was achieved by Auffret et al. (2009) using a BTEX and aliphatic hydrocarbon mixture to isolate a *Rhodococcus wratislaviensis* strain. However, Taki et al. (2006) reported the same xylene isomer preference as 21198 (m-X > p-X > o-X) with a *Rhodococcus* consortia despite using o-X as the consortia's enrichment substrate. 21198's ability to cometabolically degrade all xylene isomers, while not requiring their presence during its growth phase, indicates the relaxed substrate specificity of the enzyme(s) involved in their degradation. Abiotic losses in these experiments were minimal compared to transformation of contaminants observed in active bottles, and are reported in Table S2.

Along with the rate of contaminant degradation, the extent of degradation was impacted by growth substrate. While complete contaminant degradation was achieved by isobutane grown cells for all BTEX components, 1-butanol and 2-butanol grown cells were unable to fully degrade o-X in the duration of the experiment. 1-butanol grown cells were also unable to fully degrade p-X. A lower transformation capacity, or mass of contaminant able to be transformed by a certain resting cell mass, for o-X and p-X may be the result of stress to the microbes such as transformation product toxicity or depletion of the cells' energy reserves.

3.1.2 MTBE and TBA

MTBE transformation progressed slower than the BTEX compounds across all growth substrates, as shown in Figure II-2A. However, the relative rate and extent of degradation followed the same pattern amongst the growth substrates as observed with BTEX (isobutane > 2-butanol > 1-butanol).

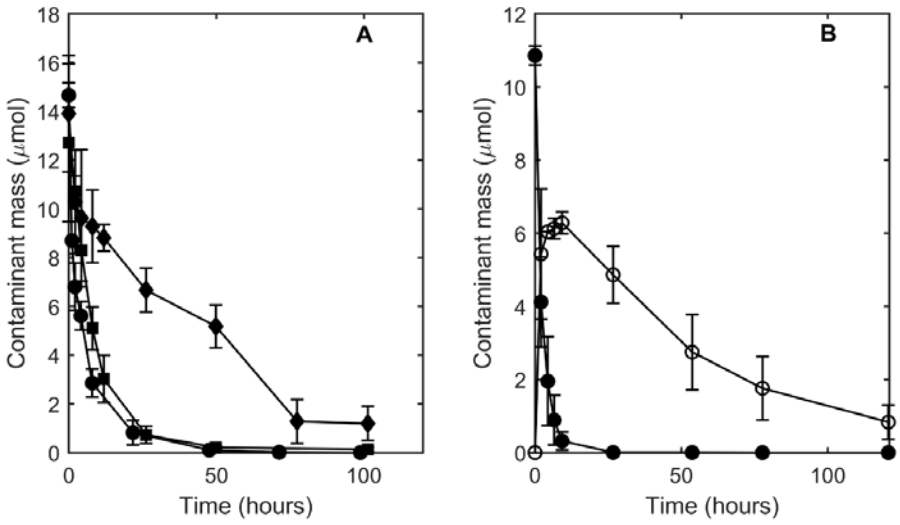

Fig. II-2 Transformation of MTBE by 21198 grown on isobutane (circles), 1-butanol (diamonds), or 2-butanol (squares) shown in A. Simultaneous MTBE (filled circle) transformation and TBA (open circle) production by isobutane grown 21198 shown in B. Error bars represent standard deviation between triplicates in A and duplicates in B

No lag period was observed for MTBE transformation by cells grown on either isobutane or butanol. Isobutane grown cells achieved MTBE concentrations below the EPA action level concentration (20 μg/L) after 76 hours of incubation, while 1-butanol and 2-butanol grown cells reached concentrations of 1.2 mg/L and 0.12 mg/L, respectively, after 100 hours of incubation. TBA was identified as the major transformation product of MTBE produced by 21198. TBA is the most common intermediate reported in MTBE aerobic degradation pathways (Nava et al. 2007; Fiorenza and Rifai, 2003). Some microorganisms such as *Arthrobacter* ATCC 27778 (Liu et al., 2001), *Acinetobacter* Sp. Strain SL3 (Li et al. 2019b) and ENV425 ATCC 55798 (Steffan et al., 1997) are able to utilize the same enzyme for MTBE and TBA oxidation, producing precursors for intermediates, such as 2-hydroxyisobutyric acid (HIBA). Other microorganisms utilize different enzymes for MTBE and TBA oxidation, such as *Mycobacterium austroafricanum* IFP 2012 (François et al., 2002) and *Methylibium petroleiphilum* strain PM1 (Deeb and Alvarez-Cohen, 2000). However, many MTBE oxidizing organisms are unable to further oxidize TBA, including *Pseudomonas mendocina* KR-1 (Smith et al. 2003), *Pseudomonas putida* GPo1 (Smith and Hyman, 2004), and *Gordonia terrae* IFP 2001 (Hernandez-Perez et

al. 2001). Accumulation of TBA is not desirable, as TBA has similar properties, including toxicity, to MTBE (Nava et al.2007).

The transformation of TBA was observed in MTBE batch tests with resting isobutane grown 21198 cells as shown in Figure II-2B, indicating that the transformation of MTBE does not end at TBA, however the transformation of TBA occurs more slowly than that of MTBE. House and Hyman (2010) observed slower TBA oxidation rates compared to MTBE as well with *Mycobacterium austroafricanum* JOB5. It was concluded that TBA and MTBE compete for the same monooxygenase, and that the lower TBA transformation rate is due to a higher K_s value for TBA compared to MTBE. Catalytic similarities between 21198 and JOB5 with regards to both BTEX and MTBE degradation suggest that this phenomenon documented in JOB5 may also be occurring in 21198.

3.1.3 Connections to Additional Contaminants of Concern

The relative activity of 21198 grown on different substrates towards BTEXM follows trends observed with 21198 transforming CAHs and 1,4-D reported previously (Bealessio 2021). This trend is reflective of the extent of expression of enzyme(s) capable of cometabolizing these contaminants. Murnane et al. (2021) used activity-based profiling to demonstrate that the alkane monooxygenase responsible for oxidizing CAHs and 1,4-D is expressed highly in isobutane grown 21198, moderately in 2-butanol grown cells, and minimally in 1-butanol grown cells. This is presumably due to the need for the alkane monooxygenase to initiate isobutane metabolism, but not butanol metabolism. Rather, butanol metabolism is initiated by an alcohol dehydrogenase, which cannot initiate cometabolism of BTEXM. A similar explanation for lag periods has been suggested with a *Rhodococcus aetherivorans* strain grown on 1-butanol (Inoue et al., 2018).

Murnane et al. (2021) also observed an acceleration in rates of 1,4-D cometabolism with time for 1-butanol grown cells, which is consistent with observations in B and T individual tests shown in Figure II-1A and B and indicative of increased monooxygenase production with time. The similarity in trends observed

across growth substrates for BTEXM, CAHs, and 1,4-D indicates that the alkane monooxygenase involved in CAH and 1,4-D oxidation may also be involved in the oxidation of BTEXM.

3.2 Contaminant Mixture Batch Experiments

3.2.1 BTEX Mixture

Contaminant mixtures were tested with 21198 after confirming its ability to degrade all components of BTEXM individually. The order of contaminant degradation and emergence of lag periods shown in Figure II-3 illustrate the impact of contaminant mixtures on 21198, and how that impact differs based on the substrate used to grow the cells.

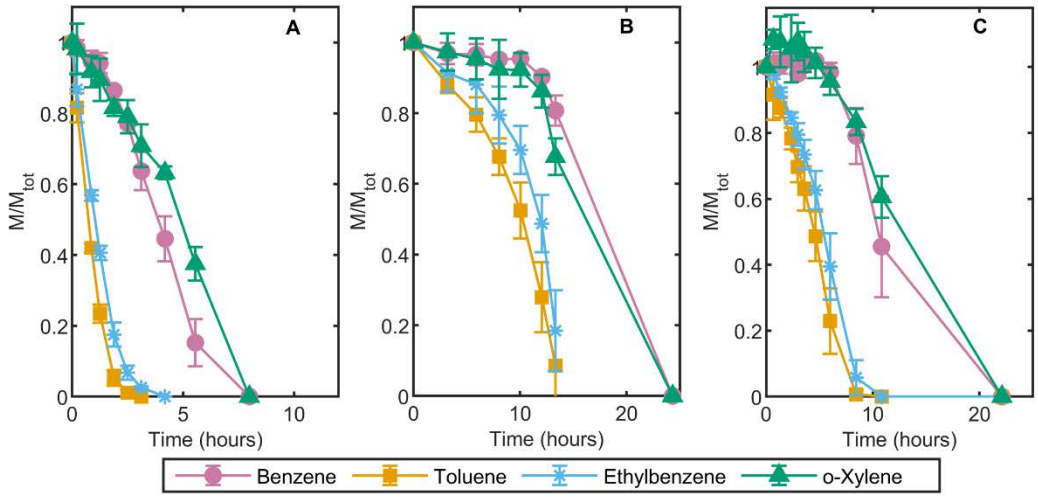

Fig. II-3 Degradation of BTEX in resting cell mixture batch tests by isobutane (A), 1-butanol (B), or 2-butanol (C) grown 21198. Error bars represent standard deviation between triplicates. Data normalized to initial masses for each contaminant. Initial mass of each contaminant is reported in Table S4

The order of contaminant transformation followed the relative rates of transformation established in the individual contaminant tests, with contaminant degradation commencing as T > E > B > o-X for all growth substrates. As observed in the individual contaminant tests, there was no lag period in TEX transformation with isobutane grown cells, however a short lag period of 1.3 hours was observed for B. A

lag period was observed for B, T, and o-X in tests conducted with 1-butanol grown cells, and B and o-X in tests conducted with 2-butanol grown cells (Table II-1). For 1-butanol grown cells, this lag period may be representative of combined effects of inhibition and induction.

Lag periods were observed for B and T in individual contaminant tests and were therefore expected to be observed in mixture tests as well. The lag periods observed in BTEX mixture tests were similar in length to those observed in individual tests, however the presence of lag periods for contaminants in mixture tests that were not observed in individual tests indicate that other factors, such as inhibition, may be contributing to the lag in transformation. Inhibition by the presence of T and E is a commonly reported phenomenon among BTEX mixture transformation (Jung and Park 2004; Deeb and Alvarez-Cohen 1999). This hypothesis is further supported by the fact that significant B and o-X transformation progressed only after T and E concentrations were significantly reduced.

These interactions were also observed with 2-butanol grown cells. For 1-butanol and 2-butanol grown cells, the presence of other aromatic compounds had a positive effect on the extent of o-X degradation, as they were able to fully transform o-X in the mixture tests. Enhanced degradation when BTEX compounds are present in a mixture has been reported for other microorganisms as well (Benedek et al., 2021; Khodaei et al., 2017; Wongbunmak et al., 2020), with authors attributing this observation to microbial growth supported by components of BTEX and/or enhanced expression of enzymes required for BTEX transformation.

3.2.2 BTEXM Mixture

The order of BTEX degradation followed the same pattern as described in the previous section, with MTBE transformation occurring slower than all BTEX components as shown in Figure II-4. Abiotic losses in these experiments were minimal and are reported in Table A3. The presence of MTBE in the BTEX mixture impacted transformation rates differently depending on the substrate the cells were grown on, although the rate of B transformation for all growth substrates was not significantly impacted by the presence of MTBE in the BTEX mixture.

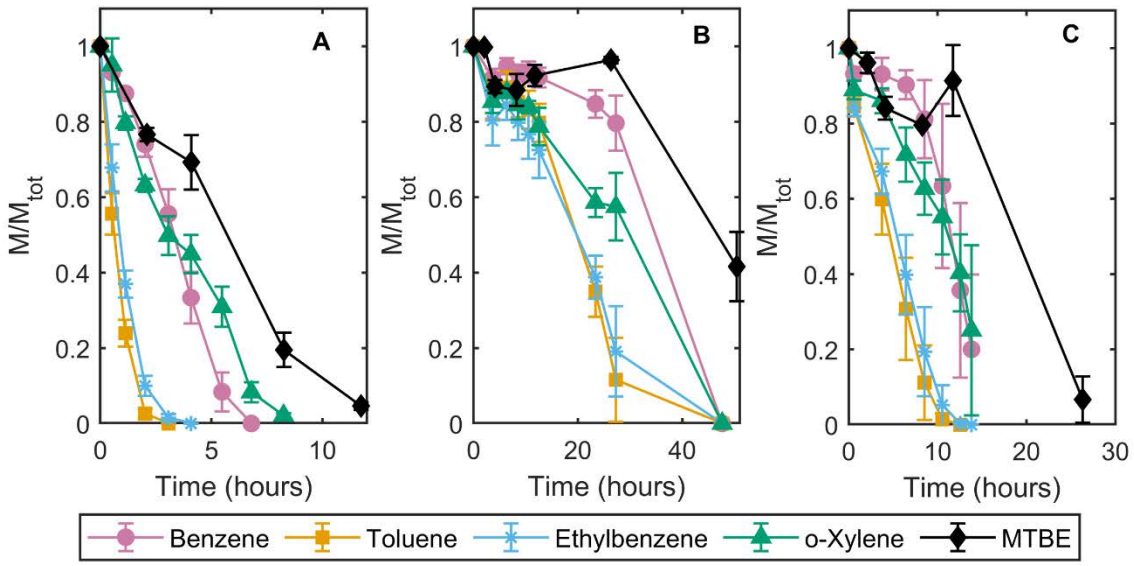

Fig. II-4 Degradation of BTEXM in resting cell mixture batch tests by isobutane (A), 1-butanol (B), or 2-butanol (C) grown 21198. Error bars represent standard deviation between triplicates. Data normalized to initial masses for each contaminant. Initial mass of each contaminant is reported in Table S4

For isobutane grown cells, an increase in zero-order transformation rate was observed for T, E, and o-X in the presence of MTBE. The opposite was observed for 1-butanol grown cells, with T, E, and o-X degradation rates decreasing in the presence of MTBE. Interestingly, for 2-butanol grown cells, no significant impact on BTEX transformation rate was observed with the presence of MTBE in the BTEX mixture (Table II-1). No lag periods were observed for isobutane grown cells, while B and o-X lag periods observed for 2-butanol grown cells were consistent with observations from the BTEX mixture test. An extended lag period for B and MTBE were observed for 1-butanol grown cells, which was twice as long as that observed in the BTEX mixture test. MTBE degradation commenced once significant transformation of BTEX was achieved by 1-butanol grown cells, suggesting that BTEX inhibits the transformation of MTBE. MTBE inhibition by BTEX is a commonly reported phenomenon (Deeb and Alvarez-Cohen, 2000; Lee and Cho, 2009; Raynal and Pruden, 2008). Similar lag periods were also observed by Zhou et al. (2016) with

BTEX and 1,4-dioxane mixtures, with lag being attributed to enzyme competition, intermediate toxicity, and/or energy deficits.

Despite the initial inhibition of MTBE transformation, as BTEX concentrations decreased, rapid transformation of MTBE was observed. What's more, lower concentrations of MTBE were achieved in BTEXM mixture tests than in tests conducted with MTBE alone as shown in Figure II-5, despite there being a greater mass of contaminants for 21198 to transform.

Fig. II-5 Comparison of MTBE transformation by isobutane (A), 1-butanol (B), and 2-butanol (C) grown 21198 in individual contaminant tests (diamonds/solid) and BTEXM mixture tests (circles/dashed). Note the y-axis is in log scale. The red line represents the 20 µg/L EPA advisory concentration of MTBE. Error bars represent standard deviation among triplicates

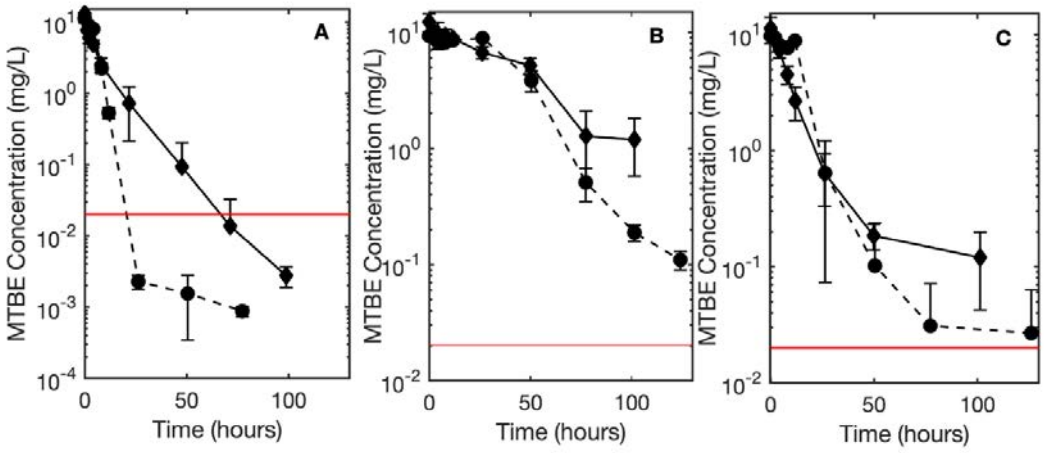

For microorganisms that are able to transform MTBE in the presence of BTEX, several studies have reported no detrimental effect to MTBE transformation (Pruden et al. 2003; Pruden and Suidan 2004; Sedran et al. 2002). However, it is uncommon for MTBE transformation to be enhanced by the presence of BTEX. Aufrett et al. (2009) reported that MTBE could only be degraded by a novel *Rhodococcus wratislaviensis* isolate when present in a mixture of aromatic and aliphatic hydrocarbons. It was suggested that this is due to enhanced cometabolic activity towards MTBE when present in a mixture with other hydrocarbons. This enhanced activity observed with 21198 could be due to BTEX acting as stronger inducers of relevant enzymes than MTBE alone, or due to the additional energy provided from hydrocarbon metabolism.

3.3 Growth Batch Reactors

A low initial biomass loading, one hundredth of what was added to the resting cell batch reactors, was studied in the growth batch reactors. Startup time, defined as the time required to transform the initial mass of BTEX in the batch reactors, was influenced by the absence or presence of an added growth substrate. Progression of BTEXM degradation followed the same order as observed in BTEXM mixture tests with resting cells. Oxygen consumption and microbial growth, reported in Table A6, support the contaminant transformation and growth substrate utilization trends shown in Figure II-6.

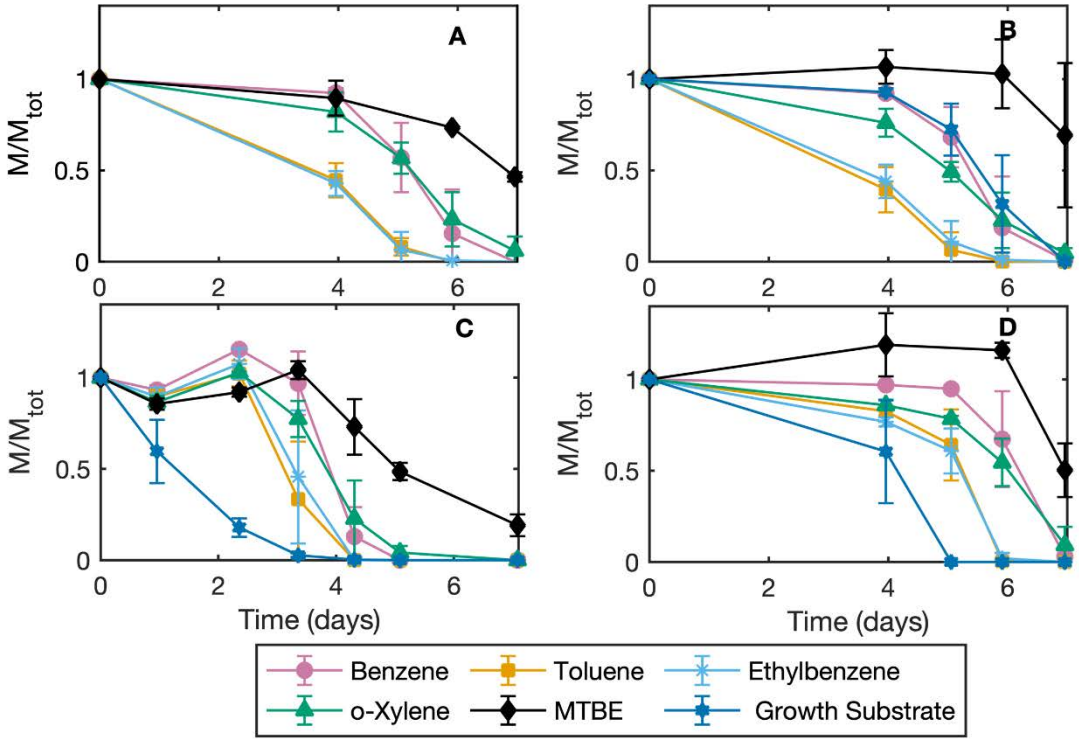

Fig. II-6 Degradation of BTEXM and consumption of growth substrate in no substrate (A), isobutane (B), 1-butanol (C), or 2-butanol (D) microcosms in first 7 days post-inoculation. Error bars represent standard deviation among triplicates. Data normalized to initial masses for each contaminant. Initial mass of each contaminant is reported in Table S4

1-butanol was most rapidly utilized, followed by 2-butanol, and then isobutane. O_2 consumption in the no substrate added batch bottles is representative of the oxygen demand of the resting cells and their oxidation of the added contaminants, while the

increases in oxygen consumption for isobutane, 1-butanol, and 2-butanol amended batch bottles demonstrate the oxygen demand associated with the resting cells, BTEXM transformation and growth substrate utilization.

As expected, optical density increased slightly more in batch bottles with added growth substrate compared to those without substrate. Increases in OD_{600} for all batch bottles indicate that 21198's growth is not inhibited by the presence of BTEXM. Additionally, an increase in the OD_{600} in bottles that did not receive any additional substrate alluded to the possibility that contaminant metabolism, rather than exclusively cometabolism, was occurring. This was further investigated in individual substrate growth tests described in Section 3.4.

Isobutane and 2-butanol amended batch bottles transformed BTEXM similarly to the batch bottles with no added growth substrate. A lag period in isobutane consumption was observed for the first 4 days, during which time T and E were transformed. This preferential transformation of T and E over isobutane utilization may be a result of the lower aqueous concentration of isobutane compared to T and E due to its higher volatility, and/or competition between the compounds for the same enzyme (Deeb et al., 2001). Despite 1-butanol grown cells consistently exhibiting the lowest transformation rates and capacities towards BTEXM in resting cell tests, the 1-butanol amended batch bottles required the shortest start up time for growth substrate utilization and contaminant transformation.

The 1-butanol amended batch bottles indicated the combined advantage of rapid substrate utilization, cell growth, the presumed high enzyme expression associated with the initial addition of isobutane grown cells and maintained enzyme expression, possibly due to the potential inductive effects of BTEX, to promote cometabolic transformation of MTBE. The use of alcohols to support growth and BTEXM transformation also avoids introducing competition between the growth substrate and contaminants, as 1-and 2-butanol do not require initial oxidation by a monooxygenase. The high performance of the 1-butanol amended batch bottles and the increase in OD_{600} in batch bottles without growth substrate prompted further investigation into the potential for utilization of BTEXM as carbon and energy sources by 21198.

3.4 21198 Growth Experiments

ATCC Strain 21198's ability to utilize a wide range of aliphatic growth substrates, including isobutane, 1-butanol, and 2-butanol, has been established previously (Chen 2016). A summary of these results is reported in Table II-2.

Table II-2. OD_{600} measurements from 21198 growth experiments reported as OD_{600} < 0.1 (-), OD_{600} > 0.1 (+), OD_{600} > 0.3 (++), OD_{600} > 0.6 (+++) among triplicates or duplicates (denoted with an asterisk). Substrates that supported 21198 growth are bolded.

Growth Substrate	Day 3	Day 7	Day 14
Isobutane	+	+++	+++
1-Butanol	++	++	++
2-Butanol	-	+	+++
Benzene	-	++	++
Toluene	-	+	++
Ethylbenzene	-	-	-
o-Xylene	-	-	-
m-Xylene*	-	-	-
p-Xylene*	-	-	-
Phenol	+	++	++
m-Cresol	-	-	-
p-Cresol*	-	-	-
Benzyl Alcohol	++	++	++
Benzyl Aldehyde	-	-	+
Benzoic Acid*	+	++	++
MTBE*	-	-	-
Control	-	-	-

Growth tests conducted with BTEX and MTBE revealed that B and T can be used as the sole carbon and energy source by 21198, but E, X, and MTBE cannot. Therefore, transformations of E, X, and MTBE observed with 21198 cells are

indicative of cometabolic processes, whereas those observed with B and T are representative of utilization through metabolic processes. Results from the growth experiments along with KEGG pathways for B and T and the annotated genome of 21198 sequenced previously (Shields-Menard et al., 2014) were used to construct possible metabolic pathways for 21198's metabolism of B and T, shown in Figure S1. Initial oxidation with a monooxygenase is proposed for B and T, however T metabolism may also be initiated with a toluene hydroxylase. It is hypothesized that T oxidation must be initiated at the methyl group, as growth was observed on benzyl alcohol but not p- or m- cresol. B and T metabolic pathways merge at a catechol intermediate, however it requires several more enzymatic steps for T to be transformed into catechol than B, which is supported by the faster growth observed on B compared to T.

21198 has genes for both a catechol-1,2-dioxygenase and catechol-2,3-dioxygenase, therefore catechol ring cleavage may occur in either the 1,2 or 2,3 position. Enzymes required to breakdown products of either catechol dioxygenase to substrates for glycolysis or the TCA cycle were found to be present in 21198's genome. Tools such as proteomics, differential gene expression analysis, or gene knockout studies are needed to confirm the proposed metabolic pathways.

Growth on B was delayed compared to substrates such as isobutane, 1-butanol, phenol, and benzyl alcohol, which all supported observable growth (OD_{600} > 0.1) within 3 days of incubation. Generally, faster growth was observed with the more oxidized substrates. For example, growth on 1-butanol commenced more rapidly than growth on isobutane. Similarly, growth on phenol or benzyl alcohol was more rapid than growth on B or T. Exceptions are 2-butanol and benzyl aldehyde, which took longer to grow cells than isobutane and T.

Growth on B and T by *Rhodococcus rhodochrous* strains has been reported previously (Deeb and Alvarez-Cohen 1999; Vanderberg et al. 2000; Warhurst et al. 1994), but to the authors' knowledge this is the first demonstration of B and T metabolism by 21198. Cometabolism of E, X, and MTBE likely involves the same enzymes used in the beginning steps of the B and T metabolic pathways shown in Figure A1. However, because growth was not observed on these substrates, the

cometabolic transformations likely lead to dead end products. Identifying dead end products that accumulate during BTEXM degradation would inform the extent of transformation and enzymes involved in the cometabolism of E, X, and MTBE.

The identification of these novel growth substrates corroborates the findings of enhanced contaminant transformation in BTEX and BTEXM mixture tests. Energy gained from B and T metabolism likely supported the cometabolism of cometabolic substrates such as o-X and MTBE. This is reflected in the greater transformation capacity of o-X and MTBE observed in mixture tests compared to the individual contaminant tests.

These findings also explain the increase in optical density in the growth batch reactors that were not supplied additional growth substrates (Table A6). The increase in OD_{600} measured in these bottles is the result of growth from B and T metabolism, while the greater OD_{600} in the growth substrate amended bottles is the result of the combined growth on B, T, and either isobutane, 1-butanol, or 2-butanol.

4.0 Conclusions

The results demonstrate that 21198 is capable of degrading all components of BTEXM individually and in mixtures using a combination of metabolic and cometabolic processes. While isobutane, 1-butanol, and 2-butanol all supported 21198's growth and degradation of BTEXM, resting 21198 cells' performance was optimized by growth on isobutane and minimized by growth on 1-butanol. However, 1-butanol was found to be an effective substrate for supporting the growth of 21198 in the presence of BTEXM as it is most rapidly utilized by 21198 compared to isobutane and 2-butanol, and likely does not compete for enzymes involved in BTEXM oxidation. Positive outcomes such as increased rate and extent of degradation followed the initial lag periods that were observed in BTEX and BTEXM mixture tests. 21198's ability to degrade all components of BTEXM, particularly B and T, allows for more rapid and complete MTBE transformation. This work demonstrates the possible utility of primary and secondary alcohols to support biodegradation of BTEXM in batch studies that can be expanded to continuous flow treatment studies in the future. The results also illustrate complex interactions of B

and T metabolism and cometabolic transformation of MTBE that require further investigation. Finally, the utility of 21198 for bioremediation applications has been expanded to include MTBE, TBA, and monoaromatic hydrocarbons.

5.0 Acknowledgements

The authors wish to thank Dr. Michael Hyman for valuable discussions and insights on the research and Dr. Mohammad Azizian for support on the analytical methods. Research reported in this publication was supported by the National Institute of Environmental Health Sciences of the National Institutes of Health under Award Number P42ES016465. The content is solely the responsibility of the authors and does not necessarily represent the official views of the National Institutes of Health.

CHAPTER III

Fluorescent spectroscopy paired with parallel factor analysis for quantitative monitoring of phenanthrene biodegradation and metabolite formation

Juliana Huizenga[a] (ORCID: 0000-0002-1242-0948) huizengj@oregonstate.edu
Lewis Semprini[a] (ORCID: 0000-0002-9174-4464) Lewis.Semprini@oregonstate.edu
[a] Oregon State University, School of Chemical, Biological, and Environmental Engineering
Corresponding Author: Lewis.Semprini@oregonstate.edu

Appears in:
Chemosphere
2023 Volume 316 Article 137771
DOI: https://doi.org/10.1016/j.chemosphere.2023.137771

Chapter III: Fluorescent spectroscopy paired with parallel factor analysis for quantitative monitoring of phenanthrene biodegradation and metabolite formation

Abstract

Polycyclic aromatic hydrocarbons (PAHs) are a class of environmental contaminants released into the environment from both natural and anthropogenic sources that are associated with carcinogenic, mutagenic, and teratogenic health effects. Many remediation strategies for the treatment of PAH contaminated material, including bioremediation, can lead to the formation of toxic transformation products. Analytical techniques for PAHs and PAH transformation products often require extensive sample preparation including solvent extraction and concentration, chromatographic separation, and mass spectrometry to identify and quantify compounds of interest. Excitation-emission matrix (EEM) fluorescent spectroscopy paired with parallel factor analysis (PARAFAC) is an approach for analyzing PAHs that eliminates the need for extensive sample preparation and separation techniques before analysis. However, this technique has rarely been applied to monitoring PAH biotransformation and formation of PAH metabolites. The objectives of this research were to compare an established targeted analytical method to two-dimensional fluorescent spectroscopy and combined EEM-PARAFAC methods to monitor phenanthrene degradation by a bacterial pure culture, *Mycobacterium* Strain ELW1, identify and quantify phenanthrene transformation products, and derive kinetic constants for phenanthrene degradation and metabolite formation. Both phenanthrene and its primary transformation product, *trans*-9,10-dihydroxy-9,10-dihydrophenanthrene, were identified and quantified with the EEM-PARAFAC method. The value of the EEM-PARAFAC method was demonstrated in the superiority of sensitivity and accuracy of quantification to two-dimensional fluorescent spectroscopy. Quantification of targets and derivation of kinetic constants using the EEM-PARAFAC method were validated with an established gas chromatography-mass spectrometry (GC-MS) method. To the authors' knowledge, this is the first study to use an EEM-PARAFAC method to monitor, identify, and

quantify both PAH biodegradation and PAH metabolite formation by a bacterial pure culture.

1.0 Introduction

Polycyclic aromatic hydrocarbons (PAHs) are a class of environmental contaminants released into the environment from both natural and anthropogenic sources, such as forest fires and the use of petroleum products (Patel et al. 2020; Alegbeleye et al. 2017), that are associated with carcinogenic, mutagenic, and teratogenic health effects (Ghosal et al., 2016; Krzyszczak and Czech, 2021). Sixteen PAHs are listed as priority pollutants by the EPA (US EPA 2014) and although PAH exposure is more commonly associated with inhalation or food ingestion over drinking water (Bansal and Kim, 2015; Patel et al., 2020; Phillips, 1999), the EPA has set a maximum contaminant level (MCL) of 0.2 μg/L for benzo(a)pyrene in drinking water (US EPA 2009). In addition, many regulations exist in the US and other countries for PAH content in industrial soils (Chibwe et al., 2015).

Common remediation techniques for PAHs include soil washing, photooxidation, chemical oxidation, and biodegradation (Gan et al. 2009; Sakshi and Haritash 2020; Kumar et al. 2021). PAH transformation products are often produced during chemical or biological remediation processes, with several studies finding these products to be equally, if not more, toxic than their parent compounds (Andersson et al. 2009; Trine et al. 2019; Titaley et al. 2020). Therefore, monitoring both PAHs and their transformation products during and after treatment is of interest in remediation studies.

PAHs typically exist as mixtures in relatively low concentrations in the environment, thus chemical analysis of environmental samples often require extraction, concentration, and separation techniques before identification and quantification of compounds of interest. Several standard methods have been developed by the US-EPA for analysis of PAHs in aqueous matrices such as methods 610, 625, 525, and 8310 that use combinations of extraction, chromatography, and detection techniques (Gitipour et al., 2018). When considering PAH transformation products, more sophisticated analytical techniques are generally required to resolve a

complex mixture of PAH transformation products that can have great diversity in structure and chemical properties (Titaley et al., 2020). The time, materials, and costs associated with these techniques has motivated the development of more rapid and less expensive analyses for PAHs and PAH transformation products.

One such analytical technique that forgoes extraction and separation before analysis is fluorescent spectroscopy. Fluorescent spectroscopic analysis can be conducted in 2 dimensions, where fluorescent emissions are measured for one excitation wavelength (λ_{ex}) and a range of emission wavelengths (λ_{em}), or three dimensions, where fluorescent emissions are measured for a range of λ_{ex} and λ_{em}. Excitation-emission matrices (EEMs) are data sets produced by three dimensional scans that are a common tool for environmental monitoring studies, as they are non-destructive, rapidly collectable, and require minimal sample preparation (Yang et al., 2016). While EEMs provide qualitative information of sample composition, decomposition of the fluorescent spectra produced from a bulk sample is often necessary to interpret EEMs (Rutherford et al., 2020) .

A tool commonly used to accomplish this decomposition is parallel factor analysis (PARAFAC), a statistical technique that models EEMs as combinations of components with specific excitation and emission spectra (Bro, 1997). Advantages of PARAFAC decomposition include uniqueness, such that pure spectra are obtained from the model (Nahorniak and Booksh, 2006), as well as a second-order advantage, which enables concentrations to be measured even in the presence of unexpected interferences (Gómez and Callao, 2008; Olivieri et al., 2004). As such, components obtained from PARAFAC models can be identified and quantified using external standard calibration.

EEM-PARAFAC methods have been used in monitoring studies to investigate the PAH content of oils (Alostaz et al., 2008; Christensen et al., 2005), seawater (Driskill et al., 2018; Ferretto et al., 2014), and freshwater (Yang et al., 2016) samples. PARAFAC components can be identified based on characteristics such as Stokes shift that can be compared with standards or literature values. Targeted chemical analyses such as gas chromatography-mass spectrometry (GC-MS) can also be used to validate sample composition. Aside from environmental monitoring,

EEM-PARAFAC analysis has also been used in kinetic experiments to monitor the degradation of PAHs. Several studies have used EEM-PARAFAC to monitor PAHs undergoing photodegradation, Fenton oxidation, biodegradation, and combined treatment techniques. A summary of these studies is provided in Table III-1.

Varying success has been reported in identifying PARAFAC components. Often, components were reported as a collection of compounds, such as humic-like substances or amino acid-like substances. This is due in part to the complexity of the compound mixtures investigated in studies included in Table III-1. As the number of initial fluorescent compounds increases, so does the possibility of overlapping fluorescent spectra and similar degradation kinetics. Thus, it is more likely that the spectra of compounds will be modeled together as one component that will not match the spectrum of any one compound. Because fluorescent degradation products can be produced in these PAH degradation experiments, such compounds can also be represented in PARAFAC components, although few studies have made these observations. For example, in PAH photodegradation experiments, Seopela et al. identified a single fluoranthene photodegradation product, 2-(3,4)-dihydronaphthalene-1-yl acetic acid, with EEM-PARAFAC analysis, however remaining PARAFAC components were defined as unresolved photoproduct mixtures (Seopela et al., 2021a).

Table III-1. Compilation of literature investigating PAH degradation kinetics and using EEM-PARAFAC monitoring methods

Compounds Studied	Matrix	Treatment	Component Identification Method	Components Identified	Citation
naphthalene, anthracene, benzo(a)anthracence, benzo(a)pyrene, benzo(ghi)perylene	Water with NOM	Photo-degradation	Literature Comparison, GC-MS Validation	2-(3,4)-dihydronaphthalene-1-yl acetic acid, unresolved photoproduct mixtures	(Seopela et al., 2021a)
dibenz(a,h)anthracene, benz(a)anthrancence, benzo(a)pyrene, benzo(k)fluoranthene	Water/alcohol/solvent mixture	Photo-degradation	Standard Comparison	dibenz(a,h)anthracene, benz(a)anthrancence, benzo(a)pyrene, benzo(k)fluoranthene	(Bosco et al., 2006)
Benzo(a)pyrene, dibenz(a,h)anthracene, benzo(b)fluoranthene, benzo(k)fluoranthene, benz(a)anthracene	Methyl-β -cyclodextrin, acetic/acetate buffer solution	Fenton degradation	Standard Comparison	Benzo(a)pyrene, dibenz(a,h)anthracene, benzo(b)fluoranthene, benzo(k)fluoranthene, benz(a)anthracene	(Carabajal et al., 2017)
Diesel	Ultra-pure water/Tween 80	Electro-Fenton and Electrochemical degradation	Literature Comparison	Fluorene-like, naphthalene/methylnaphthalene-like, BTEX	(Liu et al., 2020)
PAH Mixture	Biochar amended sediment	Biodegradation	Literature Comparison	Tyrosine-like, tryptophan- and soluble microbial byproduct-like, fulvic-like, humic-like	(Hung et al., 2022a)
Crude oil	DI water/seawater Samples	Photo-degradation and biodegradation	GC-FID/GC-MS Validation	Oil-related, Natural DOM	(Zhou et al., 2013)
Complex Mixture	Coal mining wastewater	Fenton degradation, biodegradation, ozonation	Literature Comparison, GC-MS Validation	Humic-like, PAHs, organic acids, phenolic compounds, quinones, ketones	(Peng et al., 2018a)

Very few studies have applied an EEM-PARAFAC approach to monitor PAH biodegradation and identify biological transformation products. Those that have investigated biological transformation have been conducted using biostimulation or natural attenuation methods, rather than a bioaugmentation method with known microorganisms.

When cellular material is present in the samples, sample turbidity becomes a challenge in detecting fluorescent emissions. Various solutions have been proposed to account for the effect of sample turbidity on fluorescent emissions. Several mathematical models have been developed to model and correct the effects of turbidity on fluorescent measurements (Chen et al., 2013; Kanick et al., 2012; Wu et al., 1993), however in controlled situations where sample turbidity is consistent across samples, less extensive measures can be taken to account for interreferences. The inclusion of standard scans in data sets used to develop PARAFAC models has been demonstrated to aid in the quantification of target compounds (Elcoroaristizabel et al, 2014; Maggio et al., 2010), as it has been demonstrated that accuracy of quantitation is inversely related to the presence of interfering compounds (Ferretto et al., 2014).

Mycobacterium Sp. Strain ELW1 (ELW1) was the aerobic bacterium used in this investigation. ELW1 was isolated from stream sediment using isobutene as the sole carbon and energy source (Kottegoda et al., 2015b). ELW1's cometabolic potential has been probed for both chlorinated aliphatic hydrocarbons (Krippaehne 2018, Rich 2015) and phenanthrene (Schrlau et al., 2017). Previous work with ELW1 demonstrated the cometabolism of phenanthrene to a mixture of hydroxylated products, as identified by GC-MS analysis, but the full composition of the metabolite mixture was not resolved. The primary metabolite observed in this work was *trans*-9,10-dihydroxy-9,10-dihydrophenathrene (P1) (Schrlau et al., 2017). The objectives of this research were to compare an established targeted analytical method using solid phase extraction and GC-MS analysis to 2D fluorescent spectroscopy (2D) and EEM-PARAFAC methods to monitor, quantify, and derive kinetic parameters for phenanthrene degradation and P1 formation by ELW1.

2.0 Materials and Methods

2.1 Chemicals

A list of the purity and vendors of phenanthrene, seven hydroxylated phenanthrenes, and three isotope labeled PAHs is provided in Table S1. All solvents used in solid phase extraction and GC-MS analysis: methanol, dichloromethane,

acetone, ethyl acetate, acetonitrile, and toluene, were analytical grade purity and purchased from various vendors. Isobutene (99%), 1-octyne (98%) and the derivatizing agent *N*,*O*-Bis(trimethylsilyl)trifluoroacetamide (BSTFA) (>97%) were purchased from Sigma-Aldrich (Milwaukee, WI).

2.2 Experimental Set Up

ELW1 was provided by Dr. Michael Hyman from North Carolina State University and was grown on isobutene as the sole carbon and energy source. Detailed methods on cell culturing are provided in Appendix B. Cells were harvested during the late exponential growth phase for use in phenanthrene transformation studies. Resting cell transformation studies were performed in batch bottles prepared in baked Wheaton 500 mL media bottles (nominal volume 720 mL) with solvent washed butyl septa caps. All batch bottles were prepared in a laminar flow hood to maintain aseptic conditions.

Active bottles, prepared in triplicate, contained 300 mL of mineral salt media, 90 mg of isobutene grown ELW1 cells, and approximately 1 mg/L phenanthrene added from a concentrated methanol stock. Cells were added to active bottles after the initial liquid samples were taken. Enzyme inhibited bottles were prepared in duplicate as active bottles, but with 45 mg of cells and 1-octyne, a monooxygenase inhibitor, present to block the transformation of phenanthrene. 1-octyne was added from a 1 mM gaseous stock prepared according to (Taylor et al., 2013) at a 3.5% (v/v) headspace concentration. Both active and enzyme inhibited bottles were incubated at 30 ^{o}C on a 150 RPM shaker table for the 76-hour duration of the experiment.

Liquid samples were taken through the cap septa at set times throughout the experiment with a sterile glass syringe. 8 mL of liquid sample was removed at each sampling time, with 2.5 mL analyzed immediately with fluorescent spectroscopy. Cells were not removed from samples prior to fluorescent spectroscopic analysis. The remaining 5.5 mL sample was spiked with a labeled surrogate standard mix (Table B2) and extracted with solid phase extraction (SPE) with a previously published

extraction method (Schrlau et al. 2017) using Bond Elut Plexa (60 mg, 3 mL) cartridges (Agilent Technologies, New Castle, DE).

2.3 Targeted Analysis

Extracts analyzed for phenanthrene (PPAH samples) were nitrogen line dried to 225 µL in 300 µL autosampler vials. Seventy-five µL of an internal standard mixture (Table B3) was added to reach a final sample volume of 300 µL. Preparation of hydroxylated PAHs (OHPAHs) samples was carried out with a modified published method (Schrlau et al., 2017) . Briefly, 50 µL of prepared PPAH sample was added to a 300 µL spring insert containing 120 µL of a 5:1 acetonitrile: toluene solvent mixture. This mixture was dried under a nitrogen stream to 20 µL. 30 µL of BSTFA was then added as a derivatizing agent, and the sample was incubated at 60 ^{o}C for 25 minutes. PPAH and OHPAH samples were analyzed using an Agilent 6890 GC equipped with an Agilent DB-5ms (30m x 0.25 mm x 0.25 µm) capillary column coupled to an Agilent 5977A mass spectrometer detector with electron impact ionization operated in SIM mode. GC-MS instrument parameters are provided in Appendix B.

2.4 Fluorescent Spectroscopy

All samples were analyzed with a Varian Cary Eclipse fluorescent spectrophotometer operated in emission (2D) or 3D mode. Samples were scanned in a 4-sided quartz cuvette. 2D scans were conducted with a λ_{ex} of 250 nm and 270 nm, optimized for phenanthrene and P1 respectively, for a λ_{em} range of 300 nm to 450 nm. EEMs were collected for an λ_{ex} range of 200 nm to 300 nm with a 10 nm increment and an emission wavelength range of 300 nm to 600 nm with a 1 nm increment. Excitation and emission slit widths were each 5 nm, and the scan rate was 600 nm/minute, resulting in a 3D scan time of 5 minutes per sample. It should be noted that the scan time was very short in comparison to the rate of reaction observed, therefore changes in sample composition during scanning were considered negligible. The instrument was zeroed with a deionized water blank in between scans.

2.5 PARAFAC Model Development

PARAFAC models were developed using the drEEM v0.6.2 MATLAB toolbox developed by Murphy et al. (Murphy et al., 2013). The data set used to develop the final PARAFAC models consisted of an experimental data set that included EEMs from active triplicates (n=24) and enzyme inhibited controls (n=16), and a calibration data set that included EEMs for phenanthrene standards (n=18) and P1 standards (n =15). Additional PARAFAC models were developed without the calibration data set to assess the influence of the calibration set on model output. A convergence constraint of 10^{-6} for relative change of fit was used to develop all models.

2.5.1 Data Pre-Processing

First order Raman scattering was corrected by subtracting a matrix blank spectrum from each sample's spectrum. First and second order Rayleigh scattering was corrected by excision of scattering within tolerances defined in the drEEM toolbox. Scattering was replaced with missing values (NaN), rather than zeros, as it has been demonstrated that the inclusion of zeros can negatively impact the tri-linearity of the data set (Anderson and Bro 2003). No other adjustments were made to the EEMs. A non-negativity constraint was applied when generating PARAFAC models, as negative values in spectroscopy do not have physical meaning. The data set was inspected for outliers by identifying samples with excessively high leverages and removing them from the data set before it was read into the drEEM toolbox.

2.5.2 Model Component Determination

Several metrics can be used to determine the appropriate number of PARAFAC components for a given data set. First, visual inspection of the components' excitation and emission loadings can be used to identify components resembling noise rather than fluorescent compounds. Three numerical metrics, sum of squared error (SSE), percent explained, and core consistency, are reported by the

drEEM toolbox for each model. While SSE is ideally minimized and the latter metrics are ideally maximized by the proper number of components, analyzing the trends of these metrics as the number of components used increases also provides valuable information. Diminishing returns on percent explained and SSE reduction as components are added to the model can indicate that the appropriate number of components has been exceeded (Stedmon and Markager, 2005). Similarly, a steep decline in core consistency as components are added to the model can also indicate overfitting (Bro and Kiers, 2003). These trends, rather than the values of these metrics exclusively, can inform the appropriate number of components for the model.

2.5.3 Model Validation

The PARAFAC model was validated mathematically with split-half analysis, as it is a common validation tool used for PARAFAC models and the tool of choice for the drEEM toolbox developers (Murphy et al., 2013). Details of the split-half analysis are provided in Appendix B. When possible, comparisons between PARAFAC component Stokes shift and spectra and those of standard scans and literature values were used to further validate the model and identify compounds that corresponded to the PARAFAC components.

2.6 Fluorescent Target Quantification

Standards of phenanthrene and P1 were prepared in mineral salt media and scanned as described in Section 2.5. ELW1 cells were added to the appropriate concentration corresponding with active or inhibited bottles immediately before scanning each standard to accommodate the influence of turbid media on instrument response. Standard curves with varying concentrations of ELW1 cells were produced from 2D scans as shown in Figure S1 and were used to correlate 2D maximum fluorescent emission (F_{max}) measurements with target concentrations. 3D scans of these standards, referred to as the calibration data set, were included with the experimental data set in the development of PARAFAC models. The F_{max} of PARAFAC components corresponding to phenanthrene or P1 were used to develop

standard curves shown in Figure S1. Estimated method detection limits (MDLs) for 2D and EEM-PARAFAC methods were derived by dividing the standard deviation of the lowest standard by the slope of the calibration curve (Elcoroaristizabal et al., 2014) and are reported in Table B4.

2.7 Kinetic Models

Pseudo-first order models for phenanthrene degradation and P1 formation were fit to quantitated phenanthrene measurements. Cometabolism generally follows pseudo-first order kinetics, as supported by previous PAH cometabolism monitoring studies (Barret et al., 2010; Brimo et al., 2016). Phenanthrene degradation was modeled using the first order kinetic equation $C_{PAH} = C_o exp(-k_{PAH}t)$ where C_{PAH} is the concentration of phenanthrene (mg/L) at time t (hour), C_o is the initial phenanthrene concentration (mg/L), and k_{PAH} is the first order phenanthrene degradation rate constant ($hour^{-1}$). Rate of product formation constants was modeled with the following equation: $C_{P1} = C_o F(1-exp(-k_{P1}t))$ where C_{P1} is P1 concentration (mg/L) at time t (hours), C_o is the initial phenanthrene concentration (mg/L), F is the fraction of phenanthrene transformed into P1 (-), and k_{P1} is the P1 first order formation rate constant ($hour^{-1}$). MATLAB's "fitlm" and "coefCI" functions were used to generate pseudo-first order models and confidence intervals.

3.0 Results and Discussion

3.1 GC-MS

The degradation of phenanthrene and formation of one di-hydroxylated metabolite, P1, and 3 mono-hydroxylated metabolites: 1-, 4-, and 9-hydroxyphenanthrene were quantified with GC-MS, as shown in Figure B2. Phenanthrene degradation and formation of hydroxylated metabolites agreed well with the initial study of phenanthrene degradation by ELW1 (Schrlau et al., 2017). 3-hydroxyphenanthrene and 1,9-dihydroxyphenanthrene, however, were not detected above background in active samples as they were in the former study. This may be due to lower sensitivity of the GC-MS instrument used in the present study, as they

were measured in very low concentrations previously (<70 µg/L). Recoveries of phenanthrene and the hydroxylated metabolites, estimated by the recovery of the labelled surrogate compounds, were 43.2 ± 10.1 and 53.7 ± 16.7 percent, respectively.

Minor degradation of phenanthrene and accumulation of phenanthrene metabolites was observed in the 1-octyne controls, indicating that near, but not complete, inhibition was achieved. Approximately 58% of the total mass of initial phenanthrene was accounted for with the GC-MS quantified metabolites on a molar basis, demonstrating that the composition of the metabolite mixture was not fully characterized with this method. P1 and mono-hydroxylated metabolites accounted for approximately 96% and 4% of the total metabolite mass, respectively.

3.2 Fluorescent Spectroscopy

EEMs and 2D scans collected from active samples revealed a shift in fluorescent spectra over time, providing qualitative information on reaction progress, as shown in Figure III-1.

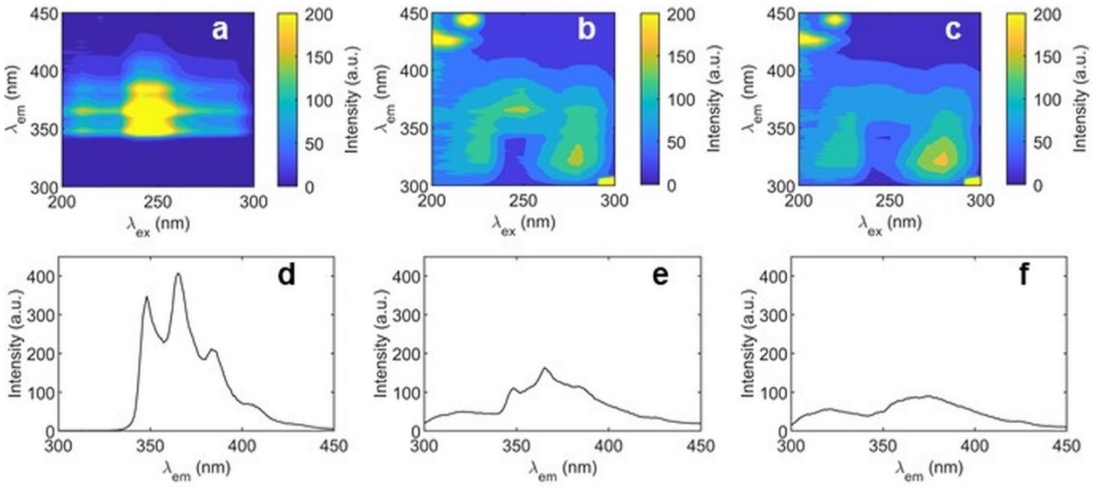

Fig. III-1 EEMs and 2D fluorescent scans (λ_{ex} = 250 nm) from an active bottle after 0 (a, d), 12 (b, e), and 28 (c, f) hours of incubation with phenanthrene

Spectra did not change significantly after 28 hours of incubation, indicating that most of the transformation occurred in the first 28 hours of incubation with the cells. Furthermore, minor changes to spectra after this time indicated the accumulation of a fluorescent metabolite.

3.2.1 PARAFAC Model Development

EEMs used to generate the PARAFAC models were reduced to a λ_{em} range of 300 nm to 450 nm, as the 450 nm to 600 nm range did not include signals above background for experimental samples and standard scans. PARAFAC models with 3 to 7 components were developed with the experimental and calibration data set and compared for over- or underfitting using visual inspection of the component emission spectra, percent explained, core consistency, and SSE. A summary of the latter three metrics is provided in Table B5. A 5-component model was determined to be the most appropriate model based on these criteria, with 98.41% explained and 87.60% core consistency. This model was validated with split-half analysis, details of which are provided in Appendix B.

3.2.2 Component Identification

Comparisons of the modeled component EEMs as well as their Stokes shifts were compared to standard scans of phenanthrene, phenanthrene metabolites, and controls to identify what compound(s) were represented by each component, as shown in Figure III-2. Component 1 (C1) was identified to be phenanthrene, and component 5 (C5) was identified as P1. Components 2 (C2) and 3 (C3) originated from the ELW1 cells present in the samples, with C2 matching literature values for the Stokes shift of the amino acid tryptophan (Hu et al., 2021; Hung et al., 2022a).

Component 4 (C4) was unable to be identified and may represent more than one compound. Comparisons to standard scans of what was identified by GC-MS eliminated mono-hydroxylated phenanthrene products as the source of this component. However, the total composition of the metabolite mixture produced by ELW1 is not resolved, as evidenced by the unknown metabolites identified in the

previous study and incomplete mass balance in the present study. These compounds, or other unknowns, may be contributing to C4.

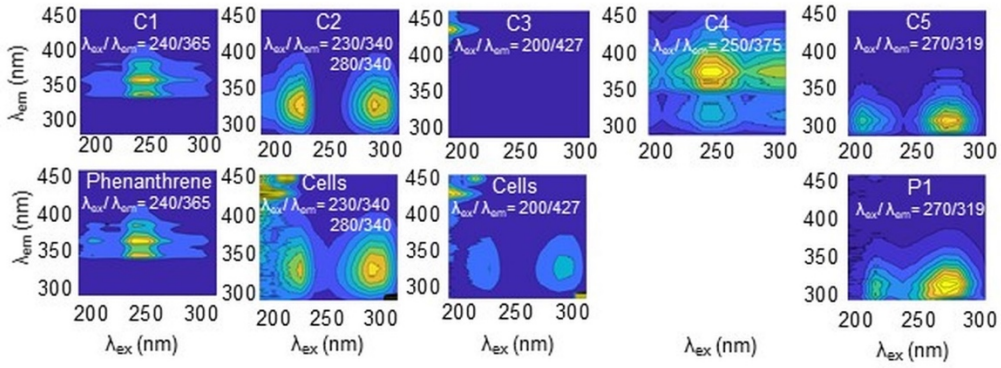

Fig. III-2 Comparison of PARAFAC components' EEMs (top row) to standard EEMs (bottom row). Fluorescent intensities of EEMs shown are arbitrary and only reflect trends in intensity as excitation wavelength changes. Text in EEMs represent Stokes shift associated with components and standards

Further investigation of the composition of components was carried out by considering their temporal variation. F_{max} values were plotted against the time of sample collection to discern temporal trends in component abundance, shown in Figure III-3.

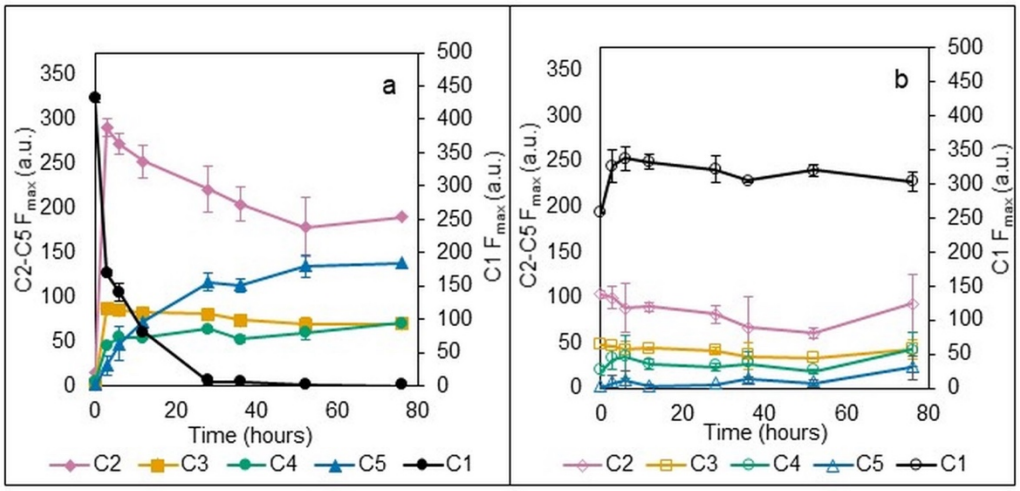

Fig. III-3 Temporal variation of PARAFAC components for active (a) and inhibited (b) bottles. Error bars represent standard deviation among triplicates in (a) and range between duplicates in (b)

The trends of reduction of C1 and production of the C5 mirror the degradation of phenanthrene and formation of P1 over time. The association of C2 and C3 with the ELW1 cells present in the sample is supported by their presence in active samples with minor temporal variation and inhibited samples with no discernable temporal variation. Additionally, these components were absent in the initial samples of active bottles that were taken prior to cell addition. The same was observed with C4, indicating that C4 may be representative of cellular material as well, rather than exclusively metabolites.

C4's Stokes shift was compared to that of common fluorophores associated with biological material reported in the literature. Fluorophores associated with cellular respiration, NADH and FAD, absorb and emit longer wavelengths of light that fall outside the scan parameters of this study (Gröning et al., 2014; Mayevsky and Rogatsky, 2007). Stokes shifts associated with the fluorescent amino acids tyrosine and phenylalanine (Hu et al., 2021) and fulvic and humic material (Alberts and Takács, 2004; Hung et al., 2022; Peng et al., 2018) do fall within the measured experimental range of λ_{ex} and λ_{em}, but do not match the Stokes shift of C4. Low amounts of C5 in inhibited controls compared to active samples support that these compounds are associated with the biological transformation of phenanthrene by ELW1.

A second PARAFAC model was generated without the calibration data set to test the influence of the calibration data on the components and model fit. As before, 5 components were needed to model the data set, and the spectra of the components were nearly identical to the model generated with the calibration data set included, indicating that the PARAFAC model could extract the pure spectra for phenanthrene and P1 without the inclusion of standards. Details of this model are provided in Figure B4.

3.2.3 Target Quantification

An inverse relationship was found for sample turbidity and sensitivity of the analysis, thus the more turbid the sample, the less sensitive the analysis. While a

significant improvement in MDL was observed for EEM-PARAFAC compared to 2D fluorescence, the EEM-PARAFAC MDLs were one to two orders of magnitude higher than the GC-MS method (Table B4). The loss of sensitivity with cell addition is likely due to fluorescent quenching from the cellular material, a phenomenon in which fluorescent emissions are reduced due to mechanisms such as absorption by other molecules (Lakowicz et al., 2002). Because of the high turbidity of samples in this study, the inclusion of interfering compounds, in this case cellular material, was critical to achieving accurate quantitation of the target compounds. Linear regression constants and goodness of fit for each standard curve developed are reported in Figure B1.

Phenanthrene and P1 quantitation by EEM-PARAFAC generally matched GC-MS quantitation within one standard deviation, as shown in Figure III-4, indicating that the impact of turbidity could be accounted for with the standard curve adjustment. Phenanthrene measurements in the 1-octyne controls matched the GC-MS results within one standard deviation as well, with more consistent measurements observed in EEM-PARAFAC samples compared to the GC-MS samples. P1 in 1-octyne controls was not measured by either fluorescent method, suggesting that concentrations may have been below the limits of detection of the fluorescent methods.

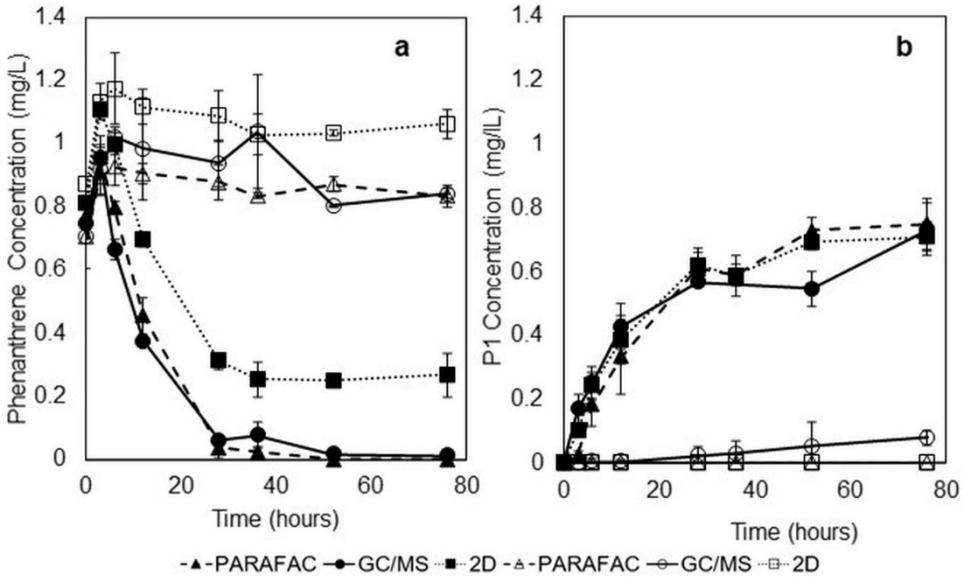

Fig. III-4 Comparison of phenanthrene (a) and trans-9,10-dihydroxy-9,10-dihydrophenathrene (b) quantitation for GC-MS (circle), EEM-PARAFAC (triangle), and 2D fluorescent spectroscopy (squares) methods. Error bars represent standard deviation among triplicates for active bottles (filled markers) and duplicates for inhibited bottles (open markers)

Results from 2D fluorescent scans on active and inhibited samples elucidate the benefits of PARAFAC modeling for fluorophore mixtures. Phenanthrene quantitation was overestimated in the first 12 hours of the experiment to a higher degree than the PARAFAC quantitation for active samples and appeared to reach an asymptote starting at hour 28. This asymptote is likely the resulting fluorescent signal of the other fluorophores in the mixture, such as the P1, that were in higher concentrations than phenanthrene at that time in the experiment. This is supported by the change in the shape of the fluorescent spectra observed in the 2D scans starting at 28 hours, as seen in Figure B6. 2D quantitation of phenanthrene in the 1-octyne controls generally fell within one standard deviation of GC-MS results, however these measurements were consistently higher than EEM-PARAFAC measurements. Quantitation of P1 was statistically indistinguishable to the quantitation with the EEM-PARAFAC method, and therefore is subject to the same comparison to GC-MS as described previously.

3.3 Kinetics

Phenanthrene transformation and P1 formation both followed first-order kinetics well, as shown in Figure III-5. The pseudo-first order rate constants for phenanthrene degradation and P1 formation derived from quantitated GC-MS data and PARAFAC C1 data have no statistically significant difference, demonstrating that the EEM-PARAFAC method provided comparable kinetic information to the GC-MS method. The initial measurement of phenanthrene was omitted from the model, as phenanthrene was not fully dissolved at this time.

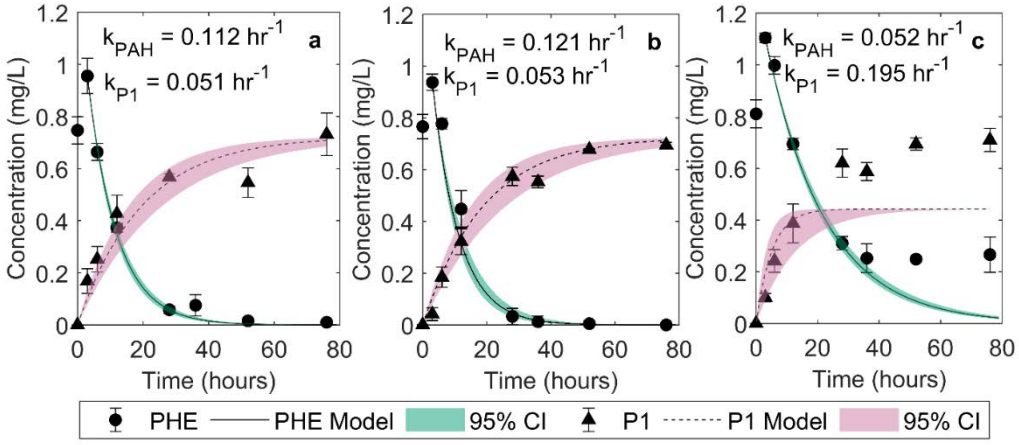

Fig. III-5 Comparison of empirical and modeled concentrations of phenanthrene and P1 derived from GC-MS (a), EEM-PARAFAC (b) and 2D fluorescent methods

This result was expected based on the good agreement of phenanthrene quantification shown in Figure III-3. Similarly, because of the poor agreement between 2D fluorescent sample phenanthrene quantitation and the other two methods, the model fit of phenanthrene degradation derived from the 2D fluorescent quantitation did not fit empirical measurements well, nor did the rate constant compared to that derived from the alternative methods. The rate of P1 formation is also significantly different than what was derived with the other methods, however, it is faster. This is due to the asymptote reached in 2D quantitated phenanthrene data, which inaccurately indicated that significantly less phenanthrene was transformed compared to what was indicated by EEM-PARAFAC or GC-MS data.

Thus, the fraction of phenanthrene transformed that was accounted for as P1 was impacted, leading to the appearance of faster product formation kinetics. This

further demonstrates the limitations of techniques such as the 2D fluorescent method that does not include separation techniques before or after analysis. Linear regions used, rate constants and goodness of fit are reported in Figure B7.

4.0 Conclusions

The method developed in this research is a rapid analytical technique that forgoes extensive sample preparation and separation techniques to monitor phenanthrene biodegradation and product formation that is comparable to an established method relying on solid-phase extraction, chromatographic separation, and mass spectrometry. The value of three-dimensional fluorescent spectroscopy paired with parallel factor analysis (EEM-PARAFAC) was demonstrated in the superiority of sensitivity and accuracy in quantification to two-dimensional fluorescent spectroscopy. A five component PARAFAC model appropriately modeled the experimental data with and without additional calibration data, from which four components were identified: phenanthrene, *trans*-9,10-dihydroxy-9,10-dihydrophenanthrene, one tryptophan-like cellular material, and one general cellular material. The unidentified component likely represents a mixture of compounds that are of cellular material origin, however based on the incomplete mass balance it is possible that unidentified phenanthrene metabolites are also associated with this component. The interference of the cellular material in the samples was accounted for with the use of standards prepared with corresponding cellular interference that were included in the PARAFAC model.

While the inclusion of standards in developing the PARAFAC models was not necessary to identify the components, it was necessary quantify the compounds of interest. Individual compounds were able to be identified with the EEM-PARAFAC method due in part to this being a single compound study. It should be noted that the complexity of component identification and quantification reflects the complexity of the initial contaminant(s) present in a study, limiting the application of this method for quantitative applications.

Quantification of targets and the development of pseudo-first order models using the EEM-PARAFAC method were validated with the established GC-MS

method. Sensitivity was enhanced with the use of the EEM-PARAFAC method compared to the 2D fluorescent method, however, it was still one to two orders of magnitude higher than the GC-MS method, highlighting the tradeoff between ease and speed of sample analysis and sensitivity of analysis. Greater sensitivity can be achieved in the EEM-PARAFAC method with additional sample preparation steps to remove cells and thus reduce sample turbidity. However, any sample preparation steps can result in losses of compounds of interest due to phenomena such as volatilization or adsorption to materials that can be difficult to account for in quantitative analyses.

The advantages of the EEM-PARAFAC method do not lie in its sensitivity, but rather in its ease and rapidity, allowing for real time monitoring of biological PAH transformation with no sample preparation steps required. To the authors' knowledge, this is the first study to use an EEM-PARAFAC method to monitor, identify, and quantify both PAH biodegradation and PAH metabolite formation by a bacterial pure culture.

5.0 Acknowledgements

The authors wish to thank Dr. Michael Hyman for providing the ELW1 pure culture, Jason Schindler for support in GC-MS sample preparation and analyses, and Dr. Mohammad Azizian for support in fluorescent spectroscopy analyses. Research reported in this publication was supported by the National Institute of Environmental Health Sciences of the National Institutes of Health under
Award Number P42ES016465. The content is solely the responsibility of the authors and does not necessarily represent the official views of the National Institutes of Health.

CHAPTER IV

Monitoring PAH Dose and Uptake Kinetics in Embryonic Zebrafish Using Fluorescent Spectroscopy

Juliana Huizenga[a] (ORCID: 0000-0002-1242-0948) huizengj@oregonstate.edu
Lisa Truong[b] (ORCID: 0000-0003-1751-4617) lisa.truong@oregonstate.edu
Lewis Semprini[a] (ORCID: 0000-0002-9174-4464) lewis.semprini@oregonstate.edu

[a] Oregon State University, School of Chemical, Biological, and Environmental Engineering
[b] Oregon State University, Department of Environmental and Molecular Toxicology

Chapter IV: Monitoring PAH Dose and Uptake Kinetics in Embryonic Zebrafish Using Fluorescent Spectroscopy

Abstract

Embryonic zebrafish (*Danio rerio*) have many qualities that make them excellent candidates for high-throughput toxicity assays and have been used extensively for screening chemicals for toxicity impacts that manifest as abnormal phenotypes, behavior, or mortality. However, knowledge of the chemical uptake in embryonic zebrafish is often minimal, as such assays are limited by the amount of material that can be sampled for chemical analyses. Typical studies of the pharmacokinetics of chemicals at this life stage require extensive sample preparation and sensitive instruments to quantify and model chemical uptake by the embryos. In this study, a fluorescent spectroscopy method was developed for monitoring the aqueous concentrations of two environmentally relevant toxicants, 2-hydroxynaphthalene and acridine, in a high-throughput (96-well plate) embryonic zebrafish toxicity assay. It was demonstrated that zebrafish embryos are tolerant to daily measurements with a fluorescent plate reader, and that background fluorescence is not impacted by normal embryo development from 6 to 120 hours post-fertilization. Abnormal embryo development, however, was found to impact background fluorescence by creating sharp peaks in background fluorescent intensity. The decreases in PAH concentrations over time were attributed to combined losses of sorption, photodegradation, and biotic uptake, models of which fit well with empirical measurements. Chemical dose, uptake rate, and abiotic loss rates were all derived from fluorescent measurements. Unexpected cranial deformities were observed in this study, suggesting further investigation of potential additive toxicity of the UV exposure from plate reader measurements and chemical exposure is needed. Nonetheless, this method provides a rapid, non-destructive tool for assessing uptake and dose of chemicals in embryonic zebrafish that can accommodate any autofluorescent chemicals of interest.

1.0 Introduction

Zebrafish (*Danio rerio*) embryos are among the top choices of model organisms for toxicity screening (Bugel et al., 2014; Li et al., 2023). Zebrafish have a high degree of homology to humans in relevant aspects such as genetics and physiology, which has positioned them as the standard experimental fish by the Organization for Economic Cooperation and Development (OECD) (Li et al., 2023; Dubey et al. 2022). Furthermore, their rapid development, small size, and transparency has made it possible to adapt zebrafish screening to high-throughput formats (Truong et al., 2016). Although toxicity assessments can be done with embryonic, larval, or adult zebrafish, embryonic zebrafish assays have the advantage of the developmental life stage, during which disturbances to the cell signaling involved in cell proliferation and differentiation can manifest as distinct phenotypes (Truong et al., 2011). In addition, embryonic zebrafish assays can be carried out in a 96-well microplate with very small embryo media (EM) volumes and chemical doses, which aid in the assay rapidity but hinder the ability to monitor the concentration of the chemical of interest.

The most common method for toxicant exposure in embryonic zebrafish assays is immersion, where the embryos reside in media that is dosed with a certain concentration of chemical (Guarin et al., 2021b). Chemical dose to the zebrafish embryos is typically reported as this nominal water concentration, however the nominal concentration is an overestimate of the actual dose to the zebrafish embryos (Geier et al., 2018; Knecht et al., 2013). Zebrafish embryos do not have gill function and exclusively feed on their yolk sac until ~5 days post fertilization (dpf), therefore exposure routes for chemical exposure occurring 0-5 dpf relies on dermal exposure, or diffusion into the yolk sac and subsequent ingestion (Sipes et al., 2011).

Thus, the uptake of chemicals is heavily dependent on its physicochemical properties and can lead to a large discrepancy between exposure and dose concentrations that is difficult to estimate. Furthermore, small embryo sizes, aqueous volumes, and chemical concentrations limit in the ability to measure chemical concentrations in EM and embryos that would inform the pharmacokinetics of toxicant exposures. Studies that investigate pharmacokinetics in zebrafish embryos typically rely on sacrificial samples in which embryos are dissected, extracted, and

analyzed with combinations of chromatographic separation and detection (Brox et al., 2016; El-Amrani et al., 2013; Halbach et al., 2020).

Aside from whole body digestion and molecular techniques, fluorescent spectroscopy is a popular, non-destructive tool used in embryonic zebrafish screening, as zebrafish embryos are translucent and therefore contribute little disruption to fluorescent signals (Ko et al., 2011; Lubin et al., 2021). A suite of fluorescent dyes and probes have been developed and used to target specific organs and enzymes in embryos (Bugel et al., 2014; Ko et al., 2011; Patton and Zon, 2001). However, the target for fluorescent spectroscopy in embryonic zebrafish assays is rarely the chemical itself, despite many relevant environmental contaminants exhibiting autofluorescent properties.

Furthermore, previous research has exclusively focused on measuring concentrations of a given toxicant in the embryonic body. For example, Guarin et al. (2021a) used 7 fluorescent dyes to investigate the impact of physicochemical properties on uptake of these compounds in zebrafish, however these dyes are not toxic or environmentally relevant. In this study, a rapid method is presented for studying the uptake of two environmentally relevant polycyclic aromatic compounds, 2-hydroxynapthalene (2-OHNAP), and acridine, using microwell media concentrations measured with a fluorescent plate reader. Additionally, the impact of fluorescent spectroscopy measurements on zebrafish embryo viability and background autofluorescence of developing embryos was investigated.

2.0 Materials and Methods

2.1 Chemicals

Acridine (99.6%) (CAS: 260-94-6) and 2-hydroxynapthalene (99.7%) (CAS: 135-19-3) and dimethyl sulfoxide (DMSO) (CAS: 67-68-5) (99.5%) were purchased from Sigma Aldrich (St. Louis, MO). Acridine and 2-hydroxynaphthalene stocks were prepared in DMSO at a concentration of 10 mM for use in zebrafish studies.

2.2 Zebrafish Husbandry

Tropical 5D wild-type zebrafish were maintained at the Sinnhuber Aquatic Research Laboratory under previously described conditions (Shankar et al., 2019). Fertilized embryos were collected at ~4 hpf and enzymatically dechorionated (Mandrell et al., 2012). One dechorionated embryo per well was hand-pipetted at ~6 hpf. Plates were placed on a 250 RPM shaker for the first 24 hours of incubation, and then transferred to a stable shelf for the remainder of the experiment. Plates were kept in a dark 30 ^{o}C room for the duration of the experiment, removed only for fluorescent measurements and morphology screening. Following the 5-day incubation period, animals were assessed for mortality and 8 developmental endpoints pertaining to: cranium (eye/snout/jaw), axis, edema (heart/yolk sac), swim bladder/somites, lower trunk/caudal fin, brain, skin, and notochord development described in Truong et al. (2011).

2.3 Fluorescent Plate Reader

All fluorescent spectroscopy methods were conducted with the BioTek Synergy Mx microplate reader in black-walled 96-well plates purchased from Life Technologies Corporation (Carlsbad, CA). All measurements were taken from the top of the plate with sensitivity and filter width settings of 75 and 20, respectively. The plate reader was validated for fluorescent measurements with the corners, sensitivity, and linearity tests per the operator manual. All measurements were corrected for Raman scattering by subtracting media blank measurements.

Detection methods for acridine and 2-OHNAP were developed for each compounds' specific Stokes shift; 350/429 and 270/355, respectively. Standard curves and method detection limits (MDLs) were determined according to EPA procedure 40 CFR 136 Appendix B. Because these measurements rely on the autofluorescence of the compounds, sensitivity is highly variable. Acridine was found to yield higher fluorescent emission intensity than 2-OHNAP, thus the MDL for acridine (452 nM) is an order of magnitude lower than that of 2-OHNAP (5 μM). However, the MDL for 2-OHNAP is still an order of magnitude lower than the initial

concentrations used in exposure tests, therefore its low sensitivity does not impede accurate measurements in exposure tests. The coefficient of determination for calibration curves of both compounds exceeded 0.99.

2.4 Abiotic Loss Experiments

PAHs are known to undergo photodegradation with exposure to UV light (Fasnacht and Blough, 2002; Nadal et al., 2006). Photodegradation experiments were carried out with the plate reader methods used in the PAH exposure experiment to determine the contribution of photodegradation to the overall abiotic losses. Experimental wells containing 100 µL of ~35 µM of 2-OHNAP or acridine were prepared in the 96-well plates, along with control wells containing 100 µL EM. Fluorescent measurements were taken in rapid succession, approximately one minute apart, to minimize the impacts of sorption of the chemicals to the well walls. Thus, the PAH losses observed with each subsequent measurement was assumed to be due to photodegradation.

PAHs are also known to adsorb to the well walls of 96-well plates due to their hydrophobicity. Chlebowski et al. (2016) investigated the adsorption losses of a suite of PAHs and nitrogen containing PAHs with polystyrene 96-well plates and reported losses up to 43% due to sorption. Acridine and 2-OHNAP have estimated k_{oc} values of 12910 and 390, respectively. Therefore, sorption losses were expected in the PAH exposure studies, particularly for acridine. To determine the impact of agitation on adsorption of the chemicals, a set of microplates were prepared as with experimental wells containing 100 µL of ~35 µM of 2-OHNAP and control wells containing 100 µL EM. Plates were measured for initial PAH concentrations with the fluorescent plate reader before being sealed with parafilm and allowed to equilibrate for 24 hours either on a 225 RPM shaker table or on a stagnant shelf in the dark. After 24 hours, plates were measured again with the fluorescent plate reader.

2.5 Exposure Tests

2.5.1 UV Only Exposure Test

The measurement wavelengths used for the compounds specific methods fall in the UVA and UVC range, which are potentially damaging to zebrafish embryos (Dong et al., 2007). However, the exposure to UV radiation is very brief (approximately 100 μs), thus it was important to determine if the UV radiation doses the embryos received were lethal or disrupted development. Zebrafish embryos were incubated in microplates with 100 μL EM per well, and one plate per measurement method. Embryos were divided into 7 groups with n=10 embryos per group. The control group (group 7) were not exposed to UV, while groups 1-6 received one UV dose/day for 1-6 days, with group number corresponding to number of days the embryos were dosed. A microwell map for this experiment is provided in Figure C1. Mortality and morphological defects were assessed at ~120 hours post-fertilization (hpf).

2.5.2 PAH Exposure Test

Duplicate 96-well microplates were prepared for PAH exposure tests, with all wells containing 100 μL of liquid volume. The target initial concentration of 2-OHNAP and acridine was 35 μM, the lowest observed adverse effect level (LOAEL) reported in a previous study (Geier et al., 2018). A combination of spectroscopy and toxicity controls were present on the plates along with the experimental zebrafish groups. A summary of these well groups is shown in Table IV-1. Aqueous solutions were hand-pipetted into microwells, and initial PAH measurements were taken with the plate reader before embryos were added. Embryos were then added to plates via hand-pipetting. Embryos were checked under a microscope for any anomalies before plates were measured again with the plate reader. Plates were sealed with parafilm in between plate reader measurements; however, these covers were temporarily removed for plate reader measurements each day. Plates were placed on a 225 RPM shaker table for the first 24 hours of the experiment, and then removed and stored on a stagnant shelf for the remainder of the experiment.

Table IV-1. Control and experimental well groups in PAH exposure test. Bolded groups were prepared as two sets, one for 2-OHNAP and one for acridine. Group name indicated if zebrafish embryos are present (Z) and if wells were measured with the plate reader (UV). A well map showing the organization of these groups on the plates is provided in Figure C3.

Group	Zebrafish Present	Fluorescent Measurement	Chemical Addition (in 100 µL EM)	n/plate
+ Control/Z	Y	N	25 µM Parathion	8
- Control/Z	Y	N	N/A	8
UV/Z	Y	Y	N/A	8
PAH/UV/Z	Y	Y	35 µM PAH	16
PAH/UV	N	Y	35 µM PAH	8
Media/UV	N	Y	N/A	8

Positive and negative control groups served as toxicity controls for embryo responses and were not measured with the plate reader. Parathion was selected as the chemical for the positive control group as standard for this experiment (Gosline et al., 2023). UV/Z groups were used to assess the effect of UV exposure on the embryos. PAH/UV/Z groups monitored changes in aqueous PAH concentrations due to embryo development, while PAH/UV groups monitored abiotic losses of PAHs. Media/UV groups served as spectroscopic controls for background fluorescence. Fluorescent measurements were collected before and after zebrafish embryos were added to the appropriate wells, followed by daily measurements for the 5-day incubation period. At ~120 hpf, zebrafish embryos were assessed for mortality and morphological abnormalities.

2.6 Data Analysis and Modeling

Statistical significance was determined with one-way ANOVA and Fisher's LSD test carried out in MATLAB.

A pseudo-first order model for the aqueous PAH concentrations over the course of the PAH exposure tests. Net uptake by zebrafish embryos, adsorption to the microwells, and photodegradation were considered in the development of the model. Volatilization of the compounds was assumed to be negligible based on their Henry's coefficients; 4E-07 atm-m^3/mol and 2.7E-08 atm-m^3/mol for acridine and 2-hydroxynapthalene, respectively. Thus, the pseudo-first order model can be described with the following equation:

$$[1] \quad C(t) = Ci*\exp(-(k_{photo} + k_{sorption} + k_{uptake})*t)$$

where C is the concentration of the PAH in the aqueous phase (μM), C_i is the initial aqueous PAH concentration (μM), $k_{sorption}$ is the rate of PAH sorption to well walls, k_{uptake} is the rate of PAH net uptake into the zebrafish embryos, and k_{photo} is the rate of PAH photodegradation. All rate constants have units of inverse hours, and were derived sequentially (k_{photo}, $k_{sorption}$, k_{uptake}).

Photodegradation rate was derived from photodegradation experiments described in section 2.4.3. Because the timeline of this experiment did not match the timeline of the PAH exposure test, the photodegradation rate was derived first as a function of the number of measurements taken. This rate was then converted to inverse hours with the ratio of measurements per hour; one measurement per 24 hours to match the daily measurement strategy in the PAH exposure test. Sorption and uptake loss rates were assumed to be negligible due to the short timescale of the experiment and absence of zebrafish embryos in the wells. Therefore, equation 1 can was simplified to the following equation:

$$[2] \quad C(t) = Ci*\exp(-(k_{photo}*t)$$

Sorption rate was derived from the losses in the abiotic wells of the PAH exposure test. Uptake losses were assumed to be zero because of the absence of zebrafish embryos in the wells, simplifying equation 1 to equation 3:

$$[3] \quad C(t) = Ci*\exp(-(k_{photo} + k_{sorption})*t)$$

where k_{photo} is a known constant, leaving $k_{sorption}$ as the only unknown. Finally, k_{uptake} was derived with the data collected from zebrafish embryo-containing wells in the PAH exposure test and the known values for k_{photo} and $k_{sorption}$ in equation 1.

3.0 Results and Discussion

3.1 Abiotic Loss Experiments

Results from the abiotic loss experiments revealed that sorption was a major contributor to abiotic losses, whereas photodegradation was a minor contributor. Photodegradation of acridine and 2-OHNAP fit first-order kinetics reasonably well as shown in Figure IV-1A and B, with fit coefficients greater than 0.8 for both compounds.

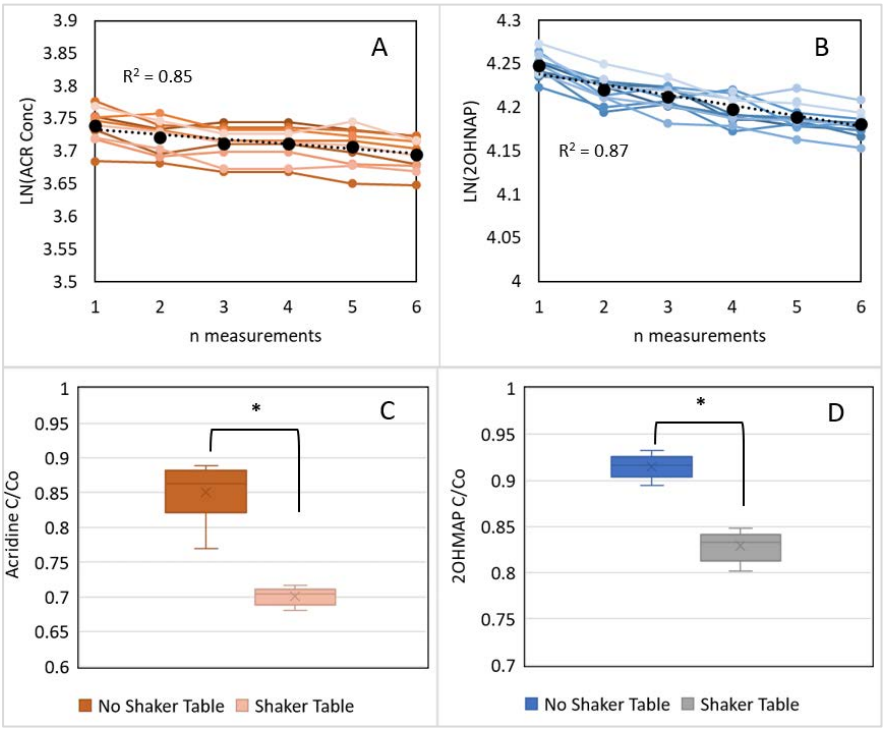

Figure IV-1. Abiotic losses from photodegradation (A, B) and sorption (C, D) for acridine (orange) and 2-OHNAP (blue). Linear regression of the average losses is shown in black in A and B. Sorption on and off the shaker table are compared as ratios of their initial concentration. Asterisks represent statistical significance with $p < 0.05$

As expected, the shaker table significantly impacted sorption losses, as shown in Figure IV-1C and D. Thus, it was necessary to consider the initial 24 hours on the shaker table when modeling data for the PAH exposure test.

3.2 UV Exposure Test

The UV exposure test produced three important findings. Primarily, the placement of zebrafish embryos resulted in a 13 ± 3 percent and 13 ± 7 percent decrease in fluorescent emission intensity for 2-OHNAP and acridine, respectively. This decrease is potentially due absorption of the excitation wavelength radiation by the embryo. However, after normalizing measurements to the initial fluorescence readings of the wells, it was observed that the development of viable embryos did not impact background fluorescence for the duration of the experiment. This is illustrated by the overlap in background fluorescence of media and embryo wells in Figure IV-2B and D.

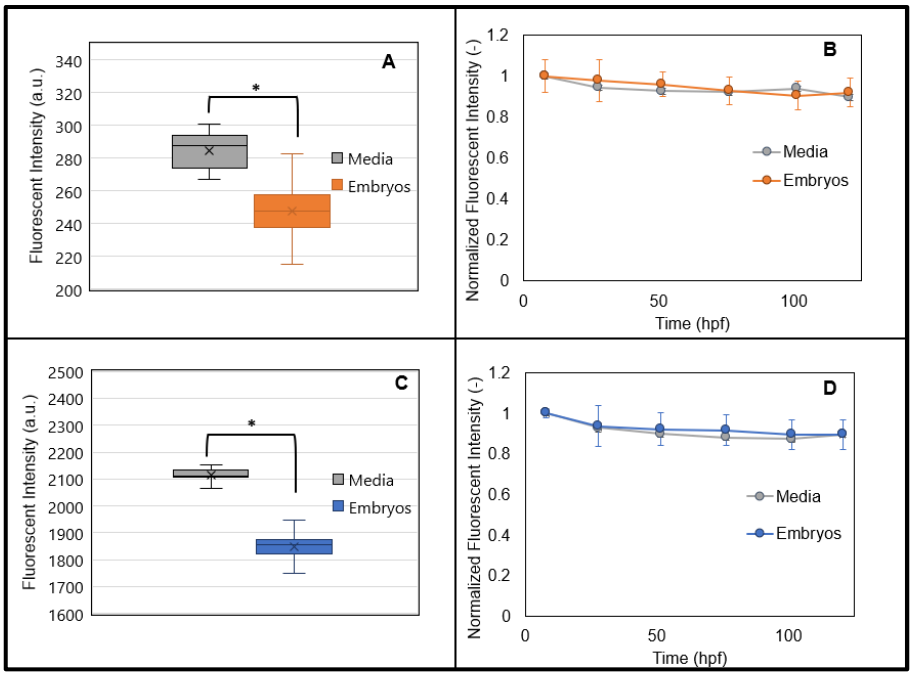

Fig. IV-2 Difference in initial fluorescent measurements for wells with and without embryos for acridine (A) and 2-OHNAP (C) methods, and changes in background fluorescence over time, normalized to initial measurements using acridine (B) and 2-OHNAP (D) methods. Asterisks represent statistical significance with $p < 0.05$

These results demonstrate that fluorescent measurements of acridine and 2-OHNAP are not obscured by the zebrafish embryos as they develop in the microwells. However, in order to account for the difference in background fluorescence shown in A and C, the matrix blank used for Raman scattering correction should match the

embryo presence in each well. Thus, a media control should be subtracted from wells that do not contain embryos, whereas a media control with an embryo should be subtracted from wells that contain embryos for the following PAH exposure study.

The second finding of importance from the UV exposure study was that embryo mortality and development was not significantly impacted by the acridine and 2-OHNAP measurement methods, as incidence of adverse effects for UV exposed embryos was not statistically significantly different than the control embryos that were not exposed to UV light, as reported in Tables C4 and C5. Therefore, the UV radiation dose the embryos received during their 5-day incubation did not lead to adverse health effects for the wavelengths used.

While there has been documentation of adverse outcomes for UV exposed zebrafish embryos, including mortality, developmental abnormalities, decreases in hatch rate, and increased inflammation, the UV doses in these studies are orders of magnitude higher than the doses received by embryos in the present study, which was estimated to be 6.1 mJ/cm^2 (Andrade et al., 2017; Dong et al., 2007; Wang et al., 2010). Banerjee and Leptin (2014) reported no significant difference in outcome for zebrafish embryos exposed to 6 mJ/cm^2, however these outcomes were reported for a single dose, whereas the present study entails 6 UV doses (one dose per day). Previous studies are limited to UVA/UVB radiation, the region in which the excitation wavelength of acridine resides. There is minimal research pertaining to UVC radiation exposures in zebrafish, the range in which the excitation wavelength for 2-OHNAP resides, presumably because UVC radiation is filtered out of sunlight by the atmosphere, and therefore has little environmental relevance (Tziortzioti, 2016).

The final compelling finding from the UV exposure study is that the death of zebrafish embryos, as well as cranial deformities, had a significant impact on the fluorescent emissions measured using acridine and 2-OHNAP methods. The incidence of these endpoints was no greater than 20% of the total number of zebrafish embryos, as reported in Tables C4 and C5. A sharp increase (>20% for 2-OHNAP and >100% for acridine) in fluorescent emission was observed in all embryos that developed cranial deformities or were not alive at the time of the 120 hpf screening,

as shown in Figure C2. The increase in fluorescence in the wells that contained dead or abnormal embryos may be due to cell/yolk sac lysis and release of fluorescent material into the aqueous phase. Similar reports of increased autofluorescence following cell death have been reported for a range of biological systems, including plant cells (Koga et al., 1988), human eosinophils (Stern et al., 1992), and indeed zebrafish embryos, where increased fluorescent emissions were attributed to lipofuscin-like autofluorescence (Yan et al., 2023).

These results indicate that measurements for the target compounds may be obscured by embryo death. Therefore, in the following PAH/UV experiments, sharp increases in fluorescence, defined as an inflection point in the first derivative of the measured PAH concentrations, were considered to indicate embryo abnormality. Subsequent measurements from those wells were removed from further data analysis. Criteria used to evaluate embryo mortality with the fluorescent data is provided in Appendix C. Embryo mortality predictions with fluorescent inflections were 90% and 97% accurate for 2-OHNAP and acridine, respectively (Table C6).

3.3 PAH Exposure Test

3.3.1 PAH Quantification

Although less than 0.5 hours separated initial measurements of the microplates before and after embryo addition, a significant decrease in PAH concentrations was measured in all PAH containing wells, shown in Figure C4. In control wells that did not receive an embryo, this difference amounted to 9.4 ± 1.5 percent loss in 2-OHNAP and 6.5 ± 0.7 percent loss in acridine, whereas the loss in wells that did receive an embryo was 31.4 ± 5.5 percent for 2-OHNAP and 18.7 ± 3 percent loss in acridine.

As discussed previously, background fluorescence decreased in wells after embryo addition in the UV exposure test, however this decrease was ~ 13% for both methods. Thus, the losses observed in the PAH exposure study cannot be fully attributed to absorbance of the excitation radiation by the embryos and abiotic losses of the chemical for 2-OHNAP, but this may account for the losses observed for wells

containing embryos exposed to acridine. This may indicate the potential for a significant influx of 2-OHNAP into the zebrafish embryos immediately upon exposure to 2-OHNAP.

An important factor to consider in the diffusion of the chemicals into the embryos is the proportion of the 2 main embryo compartments: embryonic body and yolk sac. The yolk sac comprises the majority of embryo volume and weight until approximately 48 hpf, at which point the embryotic body volume overtakes the yolk sac volume, followed by overtaking the dry weight at 72 hpf (Halbach et al., 2020). Diffusion into the yolk sac may be favorable to the PAHs due to its high lipid content compared to the embryonic body, therefore the prevalence of the yolk sac in the first 48 hpf may contribute to the prominent initial influx of PAHs into the embryos. Following the initial decrease in contaminant mass, contaminant concentrations continued to decrease over the 5-day incubation period, as illustrated in Figure IV-3.

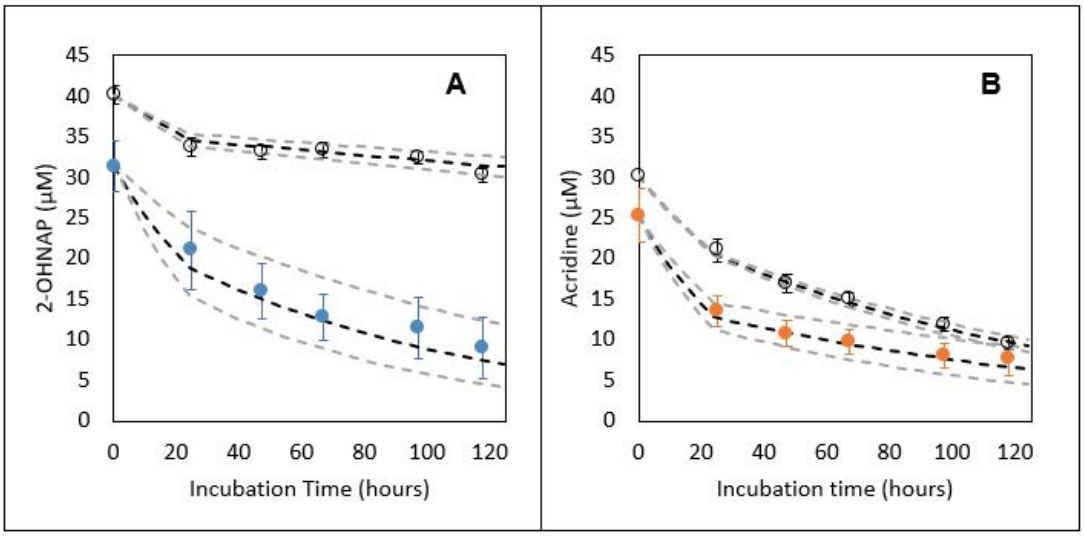

Fig. IV-3 Experimental data for wells containing zebrafish embryos (filled circles), control wells (open circles), and modeled concentrations (black dotted lines) for 2-OHNAP (A) and acridine (B). Standard deviations of modeled concentrations are shown in grey dotted lines

Although chemical concentrations decreased in controls for both PAHs in the first 24 hours, 2-OHNAP control concentrations stabilized after 24 hours of incubation, whereas acridine control concentrations continued to decline. Agitation of the plates on the shaker table played a significant role in the movement of PAHs, as has been well documented, thus rates of sorption and uptake in the first 24 hours of

incubation were significantly higher than those after 24 hours. Furthermore, acridine is expected to adsorb to the well walls to a greater extent than 2-OHNAP due to its higher k_{oc} value, therefore it is expected that more abiotic losses attributed to sorption occurred even after plates were removed from the shaker table.

While aqueous PAH concentrations in embryo containing wells decreased significantly in the first 24 hours of incubation compared to controls for both PAHs, 2-OHNAP concentrations continued to decline for the entire experiment duration compared to controls, whereas acridine concentrations did not decrease more than controls after 24 hours of incubation (32 hpf). Total uptake mass, corrected for abiotic losses, was 1.83 ± 0.85 nmol and 1.99 ± 0.30 nmol for 2-OHNAP and acridine, respectively, both of which are significantly lower than the respective exposure masses of 4.56 ± 0.16 nmol and 3.18 ± 0.09 nmol.

3.3.2 Kinetics

Changes in PAH concentrations for both control wells and embryo wells fit first order kinetics well, as shown in Figure IV-3. This supports that the assumption of chemical movement following first-order kinetics was reasonable for this system. This is in agreeance with previous diffusion modeling of similar compounds (Li et al., 2018; Wang et al., 2020, 2018). As discussed previously, agitation via shaker table played a significant role in the rate of mass transport, therefore kinetic rate constants were derived in a piecewise manner. Initial sorption rate in the first 24 hours of incubation (6-32 hpf) were significantly faster than the following 96 hours (32-120 hpf) for both compounds. However, uptake rate was significantly faster in the first 24 hours for acridine, whereas uptake rate was not significantly different for 2-OHNAP for incubation on and off the shaker table, as shown in Table IV-2.

Table IV-2. Summary of kinetic constants derived from experimental data and used to model PAH concentrations in controls well and embryo wells. Error represents standard deviation.

Time	Acridine			2-OHNAP		
	$k_{sorption}$ ($hour^{-1}$)	k_{uptake} ($hour^{-1}$)	k_{photo} ($hour^{-1}$)	$k_{sorption}$ ($hour^{-1}$)	k_{uptake} ($hour^{-1}$)	k_{photo} ($hour^{-1}$)
$t \leq 32$ hpf	0.016 ± 0.0005	0.014 ± 0.002	0.0003 ± 5E-04	0.009 ± 0.0004	0.012 ± 0.009	0.0005 ± 8E-04
$t > 32$ hpf	0.008 ± 0.0007	-0.001 ± 0.002	0.0003 ± 5E-04	0.001 ± 0.0002	0.009 ± 0.003	0.0005 ± 8E-04

Photodegradation contributed minorly to the overall abiotic losses, seen in the order of magnitude difference with $k_{sorption}$. Greater error associated with the models for embryo wells reflects the heterogeneity of PAH uptake kinetics by individual embryos. This is especially prominent for 2-OHNAP shown in Figure IV-2A, where embryos generally lived longer and thus developed more completely than those exposed to acridine. The number of zebrafish embryos included in model development for each time point is reported in Table C7.

A limitation of this study is the inability to distinguish between PAH accumulation and PAH metabolism. PAH metabolism is predominantly carried out by CYP enzymes, which are both expressed and active in embryonic zebrafish (Loerracher and Braunbeck, 2021). Therefore, uptake rate cannot be equated to bioaccumulation rate, as this would overestimate bioaccumulation by neglecting metabolism. Further work on the analysis of PAH content in the embryos, as well as PAH metabolites, would help differentiate between diffusion, metabolism, and bioaccumulation.

3.3.3 Toxicity Results

Endpoints that were observed in a previous report of toxic effects of exposures to acridine and 2-OHNAP in embryonic zebrafish were also observed in the PAH exposure studies in this work (Geier et al., 2018). Several endpoints were observed for embryos exposed to acridine or 2-OHNAP, namely mortality, yolk sac and pericardial edema, and pectoral fin malformation. Axis and cranial deformities were also observed in embryos exposed to acridine. A summary of the endpoints observed in the previous and present studies is provided in Table C8. All measured endpoints for acridine matched the expected endpoints, however we report additional endpoints that were not observed previously for 2-OHNAP exposure.

While both studies of 2-OHNAP show consistent results for mortality and edema endpoints, cranial deformities were observed only in the present study. These additional deformities may reflect additive toxicity effects from the 2-OHNAP and UV co-exposure that could not be accounted for by individual exposures. Almeida et al. (2015) reported similar phenomena for zebrafish embryos exposed to UV and triclosan, denoting that increases in toxicity may also be due to photodegradation of the compound. However, further work is needed to elucidate potential products of photodegradation, and their toxicity to zebrafish embryos. A comparison of mortality predictions based of fluorescent inflection and results from morphology screening, presented in detail in SI, showed 83% and 81% agreement between acridine and 2-OHNAP exposed embryos (Table C6).

4.0 Conclusions

The fluorescent spectroscopy method developed in this study provided insights into the uptake of 2-hydroxynaphthalene and acridine by embryonic zebrafish with rapid measurements of toxicant concentrations in the embryo media. No significant impact on embryo viability and development was observed in response to the irradiation of the embryos from the plate reader measurements. Furthermore, embryo development did not impact background fluorescence except in the instance of cranial deformation or embryo mortality, where a significant increase in fluorescent emission was observed. This observation prompted the development of a

technique for predicting embryo mortality based on inflection of the first derivative of the fluorescent emissions that was 81% to 97% accurate. Significant decreases in aqueous PAH concentrations were monitored for both chemicals from the combined losses of abiotic and biotic losses. Pseudo-first order kinetic models considering embryo uptake, photodegradation, and sorption fit well with empirical measurements, with uptake and sorption being the major contributors to overall PAH losses. Phenotypic outcomes and embryo mortality were consistent with previous reports, except for additional cranial deformities observed in the present study with 2-OHNAP. This cautions potential additive toxicity of the UV exposure and chemical exposure that this plate reader method entails, necessitating further investigation with a larger suite of chemicals. Nevertheless, this rapid, non-destructive technique is novel tool that is suitable for adaptation to any autofluorescent compound of interest.

5.0 Acknowledgements

The authors wish to acknowledge the Sinnhuber Aquatic Research Laboratory (SARL) screening team, particularly Emma Odone, Julia Jamison, Jay Adams, and Connor Johnson. Research reported in this manuscript was supported by the National Institute Of Environmental Health Sciences of the National Institutes of Health as a Trainee Initiated Collaborative Grant associated with Award Number P42ES016465 and T32ES007060. The content is solely the responsibility of the authors and does not necessarily represent the official views of the National Institutes of Health.

CHAPTER V

PAH Bioremediation with *Rhodococcus rhodochrous* ATCC 21198: Impact of Cell Immobilization and Surfactant Use on PAH Treatment and Post-Remediation Toxicity

Juliana Huizenga[a] (ORCID: 0000-0002-1242-0948) huizengj@oregonstate.edu
Jason Schindler[b] (ORCID: 000-0002-9848-0473) schindlj@oregonstate.edu
Michael Simonich[b] (ORCID: 0000-0003-2277-5192) mtsimonich@oregonstate.edu
Lisa Truong[b] (ORCID: 0000-0003-1751-4617) lisa.truong@oregonstate.edu
Manuel García-Jaramillo[b] (ORCID: 0000-0003-2987-2913)
manuel.g.jaramillo@oregonstate.edu
Robyn Tanguay[b] (ORCID: 0000-0001-6190-3682) robyn.tanguay@oregonstate.edu
Lewis Semprini[a] (ORCID: 0000-0002-9174-4464) lewis.Semprini@oregonstate.edu

[a] Oregon State University, School of Chemical, Biological, and Environmental Engineering
[b] Oregon State University, Department of Environmental and Molecular Toxicology

Chapter V: PAH Bioremediation with *Rhodococcus rhodochrous* ATCC 21198: Impact of Cell Immobilization and Surfactant Use on PAH Treatment and Post-Remediation Toxicity

Abstract

Polycyclic aromatic hydrocarbons (PAHs) are prevalent environmental contaminants that are harmful to ecological and human health. Bioremediation is a promising technique for remediating PAHs in the environment because of low costs, chemical, and energy inputs. However, bioremediation often results in the accumulation of PAH transformation products that can be more toxic than their parent compounds. Therefore, transformation product accumulation and post-remediation toxicity are important metrics for interpreting remediation success that are currently underutilized in remediation studies. The objectives of this research were to first demonstrate the cometabolic treatment of a mixture of PAHs by a pure bacterial culture, *Rhodococcus rhodochrous* ATCC 21198, and investigate transformation product formation and toxicity. Additionally, the surfactant Tween ® 80 and cell immobilization techniques were investigated to enhance bioremediation, compared to suspended cells alone. Several tools were used to monitor remediation progress and assess its success, namely fluorescent spectroscopy for rapid monitoring of PAH biotransformation, GC-MS for parent PAHs, UPLC-HRMS for PAH transformation products, and embryonic zebrafish toxicity assays for pre- and post-remediation toxicity. Transformation of all four PAHs was observed in batch tests, with cell immobilization generally improving the rate and extent of PAH transformation, especially when combined with the surfactant. Toxicity was only observed in extracts from remediated material, manifesting as mortality and developmental effects in embryonic zebrafish. Identification of PAH metabolites produced by 21198 revealed a complex mixture of hydroxylated compounds, quinones, and ring-fission products, among many other unidentified compounds. While this study highlights the importance of investigating transformation products and post-remediation toxicity, nevertheless, 21198's ability to rapidly transform PAHs of a variety of molecular structures and sizes suggests that 21198 can be a valuable microorganism for catalyzing the transformation of PAHs. Implementing further downstream processes to treat the PAH transformation

products produced by 21198 should be pursued to help lower post-treatment toxicity in future studies.

1.0 Introduction

Polycyclic aromatic hydrocarbons (PAHs) are a class of ubiquitous environmental contaminants that arise from both natural and anthropogenic sources and exhibit mutagenic, teratogenic, and carcinogenic properties (Gitipour et al., 2018; Mojiri et al., 2019). The broad range of physicochemical properties of PAHs reflects their range of molecular structures and sizes. A variety of characteristics can be used to organize PAHs into categories, including: molecular weight (low molecular weight (LMW) for three fused benzene rings or fewer, high molecular weight (HMW) for more than three fused benzene rings), structure (linear, angular, cluster), and aromaticity (alternant and non-alternant) (Patel et al., 2020; Sakshi and Haritash, 2020).

Remediation goals typically take the form of a permissible concentration of the contaminants of interest (Yu et al., 2023). However, this relies on the assumption that any transformation products produced from the remediation process are not as toxic as the parent compound(s). This assumption, while true for many contaminants, is not necessarily true for PAHs. Several studies have reported increases in toxicity after chemical or biological treatment (Andersson et al., 2009; Chibwe et al., 2015; Schrlau et al., 2017; Wang et al., 2021b), due to the formation of transformation products that are more bioavailable and more toxic that their parent compounds. Despite these findings, it is still very uncommon for transformation products or toxicity to be monitored in PAH remediation studies (Titaley et al. 2020).

An attractive option for the remediation of PAH contaminated material is bioremediation, as it is less expensive and less invasive than physical and chemical removal strategies (Kuppusamy et al., 2017; Thacharodi et al. 2023). However, bioremediation can lead to the formation and accumulation of toxic transformation products (Andersson et al., 2009; Schrlau et al., 2017). Microorganisms can transform PAHs through metabolism, where the contaminants are used as carbon and energy sources, or cometabolism, where the contaminants are transformed fortuitously without any carbon or energy gain (Hazen 2010).

Although many microorganisms have been isolated that degrade PAHs via metabolic processes (Ghosal et al., 2016; Imam et al., 2022; Lu et al., 2011), the application of these microorganisms is limited, as they are dependent on PAHs for their survival and are unable to degrade the contaminants to very low concentrations (Hazen 2010). Microorganisms that cometabolize contaminants are not limited in this way and are therefore better equipped to degrade PAHs to remediation goal concentrations. However, complete mineralization is difficult to achieve with cometabolism, thus the potential to accumulate toxic PAH transformation products should be considered.

Whether a process is metabolic or cometabolic, one of the biggest challenges in PAH bioremediation is the bioavailability of PAHs (Duan et al., 2015). PAHs sorb strongly to soil and sediment in the environment due to their hydrophobicity. Sorbed PAHs are not accessible to microorganisms, therefore treatment is often limited by the desorption rate of PAHs from the solid phase to the aqueous phase, as concentrations are only reduced by microorganisms in the aqueous phase (Lamichhane et al., 2016; Mohan et al., 2006). A common method used to overcome the bioavailability barrier is the use of surfactants to solubilize sorbed PAHs through a process known as soil washing (Cheng et al., 2018; Mulligan et al., 2001). Surfactants aid in the solubilization of PAHs by creating micelles that are suspended in the aqueous phase but have hydrophobic centers capable of accumulating PAHs (Mulligan et al., 2001; Peng et al., 2011).

Surfactants are typically categorized as cationic, anionic, or nonionic. Nonionic surfactants are most commonly used for soil washing, as cationic surfactants are prone to adsorption to soil and anionic surfactants prone to precipitation out of the aqueous phase (Bai et al., 2019; Zhang and Zhu, 2010). The nonionic surfactant Tween ® 80 (T80) has been studied extensively for soil washing applications, particularly in combination with bioremediation, as it has been shown to have minimal toxicity and disruption to its areas of use, including minimal to no impacts to fungal communities, plants, and soil microbiome (Cheng et al., 2017). However, all surfactants, including T80, are toxic to microorganisms at high enough concentrations, as they can disrupt cellular membranes and cause cell lysis (Gharibzadeh et al., 2016). Because of the

inherent toxicity of surfactants, protecting cells from surfactants is necessary for extending the lifetime of bacteria used for bioremediation.

One approach used to protect cells from surfactant toxicity is immobilizing cells in hydrogels made from biocompatible polymers such as alginate, polyvinyl alcohol, or chitosan (Mehrotra et al., 2021). The benefits of using immobilized cells in bioremediation applications has been discussed extensively in a variety of reviews, and include advantages such as increasing the activity and viability of biomass, providing opportunities for cell recovery and reuse, and protecting cells from harsh environmental conditions (Bayat etl a. 2015; Mehrotra et al., 2021; Partovinia and Rasekh, 2018; Patel et al., 2020). Of studies that have investigated PAH bioremediation using surfactants and immobilized cells, improved PAH treatment with immobilized cells compared to suspended cells has consistently been demonstrated and attributed to increased resistance to surfactant toxicity, improved mass transfer performance, bacterial growth retention in the hydrogel matrix, and sorption of PAHs to hydrogels (Chen et al., 2021; Wen et al., 2021; Xu et al., 2019).

Rhodococcus rhodochrous ATCC 21198 (21198) was the gram-positive pure bacterial culture used in the present bioremediation study. The genera *Rhodococcus* is very popular in remediation applications because of its many useful qualities such as its tolerance of harsh environments, metabolic diversity, and expression of enzymes that can transform a wide range of relevant environmental contaminants (Krivoruchko et al., 2019; Nazari et al., 2022). Indeed, 21198 has been used for the remediation of chlorinated solvents (Rolston et al., 2022), 1,4-dioxane (Rasmussen et al., 2020), monoaromatic hydrocarbons, and MTBE (Huizenga and Semprini, 2023a), however 21198 has not yet been studied for the remediation of PAHs.

The objectives of this research were to demonstrate the cometabolic treatment of a mixture of four PAHs, each representing a different structural class: fluorene (non-alternant), phenanthrene (bent), anthracene (linear), and pyrene (cluster), by 21198. The impact of T80 and cell immobilization on PAH treatment, formation of PAH transformation products, and post-remediation toxicity were evaluated using a variety of tools. Gas chromatography-mass spectrometry (GC-MS) was used to measure parent PAHs, while ultra-high performance liquid chromatography coupled with high

resolution mass spectrometry (UPLC-HRMS) was used to identify PAH transformation products. Fluorescent spectroscopy was used to monitor PAH degradation and metabolite formation in real-time, and finally, embryonic zebrafish assays were used to assess toxicity before and after remediation.

2.0 Materials and Methods

2.1 Chemicals

A full list of the PAHs, isotope labelled PAHs, and PAH transformation products included in this study is provided in Appendix D. Compressed gases were purchased from Gas Innovations (La Porte, TX): Isobutane (99.99%) and Airgas Inc. (Radnor, PA): Oxygen (100%). 1-Butanol (99.4%) was purchased from Acros Organics (MA). Polymers were purchased from Sigma Aldrich (St. Louis, MO): polyvinyl alcohol (>99%) with a molecular weight distribution of 85,000-124,000 and Cape Crystal Brands (Summit, NJ): sodium alginate of food grade purity. Crosslinkers were purchased from Honeywell (Charlotte, NC): Boric acid (>99.8%) and Millipore Sigma (Burlington, MA): Calcium chloride dihydrate (>95%). Tween ® 80 (T80) was purchased from Sigma Aldrich (St. Louis, MO). All solvents used were of analytical grade purity and purchased from various vendors.

2.2 Cell Culturing

The pure culture *Rhodococcus rhodochrous* ATCC 21198 (21198) was obtained from Dr. Michael Hyman at North Carolina State University. 21198 was maintained as a pure culture on minimal agar plates in a sterile airtight container with 1.5% v/v isobutane supplied as the sole carbon and energy source. Batch growth reactors were prepared as described in (Huizenga and Semprini, 2023a). Briefly, an inoculum scraped from a minimal plate was added to a 500 mL Wheaton glass media bottle containing 300 mL of sterile mineral salt media (MSM) (Kottegoda et al. 2015) amended with 10% v/v isobutane in excess based on the oxygen content of a sealed bottle.

Growth reactors were incubated in the dark at 30 ºC on a 150 RPM shaker table. After 5 days of incubation, cells in late exponential growth phase were concentrated via centrifugation as described in Murnane et al. (2021), and biomass content of the concentrate was measured using a total suspended solids (TSS) analysis (Baird et al. 2017). Concentrated cell solutions were stored at 4 ºC for no longer than two days before use in experiments.

2.3 Cell Immobilization

21198 cells were immobilized in sodium alginate (NaAlg)/polyvinyl alcohol (PVA) beads using a modified version of the technique described in Harris et al. (2022). Briefly, isobutane grown 21198 cells were added to a 2% w/v NaAlg/3% w/v PVA mixture at a concentration of 0.5 mg cells/mL. This mixture was transferred to 60 mL sterile syringes and dropped into a 500 mL crosslinking solution consisting of boric acid (3% w/v) and calcium chloride (1.5% w/v) with a syringe pump to create spherical hydrogel beads. Beads were crosslinked for 1 hour before being rinsed with autoclaved water.

In order to increase the biomass concentration and activity in the beads, rinsed beads were transferred to growth reactors prepared as described in section 2.1; however, the beads were present in the reactors (~20 g per reactor) rather than a suspended cell inoculum. This process was repeated without the addition of cells to produce abiotic control beads. Abiotic and active beads were prepared at the same time to maximize consistency between bead batches.

Isobutane consumption, shown in Figure D1, was monitored during incubation with a previously established gas chromatography-flame ionization detection (GC-FID) method using a Series 6890 Hewlett Packard gas chromatograph equipped with a capillary column (Agilent DB-624 UI 30m x 0.53mm) and a flame ionization detector operating under conditions described in Huizenga and Semprini (2023a). Beads were removed from growth reactors following the five-day incubation period, rinsed with autoclaved DI water, and stored in an autoclaved 50 mM phosphate buffer (pH = 7) for approximately 24 hours until use in batch experiments.

2.3.1 T80 Sensitivity and Transformation Tests

The sensitivity of suspended and immobilized 21198 was assessed in batch tests with a range of T80 concentrations. Batch bottles were prepared in 27 mL vials with butyl septa crimp tops. Stock solutions with a range T80 concentrations (0 mg/L to 5000 mg/L) in MSM were prepared, and 10 mL of solution was added to the 27 mL vials. Each concentration was prepared in triplicate. 21198 was added to bottles as suspended cells (0.5 mg cells/bottle) or immobilized cells (2 mg cells/bottle). Note that beads used in these experiments were not incubated.

After sealing the vials, 0.2 mL of isobutane was added to the headspace with a syringe and subsequently monitored with GC-FID. Equilibrium was maintained at 30 ^{o}C on a 150 RPM shaker table for the duration of the experiments. Zero-order biomass normalized rates of isobutane utilization were determined and compared to evaluate the impact of T80 on cell activity.

Because T80 is a biodegradable surfactant, a set of batch tests were conducted to determine the ability of 21198 to degrade T80. These tests were carried out in 125 mL Wheaton glass media bottles (nominal volume 155 mL) with butyl septa caps. The aqueous phase of batch bottles was 100 mL of 10x diluted MSM with 1 g/L T80, to which 30 mg of isobutane grown 21198 was added. Batch bottles were placed on a 150 RPM shaker table in a 30 ^{o}C room during the three-day incubation period. During this time, 2 mL samples were periodically removed from the bottles with a syringe through the cap septa, filtered through a 0.2 um PVDF filter, and were analyzed for T80 using the fluorescent spectroscopy method described in Mousset et al. (2013).

2.3.2 Oxygen Uptake Tests

To compare the activity of suspended cells and immobilized cells, oxygen uptake experiments were conducted with cells before and after immobilization and bead incubation, with the same cell concentrate immobilized in beads tested as suspended cells. Batch tests were conducted in 27 mL vials with butyl septa crimp tops. Each bottle contained 10 mL MSM with 40 mg/L 1-butanol, and approximately 1 mg of suspended cells or 1 g of beads. Active bottles were prepared in triplicates,

while abiotic controls were prepared in duplicates. Headspace oxygen was monitored after addition of cells using a Hewlet Packard 5890 Series Gas Chromatograph equipped with thermal conductivity detector (GC-TCD) and capillary column (Supelco 60/80 Caroboxen 1000). Helium flowed at 30 mL/minute was used as the carrier gas with the oven temperature held constant at 40 ^{o}C. Equilibrium was maintained at 30 ^{o}C on a 150 RPM shaker table for the duration of the experiments. The zero-order biomass normalized oxygen utilization rate (k_{O2}) for suspended cells was compared to that of the immobilized cells to estimate the bead mass needed per batch bottle to achieve comparable microbial activity to suspended cells.

2.4 Batch Bottle Preparation

PAH bioremediation experiments were carried out in 125 mL Wheaton glass media bottles (nominal volume 155 mL) with butyl septa caps. Experiments were conducted in four sets; set 1 with suspended cells, set 2 with suspended cells and T80, set 3 with immobilized cells, and set 4 with immobilized cells and T80. The aqueous phase of batch bottles was 100 mL of 10 times diluted MSM, with 1 g/L T80 added to the solution for batch sets 2 and 4. PAHs were added to batch bottles from concentrated DMSO stock solutions to reach approximate initial concentrations of 1 mg/L of fluorene and phenanthrene, 0.5 mg/L anthracene, and 0.1 mg/L pyrene. Initial concentrations reflect the PAH's aqueous solubility limits. 1-Butanol was added as a neat liquid at an initial concentration of 40 mg/L. The oxygen demand associated with the 1-butanol utilization did not deplete the available oxygen in sealed bottles.

Batch bottles were placed on a 150 RPM shaker table in a 30 ^{o}C room before cell addition to allow dissolution of the PAHs. Biomass was added to active bottles as either 30 mg of suspended cells or 28 g of beads (representing ~30 mg cells) at time zero, after which initial samples were taken. Batch bottles were kept in the dark at 30 ^{o}C on a 100 RPM shaker table for the duration of the experiment. Active bottles were prepared in triplicates, while autoclaved cell controls (prepared as active bottles with

autoclaved cells or abiotic beads), and abiotic controls, (prepared as active bottles with no cells) were prepared in duplicates.

Batch bottles were opened in a laminar flow hood every 24 hours to refresh oxygen, and an additional dose of 1-butanol was added every three days to active bottles. Batch sets 3 and 4 had a reduced headspace volume due to the bead volume, and therefore received an additional 5 mL of pure oxygen at the start of the experiment and every subsequent 24 hours to match the headspace oxygen content in batch sets 1 and 2. Beads were harvested from batch bottles after the final timepoint samples were taken and tested for oxygen uptake as described in section 2.3.1 to compare bead activity before and after PAH exposure.

2.5 Chemical Analyses

2.5.1 Liquid-Liquid Extraction and GC-MS

Throughout the course of the batch experiments, 0.7 mL liquid samples were taken from the batch bottles using a sterile glass syringe through the cap septa. These samples were transferred to microcentrifuge tubes and spiked with an isotope-labeled PAH surrogate mixture (Table D2) to monitor PAH losses that occurred during sample processing and storage. Samples were extracted using the following liquid-liquid extraction (LLE) method. Equal volumes of ethyl acetate were added to microcentrifuge tubes containing the 0.7 liquid sample, vortexed for five minutes, and then centrifuged at 8000 RPM for 2 minutes to separate the ethyl acetate and aqueous phase. The ethyl acetate phase was removed and stored in an amber autosampler vial with a PET lined screw cap. This process was repeated three times for each sample for a final extract volume of ~2 mL. Extracts were then dried under a nitrogen stream to 225 µL before and spiked with 75 µL of acenaphthene-d10 in ethyl acetate as an internal standard for a final sample volume of 300 µL. Samples were then analyzed with GC-MS for parent PAHs using a previously reported method (Huizenga and Semprini, 2023b).

2.5.2 EEM-PARAFAC

Concurrently with GC-MS samples, 2 mL liquid samples were taken from active bottles for fluorescent spectroscopy analysis over the duration of the experiments. Samples were transferred to a four-sided quartz cuvette (Starna Cells) and scanned using a Varian Cary Eclipse fluorescent spectrometer. Samples were scanned in 3D mode through excitation and emission wavelength ranges of 200 to 300 nm and 300 to 450 nm, respectively. The scan speed was 600 nm/min, and excitation and emission slit widths were both 5 nm. Excitation-emission matrices (EEMs) were processed further with parallel factor analysis (PARAFAC) using the drEEM MATLAB toolbox (Murphy et al., 2013) as described in (Huizenga and Semprini, 2023b).

Separate PARAFAC models were generated with EEMs from active batch bottles for each experiment set (n = 21 or 24) as well as with the combined EEMs from all experiments (n = 90). The most appropriate number of components for each model was determined based on the trends of three metrics: percent explained, core consistency, and sum of squared error. All final models were validated with split half analysis.

2.5.3 SPE and UPLC-HRMS

The remaining liquid volume in the batch bottles after all timepoint samples (~190 to ~235 mL) were taken and stored at -20 ºC until samples could be extracted using a previously described solid-phase extraction (SPE) method (Schrlau et al., 2017) using Bond Elut Plexa (60 mg, 3 mL) cartridges (Agilent Technologies, New Castle, DE). One method amendment was made for samples from batch sets 3 and 4, as cartridge clogging from free polymer released from the beads was a barrier for successful extraction. Boric acid and calcium chloride were added to samples after thawing to re-crosslink free polymer in solution. After five minutes of mixing on a magnetic stir plate, precipitate was removed from the sample before extraction.

Extracts were split 80/20 for toxicity and chemical analysis. Ultra-high performance liquid chromatography (UPLC – Sciex ExionLC AD) coupled to high-

resolution mass spectrometry (HRMS - a ZenoTOF 7600) were used for the identification of PAH transformation products. Separation was achieved with an ACE Excel column (1.7 μm; 2.1x100 mm, Hichrom Limited, UK) and a gradient of nanopure water with 0.1% formic acid and acetonitrile with 0.1% formic acid. Samples (2 μL injection) were analyzed in both positive and negative electro spray ionization (ESI) modes. Acquisition and processing computers are equipped with up-to-date Sciex OS software licenses. Full details of the LC-MS parameters, along with the PAH transformation product library used to screen samples, are provided in Appendix D.

2.7 Embryonic Zebrafish Assay

The extract fraction dedicated to toxicity testing was blown to dryness under a nitrogen stream and reconstituted in DMSO. Toxicity was evaluated using the embryonic zebrafish assay described in Truong et al. (Truong et al., 2016) at the Sinnhuber Aquatic Research Laboratory (SARL) at Oregon State University (Corvallis, OR, USA). Zebrafish were maintained according to Institutional Animal Care and Use committee protocols.

To summarize, dechorionated tropical 5D wild-type zebrafish (*Danio rerio*) embryos were statically exposed to extracts at 6 hours post fertilization (hpf) for 120 hours. A 12-point concentration curve was run in duplicate plates for each extract with 7 animals exposed per concentration per plate. Three developmental toxicity endpoints were assessed at 24 hpf, while 10 developmental endpoints were assessed at 120 hpf. Changes in toxicity before and after treatment were assessed by comparing embryo responses of extracts from control batch bottles to extracts from active batch bottles.

2.8 Statistical Analysis

Statistical significance of PAH transformation was determined using one-way ANOVA analysis and Fisher's least squared difference test assuming equal variance among comparison groups with statistical significance reported for $p \leq 0.05$.

Statistical analysis was carried out in MATLAB. Statistical significance of toxicity responses in embryonic zebrafish assays was determined according to previously published procedures (Truong et al., 2014)

3.0 Results and Discussion

3.1 T80 Sensitivity and Transformation Tests

Results from the T80 sensitivity tests, shown in Figure D2, indicate that the tolerance of T80 for suspended and immobilized cells is approximately 1 g/L. No difference was observed in isobutane consumption for T80 concentrations of 1 g/L and below compared to controls for extended incubation times, indicating that these concentrations did not cause significant cell distress. This is in good agreement with previously reported T80 tolerances for bacterial strains in the *Rhodococcus* genera, which typically range from 1 g/L to 2 g/L (Chen et al., 2012; Hu et al., 2020; Lee et al., 2006). Conversely, it was observed that T80 concentrations of 5 g/L and 2.5 g/L significantly reduced isobutane consumption after approximately 8 hours of incubation, and completely halted isobutane consumption after 24 hours of incubation Isobutane consumption and calculated rates are reported in Table D5. The 1 g/L T80 concentration selected for batch experiments is well above its critical micelle concentration of approximately 15 mg/L (Mahmood, 2013; Pinto and Moore, 2000), therefore T80 exists predominantly as micelles at this concentration..

Rapid removal of T80 from the aqueous was observed in T80 transformation tests, with less than 5% of T80 remaining after 3 days, as shown in Figure D3. It is hypothesized that this is a cometabolic process involving an esterase, as has been reported with other bacterial strains (Wang et al., 2011). This hypothesis for 21198 is supported by similar T80 removal in active cells and monooxygenase-inhibited cells and inability to culture 21198 with T80 as a carbon source. Thus, T80 concentration is not considered to be constant in PAH transformation tests, although its transformation was likely not competitive to PAH transformation, as the transformation of these substrates is catalyzed by different enzymes.

3.2 Oxygen Uptake Tests

A comparison of the rate of oyxgen uptake (k_{O2}) for suspended cells compared to immobilized cells, as shown in Figure D4, resulted in an estimated biomass concentration in the beads of 1.1 ± 0.05 mg cells/g bead, indicating that bead biomass content was approximately doubled after incubation. No statistically significant difference was observed in zero-order oxygen utilization rate for used beads in either diluted MSM (set 3) or T80 solution (set 4), indicating that PAH exposure and transformation did not significantly impact cell respiration or viability, nor did the incubation with T80. Significant changes to bead integrity and 21198 activity were not observed after use in the batch experiments, therefore beads may be reused in further PAH biotransformation batch experiments.

3.3 EEM-PARAFAC Results

Treatment progress was assessed in quasi-real time with the fluorescent spectroscopy measurements, with further interpretation was made possible with the PARAFAC modeling results. Preliminary PARAFAC models for individual experiments revealed a high degree of similarity between the components generated to model the data sets. Therefore, it was appropriate to combine data sets and generate one PARAFAC model to allow for comparison of component scores between all experiments. This was expected due to the similarity in experimental set up between the four batch set ups.

Only scans from the first timepoint samples of experiment set three were found to be outliers due to excessively high leverages and were therefore removed from the data set. Fitting metrics for preliminary models with 3 to 7 components are shown in Table D6. The final model using all data sets required four PARAFAC components to appropriately model the data set, with 79% core consistency, 96.5% explained, and 5.7E6 SSE. Components were identified by comparing component Stokes shift and spectra to standard scans and literature values, as shown in Figure D5.

Component one (C1) was identified as a mixture of metabolites and cellular material, component two (C2) was identified to be a mixture of anthracene and phenanthrene, component three (C3) was identified to be fluorene, and component four (C4) was identified to be of cellular material origin. The temporal trends of each component are shown in Figure V-1.

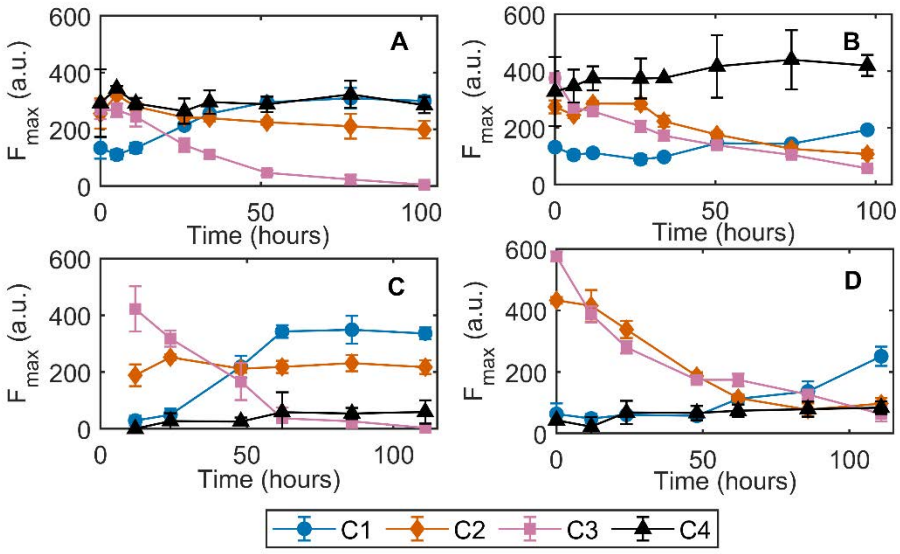

Fig. V-1 Temporal trends of PARAFAC components for each experimental set: set 1/suspended cells (A), set 2/suspended cells+T80 (B), set 3/immobilized cells (C), set 4/immobilized cells+T80 (D). Error bars represent standard deviation among triplicates

Trends in component F_{max} with time supported their suggested composition. C1 increased with time for all experiments, which is likely due to the formation of fluorescent PAH metabolites. The presence of C1 in initial timepoint samples may be due to the cellular material present in set 1 and set 2 samples, as the cellular material does fluoresce in the same region as C1. Lower initial amounts of C1 in sets 3 and 4 were expected, as minimal cellular material was present in the aqueous phase. The emergence of C1 with time also informs the nature of these metabolites. Because C1 concentrations do not increase and then decrease with time, these are hypothesized to be dead-end products, rather than intermediates in the PAH degradation process.

Furthermore, the location of their spectra in this range of excitation and emission wavelengths suggests that they contain at least two fused benzene rings, as compounds with a single benzene ring do not fluoresce in the region C1 appears (Schwarz and Wasik, 1976). However, this region does match reported spectra for PAH-quinones (Peng et al., 2018b). C2 and C3 both decreased with time, representing the transformation of PAHs that occurred over the 5-day incubation. A less apparent decrease in C2 was observed in set 1 and set 3, possible due to spectral interferences from the cellular material or production of PAH metabolites that are not represented by C1.

Finally, C4 remained relatively constant throughout the experiments, which is to be expected, as it arises from sample turbidity. Furthermore, its minor presence in set 3 and set 4 support its correlation to suspended cellular material in the aqueous samples, as this was very minor in experiments that used immobilized cells.

3.4 GC-MS Results

While EEM-PARAFAC allowed for rapid, qualitative information regarding the PAH concentration changes with time, GC-MS results fully elucidate the quantitative changes in PAH concentrations throughout the experiments. The reduction in PAH concentration for active batch bottles in each experiment set are shown in Figure V-2. The equivalent data for controls in each experiment are shown in Figure D6.

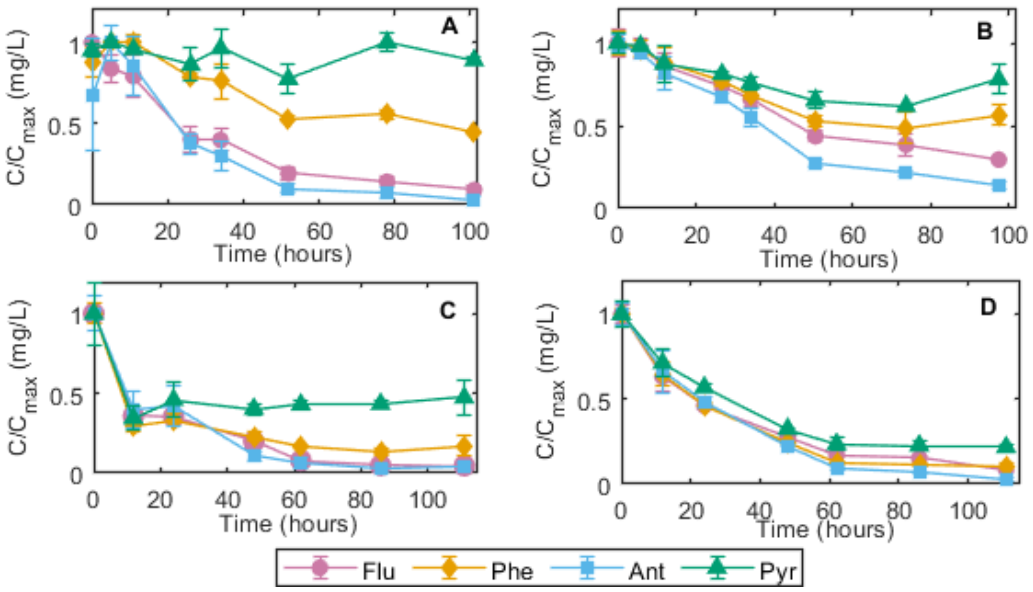

Fig. V-2 Normalized concentrations of PAHs over time for experiment set 1/suspended cells (A), set 2/suspended cells+T80 (B), set 3/immobilized cells (C), set 4/immobilized cells+T80 (D). Note that concentrations were normalized to their initial concentrations, reported in Table D11. Error bars represent standard deviations among triplicates.

Degradation of the LMW PAHs, fluorene, phenanthrene, and anthracene, was observed in all experiments, while degradation of the HMW PAH, pyrene, was not observed to be significant in experiment sets that did not contain T80. Minor degradation of pyrene was observed in set 2, while significant degradation was observed in set 4. It was expected that the presence of surfactant would impact pyrene degradation the most, as it is the least soluble and therefore least accessible to the bacteria. Thus, its bioavailability is most improved by the presence of surfactant. The degradation of the three LMW PAHs demonstrates that 21198 is capable of transforming PAHs of various geometries, including the linear and cluster geometries, which are often considered to be the most recalcitrant geometry of LMW PAHs (Abdel-Shafy and Mansour, 2016).

Adsorption of PAHs to the hydrogels is suggested by the trends in PAH concentrations for batch set 3 (Figure V-2C), as there was a rapid decrease in PAH concentration in the first 12 hours of incubation, followed by slower decreases for the remaining ~100 hours. This same observation can be seen in the controls illustrated in Figure D6. Therefore, the total losses observed in active bottles in batch set 3 may be

a combination of biotransformation and adsorption. Adsorption of the PAHs to beads in set 4 was not observed in active or control bottles, presumably due to the increased solubility of PAHs with the presence of T80.

3.4.1 Total PAH Losses

While the transformation of the PAHs by 21198 alone is a novel finding, the impact of immobilization and presence of T80 were of interest in this study as well. To further compare the different treatments in the experiment sets, the total losses and biotic losses (losses in active bottles minus losses in autoclaved cell control bottles) were calculated and are presented in Figure V-3. The impact of T80 in suspended and immobilized cells was investigated by comparing set 1 to 2 and 3 to 4, respectively, while the impact of immobilization in batch tests without and with T80 was investigated by comparing set 1 to 3 and 2 to 4, respectively.

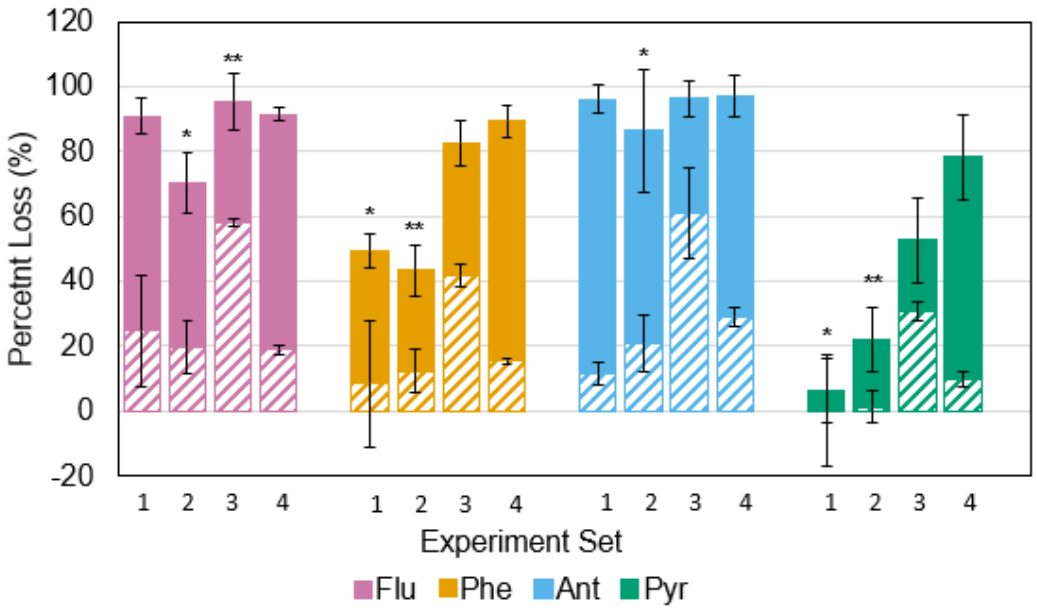

Fig. V-3 Total losses (solid filled) and abiotic losses (stripe filled) for each experiment set organized by PAH. Error bars represent one standard deviation. Statistical significance for total losses is represented by asterisks above bars with comparisons between batch sets for each PAH. Values are provided in Table D10 while P-values are reported in Table D7

As shown in Figure V-3, total fluorene losses were lower for batches containing T80 for both suspended and immobilized cells. This same observation is true for suspended cells with phenanthrene and anthracene, although phenanthrene and anthracene total losses were not impacted by T80 in sets with immobilized cells. Total pyrene losses were increased with the presence of T80 for suspended and immobilized cells.

In comparing PAH total losses for suspended and immobilized cells, significant increases were observed with immobilized cells for sets with and without T80 except for anthracene, for which no significant difference was found between sets 1, 3, and 4. This suggests that immobilized cells transformed more of the total PAH mixture than the suspended cells. This could be due to multiple factors, including greater cell biomass, higher cometabolic activity, or more interactions between PAHs and cells facilitated by the hydrogel matrix, as discussed in similar studies that have made the same observations (Wang 2019, Wen 2021, Xu 2019, Chen 2021).

The lack of methods to quantify live immobilized biomass is a significant limitation of this study, thus it is possible that more cells were present in the beads than was discernable from the oxygen uptake tests used to compare suspended and immobilized cells. This also makes it difficult to compare PAH removal efficiencies and rates with similar studies, as other studies have the same limitation. Nevertheless, biotic and abiotic PAHs observed in this study are similar to those reported with other microorganisms and bead formulations. Several studies have immobilized PAH-metabolizing bacteria at lower biomass loadings in beads than the present study for use in PAH treatment studies, results from which are summarized in Table V-1.

Table V-1. Comparison of PAH removal and control bead PAH loss for studies of PAH biodegradation with immobilized bacteria. Note that Fla is fluoranthene, while Flu is fluorene.

Bead formula	Biomass Loading	Surfactant	Time incubated (days)	PAHs studied	Bead PAH removal (%)	Control Bead PAH Removal (%)	Ref.
3% Ca-Alg	1/40 (w/v)	N/A	42	Phe	63.16	17.79	Wang et al., 2019
				Fla	56.94	13.40	
10% PVA 0.8% Na-Alg 0.7% ALNPs	1/5 (v/v)	2.5 g/L T80	30	Phe	92.21	34.76	Wen et al. 2021
				Fla	87.97	30.53	
				Pyr	88.81	26.21	
10% PVA 0.8% Na-Alg 0.7% ALNPs	1/10 (v/v)	2.5 g/L T80	30	Phe	89.14	37.96	Xu et al. 2019
				Fla	81.25	33.44	
				Pyr	78.33	29.21	
3% PVA 1% Na-Alg	1/4 (v/v)	4 g/L Triton X	4	Phe	42.06	-7.31	Chen et al. 2021*
				Fla	66.84	29.59	
				Pyr	68.70	22.92	
3% PVA 2% Na-Alg	1/2 (w/v)	1 g/L T80	4	Phe	89.26	15.53	Present Study
				Flu	91.41	18.97	
				Pyr	78.19	9.76	
				Ant	97.11	28.92	

*16 priority PAHs were degraded simultaneously, the 3 PAHs reported were reported to be most significantly degraded

Comparable PAH removal to lower biomass beads incubated for an extended time was achieved by the beads in this study, despite the processes in the present study being exclusively cometabolic. Furthermore, the PAH transformation in the present study is the work of one microorganism, rather than a bacterial consortium as in Wen et al. (2019) and Wang et al. (2019).

3.4.2 Apparent Biotic PAH Losses

When accounting for abiotic losses in controls for each set, trends differ slightly from trends of total PAH losses. For suspended cells, the only difference in trends from total PAH loss trends is that significantly less pyrene transformation occurred when T80 was not present.

The difference between total and biotic PAH losses is largest for batch set 3, in which abiotic losses due to sorption were the greatest. Thus, biotic losses for all PAHs in batch set 3 were significantly lower than those for batch set 4, which also used beads but had T80 present. Similar PAH losses with control beads were reported in studies summarized in Table V-1 and may be due to a combination of sorption to beads, sorption to glassware, volatilization, or reactions with sunlight.

However, it cannot be determined with the existing measurements how much each contributed to the total losses, as it is possible that PAHs which initially sorbed to the hydrogel matrix were then desorbed and transformed by 21198. Therefore, these observations are for apparent biotic PAH losses, as actual biotic losses are underestimated by assuming all sorbed PAHs are permanently sorbed and therefore not bioavailable.

3.4.3 PAH Transformation Rates

The impact of immobilization and T80 presence was also investigated in terms of PAH transformation rates, as both rate and extent of treatment are important parameters of remediation technologies. PAH transformation followed pseudo-first order kinetics well, as typical for cometabolic processes (Geng et al., 2022). Pseudo-first order rates derived from both total and apparent biotic losses are shown in Figure V-4. It should be noted that rates derived from total losses significantly differed from the rates derived from apparent biotic losses for set 3, where significant PAH losses were observed in abiotic bead controls. This was presumably due to adsorption of PAHs to the bead polymer matrix, however as noted in section 3.4.2, these estimates for biotic PAH losses are likely underestimates.

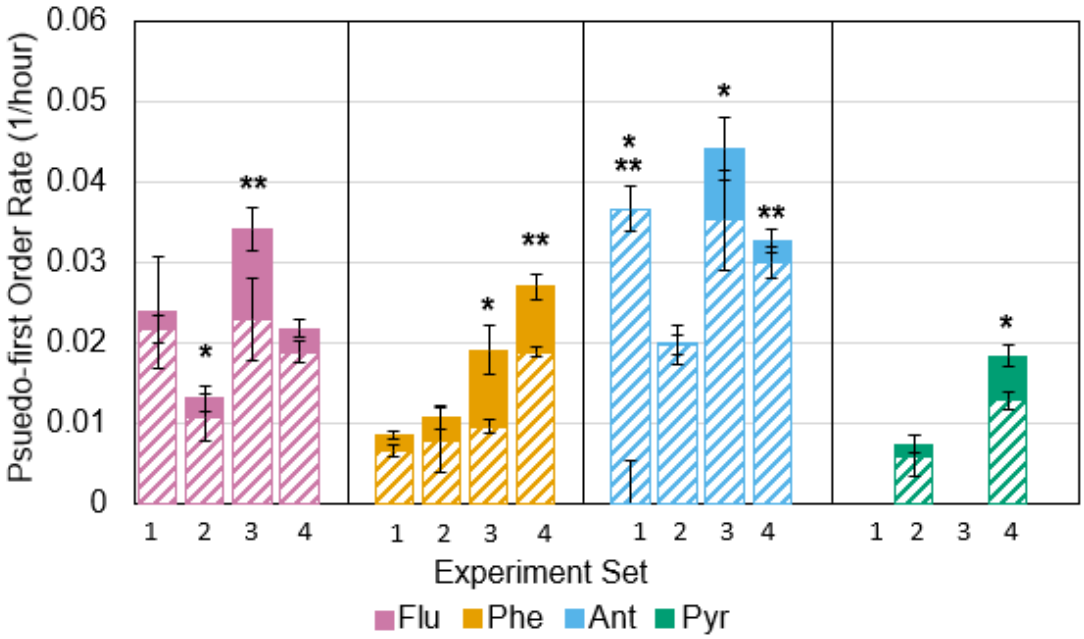

Fig. V-4 Pseudo-first order transformation rate of PAHs in active bottles derived from total PAH losses (solid bars) and biotic PAH losses (stripe fill). Error bars represent compounded standard deviation for active bars (n=3). Statistical significance for total losses is represented by asterisks above bars with comparisons between batch sets for each PAH. Values are reported in Table D10, p-values are reported in Table D7, Fit Coefficients are reported in Table D8

The presence of T80 decreased transformation rates of fluorene and anthracene for suspended and immobilized cells, increased the rate of phenanthrene degradation for immobilized cells, and increased the rate of pyrene degradation for suspended and immobilized cells. It is possible that the decrease in transformation rate for the LMW PAHs when T80 is present may be due to the increase in bioavailability and thus transformation of pyrene. Pyrene transformation rates were only derivable when surfactant was present, as surfactant was required to support pyrene transformation. The decrease in LMW PAH transformation rates may also be due to cell stress responses from the surfactant (Cheng et al., 2018, 2017).

Independent of T80 presence, transformation rates of fluorene and phenanthrene increased for immobilized cells compared to suspended cells. Anthracene transformation rates were not significantly impacted by immobilization when surfactant was not present, however a significant increase in rates were observed

when surfactant was present. The same factors discussed previously that may have contributed to the increase in total PAH losses with immobilized cells are likely to contribute to this observation as well.

3.5 EEM-PARAFAC and GC-MS Comparison

A high degree of similarity was observed between GC-MS fluorene results and C3 PARAFAC results as shown in Figure D7, indicating that the PARAFAC model was able to isolate trends in fluorene concentrations accurately throughout the experiments. The same comparison for anthracene and phenanthrene GC-MS results and C2 PARAFAC results were not as straightforward as fluorene, as they were not modeled as separate components. This may be due to the rates of anthracene and phenanthrene degradation being more similar in sets 2 and 4 compared to sets 1 and 3. The more similar the trends are for anthracene and phenanthrene, the better the PARAFAC model can use one component to model them together. Phenanthrene and anthracene share very similar spectra, thus it is expected that they be grouped together, however as their concentrations more greatly differ as they are degraded at different rates, the less their individual trends will resemble the combined trend modeled by C2. It is common for PARAFAC components to be the combined spectra of multiple compounds, particularly as mixture complexity increases (Hung et al., 2022b; Seopela et al., 2021b). Consequently, EEM-PARAFAC analysis provides limited quantitative data but rapid qualitative data, therefore it is best used in combination with a quantitative targeted analysis such as GC-MS.

3.6 UPLC-HRMS Results

The investigation of PAH metabolites produced from the bioremediation batch set 1 revealed a complex metabolite mixture consisting of several different compound classes: hydroxylated, ring fission, quinone, and hydroxy/quinone PAH transformation products. Multiple positions on each parent PAH are susceptible to enzymatic transformation, thus transformation pathways are presented for a generic PAH structure in Figure V-5.

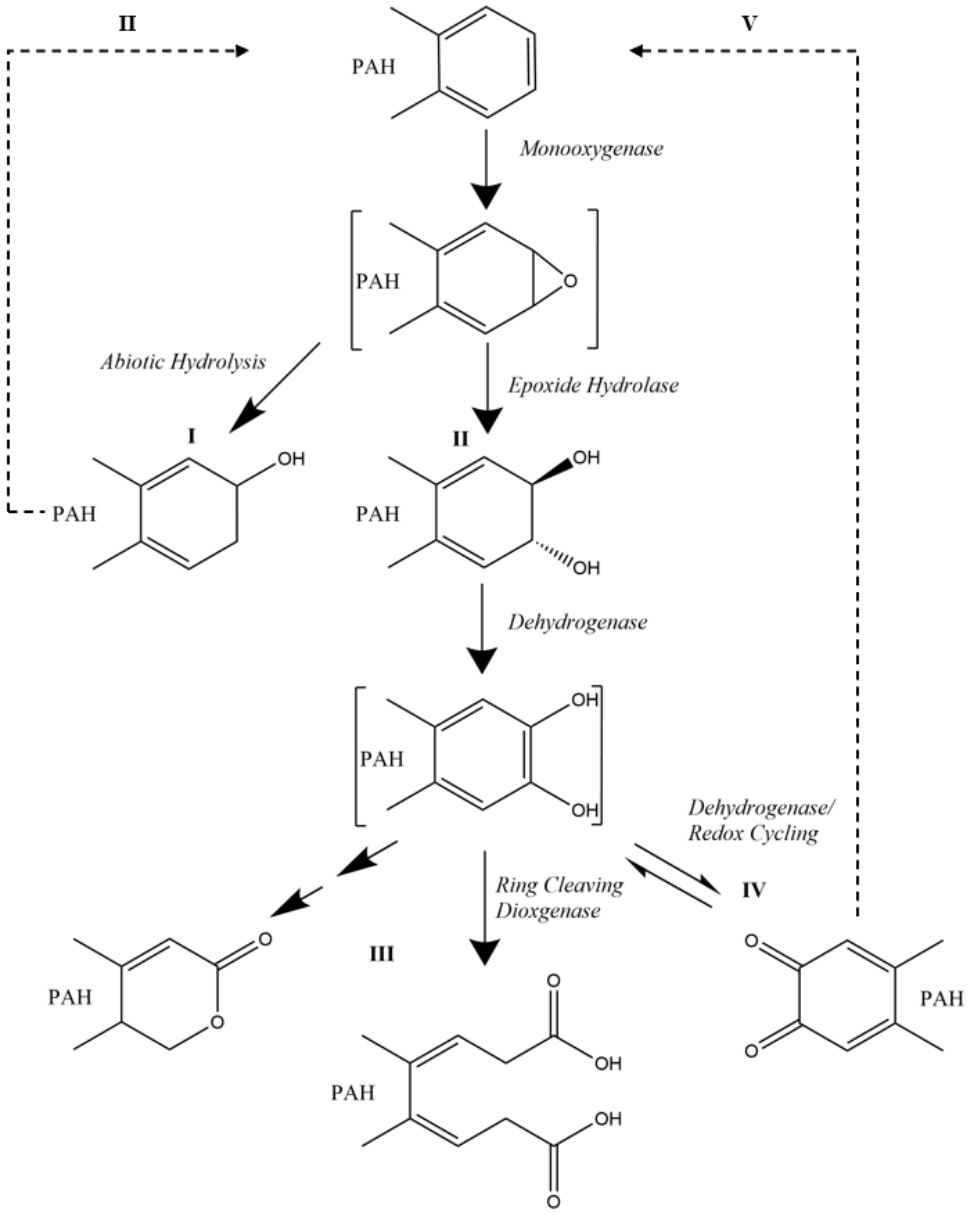

Fig. V-5. Proposed generic pathway for PAH transformation by 21198. Compounds in brackets represent undetected intermediates, while others represent compound classes identified in treated samples with high confidence: I – hydroxylated, II – dihydroxylated, III – ring fission, IV – quinone, and V – hydroxy-/dihydroxy-quinone. Confidence levels were evaluated based on (Schymanski et al., 2015) and are reported in Table D9.

The compound classes identified in remediated samples indicate that cometabolism was primarily initiated by a monooxygenase. This was an expected finding, as 21198 can expresses many monooxygenases that have broad substrate specificity, particularly the short-chain alkane monooxygenase (SCAM) highly

expressed when grown on isobutane (Bealessio et al., 2023; Murnane et al., 2021), and hydroxylated PAHs are often reported in PAH biodegradation studies with *Rhodococcus* strains (Finkelstein et al., 2003; Leneva et al., 2009; Luo et al., 2016).

Di-hydroxylated products with alcohol groups in the non-ortho position is likely the results of two separate monooxygenase attacks followed by abiotic hydrolysis of the epoxide, while products with alcohol groups in the ortho position are likely the results of enzymatic hydrolysis of the epoxide intermediate, producing a *trans*-stereoisomer intermediate. Di-hydroxylated products in the ortho position are often attributed to a naphthalene dioxygenase, however this would produce a *cis*-stereoisomer intermediate. Because a naphthalene dioxygenase has not been annotated in 21198's genome, these intermediates were not considered for this system (Shields-Menard et al., 2014) .

Another class of compounds found in 21198's PAH metabolite mixtures was ring fission products. Diphenic acid and benzocoumarin, among others, were identified in metabolite mixtures as ring fission products of phenanthrene and anthracene, suggesting the activity of intradiol-ring cleaving dioxygenase, which is present in 21198's genome. Ring-fission products have been reported for other *Rhodococcus* strains as well (Finkelstein et al., 2003; Jin et al., 2015; Leneva et al., 2009; Liu et al., 2021).

Significant biotic losses of pyrene were observed in sets 2 and 4, thus pyrene can be degraded by 21198, however, solubility limitations may have prevented significant transformation in sets 1 and 3. Thus, no pyrene metabolites were detected with high confidence in samples from batch set 1. Pyrene degradation by *Rhodococcus* strains has been reported as a significant member of a microbial consortia (Elyamine et al., 2021), however it is less commonly reported to be degraded by a single pure culture. Liu et al. (2021) reported degradation of pyrene by a *Rhodococcus ruber* strain, which degraded pyrene primarily with a catechol-1,2-dioxygenase, which has been annotated in 21198's genome (Shields-Menard et al., 2014), while Jin et al. (2015) and Walter et al. (1991) reported degradation of pyrene by *Rhodococcus* strains via a naphthalene dioxygenase, which 21198 does not possess. Further investigation of

enzyme expression and targeted analytical techniques would help elucidate the PAH transformation pathways and metabolites formed by 21198.

3.7 Embryonic Zebrafish Assay

Although parent PAH concentrations were significantly reduced in all remediation studies, post-remediation toxicity increased for all batch sets, as shown in Figure V-6. Lowest effect levels (LELs) are reported as the amount of treated material (mL) embryos are exposed to in the microwell media (µL), as described in Appendix D.

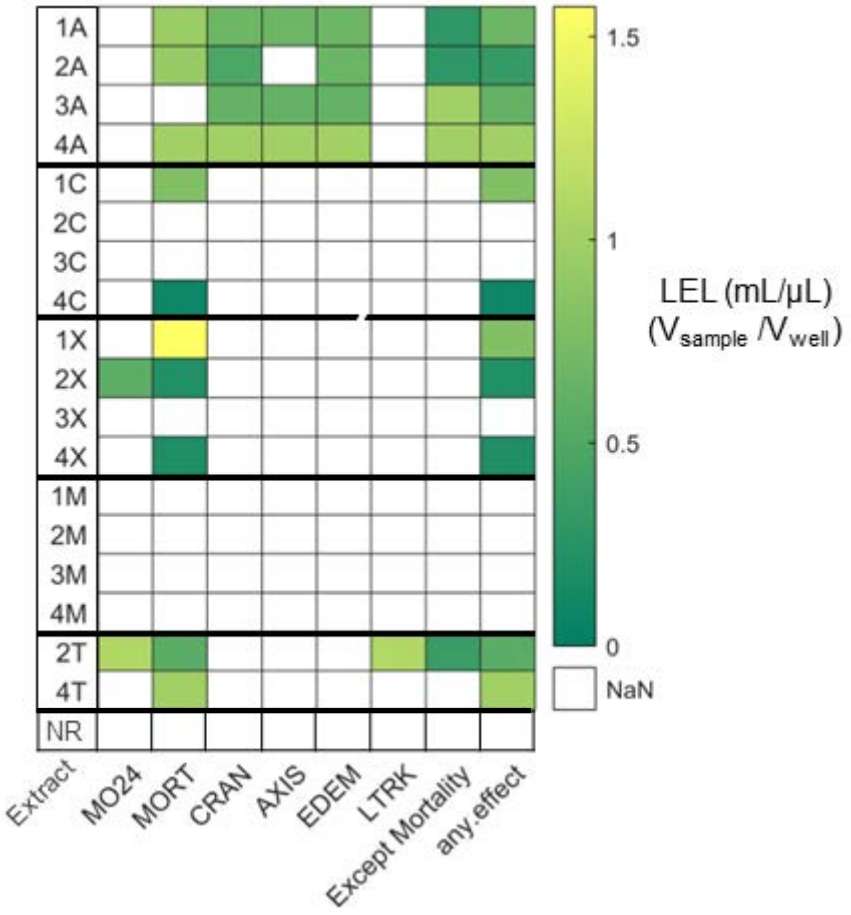

Fig. V-6 Estimated lowest effect level (LEL) based on exposure to the volume of the sample represented in the microwells. Extracts are grouped by sample type; active (A), autoclaved control (C), abiotic control (X), T80 control (T), and not remediated (NR)

The initial PAH mixture was not toxic to zebrafish, as observed in unremediated controls (NR) from the present study and individual PAH toxicity assessments conducted previously (Geier et al., 2018). After treatment, mortality and morphology impacts were observed in zebrafish embryos, indicating that mutagenic metabolites accumulated during remediation. Edema and cranial and axis deformation were observed exclusively in treated samples, suggesting that PAH metabolites are responsible for eliciting these responses. Mortality assessed at 120 hpf was also significant in three of the four remediated extracts. Extract 3A was the least concentrated and only elicited toxic responses at the highest concentration tests, therefore it is likely that the tested concentration was not high enough to cause mortality.

Mortality was observed in all abiotic controls that contained T80 (2X,4X, 2T, 4T), thus T80 was likely extracted by the SPE protocol and caused a toxic response in the zebrafish. Interestingly, this was not observed in 2C which did contain T80. This may be due to sorption of the T80 to the cell material that lowered their extraction efficiency. Similar results from active extracts with T80 present (2A and 4A) may indicate that SPE was impacted by the presence of cells, however because T80 was degraded during these experiments, T80 concentrations in active bottles were likely significantly lower than that in control bottles at the end of the experiments. Controls from experiment 1 (1C and 1X) were contaminated with cells and thus contained a small amount of PAH metabolites, supported by GC-MS data shown in Figure D6, therefore toxicity observed in zebrafish embryos exposed to these extracts do not accurately represent the toxicity of untreated samples. No toxicity was observed in media extraction blanks or solvent blanks.

Although the full content of the treated extracts is not known, several of the compounds that have been identified were assessed previously for toxicity using embryonic zebrafish assays (Geier et al., 2018; Knecht et al., 2013). From these comparisons, we see good agreement between the morphology endpoints observed in our study (mort, cran, axis, edema) to endpoints observed with transformation product compound classes that are present in remediated samples. Several of these compound classes, including anthraquinones, phenanthrene quinones, and hydroxy-fluorenones

have been found to be acutely toxic, with concentrations as low as 1.5 μM eliciting toxic responses in zebrafish embryos (Knecht et al., 2013). Therefore, it is feasible that the minor PAH transformation observed in contaminated controls from batch set 1 resulted in toxic responses. Nevertheless, the consistent trends in toxicity before and after treatment with 21198 indicates that formation of transformation products is an important factor in assessing overall remediation success and warrants further efforts to resolve the complex mixture of PAH transformation products produced by 21198.

4.0 Conclusions

The present study demonstrated the ability of 21198 to transform a mixture of PAHs in a variety of conditions that combined T80 and cell immobilization. Comparisons of PAH losses and transformation rates demonstrated that immobilized cells were positively impacted by T80, presumably due to the increased apparent solubility of the PAHs. Contrarily, suspended cells were negatively impacted by T80, except for pyrene, that was transformed more significantly and rapidly in the presence of T80. PAH total losses and transformation rates were positively impacted by cell immobilization for conditions with and without T80.

Although the initial PAHs concentrations were not toxic to zebrafish embryos, toxicity was observed in all treatments, as observed in mortality and developmental effects in embryonic zebrafish, supporting that the PAH metabolites were more toxic than their parent compounds. Preliminary identification of PAH metabolites produced by 21198 revealed a complex mixture of mono- and di-hydroxylated compounds, quinones, and ring-fission products, some of which have been previously demonstrated to elicit the same toxic responses observed in the present study. Results from this study demonstrate that although the surfactant and cell immobilization technique improve the rate and amount of PAH transformation, the toxicity of post-remediated material is not dictated by concentrations of parent PAHs alone.

The importance of including metrics other than PAH removal, such as formation of PAH metabolites and post-remediation toxicity, is highlighted by this study and motivates the development of alternative remediation strategies that reduce

PAH concentrations and material toxicity. 21198's ability to rapidly transform PAHs of a variety of molecular structures and sizes suggests that 21198 can be a valuable agent in catalyzing the transformation of PAHs, particularly in the presence of T80. Implementing further downstream processes to treat the PAH transformation products produced during initial treatment with 21198 should be pursued to help lower post-treatment toxicity in future studies.

5.0 Acknowledgements

Research reported in this manuscript was supported by the National Institute Of Environmental Health Sciences of the National Institutes of Health as a Trainee Initiated Collaborative Grant associated with Award Number P42ES016465. The content is solely the responsibility of the authors and does not necessarily represent the official views of the National Institutes of Health.

Chapter VI: Conclusions

1.0 Summary

The contents of this dissertation spanned the detection, remediation, and toxicity of mono- and poly-cyclic aromatic hydrocarbon contaminants, namely BTEX and PAHs. Chapter II studied the remediation of BTEX and their common co-contaminant MTBE, both individually and in mixtures, with the bacterial pure culture 21198. Three growth substrates; isobutane, 1-butanol, and 2-butanol, were used to grow 21198 batches and tested separately for all batch tests to investigate the impact of growth substrate on remedial activity. In high-biomass resting cell tests, isobutane grown cells transformed contaminants most rapidly and to the greatest extent, followed by 2-butanol grown cells and then 1-butanol grown cells. This same trend was apparent for BTEX and BTEXM mixture tests. These results demonstrated that isobutane is the ideal growth substrate for resting cell transformation, likely due to high enzyme expression levels for enzymes involved in BTEXM degradation and possibly larger energy reserves in isobutane grown cells compared to the other two growth substrates. Conversely to the high-biomass resting cell batch tests, 1-butanol was found to be the ideal substrate for low-biomass growing cell batch tests. 1-butanol is most rapidly utilized by 21198, thus an active population of 21198 was able to be established most rapidly with 1-butanol. Furthermore, 1-butanol did not appear to compete with BTEX for enzymes involved in their transformation, as it does not require initial oxidation with a monooxygenase like isobutane does.

Regardless of the growth substrate, BTEX and BTEXM mixture tests revealed a consistent transformation order occurring with T and E being degraded first, then B and o-X, and finally MTBE. The primary transformation product for MTBE, TBA, was transformed after MTBE as well. The order of contaminant degradation alludes to preferential transformation of singly-substituted benzene rings over unsubstituted or poly-substituted benzene rings. Possible explanations for this preference are that the involved enzymes higher substrate affinities for E and T, or that the methyl or ethyl groups are more susceptible to enzymatic attack than the aromatic ring. This is further supported by the proposed pathway for T metabolism, where hydroxylation of the methyl group was supported by observed growth on benzyl alcohol. The multiple

methyl groups substituted on the rings for the xylenes may lead to steric hindrance that prevents their rapid transformation, despite their structural similarity to T. Overall, the results from this work not only demonstrated 21198's ability to remediate BTEXM for the first time, but it also supported further research into aromatic hydrocarbon remediation with 21198, particularly with PAHs. The investigations of growth substrates also informed the design of future remediation work to include 1-butanol as a supportive growth substrate during PAH remediation.

The development of detection methods for PAHs in aqueous samples using fluorescent spectroscopy detailed in Chapters III and IV provided valuable, rapid results regarding the extent of PAH transformation and uptake for bacterial and embryonic zebrafish systems, respectively. Chapter III utilized two-dimensional scans and three-dimensional excitation-emission matrices (EEMs) to monitor phenanthrene degradation by ELW1 and formation of trans-9,10-dihydroxy-9,10-dihydrophenanthrene (P1). Qualitative reaction progress could be observed as shifts in the 2D and 3D spectra active samples over time, however quantitative reaction progress could be assessed using a calibration data set and, in the case of 3D scans, parallel factor analysis (PARAFAC). The final PARAFAC models included 5 components that were identified as phenanthrene, P1, two from cell material, and one unknown. Because phenanthrene and P1 were separated out as individual components, they could be quantified with the inclusion of a calibration data set in PARAFAC model development. Recreating impacts of cell interference in the calibration data set was necessary to achieve accurate quantification. This quantification was in good agreement with the GC-MS quantification. Quantification of phenanthrene and P1 using the 2D fluorescent method was in poor agreement with PARAFAC and GC-MS results, highlighting the need for a separation step such as PARAFAC to decompose the fluorescent spectra of a mixture of fluorophores.

The quantification of PAHs in aqueous samples based on their autofluorescence presented in Chapters III inspired a novel fluorescent plate reader method presented in Chapter IV for use in embryonic zebrafish assays. Unlike Chapter III, the method developed for embryonic zebrafish relied on single excitation and emission wavelengths, optimized for each analyte. This ensured that zebrafish

embryos were exposed to as little UV radiation as possible. The methods were developed to measure 2-hydroxynaphthalene (2-OHNAP) and acridine and used to measure both background fluorescence and PAH concentrations in a UV exposure study and PAH exposure study, respectively. The UV exposure study revealed that the background fluorescence was not significantly impacted by normal developing zebrafish, nor was zebrafish embryo development impacted by the UV exposure the fluorescent plate reader measurements entail. It was observed, however, that abnormal development of zebrafish embryos manifesting as cranial deformities or mortality did significantly impact background fluorescence in a predictable manner.

These methods were successful in quantitatively monitoring PAH concentrations decreasing with time in the PAH exposure study. Major contributors to PAH concentration reduction in this study were attributed to abiotic losses (photodegradation, sorption to well walls), and diffusion (uptake) into the zebrafish embryo. These losses could be modeled well with first-order kinetics, results of which suggested several factors impacted PAH movement in this system: physicochemical properties of the PAHs, yolk sac to embryotic body ratio, and agitation via the shaker table. Minor deviation from expected toxicity outcomes for 2-OHNAP exposed embryos suggested that there is potential for an additive toxic effect of the PAH and the UV exposure, and further work is required to investigate this possibility.

The final manuscript presented in Chapter IV combines knowledge gained from the BTEXM work with 21198 presented in Chapter II, the EEM methods presented in Chapter III, and the toxicity assay studied in Chapter IV to investigate PAH bioremediation with 21198. Surfactant enhanced bioremediation and cell immobilization were used to enhance bioremediation of PAHs, with remediation success assessed with measurements of PAHs, PAH transformation products, and post-remediation toxicity to embryonic zebrafish. 21198 cometabolized all components of the PAH mixture: fluorene, phenanthrene, anthracene, and pyrene. Pyrene degradation required the presence of surfactant to achieve significant degradation, likely due to the slow aqueous solubility of pyrene. The presence of surfactant and the use of immobilized cells compared to suspended cells both generally improved the extent and rate of transformation of PAHs. However, in all

cases, toxic transformation products accumulated during remediation. Identified transformation products included mono-and di-hydroxylated products, quinones, and ring fission products.

Several of these compound classes have been reported to elicit the developmental effects observed in embryos exposed to post-remediation material from these studies, namely mortality, edema, and deformation of the cranium and axis. The PAH transformation products and post-remediation toxicity suggest that the transformation of the PAHs was limited to a few enzymatic steps that lead to the production of dead-end products that are more bioavailable and more toxic than their precursors. As such, the remediation strategies developed in this chapter were successful at degrading PAHs, but not successful at reducing post-remediation toxicity. Although the former is the only metric typically used to assess remediation success, the use of additional tools such as LC-MS and toxicity assays demonstrated that this metric alone is not appropriate for determining the suitability of the presented PAH remediation strategies for field use.

1.2 Conclusions

Returning to the overall objectives of this dissertation work presented in Chapter 1, the overall conclusions of this work can be summarized as the following:

1) Determine suitability of a bacterial pure culture for aromatic hydrocarbon bioremediation using BTEX as model aromatic hydrocarbons
    - 21198 is a competent microorganism for the degradation of aromatic hydrocarbons. 21198 expresses enzymes that can accommodate substituted and unsubstituted monoaromatic hydrocarbons, and PAHs comprised of two to four aromatic rings. Aromatic hydrocarbon degradation by 21198 is the result of predominantly cometabolic activity, although benzene and toluene can be metabolically degraded by 21198.
2) Develop rapid detection methods for monitoring aqueous PAH concentrations changing in response to biological activity

- Fluorescence spectroscopy is a rapid, non-destructive technique that can be used to measure aqueous PAH concentrations using single excitation/emission measurements, two-dimensional scans, and 3-dimensional EEMs. EEMs can be further interpreted with parallel factor analysis to provide quantitative results for specific compounds in simple mixtures. These techniques are compatible with suspended bacterial cells and embryonic zebrafish.

3) Expand investigations in (1) to PAH remediation strategies using treatment and toxicity metrics to assess remediation success
    - Presence of surfactant and cell immobilization generally improved the extent and rate of 21198's PAH degradation; however, toxicity of post-remediated material was consistently greater than un-remediated material regardless of treatment strategy. Thus, transformation of PAHs alone should not be used to assess remediation success; investigating PAH-transformation products and post-remediation toxicity revealed that more complete transformation of PAHs is required to reduce post-remediation toxicity.

1.3 Recommendations for Future Work

In a true testament to the expansive nature of scientific research, this work has generated more questions than it has answered. It should be acknowledged that this work generated a foundation of knowledge in ideal lab conditions to build from, and as such, expansion of these remediation and detection technologies to include more aromatic contaminants in complex mixtures, as well as contaminated material (groundwater, soil, sediment, etc.) from Superfund sites would inform how well these results can be recreated in more realistic conditions. The expansion of the compounds studied would also inform the scope of suitable compounds for fluorescent detection, as few libraries exist for fluorescent spectra of PAHs and their transformation products. In addition, the extensive degradation abilities of 21198's warrant further investigation into the enzymes involved in aromatic hydrocarbon degradation using molecular tools such as differential protein expression analysis and proteomics. Of particular interest to aromatic hydrocarbon remediation are monooxygenases, toluene

hydroxylase, and ring-cleaving dioxygenases. Similarly, confirmation of the proposed benzene and toluene metabolism with 21198, and the remediation capabilities of 21198 grown on these substrates is of interest, as the discovery of these growth substrates for 21198 was an exciting and unexpected outcome of this research. Methods developed in Chapter IV should be validated with an alternative, traditional method such as GC-MS, as was conducted in Chapter III. In addition, additive toxicity from chemical and UV exposure should be investigated further to confirm UV exposure from a fluorescent plate reader does not impact toxicity outcome.

Many questions remain as to the composition of the PAH-transformation products produced by 21198 and their relative contribution to toxicity outcomes observed in zebrafish. Developing a quantitative LC-MS method for PAH-transformation products would allow a mass balance to be created and prioritize transformation products for individual toxicity analyses. Furthermore, studies that do not include parent PAH isomers such as phenanthrene and anthracene, would aid in the separation and identification of PAH metabolites. This would also aid in the comparison of toxicity outcomes between treatment strategies, as these comparisons were not possible without measured concentrations of the individual compounds in the remediated mixture. Expanding toxicity assessments to include cell-based reporter assays should also be investigated to align with Tox21 initiatives to reduce animal testing.

Finally, the promising results of surfactant enhanced bioremediation and immobilized 21198 supports the development of more complex engineered systems, such as a flow-through bead pack, for water contaminated with BTEXM and/or PAH mixtures. The work in Chapter V simulates contaminated soil washing effluent, thus Chapter V's remediation strategies to real contaminated soil washing effluent would be a logical next step in challenging 21198 with more realistic conditions. Exploration of additional remediation strategies to add before or after bioremediation with 21198, such as chemical oxidation or additional bacterial cultures, may help lower post-remediation toxicity by breaking down toxic metabolites produced by 21198.

References

Abdel-Shafy, H.I., Mansour, M.S.M., 2016. A review on polycyclic aromatic hydrocarbons: Source, environmental impact, effect on human health and remediation. Egypt. J. Pet. 25, 107–123. https://doi.org/10.1016/j.ejpe.2015.03.011

Alberts, J.J., Takács, M., 2004. Total luminescence spectra of IHSS standard and reference fulvic acids, humic acids and natural organic matter: comparison of aquatic and terrestrial source terms. Org. Geochem. 35, 243–256. https://doi.org/10.1016/j.orggeochem.2003.11.007

Alegbeleye, O.O., Opeolu, B.O., Jackson, V.A., 2017. Polycyclic Aromatic Hydrocarbons: A Critical Review of Environmental Occurrence and Bioremediation. Environ. Manage. 60, 758–783. https://doi.org/10.1007/s00267-017-0896-2

Alfoldy, B., Mahfouz, M.M.K., Yigiterhan, O., Safi, M.A., Elnaiem, A.E., Giamberini, S., 2019. BTEX, nitrogen oxides, ammonia and ozone concentrations at traffic influenced and background urban sites in an arid environment. Atmospheric Pollut. Res. 10, 445–454. https://doi.org/10.1016/j.apr.2018.08.009

Almeida, A.R., Andrade, T.S., Burkina, V., Fedorova, G., Loureiro, S., Soares, A.M.V.M., Domingues, I., 2015. Is UV radiation changing the toxicity of compounds to zebrafish embryos? Ecotoxicol. Environ. Saf. 122, 145–152. https://doi.org/10.1016/j.ecoenv.2015.07.021

Alostaz, M., Biggar, K., Donahue, R., Hall, G., 2008. Petroleum contamination characterization and quantification using fluorescence emission-excitation matrices (EEMs) and parallel factor analysis (PARAFAC). J. Environ. Eng. Sci. 7, 183–197. https://doi.org/10.1139/S07-049

Andersson, E., Rotander, A., von Kronhelm, T., Berggren, A., Ivarsson, P., Hollert, H., Engwall, M., 2009. AhR agonist and genotoxicant bioavailability in a PAH-contaminated soil undergoing biological treatment. Environ. Sci. Pollut. Res. 16, 521–530. https://doi.org/10.1007/s11356-009-0121-9

Andrade, T.S., Henriques, J.F., Almeida, A.R., Soares, A.M.V.M., Scholz, S., Domingues, I., 2017. Zebrafish embryo tolerance to environmental stress factors—Concentration–dose response analysis of oxygen limitation, pH, and UV-light irradiation. Environ. Toxicol. Chem. 36, 682–690. https://doi.org/10.1002/etc.3579

Ashton, R., Wever, B.D., Fuchs, H.W., Gaca, M., Hill, E., Krul, C., Poth, A., Roggen, E.L., n.d. State of the Art on Alternative Methods to Animal Testing from an Industrial Point of View: Ready for Regulation? 7.

Auffret, M., Labbé, D., Thouand, G., Greer, C.W., Fayolle-Guichard, F., 2009. Degradation of a Mixture of Hydrocarbons, Gasoline, and Diesel Oil Additives by *Rhodococcus aetherivorans* and *Rhodococcus wratislaviensis*. Appl. Environ. Microbiol. 75, 7774–7782. https://doi.org/10.1128/AEM.01117-09

Bai, X., Wang, Y., Zheng, X., Zhu, K., Long, A., Wu, X., Zhang, H., 2019. Remediation of phenanthrene contaminated soil by coupling soil washing with

Tween 80, oxidation using the UV/S2O82− process and recycling of the surfactant. Chem. Eng. J. 369, 1014–1023. https://doi.org/10.1016/j.cej.2019.03.116

Banerjee, S., Leptin, M., 2014. Systemic Response to Ultraviolet Radiation Involves Induction of Leukocytic IL-1β and Inflammation in Zebrafish. J. Immunol. 193, 1408–1415. https://doi.org/10.4049/jimmunol.1400232

Bansal, V., Kim, K.-H., 2015. Review of PAH contamination in food products and their health hazards. Environ. Int. 84, 26–38. https://doi.org/10.1016/j.envint.2015.06.016

Barboni, T., Chiaramonti, N., 2010. BTEX Emissions During Prescribed Burning in Function of Combustion Stage and Distance From Flame Front. Combust. Sci. Technol. 182, 1193–1200. https://doi.org/10.1080/00102201003660199

Barret, M., Carrère, H., Delgadillo, L., Patureau, D., 2010. PAH fate during the anaerobic digestion of contaminated sludge: Do bioavailability and/or cometabolism limit their biodegradation? Water Res. 44, 3797–3806. https://doi.org/10.1016/j.watres.2010.04.031

Bealessio, A.D., Chen, W., Krippaehne, K.J., Murnane, R.A., Hyman, M.R., Semprini, L., 2023. Alcohol-Dependent Cometabolic Degradation of Chlorinated Aliphatic Hydrocarbons and 1,4-Dioxane by *Rhodococcus rhodochrous* strain ATCC 21198. Environ. Eng. Sci. 40, 494–505. https://doi.org/10.1089/ees.2023.0058

Beitel, S.C., Flahr, L.M., Hoppe-Jones, C., Burgess, J.L., Littau, S.R., Gulotta, J., Moore, P., Wallentine, D., Snyder, S.A., 2020. Assessment of the toxicity of firefighter exposures using the PAH CALUX bioassay. Environ. Int. 135, 105207. https://doi.org/10.1016/j.envint.2019.105207

Benedek, T., Szentgyörgyi, F., Gergócs, V., Menashe, O., Gonzalez, P.A.F., Probst, A.J., Kriszt, B., Táncsics, A., 2021. Potential of Variovorax paradoxus isolate BFB1_13 for bioremediation of BTEX contaminated sites. AMB Express 11. https://doi.org/10.1186/s13568-021-01289-3

Bielefeldt, A.R., Stensel, H.D., 1999a. Modeling competitive inhibition effects during biodegradation of BTEX mixtures. Water Res. 33, 707–714. https://doi.org/10.1016/S0043-1354(98)00256-5

Bielefeldt, A.R., Stensel, H.D., 1999b. Modeling competitive inhibition effects during biodegradation of BTEX mixtures. Water Res. 33, 707–714. https://doi.org/10.1016/S0043-1354(98)00256-5

Bosco, M.V., Callao, M.P., Larrechi, M.S., 2006. Simultaneous analysis of the photocatalytic degradation of polycyclic aromatic hydrocarbons using three-dimensional excitation–emission matrix fluorescence and parallel factor analysis. Anal. Chim. Acta 576, 184–191. https://doi.org/10.1016/j.aca.2006.06.005

Brakstad, O.G., Størseth, T.R., Rønsberg, M.U., Hansen, B.H., 2018. Biodegradation-mediated alterations in acute toxicity of water-accommodated fraction and single crude oil components in cold seawater. Chemosphere 204, 87–91. https://doi.org/10.1016/j.chemosphere.2018.04.032

Brimo, K., Garnier, P., Sun, S., Bertrand-Krajewski, J.-L., Cébron, A., Ouvrard, S., 2016. Using a Bayesian approach to improve and calibrate a dynamic model

of polycyclic aromatic hydrocarbons degradation in an industrial contaminated soil. Environ. Pollut. 215, 27–37. https://doi.org/10.1016/j.envpol.2016.04.094

Bro, R., 1997. PARAFAC. Tutorial and applications. Chemom. Intell. Lab. Syst. 23.

Bro, R., Kiers, H.A.L., 2003. A new efficient method for determining the number of components in PARAFAC models. J. Chemom. 17, 274–286. https://doi.org/10.1002/cem.801

Brox, S., Seiwert, B., Küster, E., Reemtsma, T., 2016. Toxicokinetics of Polar Chemicals in Zebrafish Embryo (*Danio rerio*): Influence of Physicochemical Properties and of Biological Processes. Environ. Sci. Technol. 50, 10264–10272. https://doi.org/10.1021/acs.est.6b04325

Brum, D.M., Cassella, R.J., Pereira Netto, A.D., 2008. Multivariate optimization of a liquid–liquid extraction of the EPA-PAHs from natural contaminated waters prior to determination by liquid chromatography with fluorescence detection. Talanta 74, 1392–1399. https://doi.org/10.1016/j.talanta.2007.09.013

Brzeszcz, J., Kaszycki, P., 2018. Aerobic bacteria degrading both n-alkanes and aromatic hydrocarbons: an undervalued strategy for metabolic diversity and flexibility. Biodegradation 29, 359–407. https://doi.org/10.1007/s10532-018-9837-x

Bugel, S.M., Tanguay, R.L., Planchart, A., 2014. Zebrafish: A Marvel of High-Throughput Biology for 21st Century Toxicology. Curr. Environ. Health Rep. 1, 341–352. https://doi.org/10.1007/s40572-014-0029-5

Cachada, A., Pato, P., Rocha-Santos, T., da Silva, E.F., Duarte, A.C., 2012. Levels, sources and potential human health risks of organic pollutants in urban soils. Sci. Total Environ. 430, 184–192. https://doi.org/10.1016/j.scitotenv.2012.04.075

Carabajal, M.D., Arancibia, J.A., Escandar, G.M., 2017. Excitation-emission fluorescence-kinetic data obtained by Fenton degradation. Determination of heavy-polycyclic aromatic hydrocarbons by four-way parallel factor analysis. Talanta 165, 52–63. https://doi.org/10.1016/j.talanta.2016.12.030

Carter, J.M., Grady, S.J., Delzer, G.C., Koch, B., Zogorski, J.S., 2006. Occurrence of MTBE and other gasoline oxygenates in CWS source waters. J. - Am. Water Works Assoc. 98, 91–104. https://doi.org/10.1002/j.1551-8833.2006.tb07637.x

Chen, F.Y., Jiang, D.D., Tang, Y.B., 2012. Effects of Additional Stimulants on Phenol Degradation by a Halotolerant Rhodococcus sp. JDD1H. Appl. Mech. Mater. 253–255, 914–920. https://doi.org/10.4028/www.scientific.net/AMM.253-255.914

Chen, S.C., Chen, C.S., Zhan, K.-V., Yang, K.-H., Chien, C.-C., Shieh, B.-S., Chen, W.-M., 2011. Biodegradation of methyl tert-butyl ether (MTBE) by Enterobacter sp. NKNU02. J. Hazard. Mater. 186, 1744–1750. https://doi.org/10.1016/j.jhazmat.2010.12.079

Chen, W. (2016). *Activity-Based Protein Profiling of Alkane-Oxidizing Monooxygenases in Rhodococcus rhodochrous ATCC 21198*. [Master's Thesis, North Carolina State University] NC State University Libraries.

Chen, W., Zhang, H., Zhang, M., Shen, X., Zhang, X., Wu, F., Hu, J., Wang, B., Wang, X., 2021. Removal of PAHs at high concentrations in a soil washing solution containing TX-100 via simultaneous sorption and biodegradation processes by immobilized degrading bacteria in PVA-SA hydrogel beads. J. Hazard. Mater. 410, 124533. https://doi.org/10.1016/j.jhazmat.2020.124533

Chen, Y., Chen, Z.-P., Yang, J., Jin, J.-W., Zhang, J., Yu, R.-Q., 2013. Quantitative Fluorescence Spectroscopy in Turbid Media: A Practical Solution to the Problem of Scattering and Absorption. Anal. Chem. 85, 2015–2020. https://doi.org/10.1021/ac302815e

Cheng, M., Zeng, G., Huang, D., Yang, C., Lai, C., Zhang, C., Liu, Y., 2018. Tween 80 surfactant-enhanced bioremediation: toward a solution to the soil contamination by hydrophobic organic compounds. Crit. Rev. Biotechnol. 38, 17–30. https://doi.org/10.1080/07388551.2017.1311296

Cheng, M., Zeng, G., Huang, D., Yang, C., Lai, C., Zhang, C., Liu, Y., 2017. Advantages and challenges of Tween 80 surfactant-enhanced technologies for the remediation of soils contaminated with hydrophobic organic compounds. Chem. Eng. J. 314, 98–113. https://doi.org/10.1016/j.cej.2016.12.135

Chibwe, L., Geier, M.C., Nakamura, J., Tanguay, R.L., Aitken, M.D., Simonich, S.L.M., 2015. Aerobic Bioremediation of PAH Contaminated Soil Results in Increased Genotoxicity and Developmental Toxicity. Environ. Sci. Technol. 49, 13889–13898. https://doi.org/10.1021/acs.est.5b00499

Chlebowski, A.C., Tanguay, R.L., Simonich, S.L.M., 2016. Quantitation and prediction of sorptive losses during toxicity testing of polycyclic aromatic hydrocarbon (PAH) and nitrated PAH (NPAH) using polystyrene 96-well plates. Neurotoxicol. Teratol. 57, 30–38. https://doi.org/10.1016/j.ntt.2016.05.001

Christensen, J.H., Hansen, A.B., Mortensen, J., Andersen, O., 2005. Characterization and Matching of Oil Samples Using Fluorescence Spectroscopy and Parallel Factor Analysis. Anal. Chem. 77, 2210–2217. https://doi.org/10.1021/ac048213k

Cotelle, S., F&#xfffd;rard, J.F., 1999. Comet assay in genetic ecotoxicology: A review. Environ. Mol. Mutagen. 34, 246–255. https://doi.org/10.1002/(SICI)1098-2280(1999)34:4<246::AID-EM4>3.0.CO;2-V

Deeb, R.A., Alvarez-Cohen, L., 2000. Aerobic Biotransformation of Gasoline Aromatics in MultiComponent Mixtures. Bioremediation J. 4, 171–179. https://doi.org/10.1080/10889860091114211

Deeb, R.A., Alvarez-Cohen, L., 1999. Temperature effects and substrate interactions during the aerobic biotransformation of BTEX mixtures by toluene-enriched consortia andRhodococcus rhodochrous. Biotechnol. Bioeng. 62, 526–536. https://doi.org/10.1002/(SICI)1097-0290(19990305)62:5<526::AID-BIT4>3.0.CO;2-8

Deeb, R.A., Hu, H.-Y., Hanson, J.R., Scow, K.M., Alvarez-Cohen, L., 2001. Substrate Interactions in BTEX and MTBE Mixtures by an MTBE-Degrading Isolate. Environ. Sci. Technol. 35, 312–317. https://doi.org/10.1021/es001249j

Dobaradaran, S., Schmidt, T.C., Kaziur-Cegla, W., Jochmann, M.A., 2021. BTEX compounds leachates from cigarette butts into water environment: A primary

study. Environ. Pollut. 269, 116185. https://doi.org/10.1016/j.envpol.2020.116185

Dong, Q., Svoboda, K., Tiersch, T.R., Todd Monroe, W., 2007. Photobiological effects of UVA and UVB light in zebrafish embryos: Evidence for a competent photorepair system. J. Photochem. Photobiol. B 88, 137–146. https://doi.org/10.1016/j.jphotobiol.2007.07.002

Driskill, A.K., Alvey, J., Dotson, A.D., Tomco, P.L., 2018. Monitoring polycyclic aromatic hydrocarbon (PAH) attenuation in Arctic waters using fluorescence spectroscopy. Cold Reg. Sci. Technol. 145, 76–85. https://doi.org/10.1016/j.coldregions.2017.09.014

Duan, L., Naidu, R., Thavamani, P., Meaklim, J., Megharaj, M., 2015. Managing long-term polycyclic aromatic hydrocarbon contaminated soils: a risk-based approach. Environ. Sci. Pollut. Res. 22, 8927–8941. https://doi.org/10.1007/s11356-013-2270-0

El-Amrani, S., Sanz-Landaluze, J., Guinea, J., Cámara, C., 2013. Rapid determination of polycyclic aromatic hydrocarbons (PAHs) in zebrafish eleutheroembryos as a model for the evaluation of PAH bioconcentration. Talanta 104, 67–74. https://doi.org/10.1016/j.talanta.2012.11.025

Elcoroaristizabal, S., de Juan, A., García, J.A., Durana, N., Alonso, L., 2014. Comparison of second-order multivariate methods for screening and determination of PAHs by total fluorescence spectroscopy. Chemom. Intell. Lab. Syst. 132, 63–74. https://doi.org/10.1016/j.chemolab.2014.01.005

Elyamine, A.M., Kan, J., Meng, S., Tao, P., Wang, H., Hu, Z., 2021. Aerobic and Anaerobic Bacterial and Fungal Degradation of Pyrene: Mechanism Pathway Including Biochemical Reaction and Catabolic Genes. Int. J. Mol. Sci. 22, 8202. https://doi.org/10.3390/ijms22158202

Farhadian, M., Vachelard, C., Duchez, D., Larroche, C., 2008. In situ bioremediation of monoaromatic pollutants in groundwater: A review. Bioresour. Technol. 99, 5296–5308. https://doi.org/10.1016/j.biortech.2007.10.025

Fasnacht, M.P., Blough, N.V., 2002. Aqueous Photodegradation of Polycyclic Aromatic Hydrocarbons. Environ. Sci. Technol. 36, 4364–4369. https://doi.org/10.1021/es025603k

Ferretto, N., Tedetti, M., Guigue, C., Mounier, S., Redon, R., Goutx, M., 2014. Identification and quantification of known polycyclic aromatic hydrocarbons and pesticides in complex mixtures using fluorescence excitation–emission matrices and parallel factor analysis. Chemosphere 107, 344–353. https://doi.org/10.1016/j.chemosphere.2013.12.087

Filipkowska, A., Lubecki, L., Szymczak-Żyła, M., Ciesielski, T.M., Jenssen, B.M., Ardelan, M.V., Mazur-Marzec, H., Breedveld, G.D., Oen, A.M.P., Zamojska, A., Kowalewska, G., 2018. Anthropogenic impact on marine ecosystem health: A comparative multi-proxy investigation of recent sediments in coastal waters. Mar. Pollut. Bull. 133, 328–335. https://doi.org/10.1016/j.marpolbul.2018.05.058

Finkelstein, Z.I., Baskunov, B.P., Golovlev, E.L., Vervoort, J., Rietjens, I.M.C.M., Baboshin, M.A., Golovleva, L.A., 2003. Fluorene Transformation by Bacteria

of the Genus Rhodococcus. Microbiology 72, 660–665. https://doi.org/10.1023/B:MICI.0000008365.53111.a4

Fiorenza, S., Rifai, H.S., n.d. Review of MTBE Biodegradation and Bioremediation 36.

François, A., Mathis, H., Godefroy, D., Piveteau, P., Fayolle, F., Monot, F., 2002. Biodegradation of Methyl *tert* -Butyl Ether and Other Fuel Oxygenates by a New Strain, *Mycobacterium austroafricanum* IFP 2012. Appl. Environ. Microbiol. 68, 2754–2762. https://doi.org/10.1128/AEM.68.6.2754-2762.2002

Gan, S., Lau, E.V., Ng, H.K., 2009. Remediation of soils contaminated with polycyclic aromatic hydrocarbons (PAHs). J. Hazard. Mater. 172, 532–549. https://doi.org/10.1016/j.jhazmat.2009.07.118

Gan, X., Teng, Y., Zhao, L., Ren, W., Chen, W., Hao, J., Christie, P., Luo, Y., 2018. Influencing mechanisms of hematite on benzo(a)pyrene degradation by the PAH-degrading bacterium Paracoccus sp. Strain HPD-2: insight from benzo(a)pyrene bioaccessibility and bacteria activity. J. Hazard. Mater. 359, 348–355. https://doi.org/10.1016/j.jhazmat.2018.07.070

Geier, M.C., Chlebowski, A.C., Truong, L., Massey Simonich, S.L., Anderson, K.A., Tanguay, R.L., 2018. Comparative developmental toxicity of a comprehensive suite of polycyclic aromatic hydrocarbons. Arch. Toxicol. 92, 571–586. https://doi.org/10.1007/s00204-017-2068-9

Geng, S., Qin, W., Cao, W., Wang, Y., Ding, A., Zhu, Y., Fan, F., Dou, J., 2022. Pilot-scale bioaugmentation of polycyclic aromatic hydrocarbon (PAH)-contaminated soil using an indigenous bacterial consortium in soil-slurry bioreactors. Chemosphere 287, 132183. https://doi.org/10.1016/j.chemosphere.2021.132183

Gharibzadeh, F., Rezaei Kalantary, R., Nasseri, S., Esrafili, A., Azari, A., 2016. Reuse of polycyclic aromatic hydrocarbons (PAHs) contaminated soil washing effluent by bioaugmentation/biostimulation process. Sep. Purif. Technol. 168, 248–256. https://doi.org/10.1016/j.seppur.2016.05.022

Ghosal, D., Ghosh, S., Dutta, T.K., Ahn, Y., 2016. Current State of Knowledge in Microbial Degradation of Polycyclic Aromatic Hydrocarbons (PAHs): A Review. Front. Microbiol. 7. https://doi.org/10.3389/fmicb.2016.01369

Gitipour, S., Sorial, G.A., Ghasemi, S., Bazyari, M., 2018. Treatment technologies for PAH-contaminated sites: a critical review. Environ. Monit. Assess. 190, 546. https://doi.org/10.1007/s10661-018-6936-4

Gómez, V., Callao, M.P., 2008. Analytical applications of second-order calibration methods. Anal. Chim. Acta 627, 169–183. https://doi.org/10.1016/j.aca.2008.07.054

González, U., Schifter, I., Díaz, L., González-Macías, C., Mejía-Centeno, I., Sánchez-Reyna, G., 2018. Assessment of the use of ethanol instead of MTBE as an oxygenated compound in Mexican regular gasoline: combustion behavior and emissions. Environ. Monit. Assess. 190, 700. https://doi.org/10.1007/s10661-018-7083-7

Gosline, S.J.C., Kim, D.N., Pande, P., Thomas, D.G., Truong, L., Hoffman, P., Barton, M., Loftus, J., Moran, A., Hampton, S., Dowson, S., Franklin, L., Degnan, D., Anderson, L., Thessen, A., Tanguay, R.L., Anderson, K.A.,

Waters, K.M., 2023. The Superfund Research Program Analytics Portal: linking environmental chemical exposure to biological phenotypes. Sci. Data 10, 151. https://doi.org/10.1038/s41597-023-02021-5

Gröning, J.A.D., Kaschabek, S.R., Schlömann, M., Tischler, D., 2014. A mechanistic study on SMOB-ADP1: an NADH:flavin oxidoreductase of the two-component styrene monooxygenase of Acinetobacter baylyi ADP1. Arch. Microbiol. 196, 829–845. https://doi.org/10.1007/s00203-014-1022-y

Guarin, M., Faelens, R., Giusti, A., De Croze, N., Léonard, M., Cabooter, D., Annaert, P., de Witte, P., Ny, A., 2021a. Spatiotemporal imaging and pharmacokinetics of fluorescent compounds in zebrafish eleuthero-embryos after different routes of administration. Sci. Rep. 11, 12229. https://doi.org/10.1038/s41598-021-91612-6

Guarin, M., Ny, A., De Croze, N., Maes, J., Léonard, M., Annaert, P., de Witte, P., 2021b. Pharmacokinetics in Zebrafish Embryos (ZFE) Following Immersion and Intrayolk Administration: A Fluorescence-Based Analysis. Pharmaceuticals 14, 576. https://doi.org/10.3390/ph14060576

Halbach, K., Ulrich, N., Goss, K.-U., Seiwert, B., Wagner, S., Scholz, S., Luckenbach, T., Bauer, C., Schweiger, N., Reemtsma, T., 2020. Yolk Sac of Zebrafish Embryos as Backpack for Chemicals? Environ. Sci. Technol. 54, 10159–10169. https://doi.org/10.1021/acs.est.0c02068

Harris, C., Gedde, H., Semprini, L., Rochefort, S., Fogg, K., 2022. Development and Optimization of Poly(vinyl) Alcohol-Alginate Hydrogel Beads for Immobilization of Rhodococcus rhodochrous ATCC 21198 and Slow-Release Compounds. AICHE Annual Meeting, Phoenix, AZ, USA.

Hazen, T.C., 2010. Cometabolic bioremediation 17.

Hazrati, S., Rostami, R., Farjaminezhad, M., Fazlzadeh, M., 2016. Preliminary assessment of BTEX concentrations in indoor air of residential buildings and atmospheric ambient air in Ardabil, Iran. Atmos. Environ. 132, 91–97. https://doi.org/10.1016/j.atmosenv.2016.02.042

Hernandez-Perez, G., Fayolle, F., Vandecasteele, J.-P., 2001. Biodegradation of ethyl t -butyl ether (ETBE), methyl t -butyl ether (MTBE) and t -amyl methyl ether (TAME) by Gordonia terrae. Appl. Microbiol. Biotechnol. 55, 117–121. https://doi.org/10.1007/s002530000482

Hocinat, A., Boudemagh, A., Ali-Khodja, H., Medjemadj, M., 2020. Aerobic degradation of BTEX compounds by Streptomyces species isolated from activated sludge and agricultural soils. Arch. Microbiol. 202, 2481–2492. https://doi.org/10.1007/s00203-020-01970-4

Hogstedt, C., Jansson, C., Hugosson, M., Tinnerberg, H., Gustavsson, P., 2013. Cancer Incidence in a Cohort of Swedish Chimney Sweeps, 1958–2006. Am. J. Public Health 103, 1708–1714. https://doi.org/10.2105/AJPH.2012.300860

House, A.J., Hyman, M.R., 2010. Effects of gasoline components on MTBE and TBA cometabolism by Mycobacterium austroafricanum JOB5. Biodegradation 21, 525–541. https://doi.org/10.1007/s10532-009-9321-8

Hristova, K., Gebreyesus, B., Mackay, D., Scow, K.M., 2003. Naturally Occurring Bacteria Similar to the Methyl *tert* -Butyl Ether (MTBE)-Degrading Strain

PM1 Are Present in MTBE-Contaminated Groundwater. Appl. Environ. Microbiol. 69, 2616–2623. https://doi.org/10.1128/AEM.69.5.2616-2623.2003

Hu, X., Qiao, Y., Chen, L.-Q., Du, J.-F., Fu, Y.-Y., Wu, S., Huang, L., 2020. Enhancement of solubilization and biodegradation of petroleum by biosurfactant from *Rhodococcus erythropolis* HX-2. Geomicrobiol. J. 37, 159–169. https://doi.org/10.1080/01490451.2019.1678702

Hu, Y., Zhang, H., Zhao, D., 2021. Transform method in three-dimensional fluorescence spectra for direct reflection of internal molecular properties in rapid water contaminant analysis. Spectrochim. Acta. A. Mol. Biomol. Spectrosc. 250, 119376. https://doi.org/10.1016/j.saa.2020.119376

Huguenot, D., Mousset, E., van Hullebusch, E.D., Oturan, M.A., 2015. Combination of surfactant enhanced soil washing and electro-Fenton process for the treatment of soils contaminated by petroleum hydrocarbons. J. Environ. Manage. 153, 40–47. https://doi.org/10.1016/j.jenvman.2015.01.037

Huizenga, J.M., Semprini, L., 2023a. Influence of growth substrate and contaminant mixtures on the degradation of BTEX and MTBE by Rhodococcus rhodochrous ATCC strain 21198. Biodegradation. https://doi.org/10.1007/s10532-023-10037-2

Huizenga, J.M., Semprini, L., 2023b. Fluorescent spectroscopy paired with parallel factor analysis for quantitative monitoring of phenanthrene biodegradation and metabolite formation. Chemosphere 316, 137771. https://doi.org/10.1016/j.chemosphere.2023.137771

Hung, C.-M., Chen, C.-W., Huang, C.-P., Cheng, J.-W., Dong, C.-D., 2022a. Algae-derived metal-free boron-doped biochar as an efficient bioremediation pretreatment for persistent organic pollutants in marine sediments. J. Clean. Prod. 336, 130448. https://doi.org/10.1016/j.jclepro.2022.130448

Hung, C.-M., Chen, C.-W., Huang, C.-P., Cheng, J.-W., Dong, C.-D., 2022b. Algae-derived metal-free boron-doped biochar as an efficient bioremediation pretreatment for persistent organic pollutants in marine sediments. J. Clean. Prod. 336, 130448. https://doi.org/10.1016/j.jclepro.2022.130448

Imam, A., Kumar Suman, S., Kanaujia, P.K., Ray, A., 2022. Biological machinery for polycyclic aromatic hydrocarbons degradation: A review. Bioresour. Technol. 343, 126121. https://doi.org/10.1016/j.biortech.2021.126121

Inoue, D., Tsunoda, T., Yamamoto, N., Ike, M., Sei, K., 2018. 1,4-Dioxane degradation characteristics of Rhodococcus aetherivorans JCM 14343. Biodegradation 29, 301–310. https://doi.org/10.1007/s10532-018-9832-2

Jeong, E., Hirai, M., Shoda, M., 2008. Removal of o-xylene using biofilter inoculated with Rhodococcus sp. BTO62. J. Hazard. Mater. 152, 140–147. https://doi.org/10.1016/j.jhazmat.2007.06.078

Jin, D., Jiang, X., Jing, X., Ou, Z., 2007. Effects of concentration, head group, and structure of surfactants on the degradation of phenanthrene. J. Hazard. Mater. 144, 215–221. https://doi.org/10.1016/j.jhazmat.2006.10.012

Jin, J.-N., Yao, J., Zhang, Q.-Y., Yu, C., Chen, P., Liu, W.-J., Peng, D.-N., Choi, M.M.F., 2015. An integrated approach of bioassay and molecular docking to study the dihydroxylation mechanism of pyrene by naphthalene dioxygenase

in Rhodococcus sp. ustb-1. Chemosphere 128, 307–313. https://doi.org/10.1016/j.chemosphere.2015.02.012

Jung, I.-G., Park, C.-H., n.d. Characteristics of Rhodococcus pyridinovorans PYJ-1 for the Biodegradation of Benzene, Toluene, m-Xylene (BTX), and Their Mixtures 3.

Juwarkar, A.A., Singh, S.K., Mudhoo, A., 2010. A comprehensive overview of elements in bioremediation. Rev. Environ. Sci. Biotechnol. 9, 215–288. https://doi.org/10.1007/s11157-010-9215-6

Kanick, S.C., Robinson, D.J., Sterenborg, H.J.C.M., Amelink, A., 2012. Extraction of intrinsic fluorescence from single fiber fluorescence measurements on a turbid medium. Opt. Lett. 37, 948. https://doi.org/10.1364/OL.37.000948

Kasi, M., Wadhawan, T., McEvoy, J., Padmanabhan, G., Khan, E., 2013. Effect of carbon source during enrichment on BTEX degradation by anaerobic mixed bacterial cultures. Biodegradation 24, 279–293. https://doi.org/10.1007/s10532-012-9586-1

Khodaei, K., Nassery, H.R., Asadi, M.M., Mohammadzadeh, H., Mahmoodlu, M.G., 2017. BTEX biodegradation in contaminated groundwater using a novel strain (Pseudomonas sp. BTEX-30). Int. Biodeterior. Biodegrad. 116, 234–242. https://doi.org/10.1016/j.ibiod.2016.11.001

Kim, D., Kim, Y.-S., Kim, S.-K., Kim, S.W., Zylstra, G.J., Kim, Y.M., Kim, E., 2002. Monocyclic Aromatic Hydrocarbon Degradation by *Rhodococcus* sp. Strain DK17. Appl. Environ. Microbiol. 68, 3270–3278. https://doi.org/10.1128/AEM.68.7.3270-3278.2002

Kim Oanh, N.T., Nghiem, L.H., Phyu, Y.L., 2002. Emission of Polycyclic Aromatic Hydrocarbons, Toxicity, and Mutagenicity from Domestic Cooking Using Sawdust Briquettes, Wood, and Kerosene. Environ. Sci. Technol. 36, 833–839. https://doi.org/10.1021/es011060n

Knecht, A.L., Goodale, B.C., Truong, L., Simonich, M.T., Swanson, A.J., Matzke, M.M., Anderson, K.A., Waters, K.M., Tanguay, R.L., 2013. Comparative developmental toxicity of environmentally relevant oxygenated PAHs. Toxicol. Appl. Pharmacol. 271, 266–275. https://doi.org/10.1016/j.taap.2013.05.006

Ko, S.-K., Chen, X., Yoon, J., Shin, I., 2011. Zebrafish as a good vertebrate model for molecular imaging using fluorescent probes. Chem. Soc. Rev. 40, 2120. https://doi.org/10.1039/c0cs00118j

Koga, H., Zeyen, R.J., Bushnell, W.R., Ahlstrand, G.G., 1988. Hypersensitive cell death, autofluorescence, and insoluble silicon accumulation in barley leaf epidermal cells under attack by Erysiphe graminis f. sp. hordei. Physiol. Mol. Plant Pathol. 32, 395–409. https://doi.org/10.1016/S0885-5765(88)80033-X

Kottegoda, S., Waligora, E., Hyman, M., 2015a. Metabolism of 2-Methylpropene (Isobutylene) by the Aerobic Bacterium Mycobacterium sp. Strain ELW1. Appl. Environ. Microbiol. 81, 1966–1976. https://doi.org/10.1128/AEM.03103-14

Kottegoda, S., Waligora, E., Hyman, M., 2015b. Metabolism of 2-Methylpropene (Isobutylene) by the Aerobic Bacterium Mycobacterium sp. Strain ELW1.

Appl. Environ. Microbiol. 81, 1966–1976. https://doi.org/10.1128/AEM.03103-14
Krivoruchko, A., Kuyukina, M., Ivshina, I., 2019. Advanced Rhodococcus Biocatalysts for Environmental Biotechnologies. Catalysts 9, 236. https://doi.org/10.3390/catal9030236
Krippaehne, K. (2018). Cometabolism of 1,4-Dioxane and Chlorinated Aliphatic Hydrocarbons by Pure Cultures of Rhodococcus rhodochrous 21198 and Mycobacterium ELW1 and in Groundwater Microcosms Fed Isobutane and Isobutene as Growth Substrates. (Master's Thesis). Oregon State University.
Krzyszczak, A., Czech, B., 2021. Occurrence and toxicity of polycyclic aromatic hydrocarbons derivatives in environmental matrices. Sci. Total Environ. 788, 147738. https://doi.org/10.1016/j.scitotenv.2021.147738
Kumar, M., Bolan, N.S., Hoang, S.A., Sawarkar, A.D., Jasemizad, T., Gao, B., Keerthanan, S., Padhye, L.P., Singh, L., Kumar, S., Vithanage, M., Li, Y., Zhang, M., Kirkham, M.B., Vinu, A., Rinklebe, J., 2021. Remediation of soils and sediments polluted with polycyclic aromatic hydrocarbons: To immobilize, mobilize, or degrade? J. Hazard. Mater. 420, 126534. https://doi.org/10.1016/j.jhazmat.2021.126534
Kuppusamy, S., Thavamani, P., Venkateswarlu, K., Lee, Y.B., Naidu, R., Megharaj, M., 2017. Remediation approaches for polycyclic aromatic hydrocarbons (PAHs) contaminated soils: Technological constraints, emerging trends and future directions. Chemosphere 168, 944–968. https://doi.org/10.1016/j.chemosphere.2016.10.115
Lakowicz, J.R., Shen, Y., D'Auria, S., Malicka, J., Fang, J., Gryczynski, Z., Gryczynski, I., 2002. Radiative Decay Engineering. Anal. Biochem. 301, 261–277. https://doi.org/10.1006/abio.2001.5503
Lamichhane, S., Bal Krishna, K.C., Sarukkalige, R., 2016. Polycyclic aromatic hydrocarbons (PAHs) removal by sorption: A review. Chemosphere 148, 336–353. https://doi.org/10.1016/j.chemosphere.2016.01.036
Latif, M.T., Abd Hamid, H.H., Ahamad, F., Khan, M.F., Mohd Nadzir, M.S., Othman, M., Sahani, M., Abdul Wahab, M.I., Mohamad, N., Uning, R., Poh, S.C., Fadzil, M.F., Sentian, J., Tahir, N.M., 2019. BTEX compositions and its potential health impacts in Malaysia. Chemosphere 237, 124451. https://doi.org/10.1016/j.chemosphere.2019.124451
Lawal, A.T., 2017. Polycyclic aromatic hydrocarbons. A review. Cogent Environ. Sci. 3, 1339841. https://doi.org/10.1080/23311843.2017.1339841
Lee, E.-H., Cho, K.-S., 2009. Effect of substrate interaction on the degradation of methyl tert-butyl ether, benzene, toluene, ethylbenzene, and xylene by Rhodococcus sp. J. Hazard. Mater. 167, 669–674. https://doi.org/10.1016/j.jhazmat.2009.01.035
Lee, M., Kim, M.K., Singleton, I., Goodfellow, M., Lee, S.-T., 2006. Enhanced biodegradation of diesel oil by a newly identified Rhodococcus baikonurensis EN3 in the presence of mycolic acid. J. Appl. Microbiol. 100, 325–333. https://doi.org/10.1111/j.1365-2672.2005.02756.x
Leneva, N.A., Kolomytseva, M.P., Baskunov, B.P., Golovleva, L.A., 2009. Phenanthrene and anthracene degradation by microorganisms of the genus

Rhodococcus. Appl. Biochem. Microbiol. 45, 169–175. https://doi.org/10.1134/S0003683809020094

Li, H., Liu, Y., Chen, Q., Jin, L., Peng, R., 2023. Research Progress of Zebrafish Model in Aquatic Ecotoxicology. Water 15, 1735. https://doi.org/10.3390/w15091735

Li, S., Wang, D., Du, D., Qian, K., Yan, W., 2019a. Characterization of co-metabolic biodegradation of methyl *tert* -butyl ether by a *Acinetobacter* sp. strain. RSC Adv. 9, 38962–38972. https://doi.org/10.1039/C9RA09507A

Li, S., Wang, D., Du, D., Qian, K., Yan, W., 2019b. Characterization of co-metabolic biodegradation of methyl *tert* -butyl ether by a *Acinetobacter* sp. strain. RSC Adv. 9, 38962–38972. https://doi.org/10.1039/C9RA09507A

Li, Y., Wang, H., Xia, X., Zhai, Y., Lin, H., Wen, W., Wang, Z., 2018. Dissolved organic matter affects both bioconcentration kinetics and steady-state concentrations of polycyclic aromatic hydrocarbons in zebrafish (Danio rerio). Sci. Total Environ. 639, 648–656. https://doi.org/10.1016/j.scitotenv.2018.05.067

Li, Y., Yan, Y., Hu, D., Li, Z., Hao, A., Li, R., Wang, C., Xu, Y., Cao, J., Liu, Z., Peng, L., 2020. Source apportionment of atmospheric volatile aromatic compounds (BTEX) by stable carbon isotope analysis: A case study during heating period in Taiyuan, northern China. Atmos. Environ. 225, 117369. https://doi.org/10.1016/j.atmosenv.2020.117369

Liu, C.Y., Speitel, G.E., Georgiou, G., 2001. Kinetics of Methyl *t* -Butyl Ether Cometabolism at Low Concentrations by Pure Cultures of Butane-Degrading Bacteria. Appl. Environ. Microbiol. 67, 2197–2201. https://doi.org/10.1128/AEM.67.5.2197-2201.2001

Liu, F., Oturan, N., Zhang, H., Oturan, M.A., 2020. Soil washing in combination with electrochemical advanced oxidation for the remediation of synthetic soil heavily contaminated with diesel. Chemosphere 249, 126176. https://doi.org/10.1016/j.chemosphere.2020.126176

Liu, J., Zhang, A.-N., Liu, Y.-J., Liu, Z., Liu, Y., Wu, X.-J., 2021. Analysis of the mechanism for enhanced pyrene biodegradation based on the interactions between iron-ions and Rhodococcus ruber strain L9. Ecotoxicol. Environ. Saf. 225, 112789. https://doi.org/10.1016/j.ecoenv.2021.112789

Loerracher, A.-K., Braunbeck, T., 2021. Cytochrome P450-dependent biotransformation capacities in embryonic, juvenile and adult stages of zebrafish (Danio rerio)—a state-of-the-art review. Arch. Toxicol. 95, 2299–2334. https://doi.org/10.1007/s00204-021-03071-7

Lu, X.-Y., Zhang, T., Fang, H.H.-P., 2011. Bacteria-mediated PAH degradation in soil and sediment. Appl. Microbiol. Biotechnol. 89, 1357–1371. https://doi.org/10.1007/s00253-010-3072-7

Lubin, A., Otterstrom, J., Hoade, Y., Bjedov, I., Stead, E., Whelan, M., Gestri, G., Paran, Y., Payne, E., 2021. A versatile, automated and high-throughput drug screening platform for zebrafish embryos. Biol. Open 10, bio058513. https://doi.org/10.1242/bio.058513

Luo, A., Wu, Y.-R., Xu, Y., Kan, J., Qiao, J., Liang, L., Huang, T., Hu, Z., 2016. Characterization of a cytochrome P450 monooxygenase capable of high

molecular weight PAHs oxidization from Rhodococcus sp. P14. Process Biochem. 51, 2127–2133. https://doi.org/10.1016/j.procbio.2016.07.024

MacMichael, G.J., Brown, L.R., 1987. Role of Carbon Dioxide in Catabolism of Propane by " *Nocardia paraffinicum* " (*Rhodococcus rhodochrous*). Appl. Environ. Microbiol. 53, 65–69. https://doi.org/10.1128/aem.53.1.65-69.1987

Mahmood, M.E., 2013. Effect of Temperature Changes on Critical Micelle Concentration for Tween Series Surfactant.

Mahmoodsaleh, F., Roayaei Ardakani, M., 2021. Methyl tertiary butyl ether biodegradation by the bacterial consortium isolated from petrochemical wastewater and contaminated soils of Imam Khomeini Port Petrochemical Company (Iran). Bioremediation J. 1–11. https://doi.org/10.1080/10889868.2021.1927972

Mandrell, D., Truong, L., Jephson, C., Sarker, M.R., Moore, A., Lang, C., Simonich, M.T., Tanguay, R.L., 2012. Automated Zebrafish Chorion Removal and Single Embryo Placement: Optimizing Throughput of Zebrafish Developmental Toxicity Screens. SLAS Technol. 17, 66–74. https://doi.org/10.1177/2211068211432197

Marcé, R.M., Borrull, F., 2000. Solid-phase extraction of polycyclic aromatic compounds. J. Chromatogr. A 885, 273–290. https://doi.org/10.1016/S0021-9673(00)00428-3

Masih, A., Lall, A.S., Taneja, A., Singhvi, R., 2016. Inhalation exposure and related health risks of BTEX in ambient air at different microenvironments of a terai zone in north India. Atmos. Environ. 147, 55–66. https://doi.org/10.1016/j.atmosenv.2016.09.067

Mayevsky, A., Rogatsky, G.G., 2007. Mitochondrial function in vivo evaluated by NADH fluorescence: from animal models to human studies. Am. J. Physiol.-Cell Physiol. 292, C615–C640. https://doi.org/10.1152/ajpcell.00249.2006

Mehrotra, T., Dev, S., Banerjee, A., Chatterjee, A., Singh, R., Aggarwal, S., 2021. Use of immobilized bacteria for environmental bioremediation: A review. J. Environ. Chem. Eng. 9, 105920. https://doi.org/10.1016/j.jece.2021.105920

Mohan, S.V., Kisa, T., Ohkuma, T., Kanaly, R.A., Shimizu, Y., 2006. Bioremediation technologies for treatment of PAH-contaminated soil and strategies to enhance process efficiency. Rev. Environ. Sci. Biotechnol. 5, 347–374. https://doi.org/10.1007/s11157-006-0004-1

Mojiri, A., Zhou, J.L., Ohashi, A., Ozaki, N., Kindaichi, T., 2019. Comprehensive review of polycyclic aromatic hydrocarbons in water sources, their effects and treatments. Sci. Total Environ. 696, 133971. https://doi.org/10.1016/j.scitotenv.2019.133971

Mousset, E., Huguenot, D., Hullebusch, E.D.V., Oturan, N., Esposito, G., Oturan, M.A., n.d. A NEW INTEGRATED APPROACH TO REMOVE PAHs FROM HIGHLY CONTAMINATED SOIL: SOIL WASHING COMBINED TO ELECTRO-FENTON PROCESS AND POSSIBLE POST-BIOLOGICAL TREATMENT 9.

Mousset, E., Oturan, N., van Hullebusch, E.D., Guibaud, G., Esposito, G., Oturan, M.A., 2013. A new micelle-based method to quantify the Tween 80®

surfactant for soil remediation. Agron. Sustain. Dev. 33, 839–846. https://doi.org/10.1007/s13593-013-0140-2

Mulligan, C.N., Yong, R.N., Gibbs, B.F., 2001. Surfactant-enhanced remediation of contaminated soil: a review. Eng. Geol. 60, 371–380. https://doi.org/10.1016/S0013-7952(00)00117-4

Murnane, R.A., Chen, W., Hyman, M., Semprini, L., 2021. Long-term cometabolic transformation of 1,1,1-trichloroethane and 1,4-dioxane by Rhodococcus rhodochrous ATCC 21198 grown on alcohols slowly produced by orthosilicates. J. Contam. Hydrol. 240, 103796. https://doi.org/10.1016/j.jconhyd.2021.103796

Murphy, K.R., Stedmon, C.A., Graeber, D., Bro, R., 2013. Fluorescence spectroscopy and multi-way techniques. PARAFAC. Anal. Methods 5, 6557. https://doi.org/10.1039/c3ay41160e

Nadal, M., Wargent, J.J., Jones, K.C., Paul, N.D., Schuhmacher, M., Domingo, J.L., 2006. Influence of UV-B Radiation and Temperature on Photodegradation of PAHs: Preliminary Results. J Atmos Chem 55, 241–252. https://doi.org/10.1007/s10874-006-9037-7

Nahorniak, M.L., Booksh, K.S., 2006. Excitation-emission matrix fluorescence spectroscopy in conjunction with multiway analysis for PAH detection in complex matrices. The Analyst 131, 1308. https://doi.org/10.1039/b609875d

Nava, V., Morales, M., Revah, S., 2007. Cometabolism of methyl tert-butyl ether (MTBE) with alkanes. Rev. Environ. Sci. Biotechnol. 6, 339–352. https://doi.org/10.1007/s11157-006-9119-7

Nazari, M.T., Simon, V., Machado, B.S., Crestani, L., Marchezi, G., Concolato, G., Ferrari, V., Colla, L.M., Piccin, J.S., 2022. Rhodococcus: A promising genus of actinomycetes for the bioremediation of organic and inorganic contaminants. J. Environ. Manage. 323, 116220. https://doi.org/10.1016/j.jenvman.2022.116220

Olivieri, A.C., Arancibia, J.A., Muñoz de la Peña, A., Durán-Merás, I., Espinosa Mansilla, A., 2004. Second-Order Advantage Achieved with Four-Way Fluorescence Excitation−Emission−Kinetic Data Processed by Parallel Factor Analysis and Trilinear Least-Squares. Determination of Methotrexate and Leucovorin in Human Urine. Anal. Chem. 76, 5657–5666. https://doi.org/10.1021/ac0493065

Pantsyrnaya, T., Blanchard, F., Delaunay, S., Goergen, J.L., Guédon, E., Guseva, E., Boudrant, J., 2011. Effect of surfactants, dispersion and temperature on solubility and biodegradation of phenanthrene in aqueous media. Chemosphere 83, 29–33. https://doi.org/10.1016/j.chemosphere.2011.01.024

Partovinia, A., Naeimpoor, F., 2013. Phenanthrene biodegradation by immobilized microbial consortium in polyvinyl alcohol cryogel beads. Int. Biodeterior. Biodegrad. 85, 337–344. https://doi.org/10.1016/j.ibiod.2013.08.017

Partovinia, A., Rasekh, B., 2018. Review of the immobilized microbial cell systems for bioremediation of petroleum hydrocarbons polluted environments. Crit. Rev. Environ. Sci. Technol. 48, 1–38. https://doi.org/10.1080/10643389.2018.1439652

Patel, A.B., Shaikh, S., Jain, K.R., Desai, C., Madamwar, D., 2020. Polycyclic Aromatic Hydrocarbons: Sources, Toxicity, and Remediation Approaches. Front. Microbiol. 11. https://doi.org/10.3389/fmicb.2020.562813

Patton, E.E., Zon, L.I., 2001. The art and design of genetic screens: zebrafish. Nat. Rev. Genet. 2, 956–966. https://doi.org/10.1038/35103567

Peng, S., He, X., Pan, H., 2018a. Spectroscopic study on transformations of dissolved organic matter in coal-to-liquids wastewater under integrated chemical oxidation and biological treatment process. J. Environ. Sci. 70, 206–216. https://doi.org/10.1016/j.jes.2018.04.006

Peng, S., He, X., Pan, H., 2018b. Spectroscopic study on transformations of dissolved organic matter in coal-to-liquids wastewater under integrated chemical oxidation and biological treatment process. J. Environ. Sci. 70, 206–216. https://doi.org/10.1016/j.jes.2018.04.006

Peng, S., Wu, W., Chen, J., 2011. Removal of PAHs with surfactant-enhanced soil washing: Influencing factors and removal effectiveness. Chemosphere 82, 1173–1177. https://doi.org/10.1016/j.chemosphere.2010.11.076

Perraudin, E., Budzinski, H., Villenave, E., 2006. Kinetic Study of the Reactions of Ozone with Polycyclic Aromatic Hydrocarbons Adsorbed on Atmospheric Model Particles. J. Atmospheric Chem. 56, 57–82. https://doi.org/10.1007/s10874-006-9042-x

Phillips, D.H., 1999. Polycyclic aromatic hydrocarbons in the diet. Mutat. Res. Toxicol. Environ. Mutagen. 443, 139–147. https://doi.org/10.1016/S1383-5742(99)00016-2

Pinto, L.J., Moore, M.M., 2000. Release of polycyclic aromatic hydrocarbons from contaminated soils by surfactant and remediation of this effluent by *Penicillium* spp. Environ. Toxicol. Chem. 19, 1741–1748. https://doi.org/10.1002/etc.5620190706

Pruden, A., Sedran, M., Suidan, M., Venosa, A., 2003. Biodegradation of MTBE and BTEX in an aerobic fluidized bed reactor. Water Sci. Technol. 47, 123–128. https://doi.org/10.2166/wst.2003.0507

Pruden, A., Suidan, M., 2004. Effect of Benzene, Toluene, Ethylbenzene, and p-Xylene (BTEX) Mixture on Biodegradation of Methyl tert-Butyl Ether (MTBE) and tert-Butyl Alcohol (TBA) by Pure Culture UC1. Biodegradation 15, 213–227. https://doi.org/10.1023/B:BIOD.0000042900.29237.f1

Rasmussen, M.T., Saito, A.M., Hyman, M.R., Semprini, L., 2020. Co-encapsulation of slow release compounds and *Rhodococcus rhodochrous* ATCC 21198 in gellan gum beads to promote the long-term aerobic cometabolic transformation of 1,1,1-trichloroethane, *cis* -1,2-dichloroethene and 1,4-dioxane. Environ. Sci. Process. Impacts 22, 771–791. https://doi.org/10.1039/C9EM00607A

Raynal, M., Pruden, A., 2008. Aerobic MTBE biodegradation in the presence of BTEX by two consortia under batch and semi-batch conditions. Biodegradation 19, 269–282. https://doi.org/10.1007/s10532-007-9133-7

Rich, S. (2015) Kinetic Analysis of the Aerobic Degradation of Chlorinated Ethenes by the Mycobacterium ELW-1 and Chlorinated Ethanes and Ethenes by

Rhodococcus rhodochrous ATCC 21198. (Honor's Thesis). Oregon State University.

Rolston, H., Hyman, M., Semprini, L., 2022. Single-well push–pull tests evaluating isobutane as a primary substrate for promoting in situ cometabolic biotransformation reactions. Biodegradation 33, 349–371. https://doi.org/10.1007/s10532-022-09987-w

Rolston, H.M., Hyman, M.R., Semprini, L., 2019. Aerobic cometabolism of 1,4-dioxane by isobutane-utilizing microorganisms including Rhodococcus rhodochrous strain 21198 in aquifer microcosms: Experimental and modeling study. Sci. Total Environ. 694, 133688. https://doi.org/10.1016/j.scitotenv.2019.133688

Rutherford, J.W., Dawson-Elli, N., Manicone, A.M., Korshin, G.V., Novosselov, I.V., Seto, E., Posner, J.D., 2020. Excitation emission matrix fluorescence spectroscopy for combustion generated particulate matter source identification. Atmos. Environ. 220, 117065. https://doi.org/10.1016/j.atmosenv.2019.117065

Sairat, T., Homwuttiwong, S., Homwutthiwong, K., Ongwandee, M., 2015. Investigation of gasoline distributions within petrol stations: spatial and seasonal concentrations, sources, mitigation measures, and occupationally exposed symptoms. Environ. Sci. Pollut. Res. 22, 13870–13880. https://doi.org/10.1007/s11356-015-4615-3

Sakshi, Haritash, A.K., 2020. A comprehensive review of metabolic and genomic aspects of PAH-degradation. Arch. Microbiol. 202, 2033–2058. https://doi.org/10.1007/s00203-020-01929-5

Schrlau, J.E., Kramer, A.L., Chlebowski, A., Truong, L., Tanguay, R.L., Simonich, S.L.M., Semprini, L., 2017. Formation of Developmentally Toxic Phenanthrene Metabolite Mixtures by *Mycobacterium* sp. ELW1. Environ. Sci. Technol. 51, 8569–8578. https://doi.org/10.1021/acs.est.7b01377

Schwarz, F.P., Wasik, S.P., 1976. Fluorescence measurements of benzene, naphthalene, anthracene, pyrene, fluoranthene, and benzo[e]pyrene in water. Anal. Chem. 48, 524–528. https://doi.org/10.1021/ac60367a046

Schymanski, E.L., Singer, H.P., Slobodnik, J., Ipolyi, I.M., Oswald, P., Krauss, M., Schulze, T., Haglund, P., Letzel, T., Grosse, S., Thomaidis, N.S., Bletsou, A., Zwiener, C., Ibáñez, M., Portolés, T., de Boer, R., Reid, M.J., Onghena, M., Kunkel, U., Schulz, W., Guillon, A., Noyon, N., Leroy, G., Bados, P., Bogialli, S., Stipaničev, D., Rostkowski, P., Hollender, J., 2015. Non-target screening with high-resolution mass spectrometry: critical review using a collaborative trial on water analysis. Anal. Bioanal. Chem. 407, 6237–6255. https://doi.org/10.1007/s00216-015-8681-7

Sedran, M.A., Pruden, A., Wilson, G.J., Suidan, M.T., Venosa, A.D., 2002. Effect of BTEX on Degradation of MTBE and TBA by Mixed Bacterial Consortium. J. Environ. Eng. 128, 830–835. https://doi.org/10.1061/(ASCE)0733-9372(2002)128:9(830)

Seopela, M.P., Powers, L.C., Clark, C., Heyes, A., Gonsior, M., 2021a. Combined fluorescent measurements, parallel factor analysis and GC-mass spectrometry in evaluating the photodegradation of PAHS in freshwater systems.

Chemosphere 269, 129386. https://doi.org/10.1016/j.chemosphere.2020.129386

Seopela, M.P., Powers, L.C., Clark, C., Heyes, A., Gonsior, M., 2021b. Combined fluorescent measurements, parallel factor analysis and GC-mass spectrometry in evaluating the photodegradation of PAHS in freshwater systems. Chemosphere 269, 129386. https://doi.org/10.1016/j.chemosphere.2020.129386

Shankar, P., Geier, M.C., Truong, L., McClure, R.S., Pande, P., Waters, K.M., Tanguay, R.L., 2019. Coupling Genome-wide Transcriptomics and Developmental Toxicity Profiles in Zebrafish to Characterize Polycyclic Aromatic Hydrocarbon (PAH) Hazard. Int. J. Mol. Sci. 20, 2570. https://doi.org/10.3390/ijms20102570

Shields-Menard, S.A., Amirsadeghi, M., Sukhbaatar, B., Revellame, E., Hernandez, R., Donaldson, J.R., French, W.T., 2015. Lipid accumulation by *Rhodococcus rhodochrous* grown on glucose. J. Ind. Microbiol. Biotechnol. 42, 693–699. https://doi.org/10.1007/s10295-014-1564-7

Shields-Menard, S.A., Brown, S.D., Klingeman, D.M., Indest, K., Hancock, D., Wewalwela, J.J., French, W.T., Donaldson, J.R., n.d. Draft Genome Sequence of Rhodococcus rhodochrous Strain ATCC 21198. Genome Announc. 2.

Shim, H., Shin, E., Yang, S.-T., 2002. A continuous fibrous-bed bioreactor for BTEX biodegradation by a co-culture of Pseudomonas putida and Pseudomonas fluorescens. Adv. Environ. Res. 7, 203–216. https://doi.org/10.1016/S1093-0191(01)00132-0

Shukla, S.J., Huang, R., Austin, C.P., Xia, M., 2010. The future of toxicity testing: a focus on in vitro methods using a quantitative high-throughput screening platform. Drug Discov. Today 15, 997–1007. https://doi.org/10.1016/j.drudis.2010.07.007

Sipes, N.S., Padilla, S., Knudsen, T.B., 2011. Zebrafish-As an integrative model for twenty-first century toxicity testing. Birth Defects Res. Part C Embryo Today Rev. 93, 256–267. https://doi.org/10.1002/bdrc.20214

Smith, C.A., Hyman, M.R., 2004. Oxidation of Methyl *tert* -Butyl Ether by Alkane Hydroxylase in Dicyclopropylketone-Induced and *n* -Octane-Grown *Pseudomonas putida* GPo1. Appl. Environ. Microbiol. 70, 4544–4550. https://doi.org/10.1128/AEM.70.8.4544-4550.2004

Smith, C.A., O'Reilly, K.T., Hyman, M.R., 2003. Cometabolism ofMethyl *tertiary* Butyl Ether and Gaseous *n* -Alkanes by *Pseudomonas mendocina* KR-1 Grown on C_5 toC_8 *n* -Alkanes. Appl. Environ. Microbiol. 69, 7385–7394. https://doi.org/10.1128/AEM.69.12.7385-7394.2003

Song, G., Lu, C., Lin, J.-M., 2007. Application of surfactants and microemulsions to the extraction of pyrene and phenanthrene from soil with three different extraction methods. Anal. Chim. Acta 596, 312–318. https://doi.org/10.1016/j.aca.2007.06.004

Stedmon, C.A., Markager, S., 2005. Resolving the variability in dissolved organic matter fluorescence in a temperate estuary and its catchment using PARAFAC analysis. Limnol. Oceanogr. 50, 686–697. https://doi.org/10.4319/lo.2005.50.2.0686

Steffan, R.J., McClay, K., Vainberg, S., Condee, C.W., Zhang, D., 1997. Biodegradation of the gasoline oxygenates methyl tert-butyl ether, ethyl tert-butyl ether, and tert-amyl methyl ether by propane-oxidizing bacteria. Appl. Environ. Microbiol. 63, 4216–4222. https://doi.org/10.1128/aem.63.11.4216-4222.1997

Stern, M., Meagher, L., Savill, J., Haslett, C., 1992. Apoptosis in human eosinophils. Programmed cell death in the eosinophil leads to phagocytosis by macrophages and is modulated by IL-5. J. Immunol. 148, 3543–3549. https://doi.org/10.4049/jimmunol.148.11.3543

Sun, L., Chiu, M.-H., Xu, C., Lin, P., Schwehr, K.A., Bacosa, H., Kamalanathan, M., Quigg, A., Chin, W.-C., Santschi, P.H., 2018. The effects of sunlight on the composition of exopolymeric substances and subsequent aggregate formation during oil spills. Mar. Chem. 203, 49–54. https://doi.org/10.1016/j.marchem.2018.04.006

Taki, H., Syutsubo, K., Mattison, R.G., Harayama, S., 2006. Identification and characterization of o-xylene-degrading Rhodococcus spp. which were dominant species in the remediation of o-xylene-contaminated soils. Biodegradation 18, 17–26. https://doi.org/10.1007/s10532-005-9030-x

Taylor, A.E., Vajrala, N., Giguere, A.T., Gitelman, A.I., Arp, D.J., Myrold, D.D., Sayavedra-Soto, L., Bottomley, P.J., 2013. Use of Aliphatic *n* -Alkynes To Discriminate Soil Nitrification Activities of Ammonia-Oxidizing Thaumarchaea and Bacteria. Appl. Environ. Microbiol. 79, 6544–6551. https://doi.org/10.1128/AEM.01928-13

Titaley, I.A., Chlebowski, A., Truong, L., Tanguay, R.L., Massey Simonich, S.L., 2016. Identification and Toxicological Evaluation of Unsubstituted PAHs and Novel PAH Derivatives in Pavement Sealcoat Products. Environ. Sci. Technol. Lett. 3, 234–242. https://doi.org/10.1021/acs.estlett.6b00116

Titaley, I.A., Simonich, S.L.M., Larsson, M., 2020. Recent Advances in the Study of the Remediation of Polycyclic Aromatic Compound (PAC)-Contaminated Soils: Transformation Products, Toxicity, and Bioavailability Analyses. Environ. Sci. Technol. Lett. 7, 873–882. https://doi.org/10.1021/acs.estlett.0c00677

Trine, L.S.D., Davis, E.L., Roper, C., Truong, L., Tanguay, R.L., Simonich, S.L.M., 2019. Formation of PAH Derivatives and Increased Developmental Toxicity during Steam Enhanced Extraction Remediation of Creosote Contaminated Superfund Soil. Environ. Sci. Technol. 53, 4460–4469. https://doi.org/10.1021/acs.est.8b07231

Truong, L., Bugel, S.M., Chlebowski, A., Usenko, C.Y., Simonich, M.T., Simonich, S.L.M., Tanguay, R.L., 2016. Optimizing multi-dimensional high throughput screening using zebrafish. Reprod. Toxicol. 65, 139–147. https://doi.org/10.1016/j.reprotox.2016.05.015

Truong, L., Harper, S.L., Tanguay, R.L., 2011. Evaluation of Embryotoxicity Using the Zebrafish Model, in: Gautier, J.-C. (Ed.), Drug Safety Evaluation, Methods in Molecular Biology. Humana Press, Totowa, NJ, pp. 271–279. https://doi.org/10.1007/978-1-60761-849-2_16

Truong, L., Reif, D.M., St Mary, L., Geier, M.C., Truong, H.D., Tanguay, R.L., 2014. Multidimensional In Vivo Hazard Assessment Using Zebrafish. Toxicol. Sci. 137, 212–233. https://doi.org/10.1093/toxsci/kft235

Tu, Y.T., Ou, J.H., Tsang, D.C.W., Dong, C.D., Chen, C.W., Kao, C.M., 2018. Source identification and ecological impact evaluation of PAHs in urban river sediments: A case study in Taiwan. Chemosphere 194, 666–674. https://doi.org/10.1016/j.chemosphere.2017.12.008

Tziortzioti, R., 2016. Biological Effects of Sunlight, Ultraviolet Radiation, Visible Light, Infrared Radiation and Vitamin D for Health. ANTICANCER Res.

US EPA, 1997. Drinking Water Advisory on MTBE.

US EPA, 2009. National Primary Drinking Water Regulations. EPA 816-F-09-004.

US EPA, 2014. Priority Pollutants List. 40 CFR Part 423, Appendix A.

Vanderberg, L.A., Krieger-Grumbine, R., Taylor, M.N., 2000. Evidence for diverse oxidations in the catabolism of toluene by Rhodococcus rhodochrous strain OFS. Appl. Microbiol. Biotechnol. 53, 447–452. https://doi.org/10.1007/s002530051640

Wang, B., Liu, P., Tang, Y., Pan, H., Xu, X., Tang, R., 2010. Guarding Embryo Development of Zebrafish by Shell Engineering: A Strategy to Shield Life from Ozone Depletion. PLoS ONE 5, e9963. https://doi.org/10.1371/journal.pone.0009963

Wang, B., Xu, X., Yao, X., Tang, H., Ji, F., 2019. Degradation of phenanthrene and fluoranthene in a slurry bioreactor using free and Ca-alginate-immobilized Sphingomonas pseudosanguinis and Pseudomonas stutzeri bacteria. J. Environ. Manage. 249, 109388. https://doi.org/10.1016/j.jenvman.2019.109388

Wang, C., Mahrous, E.A., Lee, R.E., Vestling, M.M., Takayama, K., 2011. Novel Polyoxyethylene-Containing Glycolipids Are Synthesized in *Corynebacterium matruchotii* and *Mycobacterium smegmatis* Cultured in the Presence of Tween 80. J. Lipids 2011, 1–12. https://doi.org/10.1155/2011/676535

Wang, H., Li, Y., Xia, X., Xiong, X., 2018. Relationship between metabolic enzyme activities and bioaccumulation kinetics of PAHs in zebrafish (Danio rerio). J. Environ. Sci. 65, 43–52. https://doi.org/10.1016/j.jes.2017.03.037

Wang, H., Xia, X., Liu, R., Wang, Z., Lin, X., Muir, D.C.G., Wang, W.-X., 2020. Multicompartmental Toxicokinetic Modeling of Discrete Dietary and Continuous Waterborne Uptake of Two Polycyclic Aromatic Hydrocarbons by Zebrafish *Danio rerio*. Environ. Sci. Technol. 54, 1054–1065. https://doi.org/10.1021/acs.est.9b05513

Wang, Y., Nie, M., Diwu, Z., Chang, F., Nie, H., Zhang, B., Bai, X., Yin, Q., 2021a. Toxicity evaluation of the metabolites derived from the degradation of phenanthrene by one of a soil ubiquitous PAHs-degrading strain Rhodococcus qingshengii FF. J. Hazard. Mater. 415, 125657. https://doi.org/10.1016/j.jhazmat.2021.125657

Wang, Y., Nie, M., Diwu, Z., Chang, F., Nie, H., Zhang, B., Bai, X., Yin, Q., 2021b. Toxicity evaluation of the metabolites derived from the degradation of phenanthrene by one of a soil ubiquitous PAHs-degrading strain Rhodococcus

qingshengii FF. J. Hazard. Mater. 415, 125657. https://doi.org/10.1016/j.jhazmat.2021.125657

Warhurst, A.M., Clarke, K.F., Hill, R.A., Holt, R.A., Fewson, C.A., 1994. Metabolism of styrene by Rhodococcus rhodochrous NCIMB 13259. Appl. Environ. Microbiol. 60, 1137–1145. https://doi.org/10.1128/aem.60.4.1137-1145.1994

Wen, Y., Xu, Xiaoyi, Wang, B., He, Z., Bai, J., Chen, X., Cui, J., Xu, Xiaofang, 2021. PAHs biodegradation in soil washing effluent by native mixed bacteria embedded in polyvinyl alcohol-sodium alginate-nano alumina gel beads. J. Environ. Manage. 297, 113415. https://doi.org/10.1016/j.jenvman.2021.113415

Wongbunmak, A., Khiawjan, S., Suphantharika, M., Pongtharangkul, T., 2020. BTEX biodegradation by Bacillus amyloliquefaciens subsp. plantarum W1 and its proposed BTEX biodegradation pathways. Sci. Rep. 10. https://doi.org/10.1038/s41598-020-74570-3

Wu, J., Feld, M.S., Rava, R.P., 1993. Analytical model for extracting intrinsic fluorescence in turbid media. Appl. Opt. 32, 3585. https://doi.org/10.1364/AO.32.003585

Xu, X., Zhou, H., Chen, X., Wang, B., Jin, Z., Ji, F., 2019. Biodegradation potential of polycyclic aromatic hydrocarbons by immobilized Klebsiella sp. in soil washing effluent. Chemosphere 223, 140–147. https://doi.org/10.1016/j.chemosphere.2019.01.196

Yan, Y., Xing, F., Cao, J., Hu, Y., Li, L., Gao, Z., Jia, H., Miao, K., Shao, F., Deng, C.-X., Luo, K.Q., Lee, L.T. on, Liu, T.-M., 2023. Fluorescence intensity and lifetime imaging of lipofuscin-like autofluorescence for label-free predicting clinical drug response in cancer. Redox Biol. 59, 102578. https://doi.org/10.1016/j.redox.2022.102578

Yang, R., Zhao, N., Xiao, X., Yin, G., Yu, S., Liu, J., Liu, W., 2016. Quantifying PAHs in water by three-way fluorescence spectra and second-order calibration methods. Opt. Express 24, A1148. https://doi.org/10.1364/OE.24.0A1148

You, J., Du, M., Chen, H., Zhang, X., Zhang, S., Chen, J., Cheng, Z., Chen, D., Ye, J., 2018. BTEX degradation by a newly isolated bacterium: Performance, kinetics, and mechanism. Int. Biodeterior. Biodegrad. 129, 202–208. https://doi.org/10.1016/j.ibiod.2018.02.012

Yu, J., Luo, H., Yang, B., Wang, M., Gong, Y., Wang, P., Jiao, Y., Liang, T., Cheng, H., Ma, F., Gu, Q., Li, F., 2023. Risk Control Values and Remediation Goals for Benzo[*a*]pyrene in Contaminated Sites: Sectoral Characteristics, Temporal Trends, and Empirical Implications. Environ. Sci. Technol. 57, 2064–2074. https://doi.org/10.1021/acs.est.2c09553

Zampolli, J., Zeaiter, Z., Di Canito, A., Di Gennaro, P., 2019. Genome analysis and -omics approaches provide new insights into the biodegradation potential of Rhodococcus. Appl. Microbiol. Biotechnol. 103, 1069–1080. https://doi.org/10.1007/s00253-018-9539-7

Zebrafish as An Emerging Model: An Important Testing Platform for Biomedical Science, 2022. . J. Pharm. Negat. Results 13. https://doi.org/10.47750/pnr.2022.13.03.001

Zhang, M., Zhu, L., 2010. Effect of SDBS–Tween 80 mixed surfactants on the distribution of polycyclic aromatic hydrocarbons in soil–water system. J. Soils Sediments 10, 1123–1130. https://doi.org/10.1007/s11368-010-0215-5

Zhou, Z., Liu, Z., Guo, L., 2013. Chemical evolution of Macondo crude oil during laboratory degradation as characterized by fluorescence EEMs and hydrocarbon composition. Mar. Pollut. Bull. 66, 164–175. https://doi.org/10.1016/j.marpolbul.2012.09.028

APPENDICES

Appendix A: Supplementary Information for Manuscript 1

Title
Influence of Growth Substrate and Contaminant Mixtures on the Degradation of BTEX and MTBE by *Rhodococcus rhodochrous* ATCC Strain 21198
Submitted to the journal Biodegradation
Author Information

Juliana Huizenga[a] (ORCID: 0000-0002-1242-0948) huizengj@oregonstate.edu
Lewis Semprini[a] (ORCID: 0000-0002-9174-4464)
Lewis.Semprini@oregonstate.edu
[a] Oregon State University, School of Chemical, Biological, and Environmental Engineering
Corresponding Author: Lewis.Semprini@oregonstate.edu

Supplemental Information

Proposed B and T Metabolic Pathways

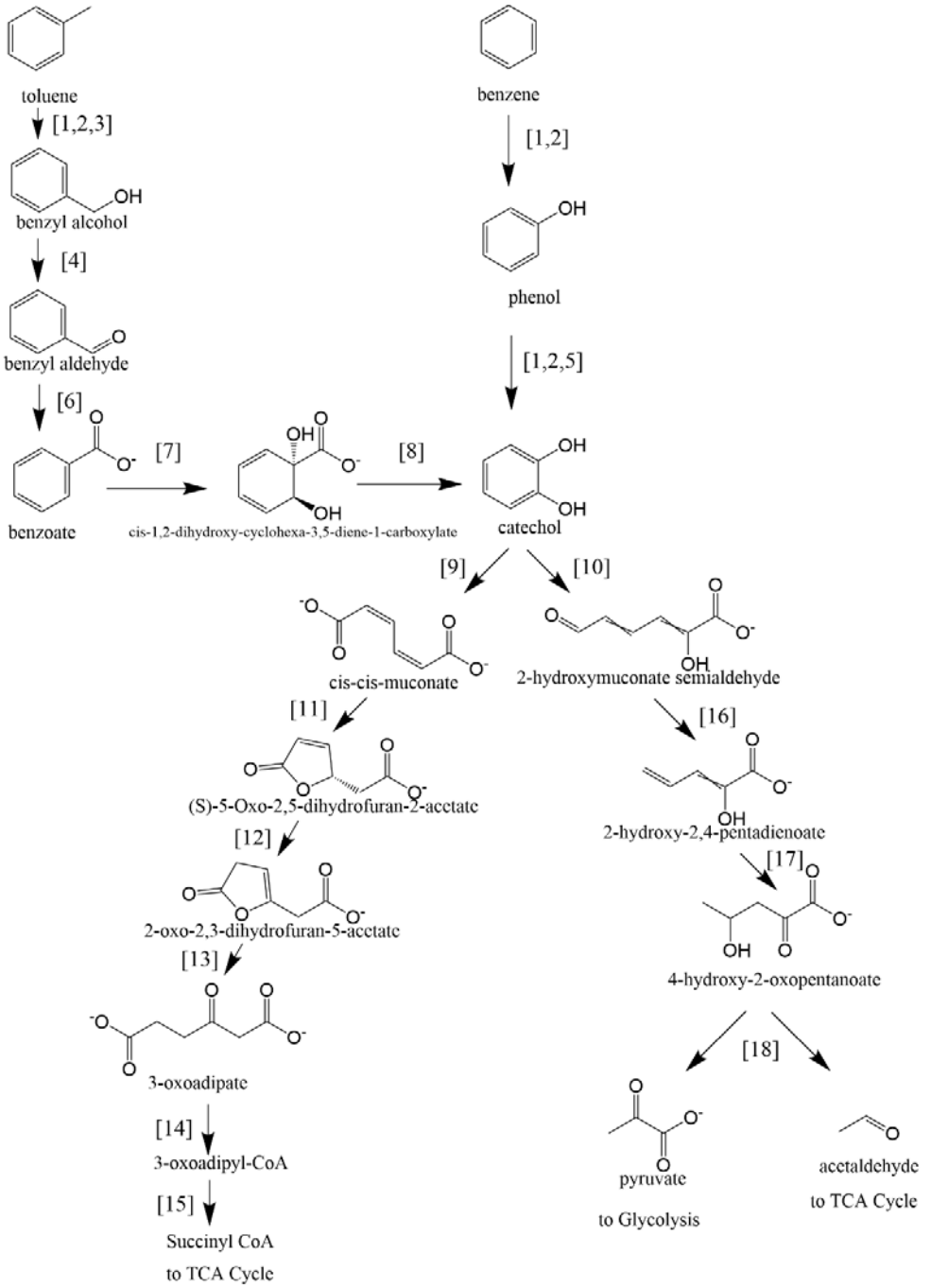

Figure A1. 21198's proposed metabolic pathways for benzene and toluene. Pathways leading to the production of dead-end products were omitted from this figure. Enzymes involved in each catalytic step appear in brackets and are as follows: [1] Methane MO, [2] Propane MO, [3] Methane/toluene/phenol hydroxylase, [4] Aryl-alcohol dehydrogenase, [5] Phenol-2-MO, [6] Benzaldehyde dehydrogenase, [7] Benzoate-1-2-dioxygenase, [8] 1,6-dihydroxycyclohexa-2,4-diene-1-carboxylate dehydrogenase, [9] Catechol-1,2-dioxygenase, [10] Catechol-2,3-dioxygenase, [11] Muconate cycloisomerase, [12] Muconate delta-isomerase, [13] 3-oxoadipate-enol-lactonase, [14] Succinate CoA Transferase, [15] Acetyl-CoA acetyltransferase, [16] Semialdehyde dehydrogenase, [17] 2-oxo-4-enoate hydratase, [18] 4-hydroxy-2-oxovalerate-aldolase.

Growth Experiment Substrate Additions

Table A1. Substrate volume added to 125 mL serum bottles for growth experiments. * Indicates addition of aqueous stock at its solubility limit rather than addition of the neat compound.

Growth Substrate	Volume Neat Stock Added (µL)
1-Butanol	17.9
2-Butanol	
Benzene	13.9
Toluene	
Ethylbenzene	13.6
o-Xylene	
m-Xylene	
p-Xylene	13.8
Phenol*	190.3
m-Cresol	14.2
p-Cresol	
Benzyl Alcohol	
Benzyl Aldehyde	16.9
Benzoic Acid	14.7
MTBE	19.9

Abiotic Controls

Table A2. Abiotic controls for individual contaminants tests reported as % remaining after experiment concluded ± range between duplicates.

Analyte	Growth Substrate		
	Isobutane	**1-Butanol**	**2-Butanol**
Benzene	110.72 ± 0.75	97.06 ± 0.29	100.86 ± 3.61
Toluene	90.23 ± 0.03	94.87 ± 8.15	92.75 ± 3.53
Ethylbenzene	91.32 ± 0.14	92.23 ± 7.84	94.02 ± 4.62
o-Xylene	109.69 ± 2.51	82.33 ± 7.99	100.58 ± 0.20
m-Xylene	97.36 ± 4.32	96.63 ± 6.69	89.01 ± 6.65
p-Xylene		86.09 ± 7.57	90.75 ± 8.98
MTBE	109.40 ± 6.07	95.06 ± 8.86	95.06 ± 8.86

Table A3. Abiotic controls for mixture experiments reported as % remaining after experiment concluded ± range between duplicates where applicable.

Analyte	BTEX Mixture Tests	BTEXM Mixture Tests	BTEXM Microcosms
Benzene	105.67 ± 1.87	96.08 ± 1.64	94.59 ± 1.93
Toluene	98.82 ± 0.98	93.65 ± 3.58	82.83 ± 5.22
Ethylbenzene	83.51 ± 0.01	90.65 ± 7.45	67.04 ± 9.64
o-Xylene	87.51 ± 4.00	92.88 ± 13.58	70.77 ± 9.31
MTBE		91.94 ± 8.72	94.16 ± 8.11
Isobutane			91.13
1-Butanol			82.96
2-Butanol			78.49

Henry's Coefficients

Table A4. Henry's coefficients used in mass calculations for headspace measurements. Constants were sourced from the Hazardous Substance Database (HSDB) and converted to dimensionless constants using the universal gas constant and appropriate temperature for experimental conditions.

Compound	Henry's Coefficient @ 20°C [-]	Henry's Coefficient @ 30°C [-]
Benzene	0.23	0.22
Toluene	0.27	0.27
Ethylbenzene	0.36	0.35
o-Xylene	0.22	0.21
m-Xylene		0.29
p-Xylene		0.28
Isobutane	49.47	47.83
O_2	0.05	0.05

Initial Contaminant Mass in Mixture Experiments

Table A5. Initial contaminant mass (μmol) of contaminants in contaminant mixture resting cell and growth batch experiments. Error represents standard deviation among triplicates. Filled cells indicate absence of compound from experimental set up.

Growth Substrate	Analyte	BTEX Mixture Tests	BTEXM Mixture Tests	BTEXM Microcosms
Isobutane	Benzene	13.04 ± 0.38	14.78 ± 0.35	10.23 ± 0.22
	Toluene	13.77 ± 1.03	16.37 ± 0.32	11.99 ± 0.56
	Ethylbenzene	8.61 ± 0.11	12.65 ± 0.38	7.72 ± 0.67
	o-Xylene	12.38 ± 0.52	18.31 ± 0.83	12.87 ± 0.96
	MTBE		13.20 ± 1.51	11.57 ± 0.09
	Isobutane			19.82 ± 1.26
1-Butanol	Benzene	7.34 ± 0.90	14.55 ± 0.04	15.37 ± 0.48
	Toluene	13.02 ± 1.44	16.35 ± 0.14	14.71 ± 0.73
	Ethylbenzene	5.44 ± 0.40	12.94 ± 0.32	8.88 ± 0.97
	o-Xylene	8.70 ± 0.32	19.33 ± 0.69	13.84 ± 0.63
	MTBE		10.51 ± 0.19	10.27 ± 0.43
	1-Butanol			13.71 ± 2.26
2-Butanol	Benzene	12.90 ± 0.56	13.29 ± 1.85	13.86 ± 0.08
	Toluene	12.10 ± 0.58	14.96 ± 1.87	11.49 ± 0.12
	Ethylbenzene	7.66 ± 0.18	11.77 ± 1.33	8.10 ± 0.24
	o-Xylene	10.90 ± 0.43	17.93 ± 0.99	12.06 ± 0.54
	MTBE		10.96 ± 0.44	13.99 ± 1.01
	2-Butanol			21.18 ± 1.76
No Substrate	Benzene			13.93 ± 0.45
	Toluene			11.95 ± 1.00
	Ethylbenzene			6.75 ± 1.52
	o-Xylene			10.04 ± 3.45
	MTBE			11.04 ± 0.50

Linear Regression Analysis

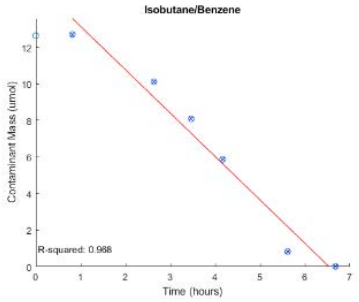

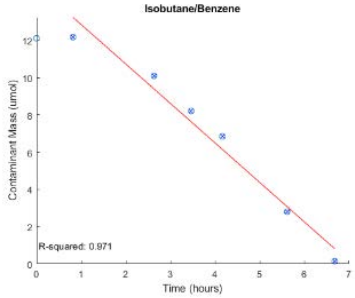

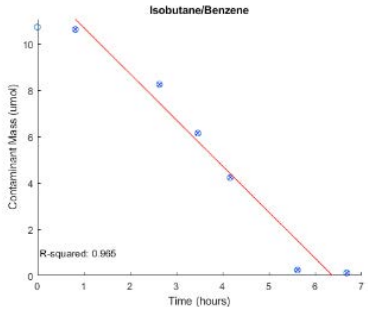

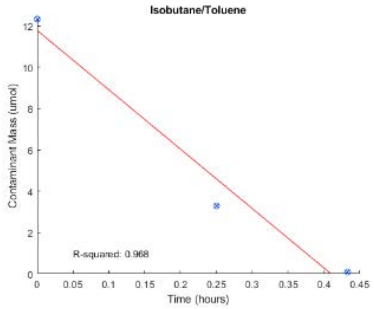

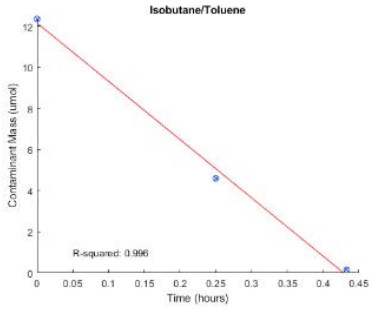

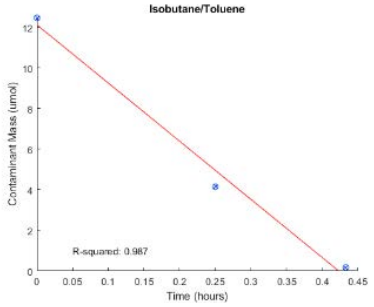

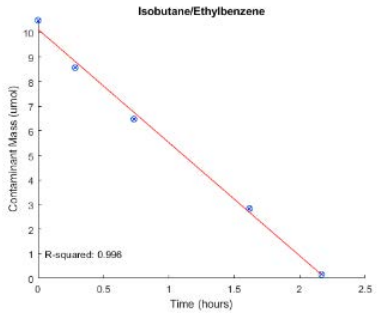
Isobutane/Ethylbenzene
Contaminant Mass (umol)
Time (hours)
R-squared: 0.998

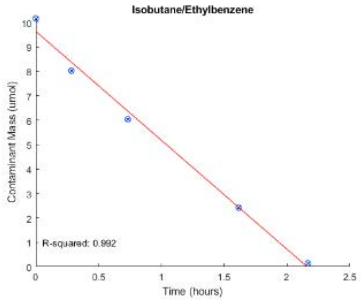
Isobutane/Ethylbenzene
Contaminant Mass (umol)
Time (hours)
R-squared: 0.992

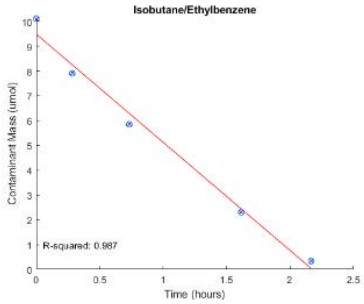
Isobutane/Ethylbenzene
Contaminant Mass (umol)
Time (hours)
R-squared: 0.987

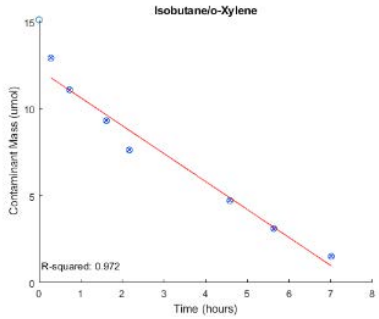
Isobutane/o-Xylene
Contaminant Mass (umol)
Time (hours)
R-squared: 0.972

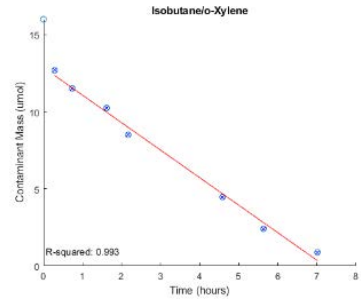
Isobutane/o-Xylene
Contaminant Mass (umol)
Time (hours)
R-squared: 0.993

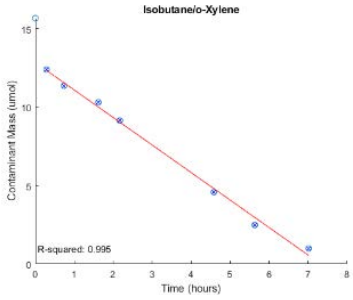
Isobutane/o-Xylene
Contaminant Mass (umol)
Time (hours)
R-squared: 0.995

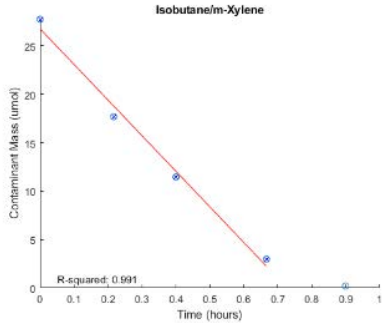
Isobutane/m-Xylene
Contaminant Mass (umol)
Time (hours)
R-squared: 0.991

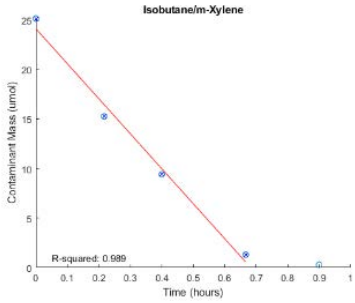
Isobutane/m-Xylene
Contaminant Mass (umol)
Time (hours)
R-squared: 0.989

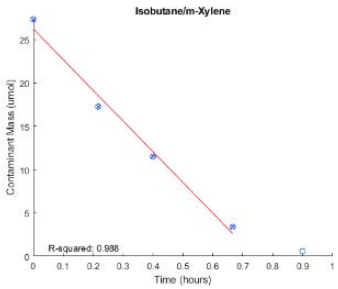
Isobutane/m-Xylene
Contaminant Mass (umol)
Time (hours)
R-squared: 0.988

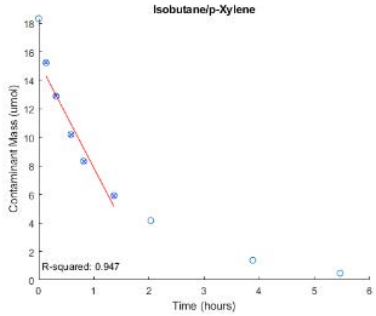
Isobutane/p-Xylene
Contaminant Mass (umol)
Time (hours)
R-squared: 0.947

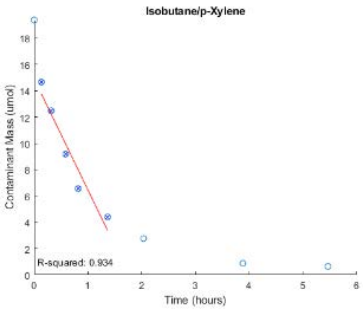
Isobutane/p-Xylene
Contaminant Mass (umol)
Time (hours)
R-squared: 0.934

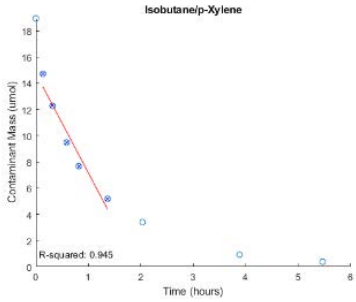
Isobutane/p-Xylene
Contaminant Mass (umol)
Time (hours)
R-squared: 0.945

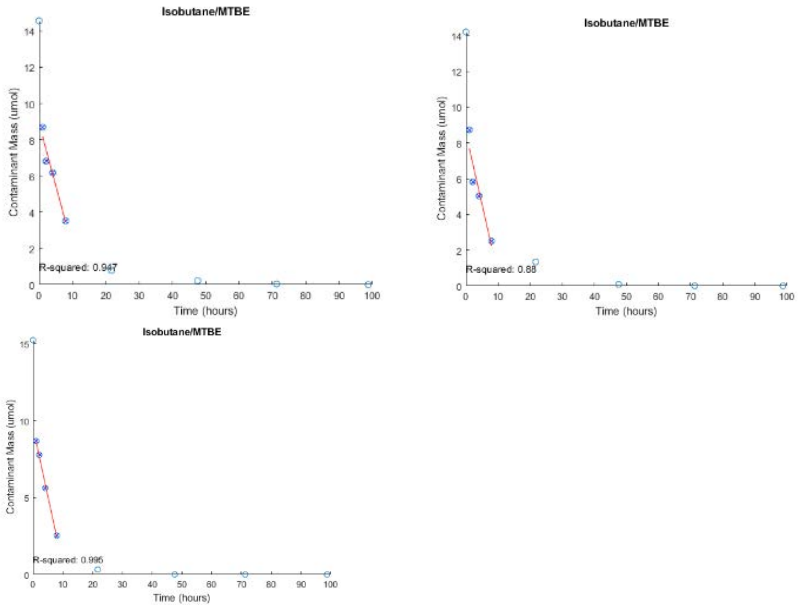

Figure A2a. Individual contaminant experiments with isobutane grown cells. Red lines indicate linear regions used to derive zero-order rate. Filled data points indicate data points included in linear regression model. R-squared value is shown in the bottom left corner of each plot.

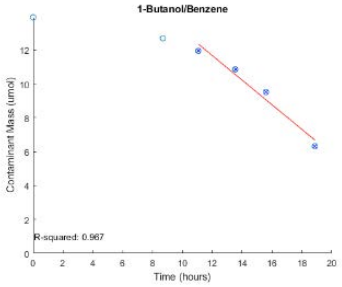
1-Butanol/Benzene
Contaminant Mass (umol)
Time (hours)
R-squared: 0.967

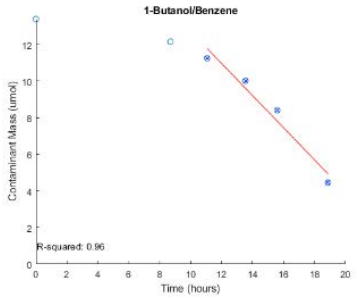
1-Butanol/Benzene
Contaminant Mass (umol)
Time (hours)
R-squared: 0.96

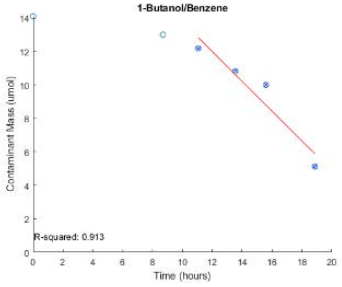
1-Butanol/Benzene
Contaminant Mass (umol)
Time (hours)
R-squared: 0.913

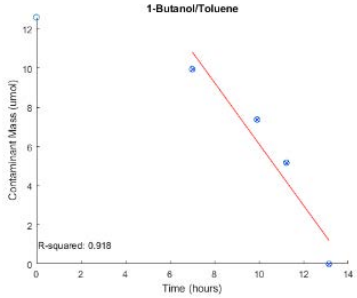
1-Butanol/Toluene
Contaminant Mass (umol)
Time (hours)
R-squared: 0.918

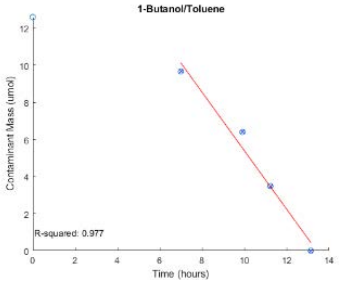
1-Butanol/Toluene
Contaminant Mass (umol)
Time (hours)
R-squared: 0.977

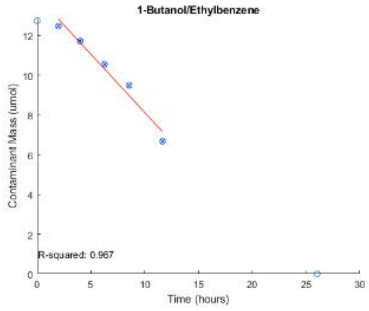
1-Butanol/Ethylbenzene
Contaminant Mass (umol)
Time (hours)
R-squared: 0.967

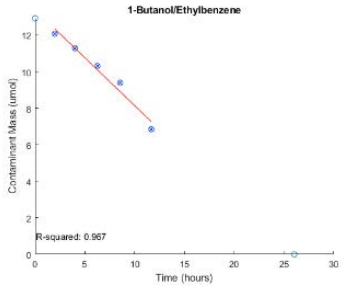
1-Butanol/Ethylbenzene
Contaminant Mass (umol)
Time (hours)
R-squared: 0.967

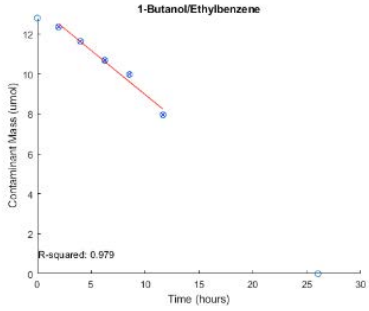
1-Butanol/Ethylbenzene
Contaminant Mass (umol)
Time (hours)
R-squared: 0.979

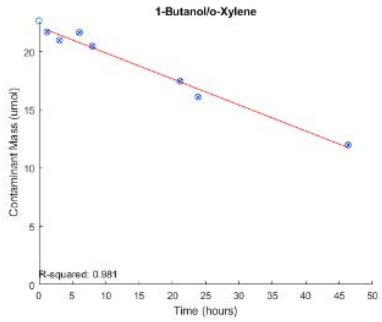
1-Butanol/o-Xylene
Contaminant Mass (umol)
Time (hours)
R-squared: 0.981

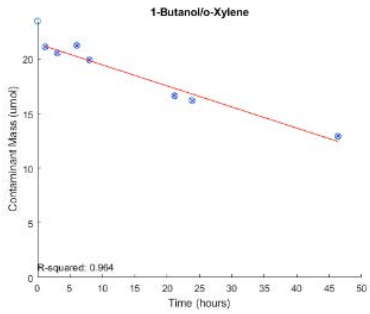
1-Butanol/o-Xylene
Contaminant Mass (umol)
Time (hours)
R-squared: 0.964

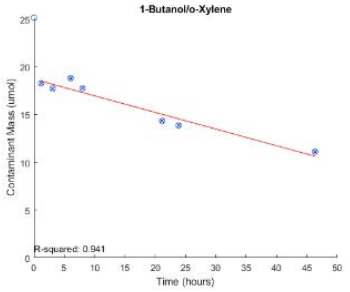
1-Butanol/o-Xylene
Contaminant Mass (umol)
Time (hours)
R-squared: 0.941

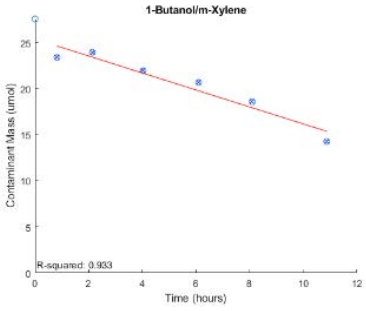
1-Butanol/m-Xylene
Contaminant Mass (umol)
Time (hours)
R-squared: 0.953

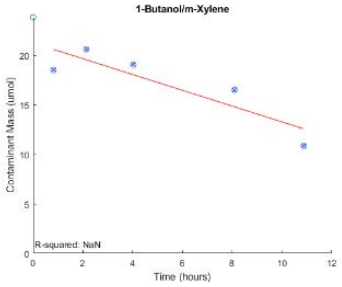
1-Butanol/m-Xylene
Contaminant Mass (umol)
Time (hours)
R-squared: NaN

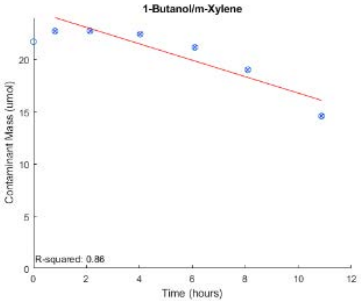
1-Butanol/m-Xylene
Contaminant Mass (umol)
Time (hours)
R-squared: 0.86

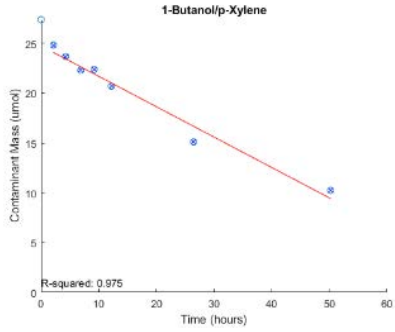
1-Butanol/p-Xylene
Contaminant Mass (umol)
Time (hours)
R-squared: 0.975

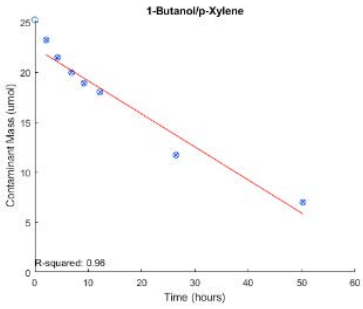
1-Butanol/p-Xylene
Contaminant Mass (umol)
Time (hours)
R-squared: 0.98

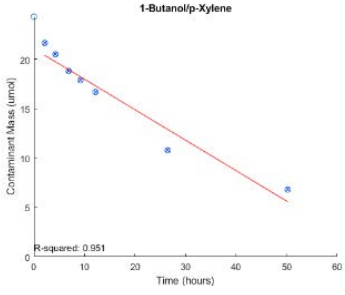
1-Butanol/p-Xylene
Contaminant Mass (umol)
Time (hours)
R-squared: 0.951

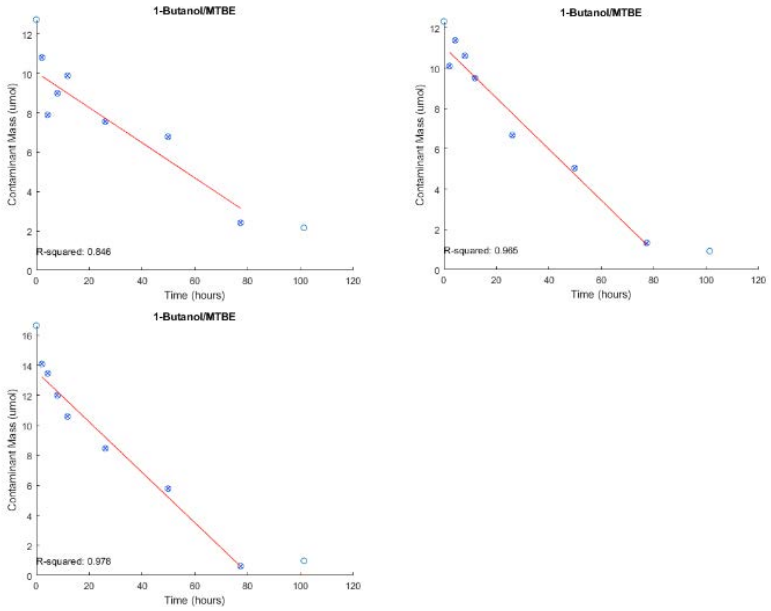

Figure A2b. Individual contaminant experiments with 1-butanol grown cells. Red lines indicate linear regions used to derive zero-order rate. Filled data points indicate data points included in linear regression model. R-squared value is shown in the bottom left corner of each plot.

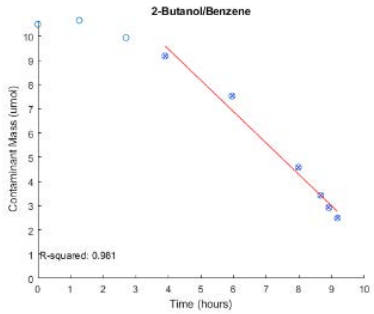
2-Butanol/Benzene
Contaminant Mass (umol)
Time (hours)
R-squared: 0.981

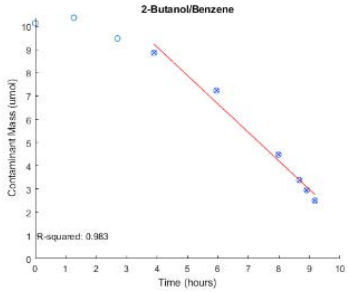
2-Butanol/Benzene
Contaminant Mass (umol)
Time (hours)
R-squared: 0.983

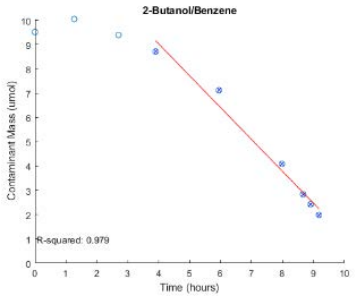
2-Butanol/Benzene
Contaminant Mass (umol)
Time (hours)
R-squared: 0.979

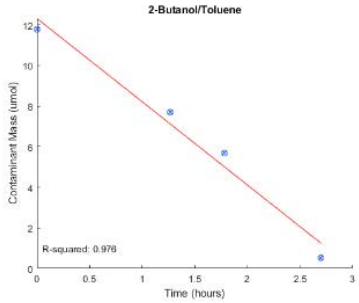
2-Butanol/Toluene
Contaminant Mass (umol)
Time (hours)
R-squared: 0.976

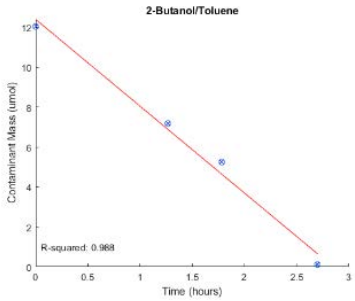
2-Butanol/Toluene
Contaminant Mass (umol)
Time (hours)
R-squared: 0.988

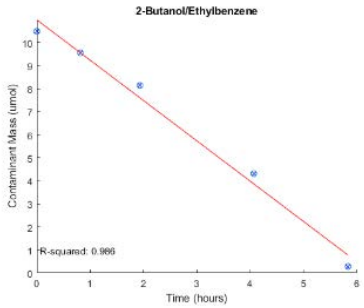
2-Butanol/Ethylbenzene
Contaminant Mass (umol)
Time (hours)
R-squared: 0.986

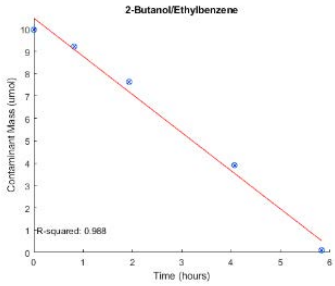
2-Butanol/Ethylbenzene
Contaminant Mass (umol)
Time (hours)
R-squared: 0.988

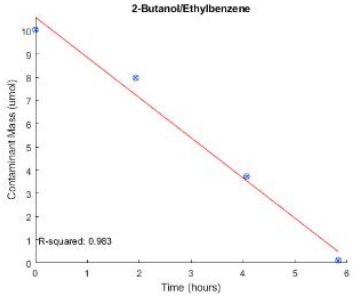
2-Butanol/Ethylbenzene
Contaminant Mass (umol)
Time (hours)
R-squared: 0.983

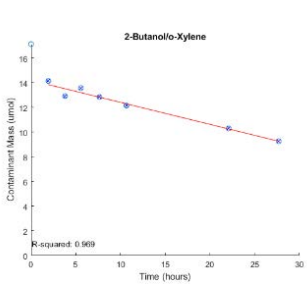
2-Butanol/o-Xylene
Contaminant Mass (umol)
Time (hours)
R-squared: 0.969

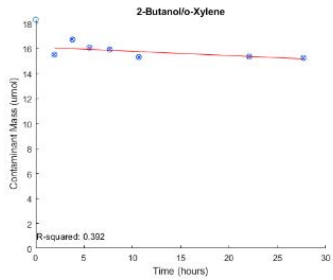
2-Butanol/o-Xylene
Contaminant Mass (umol)
Time (hours)
R-squared: 0.392

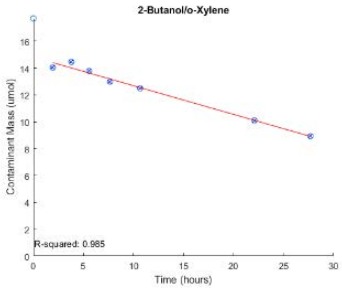
2-Butanol/o-Xylene
Contaminant Mass (umol)
Time (hours)
R-squared: 0.985

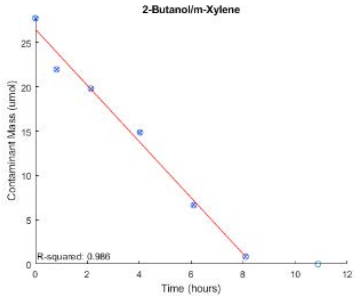
2-Butanol/m-Xylene
Contaminant Mass (umol)
Time (hours)
R-squared: 0.986

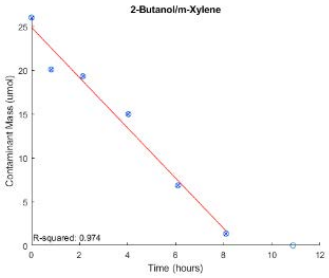
2-Butanol/m-Xylene
Contaminant Mass (umol)
Time (hours)
R-squared: 0.974

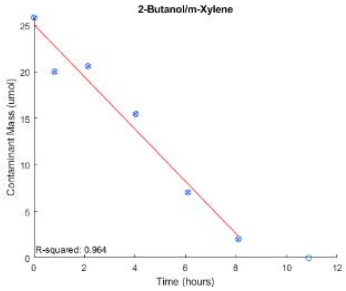
2-Butanol/m-Xylene
Contaminant Mass (umol)
Time (hours)
R-squared: 0.964

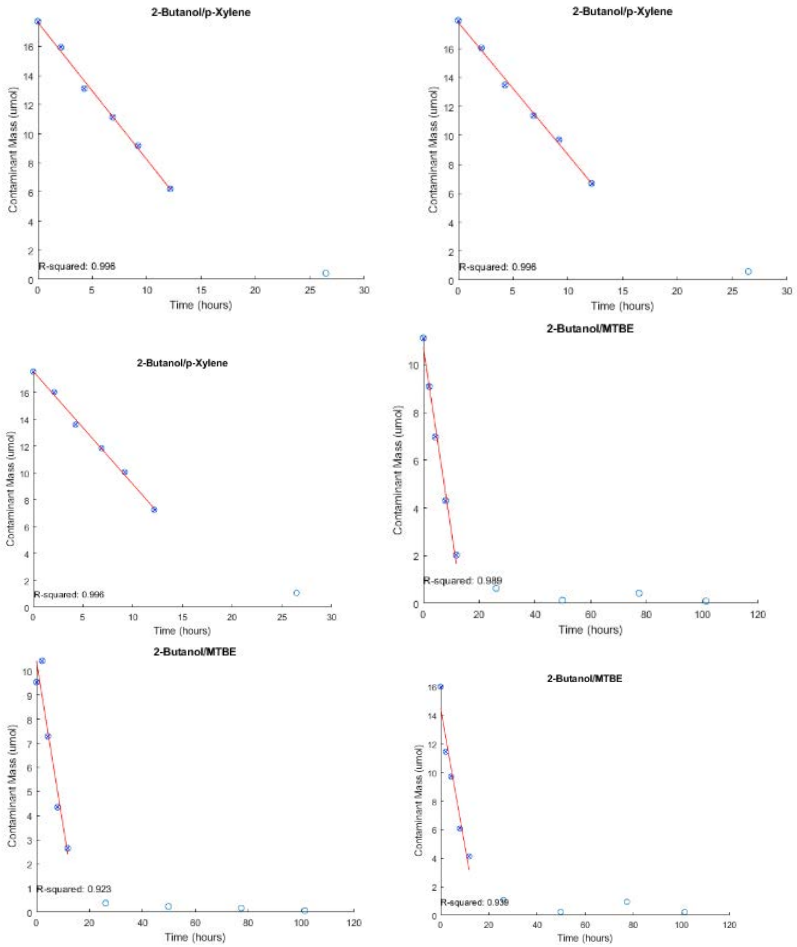

Figure A2c. Individual contaminant experiments with 2-butanol grown cells. Red lines indicate linear regions used to derive zero-order rate. Filled data points indicate data points included in linear regression model. R-squared value is shown in the bottom left corner of each plot.

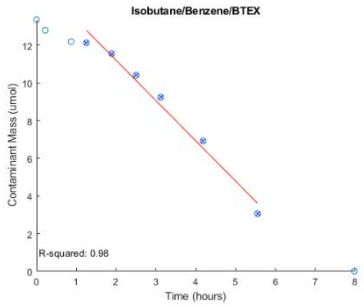
Isobutane/Benzene/BTEX
Contaminant Mass (umol)
Time (hours)
R-squared: 0.98

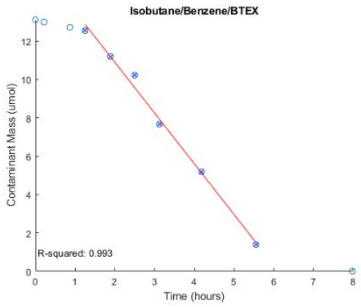
Isobutane/Benzene/BTEX
Contaminant Mass (umol)
Time (hours)
R-squared: 0.993

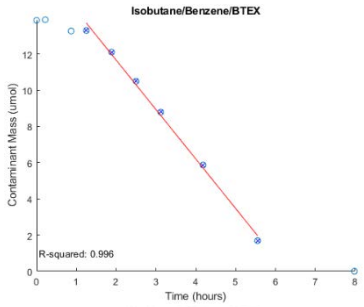
Isobutane/Benzene/BTEX
Contaminant Mass (umol)
Time (hours)
R-squared: 0.996

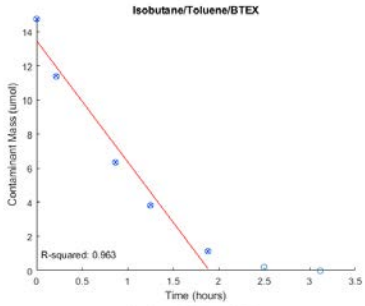
Isobutane/Toluene/BTEX
Contaminant Mass (umol)
Time (hours)
R-squared: 0.963

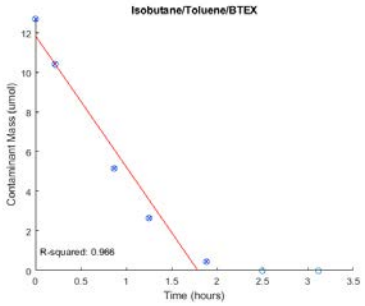
Isobutane/Toluene/BTEX
Contaminant Mass (umol)
Time (hours)
R-squared: 0.968

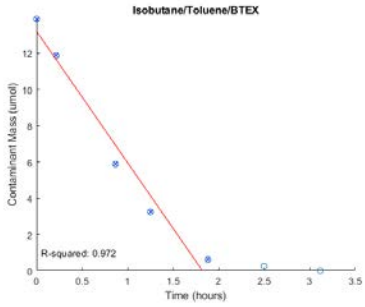
Isobutane/Toluene/BTEX
Contaminant Mass (umol)
Time (hours)
R-squared: 0.972

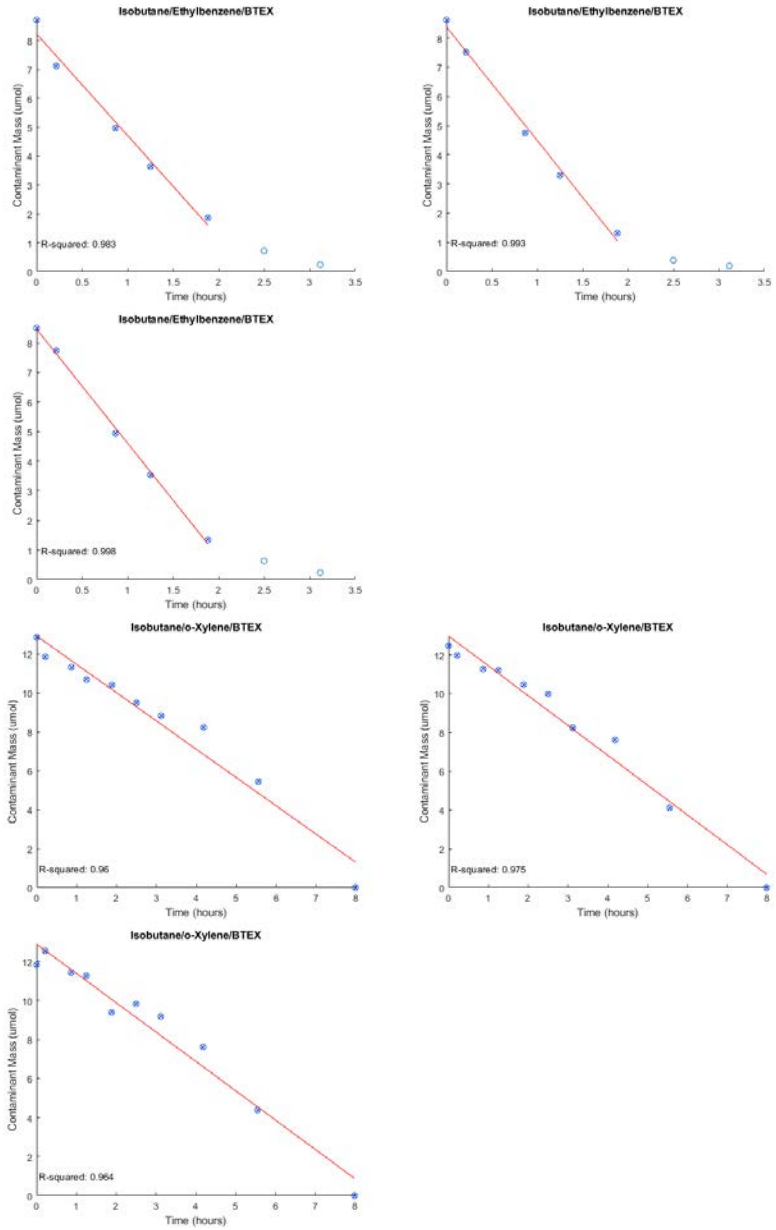

Figure A2d. BTEX mixture contaminant experiment with isobutane grown cells. Red lines indicate linear regions used to derive zero-order rate. Filled data points indicate data points included in linear regression model. R-squared value is shown in the bottom left corner of each plot.

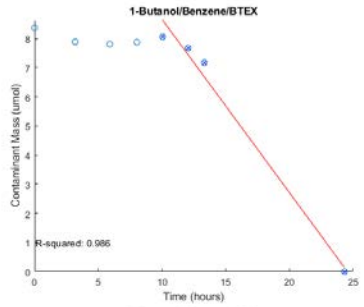
1-Butanol/Benzene/BTEX
Contaminant Mass (umol)
Time (hours)
R-squared: 0.986

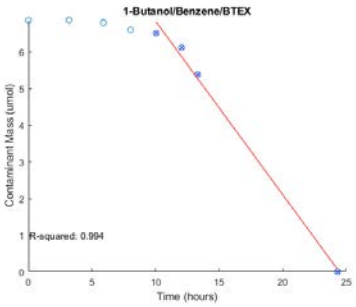
1-Butanol/Benzene/BTEX
Contaminant Mass (umol)
Time (hours)
R-squared: 0.994

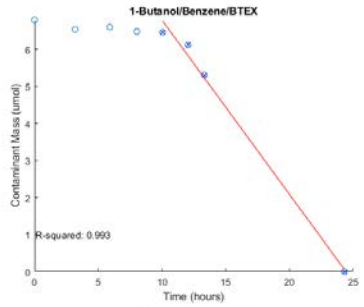
1-Butanol/Benzene/BTEX
Contaminant Mass (umol)
Time (hours)
R-squared: 0.993

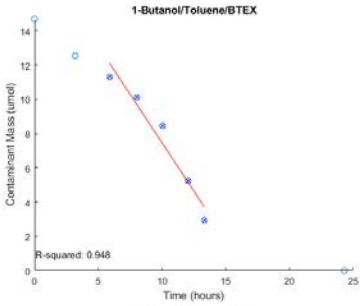
1-Butanol/Toluene/BTEX
Contaminant Mass (umol)
Time (hours)
R-squared: 0.948

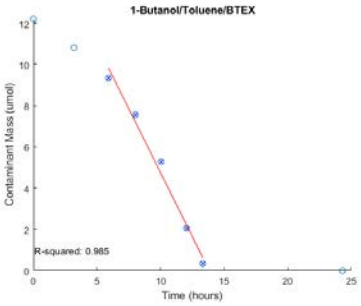
1-Butanol/Toluene/BTEX
Contaminant Mass (umol)
Time (hours)
R-squared: 0.985

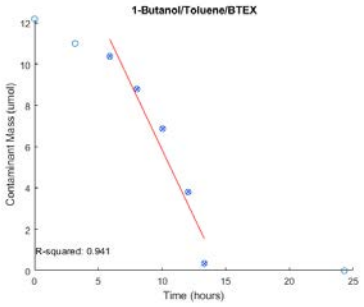
1-Butanol/Toluene/BTEX
Contaminant Mass (umol)
Time (hours)
R-squared: 0.941

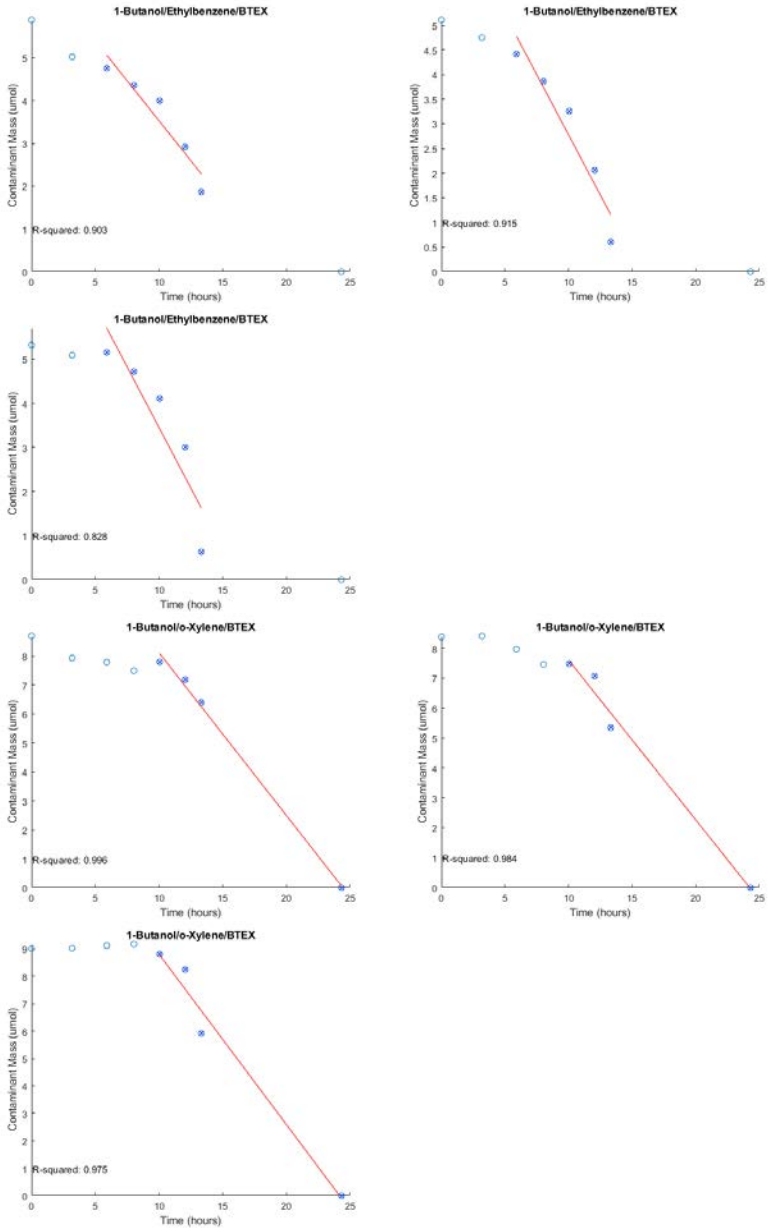

Figure A2e. BTEX mixture contaminant experiment with 1-butanol grown cells. Red lines indicate linear regions used to derive zero-order rate. Filled data points indicate data points included in linear regression model. R-squared value is shown in the bottom left corner of each plot.

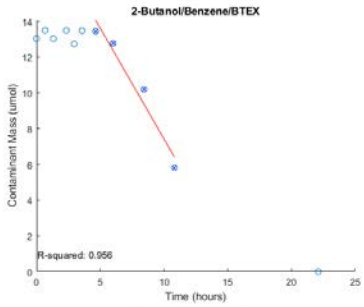
2-Butanol/Benzene/BTEX
Contaminant Mass (umol)
Time (hours)
R-squared: 0.956

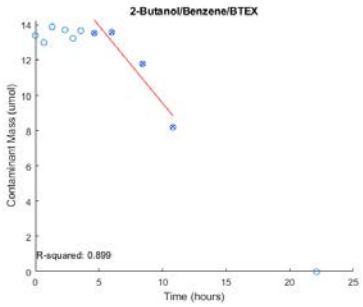
2-Butanol/Benzene/BTEX
Contaminant Mass (umol)
Time (hours)
R-squared: 0.899

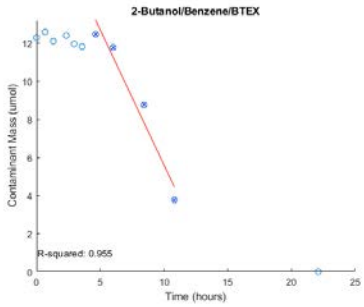
2-Butanol/Benzene/BTEX
Contaminant Mass (umol)
Time (hours)
R-squared: 0.955

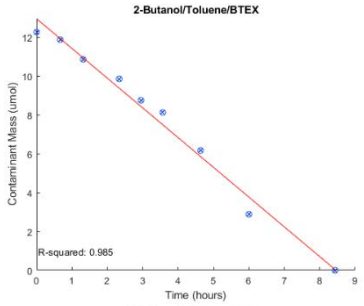
2-Butanol/Toluene/BTEX
Contaminant Mass (umol)
Time (hours)
R-squared: 0.985

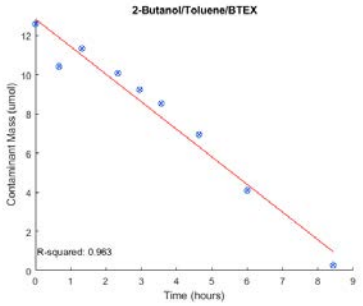
2-Butanol/Toluene/BTEX
Contaminant Mass (umol)
Time (hours)
R-squared: 0.963

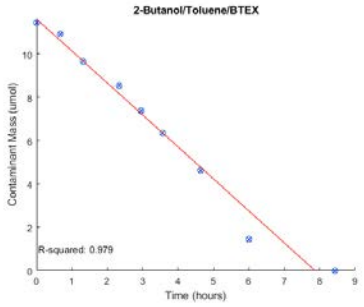
2-Butanol/Toluene/BTEX
Contaminant Mass (umol)
Time (hours)
R-squared: 0.979

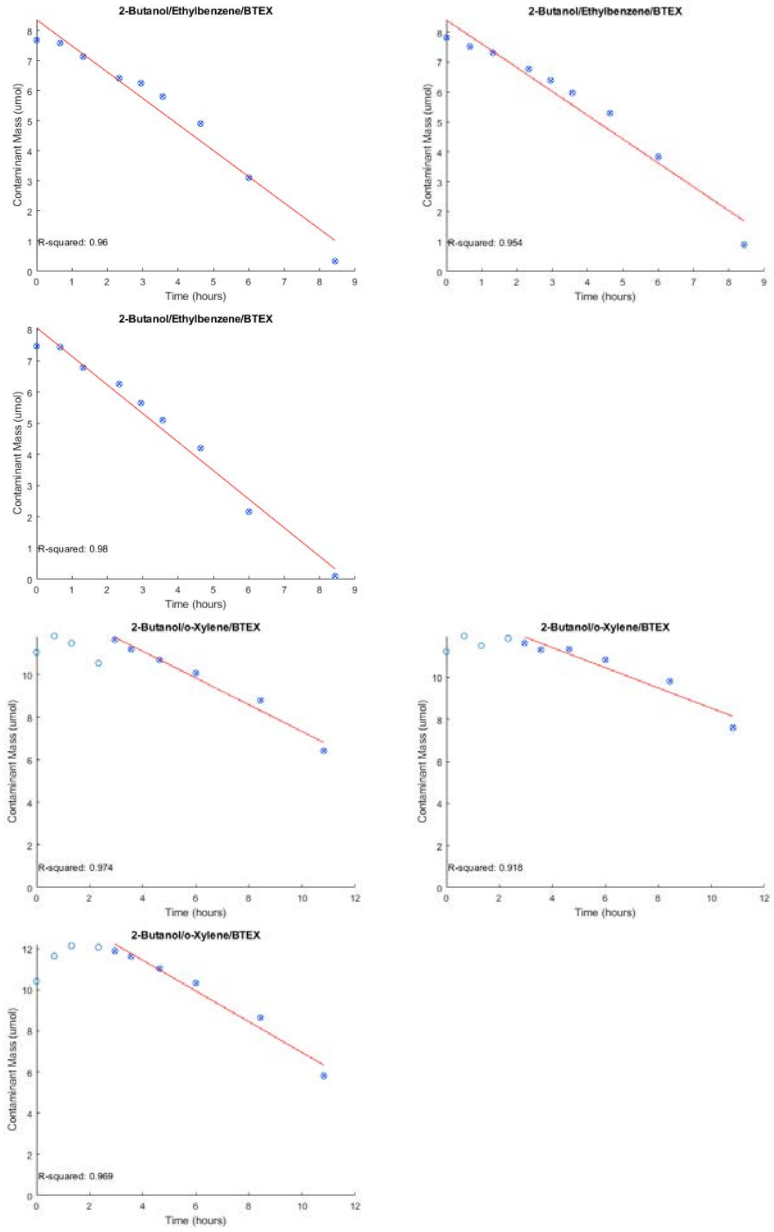

Figure A2f. BTEX mixture contaminant experiment with 2-butanol grown cells. Red lines indicate linear regions used to derive zero-order rate. Filled data points indicate data points included in linear regression model. R-squared value is shown in the bottom left corner of each plot.

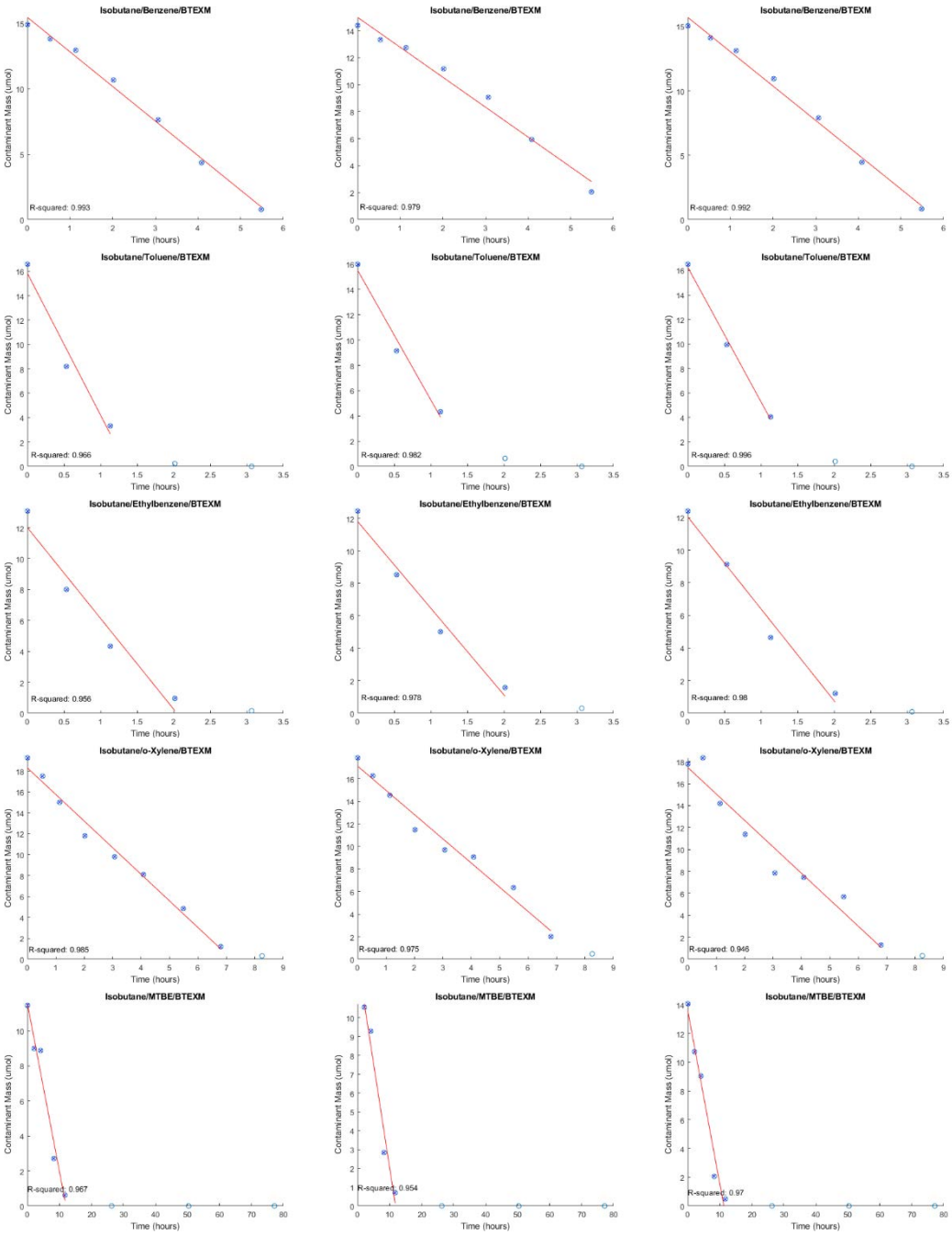

Figure A2g. BTEXM mixture contaminant experiment with isobutane grown cells. Red lines indicate linear regions used to derive zero-order rate. Filled data points indicate data points included in linear regression model. R-squared value is shown in the bottom left corner of each plot.

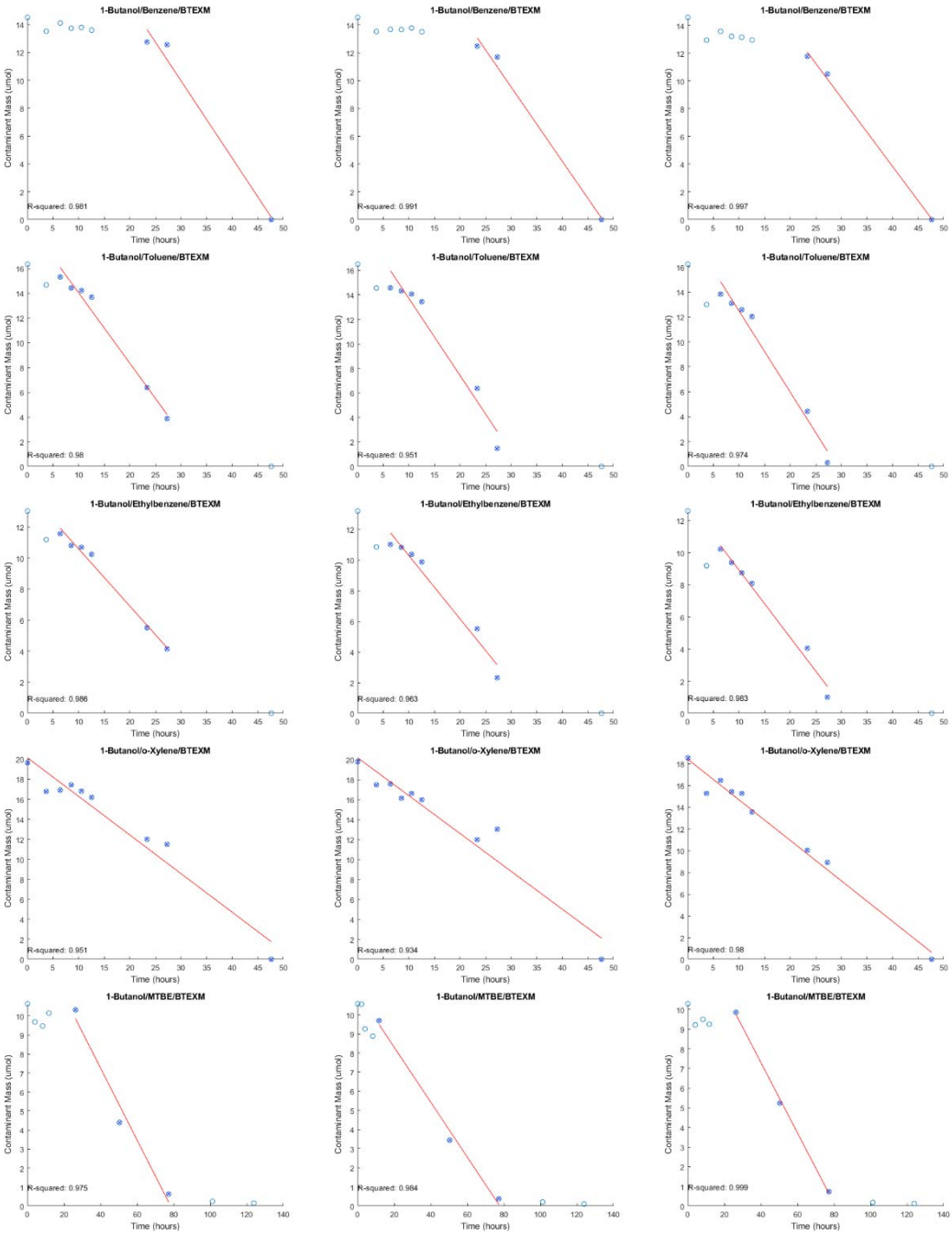

Figure A2h. BTEXM mixture contaminant experiment with 1-butanol grown cells. Red lines indicate linear regions used to derive zero-order rate. Filled data points indicate data points included in linear regression model. R-squared value is shown in the bottom left corner of each plot.

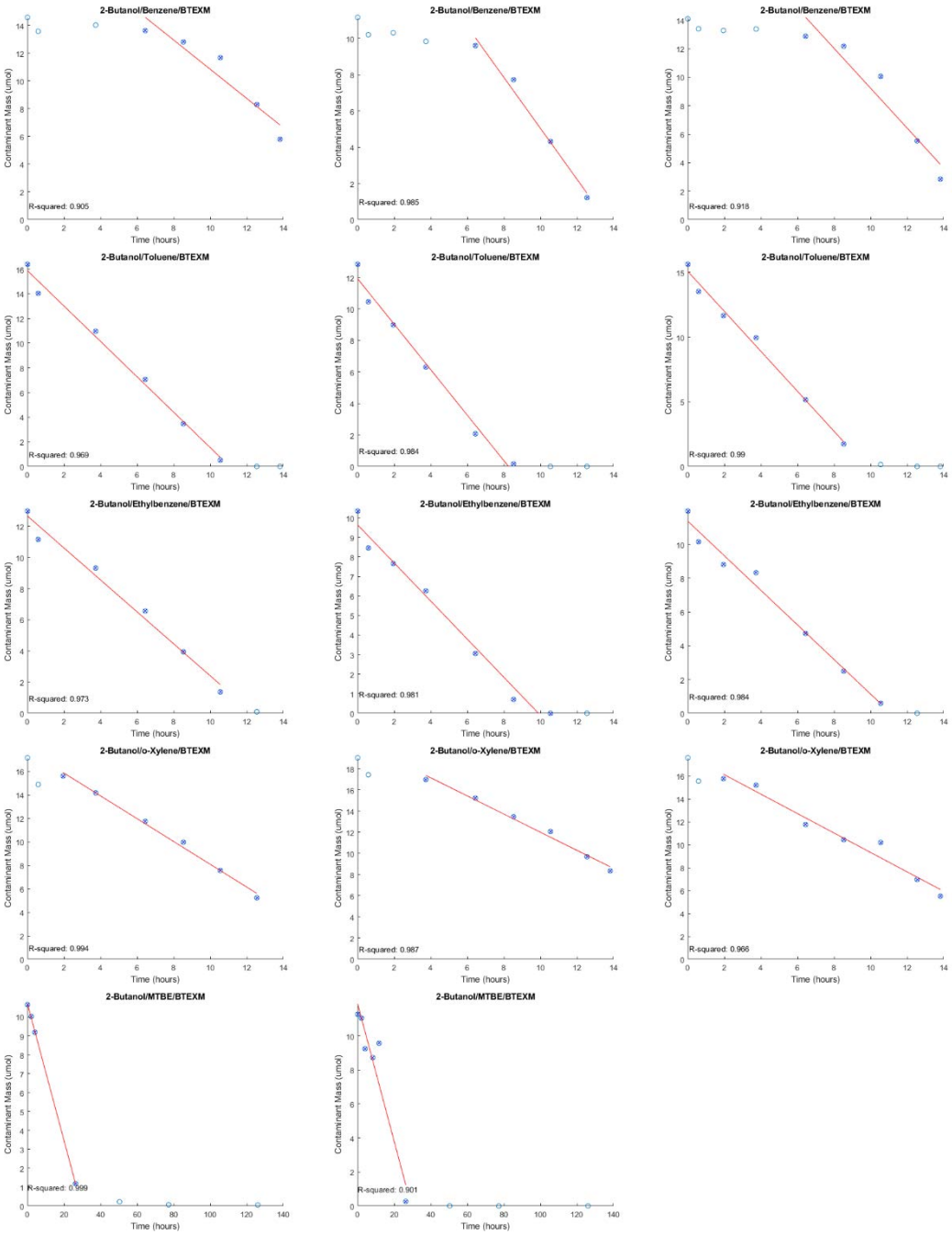

Figure A2i. BTEXM mixture contaminant experiment with 2-butanol grown cells. Red lines indicate linear regions used to derive zero-order rate. Filled data points indicate data points included in linear regression model. R-squared value is shown in the bottom left corner of each plot.

Growth Batch Experiments Optical Density and Oxygen Data

Table A6. Optical density measurements and Oxygen consumption of growth batch bottles on day 7 post-inoculation. Error bars represent standard deviation among triplicates.

Growth Substrate Added	OD_{600} (-)	O_2 Consumption (mg)
No Substrate	0.090 ± 0.003	27.76 ± 1.47
Isobutane	0.101 ± 0.008	33.44 ± 6.13
1-Butanol	0.121 ± 0.009	52.52 ± 1.70
2-Butanol	0.124 ± 0.026	69.08 ± 10.60
Abiotic Controls	0.072 ± 0.004	8.45 ± 1.19

Appendix B: Supplementary Information for Manuscript 2

Cell Culturing Methods

ELW1 was maintained as a pure culture on minimal salt media agar plates in a sterile airtight jar with isobutene supplied as the sole carbon and energy source. Growth reactors were prepared as described in Schrlau et al. (Schrlau et al., 2017). Briefly, an inoculum scraped from a minimal plate was added to a 720 mL glass bottle containing 300 mL of sterile mineral salt media (MSM) (Kottegoda et al. 2015) amended with either isobutene at 10% headspace volume. Growth reactors were incubated in the dark at 30ºC on a 150 RPM shaker table. Microbial growth was monitored via optical density absorption at 600 nm (OD_{600}) using a Thermo Scientific Orion Aquamate 8000 UV–Vis Spectrophotometer. When an OD_{600} of approximately 0.3 was reached, growth reactors were refreshed to enhance biomass growth. During refreshment, reactors were opened in a laminar flow hood to equilibrate with atmospheric oxygen and streaked on a tryptic soy glucose agar (TSGA) plate to confirm culture purity. A second addition of isobutene was added to growth reactors after reclosing them. Cells in late exponential growth phase were concentrated into a 50 mM sodium phosphate buffer via centrifugation the day after refreshing as described in Murnane et al. (Murnane et al., 2021). TSS analysis on the cell concentrate was performed according to AWWA standard protocol to determine the biomass concentration. Concentrated cell solutions were stored at 4ºC and allowed to equilibrate with ambient temperature before use in experiments.

PAH and PAH Metabolite Standards

Table B1. Purity, CAS number, and vendors of the PAHs and PAH metabolites included in this study.

Compound	CAS	Purity	Vendor
1-hydroxyphenanthrene	2433-56-9	>99%	Toronto Research Center
2-hydroxyphenanthrene	605-55-0	>99%	
3-hydroxyphenanthrene	605-87-8	98%	
4-hydroxyphenanthrene	7651-89-7	98%	
9-hydroxyphenanthrene	484-17-3	97%	
trans-9,10-dihydroxy-9,10-dihydrophenanthrene	572-41-8	98%	
1,9-dihydroxyphenanthrene	604-84-2	95%	Sigma Aldrich
phenanthrene	85-01-8	99.5%	
d_{10}-phenanthrene	1517-22-2	98%	CDN Isotopes Inc
d_{10}-acenaphthene	15067-26-2	99%	CDN Isotopes Inc
4-hydroxy[$^{13}C_4$]phenanthrene	N/A	98%	Cambridge Isotope Laboratories

Surrogate and Internal Standard Mix Compositions

Table B2. Composition of surrogate standard mixture used in sample preparation for GC/MS analysis.

Compound	Concentration
d_8-1-hydroxynaphthalene	4968 pg/uL
4-hydroxy[$^{13}C_4$]phenanthrene	5000 pg/uL
3-hydroxy[$^{13}C_6$]fluorene	5000 pg/uL
d_9-1-hydroxypyrene	4918 pg/uL
d_{10}-Phenanthrene	4952 pg/uL

Table B3. Composition of internal standard mixture used in sample preparation for GC/MS analysis.

Compound	Concentration
d_{10}-Acenaphthene	39760 pg/uL
d_{10}-Fluoranthene	39701 pg/uL
d_{12}-Benzo(k)fluoranthe	39834 pg/uL

PPAH and OHPAH GC/MS Methods

PPAH and OHPAH methods used to quantify target compounds were used in the previous study (Schrlau et al. 2017) as discussed below.

The PPAH method used to quantify phenanthrene in samples is as follows. 1 µL of sample was injected into an Agilent 6890 GC was operated in splitless mode. The injection temperature was 300ºC. The temperature program is as follows. Initial temp 60ºC for 1 minute. Ramp to 210ºC at 6ºC/minute hold for 2 minutes. Ramp to 300 ºC at rate of 6 ºC min hold for 2 minutes. Ramp to 320ºC at a rate of 40 ºC /minute hold for 1.5 minutes for a total run time of 47 minutes. Ultra-high purity helium was used as the carrier gas and flowed at a rate of 1 mL/minute.

The OHPAH method used to quantify hydroxylated phenanthrene metabolites in samples is as follows. 1 µL of sample was injected into an Agilent 6890 GC was operated in splitless mode. The injection temperature was 280ºC. The temperature program is as follows. Initial temp 70ºC for 1 minute. Ramp to 200ºC at 15ºC/minute hold for 5 minutes. Ramp to 320 ºC at rate of 10 ºC min hold for 1 minute for a total run time of 27.67 minutes. Ultra-high purity helium was used as the carrier gas and flowed at a rate of 1 mL/minute.

The ions monitored to identify and quantify the target compounds are provided in table SX.

Table B6. Mass to charge ratios (*m/z*) of ions used to identify and quantify target compounds in PPAH and OHPAH GC/MS analysis.

Compound	*m/z* 1	*m/z* 2	*m/z* 3
Phenanthrene	178.1	176.1	179.1
d_{10}-Phenanthrene	188.0	189.0	147.1
d_{10}-Acenaphthene	164.0	162.0	160.0
4-hydroxy[$^{13}C_4$]phenanthrene	255.1	239.1	312.2
1,9-dihydroxyphenanthrene	339.0	265.0	323.0
trans-9,10-dihydroxy-9,10-dihydrophenanthrene	341.0	267.0	325.0
4-hydroxyphenanthrene	251.1	235.1	308.1
9-hydroxyphenanthrene	251.1	308.2	235.1
1-hydroxyphenanthrene	251.1	235.1	308.1
2-hydroxyphenanthrene	251.1	308.2	176.1
3-hydroxyphenanthrene	251.1	308.1	195.1

Fluorescent Calibration Curves

Figure B1. Comparison of standard curves generated from 2D fluorescence and EEM-PARAFAC methods with different concentrations of cells present on a total suspended solids (TSS) basis (0 mg TSS/L, 150 mg TSS/L, 300 mg TSS/L).

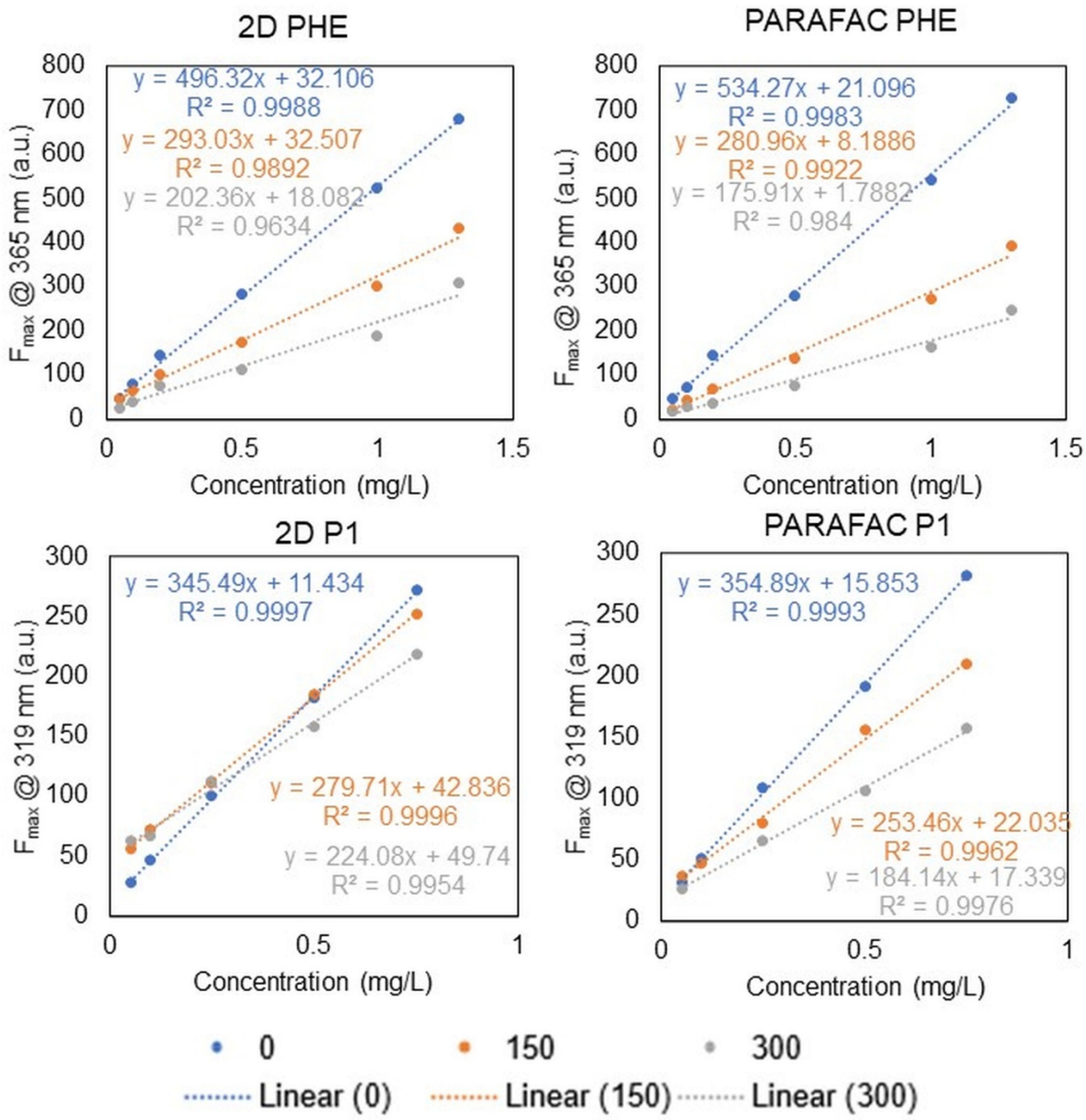

In comparing standards produced from 2D emission data versus EEM-PARAFAC data, minimal changes in slope were observed for phenanthrene and P1, however y-intercepts were consistently lower for EEM-PARAFAC standard curves, particularly in the case of P1. These trends demonstrate that the EEM-PARAFAC

method was able to separate emissions from the targets and emissions from the cellular material, increasing sensitivity in turbid conditions. However, the inverse relationship between the slope and biomass concentration in the standards for 2D and EEM-PARAFAC methods indicates that loss of sensitivity due to sample turbidity arises in part from scattering and background absorption that must be accounted for in standard curves.

Estimated Method Detection Limits

Table B4. Estimated method detection limits for phenanthrene and P1 reported for each TSS loading. All MDLs reported in units of µg/L.

Method	Phenanthrene			P1		
	0 mg/L TSS	150 mg/L TSS	300 mg/L TSS	0 mg/L TSS	150 mg/L TSS	300 mg/L TSS
GC/MS	0.5			0.5		
2D Fluorescence	13	47	80	35	101	263
3D Fluorescence	1.9	14	17	11	82	117

GC/MS PPAH and OHPAH Results

Figure B2. GC/MS results for active (left) and octyne (right) bottles including minor transformation products.

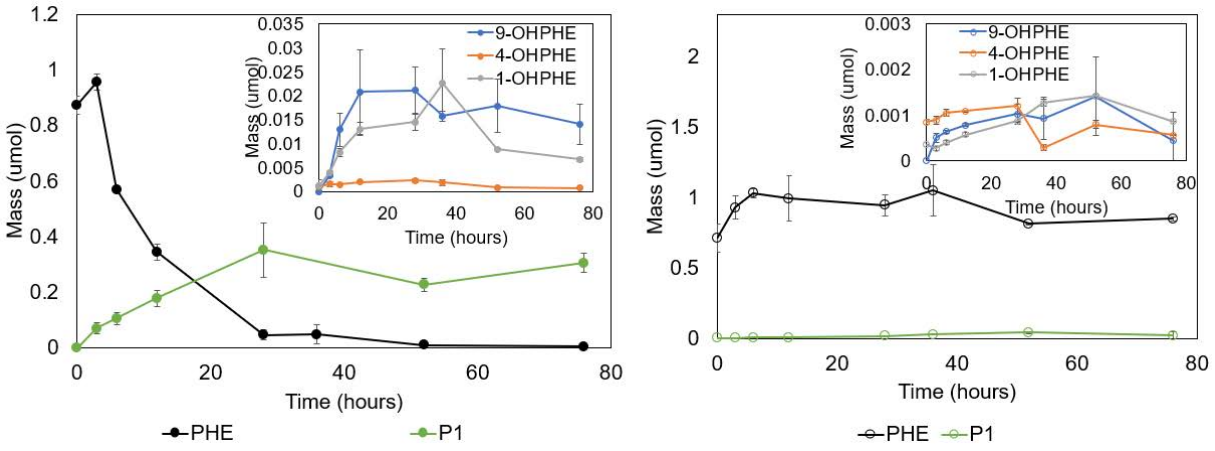

PARAFAC Model Fit Metrics

Table B5. Summary of fit parameters for PARAFAC models generated with experimental and calibration data.

Components	Percent explained	Core consistency	Error
3	96.72	93.66	8.82E+06
4	98.15	94.57	4.30E+06
5	98.41	87.60	2.84E+06
6	99.29	63.51	1.90E+06
7	99.43	18.20	1.52E+06

Five components were determined to be the appropriate number of components based on the diminishing returns of error reduction and sharp decrease in core consistency as the number of components exceeded 5.

Split Half Analysis

Split-half analysis involves splitting the original data set into multiple halves randomly, and fitting a PARAFAC model with a specific number of components to each half. The models generated from each set are then compared, and the model is considered valid if identical models are generated from each half within a certain tolerance. The drEEM toolbox default creates 4 splits of the original data set and conducts a split half analysis on all possible combinations of those 4 splits combined into 2 halves (Murphy et al., 2013).

Figure B3. Split half analysis results for 5 component PARAFAC model generated from experimental and calibration data sets. The overlap in component spectra for all plots confirms reproducibility of model output.

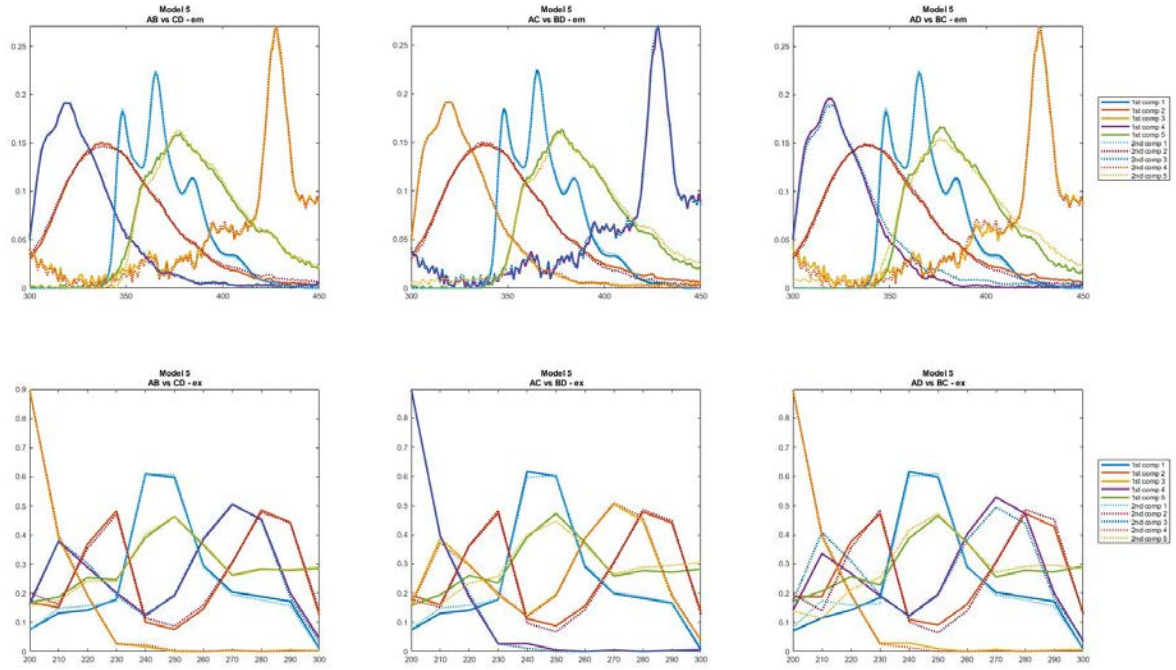

PARAFAC Model without Calibration Data

Figure B4. drEEM output for 5 component PARAFAC model generated from experimental data set exclusively. Note that the same components were output in this model as the model generated from the experimental and calibration data sets, indicating that the calibration data set is not impacting the modelled components spectra.

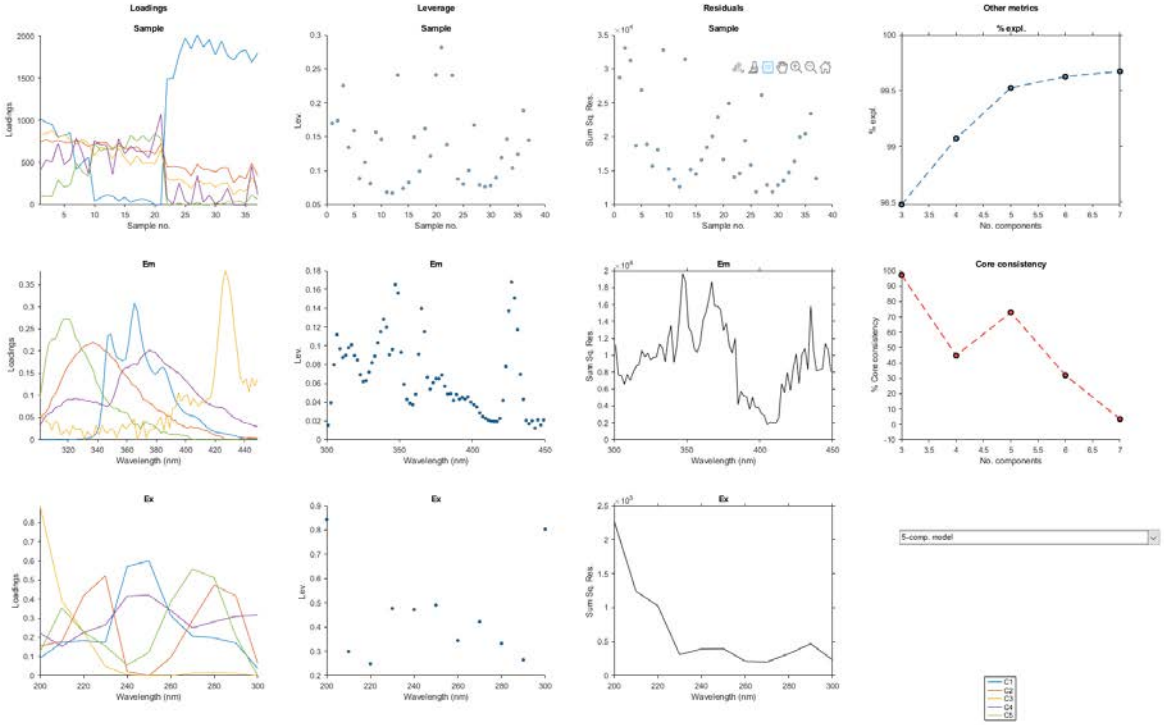

Figure B5. drEEM output of split-half validation for 5 component PARAFAC model generated from experimental data set exclusively. Reproducibility in model output regardless of data split indicates that the model is valid, and that the calibration data set is not needed for model validation.

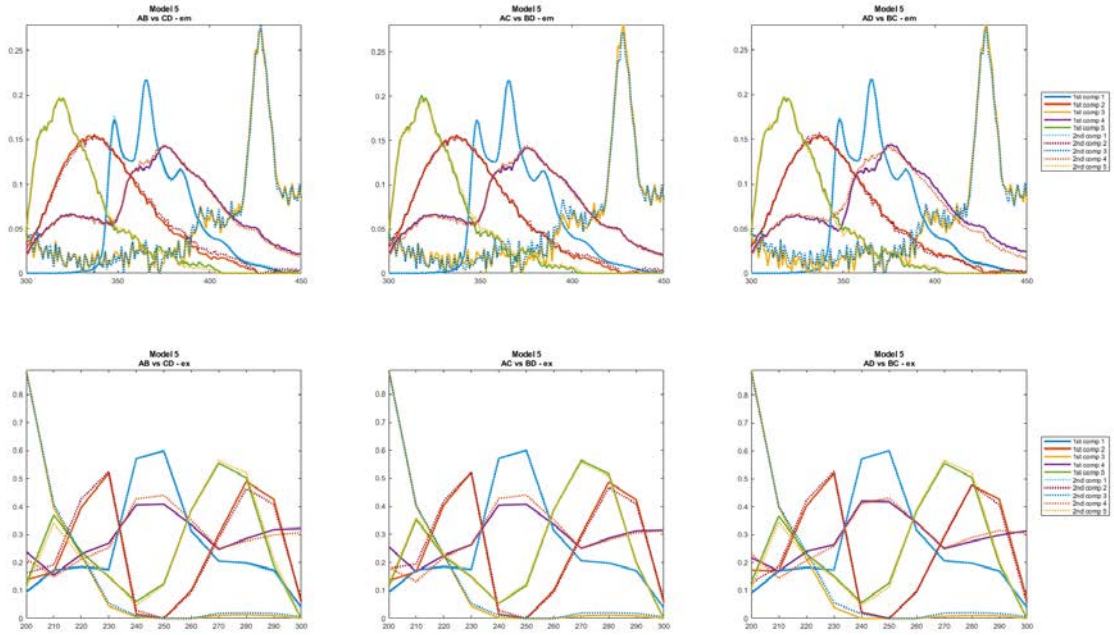

2D fluorescent spectra of active bottles over time

Figure B6. 2D fluorescent spectra for active bottle over time measured at λ_{ex} = 250 nm. Minor changes in spectra after 28 hours indicates that the majority of reaction progress occurred by hour 28.

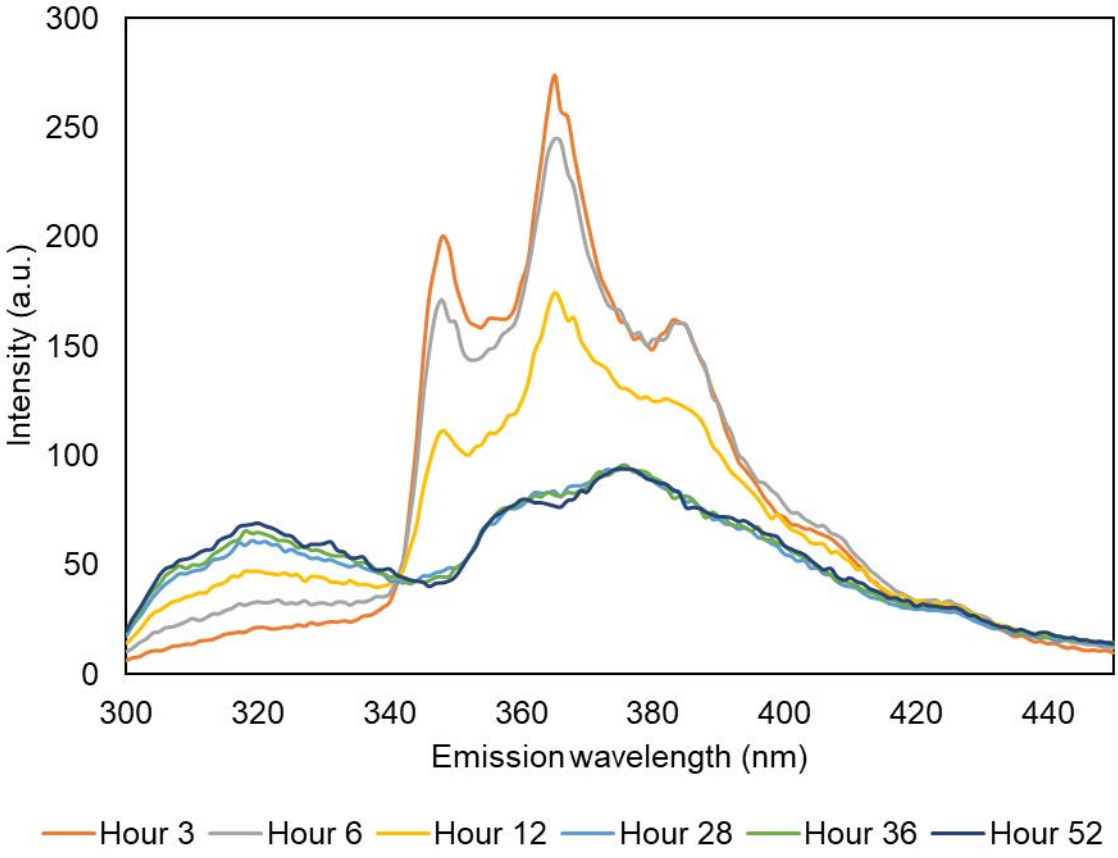

Linear Regression Models

Figure B7. Linear regression models for GC-MS, EEM-PARAFAC, and 2D fluorescent data for triplicate active bottles generated from MATLAB.

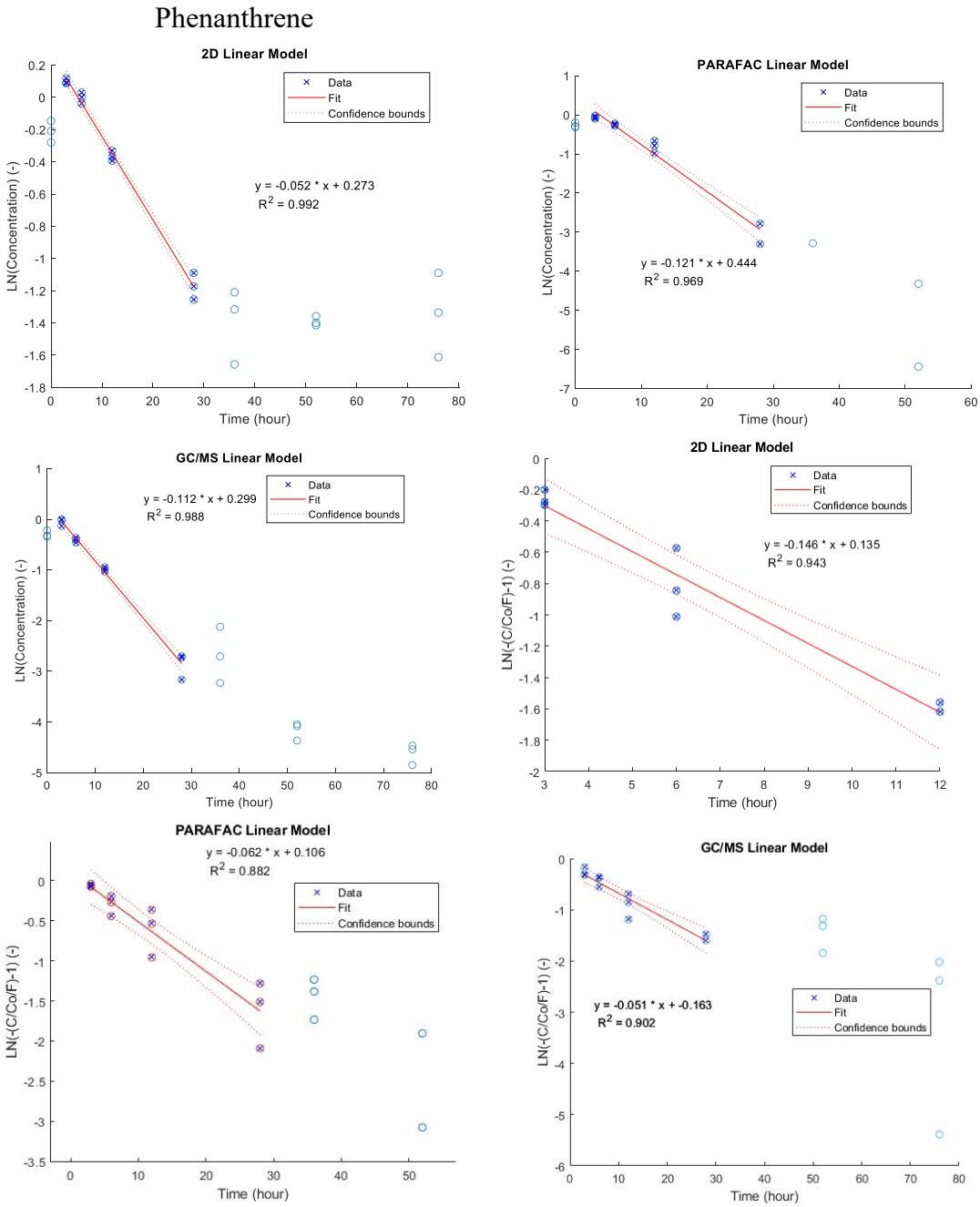

Appendix C: Supplementary Information for Manuscript 3

Fluorescent Spectroscopy Method Details

Table C1. Results from fluorescent liquid tests.

Test	Pass Criteria	Experimental Results	Pass/Fail
Corners	% CV < 3.0	% CV = 1.35	Pass
Sensitivity	MDL < 15 pM	MDL = 14 pM	Pass
Linearity	R^2 < 0.95	R^2 = 0.98	Pass

Table C2. Summary of fluorescent calibration information.

Compound	Stokes Shift (λ_{ex}/ λ_{em}) (nm)	m (uM/Intensity unit)	R^2	MDL
Acridine	270/355	8.19E-04	>0.99	452 nM
2-OHNAP	350/429	1.52E-02	>0.99	5 µM

UV Study Plate Map

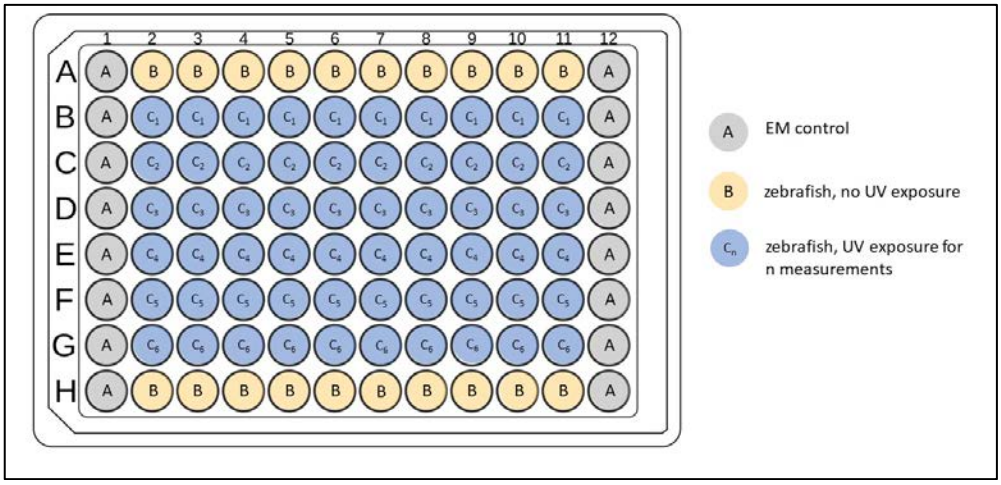

Figure C1. Design of UV study 96-well plates - one plate was made for each PAH.

UV Study Abnormal Embryos

Table C3. Incidence of endpoint (n hits/n embryos) for each embryo group measured with 2-OHNAP method (270 nm). Group number (x) corresponds with number of measurements (1/day for x days).

n	Group Number	MO120	CRAN	AXIS	EDEM
20	Negative Control	0.05	0.1	0	0
10	1	0.1	0.1	0	0.1
10	2	0.1	0	0	0
10	3	0	0.1	0.1	0.1
10	4	0.1	0	0	0
10	5	0	0.1	0	0
10	6	0.2	0	0	0

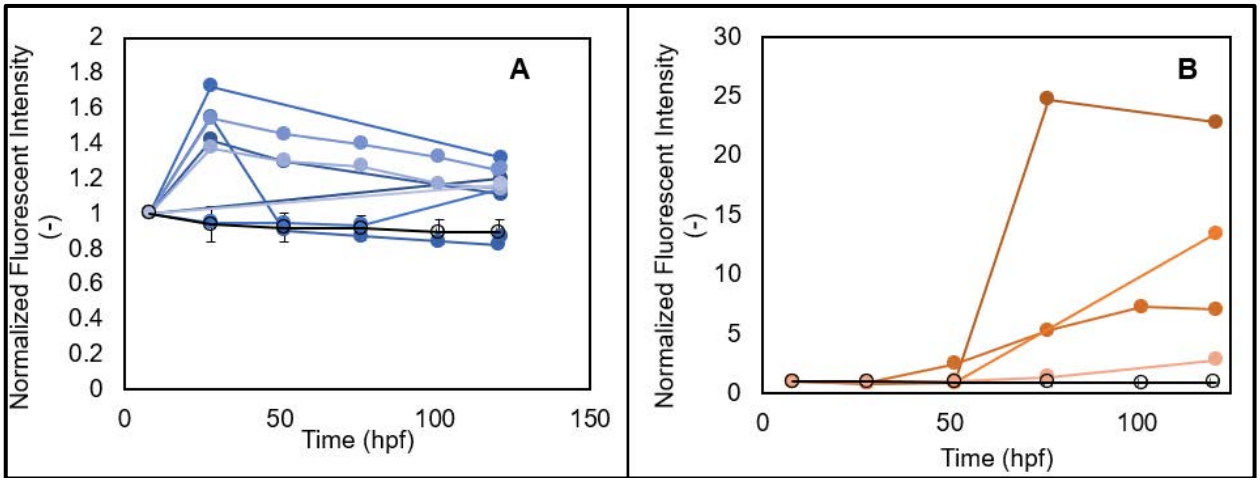

Fig. C2 Normalized fluorescent intensity for embryos measured with the 2-OHNAP method (A) or acridine method (B). Embryos with typical development is shown in the empty black circles, whereas the normalized fluorescent intensity for individual embryos with atypical development is shown in color-filled circles

UV Exposure Screening Results

Table C4. Incidence of endpoint (n hits/n embryos) for each embryo group measured with 2-OHNAP method (270 nm). Group number (x) corresponds with number of measurements (1/day for x days).

n	Set	MO120	CRAN	AXIS	EDEM
20	Negative Control	0.05	0.1	0	0
10	1	0.1	0.1	0	0.1
10	2	0.1	0	0	0
10	3	0	0.1	0.1	0.1

10	4	0.1	0	0	0
10	5	0	0.1	0	0
10	6	0.2	0	0	0

Table C5. Incidence of endpoint (n hits/n embryos) for each embryo group measured with acridine method (350 nm). Group number (x) corresponds with number of measurements (1/day for x days).

n	Set	MO120	CRAN
20	Negative Control	0.05	0.05
10	1	0	0
10	2	0	0
10	3	0.1	0
10	4	0.2	0
10	5	0.1	0
10	6	0	0

UV Dose Calculations

UV Dose (J/cm^2) = UV irradiance (W/cm^2) * Exposure time (s)

Microwell area = 0.33 cm^2

UV irradiance = 20 W (maximum from user manual)

Exposure time = 100 µseconds (Maximum of typical range for Xe flash lamps)

UV dose = 20 W * 0.33 cm^2 * 100 µs * 10^-6 s/µs = 0.0061 J/cm^2 = 6.1 mJ/cm^2

PAH Exposure Study

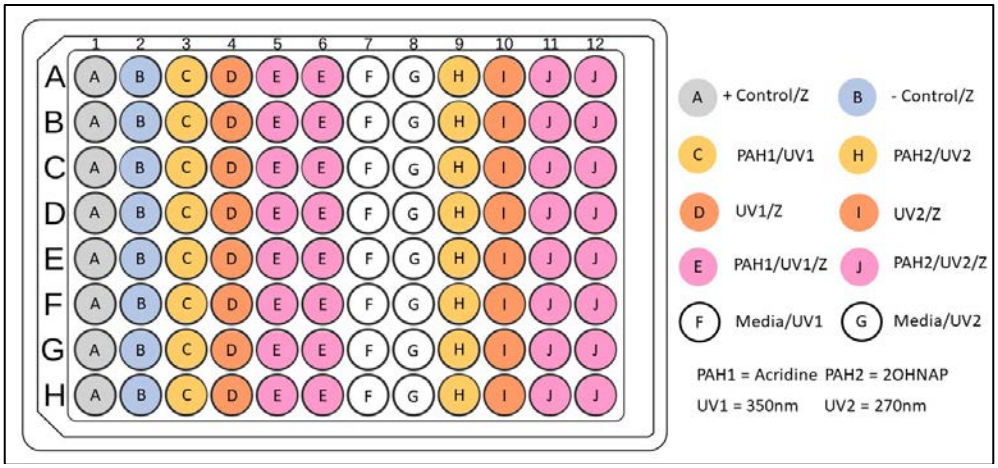

Figure C3. Design of PAH exposure study 96-well plates.

Fluorescent Inflection Predictions for Embryo Abnormality

Fluorescent inflections were used to determine embryo mortality and/or cranial deformation with the following workflow:

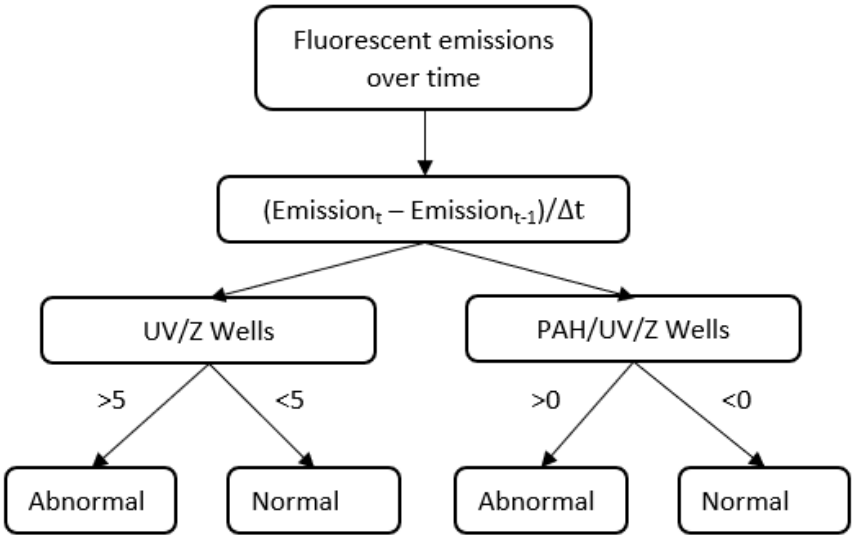

Because the emission signals from UV/Z wells were significantly smaller than those from PAH/UV/Z wells, (thus the signal to noise ratio was significantly smaller for UV/Z wells) a tolerance was needed to accommodate for instrument noise. A fluorescent inflection >5 was set to indicate an abnormality with the embryo, selected based on the maximum inflection observed in media controls. The accuracy and incidence of false positives and negatives are reported in the table below.

Table C6. Fluorescent inflection model performance compared to morphology screening results. False + indicates where fluorescent inflection indicated a normal embryo was abnormal, False – indicates where fluorescent inflection indicated an abnormal embryo was normal.

	2-OHNAP			Acridine		
	Accuracy	False +	False -	Accuracy	False +	False -
UV Only	0.90	0.083	0.017	0.97	0.017	0.017
PAH + UV	0.81	0.021	0.017	0.83	0.083	0.083

Initial PAH Losses in PAH Exposure Test

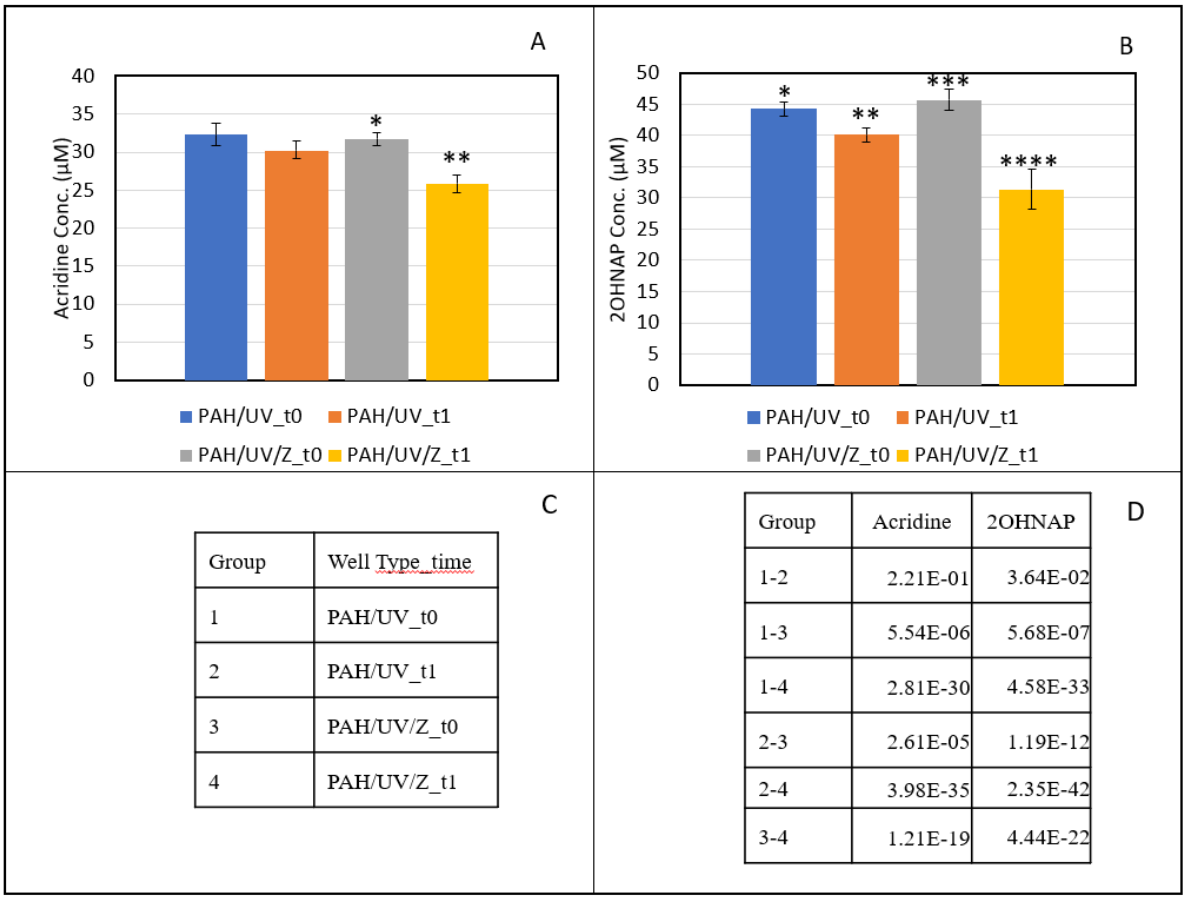

Group	Well Type_time
1	PAH/UV_t0
2	PAH/UV_t1
3	PAH/UV/Z_t0
4	PAH/UV/Z_t1

Group	Acridine	2OHNAP
1-2	2.21E-01	3.64E-02
1-3	5.54E-06	5.68E-07
1-4	2.81E-30	4.58E-33
2-3	2.61E-05	1.19E-12
2-4	3.98E-35	2.35E-42
3-4	1.21E-19	4.44E-22

Figure C4. Decrease in PAH concentrations before (t0) and immediately after (t1) embryo addition for wells that received an embryo (PAZ/UV/Z) and those without embryos (PAH/UV). Concentrations for acridine and 2OHNAP are shown in A and B respectively, while tables in C and D show statistical significance for each group type.

Zebrafish Embryos Included in Kinetic Models

Table C7. N embryos included in derivation of kinetic parameters. Embryos were removed based off fluorescent inflection information.

Time (hpf)	Viable embryos exposed to 2-OHNAP	Viable embryos exposed to acridine
6.5	31	31
31	31	31
53	25	31
73	24	22
103	12	7
124	6	2

Toxicity Endpoint Comparison

Table C8. Comparison of endpoints observed in Geier et al. and endpoints observed in the present study. Bolded X's indicate endpoints observed in only the present study, however all such endpoints occurred at an incidence < 20%, the typical threshold for significance.

Endpoint	Geier et al. Acridine	Present Study Acridine	Geier et al. 2-OHNAP	Present Study 2-OHNAP
120 Mortality	X	X	X	X
Yolk Sac Edema	X	X	X	X
Axis	X	X		
Eye	X	X		**X**
Snout	X	X		**X**
Jaw	X	X		**X**
Pericardial Edema	X	X	X	X
Brain	X	X		**X**
Somite				
Pectoral Fin	X	X	X	X
Caudal Fin	X	X		
Trunk		**X**		

PAH Exposure Screening Results

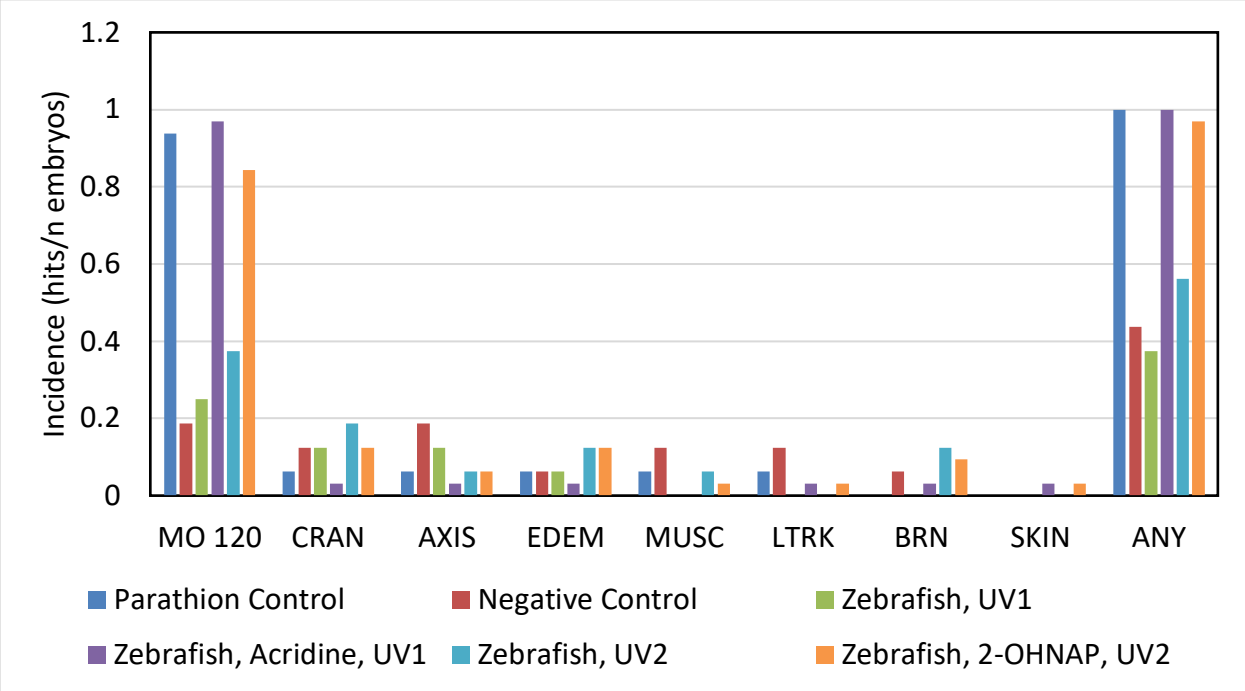

Figure C5. Incidence of endpoints observed in PAH exposure test.

Appendix D: Supplementary Information for Manuscript 4

Bead Incubation

Isobutane consumption and estimated biomass grown for immobilized 21198 is shown in Figure D1 below, along with the visual color change from 21198's growth in the hydrogel beads.

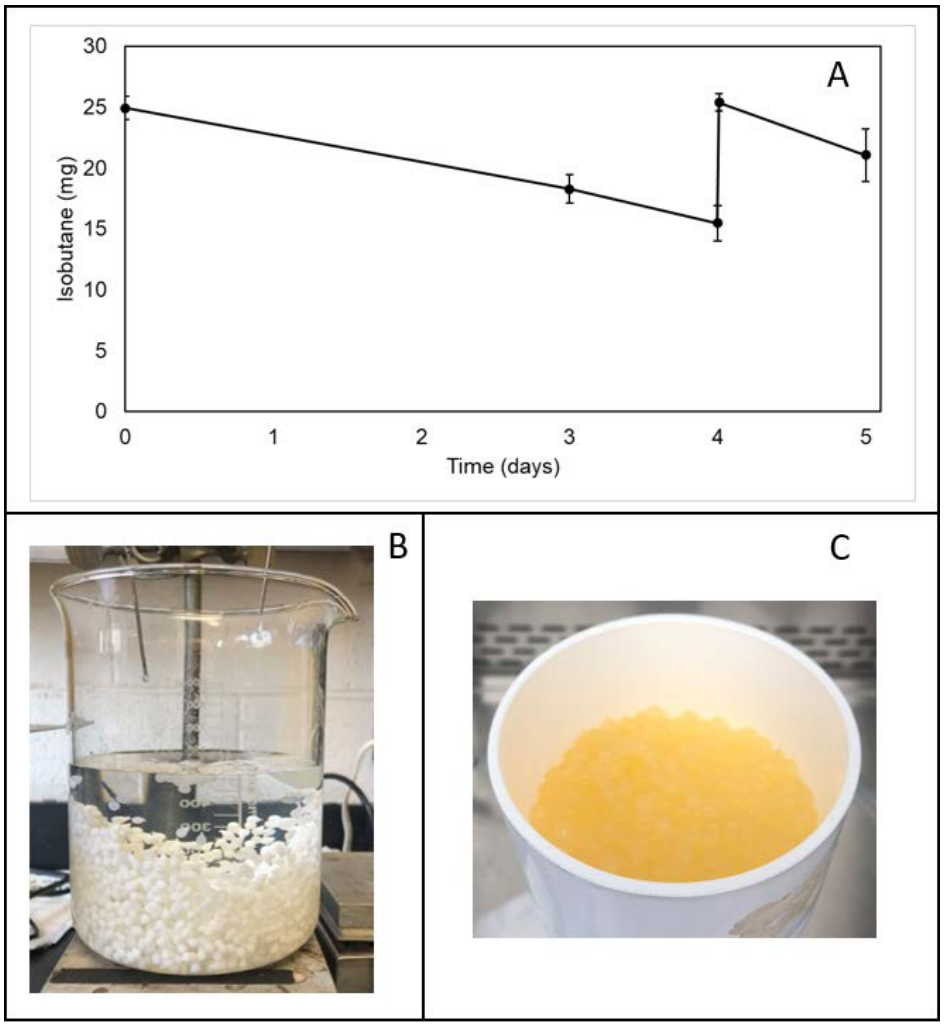

Figure D1. Average isobutane consumption during bead incubation (A), and observable color change of beads immediately after preparation (B) and after the 5-day incubation period (C). Error bars in (A) represent standard deviation between incubation batch reactors (n = 6).

The amount of biomass grown can be estimated based on the amount of isobutane consumed with the yield coefficient: 0.89 mg isobutane consumed/mg biomass grown from Rolston et. al (2019).

$$\text{Biomass grown} \approx 82.72 \text{ mg Isobutane} * \frac{1 \text{ mg } 21198}{0.89 \text{ mg isobutane}} = 92.94 \text{ mg } 21198$$

$$\text{Total Immobilized Biomass} \approx 92.94 \text{ mg } 21198 + 60.8 \text{ mg } 21198 = 153.7 \text{ mg } 21198$$

$$\text{Biomass loading} = 153.7 \text{ mg } 21198 \text{ / } 120 \text{ mL polymer solution} = 1.3 \frac{\text{mg}}{\text{mL}}$$

Note that this biomass loading is an overestimate based on the assumptions used, therefore O_2 utilization was deemed most appropriate for estimating biomass loading in beads, although there is good agreement between the two methods of estimation.

Surrogate PAH Mix

Table D2. Composition of surrogate PAH standard mix spiked into LLE samples. Target concentration in final extract ≈ 1000 pg/µL.

Compound	CAS	Purity %	Deuteration %	Concentration (pg/µL)
Naphthalene-d8	1146-65-2	99	99	6125
Phenanthrene-d10	1517-22-2	99	99.6	6095
Pyr-d10	1718-52-1	99	99.2	6087

LC-MS Parameters

LC Parameters:

Eluent A: 0.1% Formic acid in nanopure water
Eluent B: 0.1% Formic acid in Acetonitrile

Table D3. Eluent gradient for LC separation.

Time (min)	**Flow (mL/min)**	**B Conc (%)**
0	0.3	5
3	0.3	5
12	0.3	98
17	0.3	98
17.5	0.3	5
23	0.3	5

Table D4. ZenoTOF operating parameters.

Parameter	**Setting**
Source Temperature	500 oC
Curtain Gas	35
G1	45
G2	45
Source Name	TurboIonSpray (ESI)
Polarity	+ or -
Spray Voltage	5500 V
Fragmentation Mode	CID
TOF start/stop mass	40-1000 Da
Delustering Potential	80 V
Scan Type	TOFMSMS
Declustering potential	80 V
Collision energy	40 V
Zeno threshold	20000 cps

Isobutane Utilization Rates (T80 Sensitivity Tests)

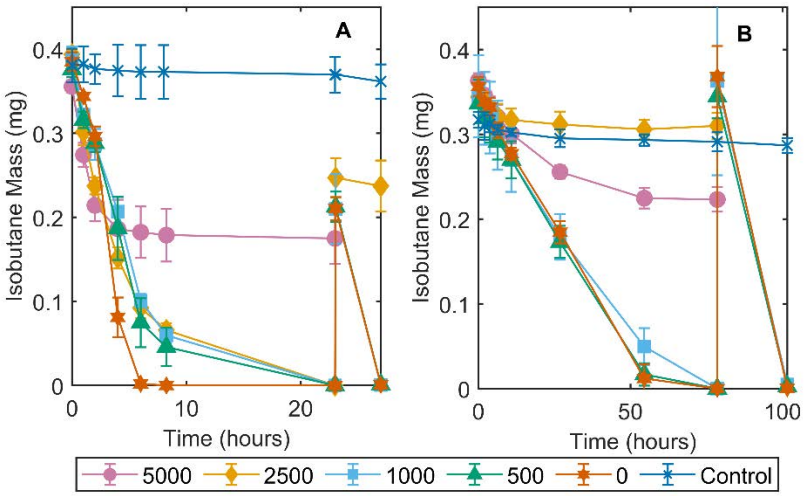

Figure D2. Isobutane consumption for suspended (A) and immobilized (B) 21198 with various concentrations of Tween 80 (mg/L). Error bars represent standard deviation among triplicates

It should be noted that the biomass normalized isobutane consumption rates were drastically different between suspended and immobilized cells for these experiments. Zero-order isobutane consumption rates for suspended and immobilized cells without Tween 80 were 0.15 ± 0.013 mg isobutane/mg biomass/hour and 0.003 ± 0.0007 mg isobutane/mg biomass/hour, respectively. This order of magnitude difference in rates is likely due to the use of beads directly after they were prepared, rather than being used after an incubation period as was done with beads used in PAH batch experiments. Immobilized cell inactivity has been observed previously and may be due to acid stress responses such as changes to the cell membrane, enzyme expression, or metabolic pathways. This inactivity may also be due to cell death within the beads, as the pH of the crosslinking solution is 4*, well below the optimal pH of 6.5-7 for 21198. Because methods measuring live immobilized biomass is lacking in this study, the importance of bead incubation and using the oxygen utilization tests to match suspended and immobilized cell activity is emphasized by these findings.

Initial zero-order isobutane consumption rates (k_{iso}) for suspended and immobilized cells normalized to starting biomass concentration in mg. This value was estimated for the immobilized cells based on the biomass concentration in the prepared beads. Note that the reported rates are initial rates, and therefore do not take into account the slowing or cessation of isobutane consumption observed at higher Tween 80 concentrations that was presumably caused by cell death.

Table D5. k_{iso} for suspended and immobilized 21198 exposed to various concentrations of Tween 80.

Tween 80 Concentration (mg/L)	Suspended Cells k_{iso} (mg isobutane/hour/mg biomass)	Immobilized Cells k_{iso} (mg isobutane/hour/mg biomass)
0	0.15 ± 0.013	0.003 ± 0.0007
500	0.09 ± 0.015	0.003 ± 0.0013
1000	0.09 ± 0.003	0.003 ± 0.0004
2500	0.12 ± 0.005	0.002 ± 0.001
5000	0.08 ± 0.02	0.003 ± 0.00005

T80 Transformation Tests

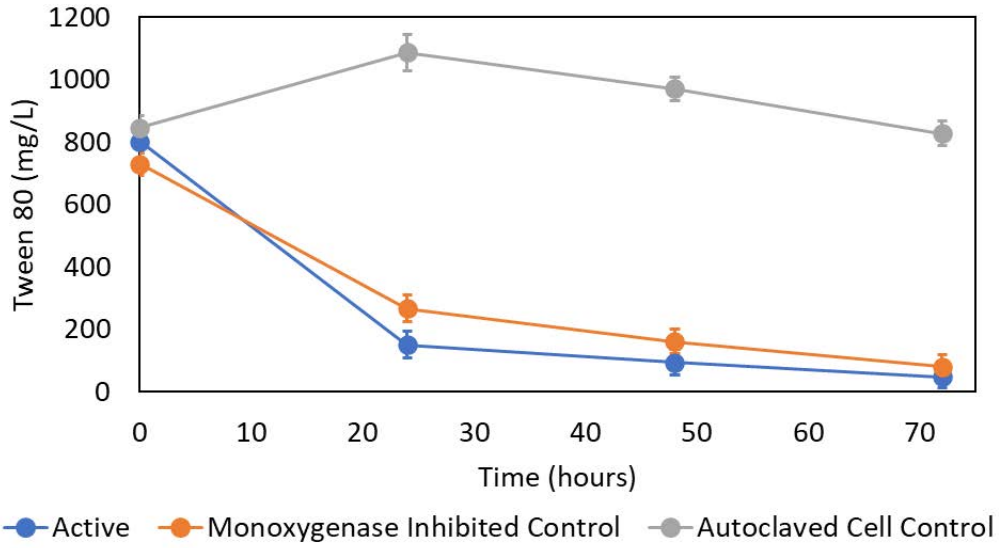

Figure D3. Transformation of T80 over time by suspended 21198 cells in solution with (orange) or without (blue) the presence of a monooxygenase inhibitor. Autoclaved cells were used to control for removal via sorption to cell material. Error bars represent standard deviation among triplicates.

Oxygen Utilization Rates (Suspended vs Immobilized Cells)

Zero-order oxygen utilization rate (k_{O2}) as calculated with a linear regression to the oxygen mass data collected over time. $R^2 > 0.96$ for all regression models. Rates are normalized to biomass in mg or bead mass in g.

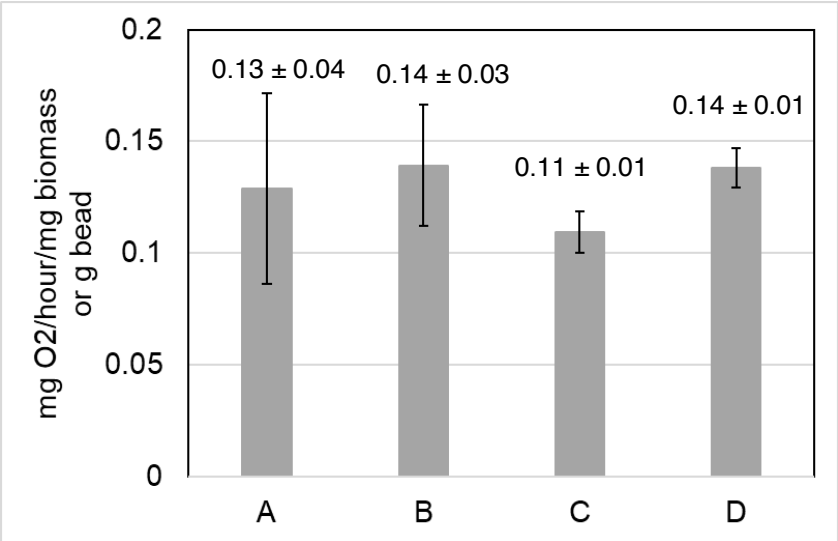

Figure D4. k_{O2} for suspended cells collected the day of cell harvesting (A), immobilized cells after incubation but before use in PAH experiments (B), immobilized cells used in experiment set 3 (C), and immobilized cells used in experiment set 4 (D). Error bars represent standard deviation among triplicates

k_{O2} of suspended and immobilized cells can be used to estimate bead biomass in the cells with the following calculations:

$$\text{Immobilized biomass} = \left(\frac{0.13 \frac{\text{mg } O_2}{\text{hour} * \text{mg biomass}}}{0.14 \frac{\text{mg } O_2}{\text{hour} * \text{g bead}}} \right)^{-1} = 1.1 \frac{\text{mg biomass}}{\text{g bead}}$$

$$\text{Error} = \sqrt[2]{0.04^2 + 0.03^2} = 0.05 \frac{\text{mg biomass}}{\text{g bead}}$$

PARAFAC Model Fit Parameters

Table D6. Model fit parameters for preliminary PARAFAC models developed with 3-7 components. The model with 4 components minimized SSE and maximized Core consistency, thus was chosen as the most appropriate model.

	3	4	5	6	7
SSE	5.80E+07	2.85E+07	1.71E+07	1.25E+07	7.73E+06
Core Consistency	77.4	79.0	52.2	35.1	14.4
Percent Explained	93.0	96.5	97.9	98.5	99.1

PARAFAC Component Identification

Comparisons of standard spectra to PARAFAC components were used to identify PARAFAC components. A 1 mg/L phenanthrene 0.5 mg/L anthracene standard is shown compared to C2, while a 0.5 mg/L fluorene standard is compared to C3 and a 300 mg/L suspension of 21198 cells is compared to C4.

C1 C2 C3 C4

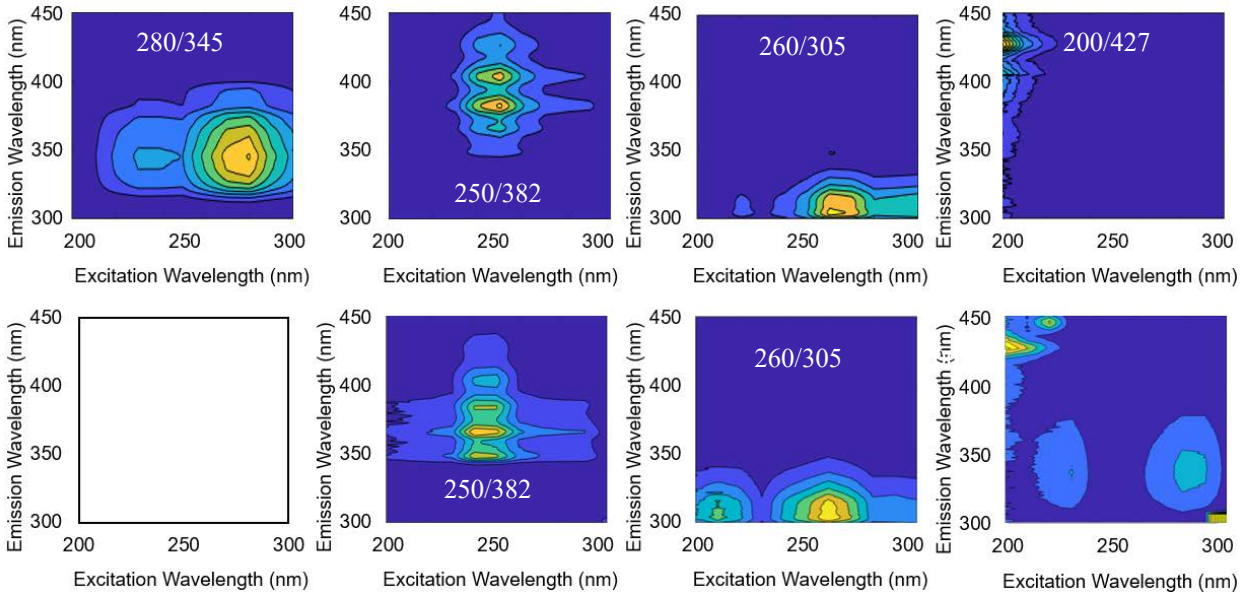

Figure D5. PARAFAC components (top row) compared to standard scans of corresponding compounds that were identified (bottom row). Note that the PARAFAC components represent general spectra trends, and are not scaled to a specific concentration, therefore no color bar is shown. Stokes shift ($\lambda_{ex/}$ λ_{em}) in nm is shown in white text inside the EEMs.

GC-MS Data for Control Batch Bottles

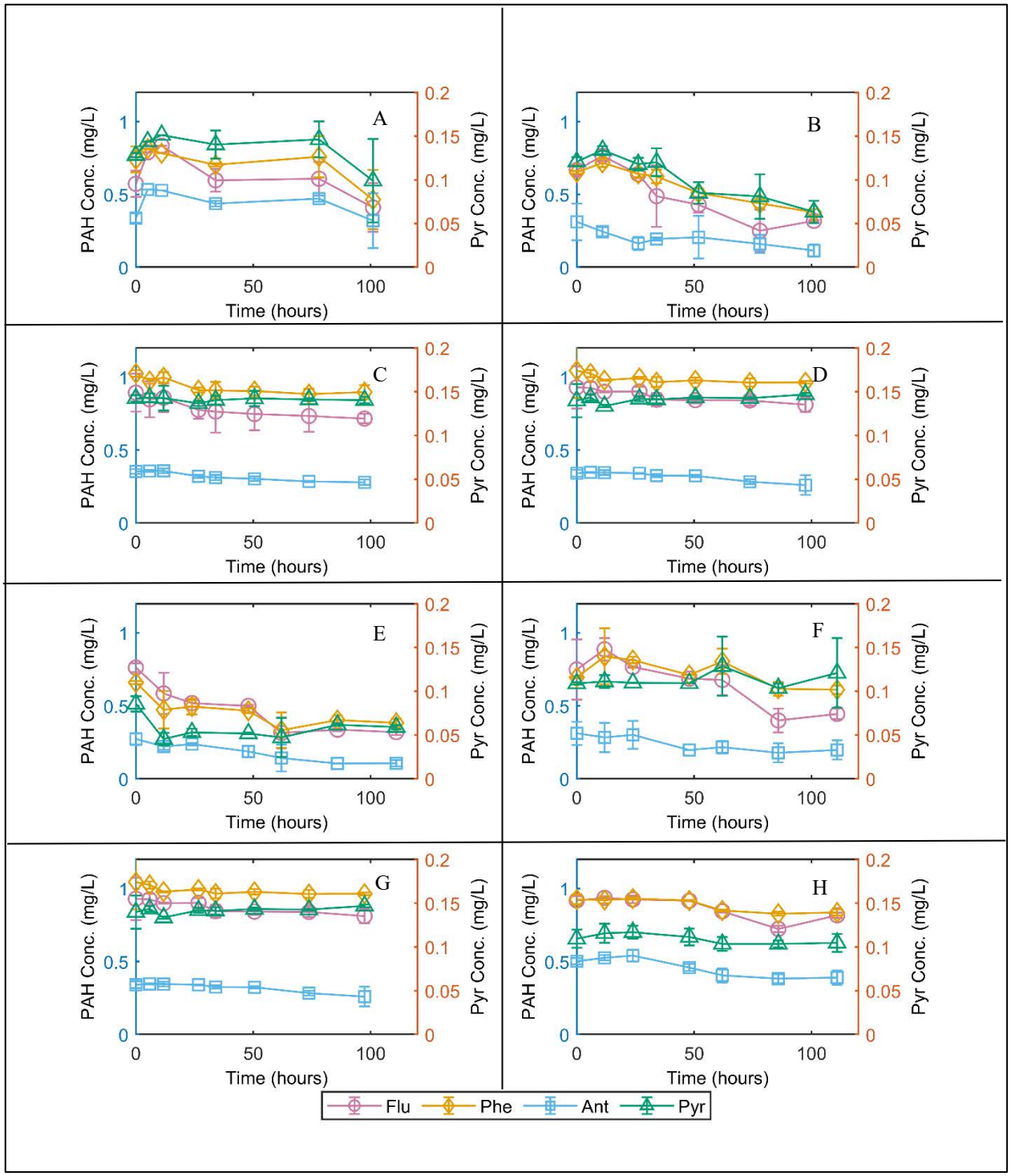

Figure D6. Autoclaved cell/bead controls (A,C,E,D) and abiotic controls (B,D,F,H) for batch set 1 (A,B), 2 (C,D), 3 (E,F), and 4 (G,H).

Statistical Significance for PAH Losses and Transformation Rates

Table D7. P-values for Total Loss and Transformation Rates for each PAH. Note that comparisons are for the same PAH in different experimental sets, no comparisons are made for different PAHs in the same experimental set.

PAH	Group A	Group B	Rate P-Value	Total Loss P-Value
Flu	1	2	2.4E-03	1.6E-06
	1	3	4.7E-03	1.1E-02
	1	4	4.7E-01	5.0E-01
	2	3	3.5E-05	2.7E-07
	2	4	6.9E-03	1.1E-06
	3	4	1.6E-03	3.2E-02
Phe	1	2	1.5E-01	2.3E-02
	1	3	1.4E-05	2.7E-04
	1	4	3.7E-07	6.5E-05
	2	3	5.6E-05	1.9E-05
	2	4	9.0E-07	6.4E-06
	3	4	4.4E-04	1.9E-01
Ant	1	2	1.1E-03	1.1E-04
	1	3	1.4E-01	5.5E-01
	1	4	2.2E-01	8.3E-01
	2	3	1.8E-04	2.0E-04
	2	4	7.1E-03	1.3E-04
	3	4	1.8E-02	7.0E-01
Pyr	1	2	9.1E-03	1.8E-01
	1	3	1.6E-01	2.6E-04
	1	4	1.9E-05	1.4E-05
	2	3	9.6E-02	1.5E-03
	2	4	5.3E-04	4.9E-05
	3	4	7.2E-05	1.4E-02

PAH Transformation Rate Fit Coefficients

Table D8. Fit coefficients (R^2) for pseudo-first order PAH transformation rates derived from 'fitlm' regression of linearized data in MATLAB. $R^2 < 0.5$ are shown in red

PAH	Replicate	Exp 1	Exp 2	Exp 3	Exp 4
Pyr	1	0.09	0.98	0.41	0.96
	2	0.01	0.98	0.04	0.91
	3	0.01	0.88	0.24	0.94
Phe	1	0.90	1.00	0.79	0.96
	2	0.93	0.99	0.73	0.95
	3	0.81	0.97	0.71	0.95
Ant	1	0.94	0.97	0.94	0.97
	2	0.96	0.98	0.95	0.99
	3	0.98	0.95	0.90	0.95
Flu	1	0.90	0.98	0.91	0.97
	2	0.97	0.98	0.95	0.97
	3	0.97	0.96	0.97	0.94

GC-MS/PARAFAC Comparison

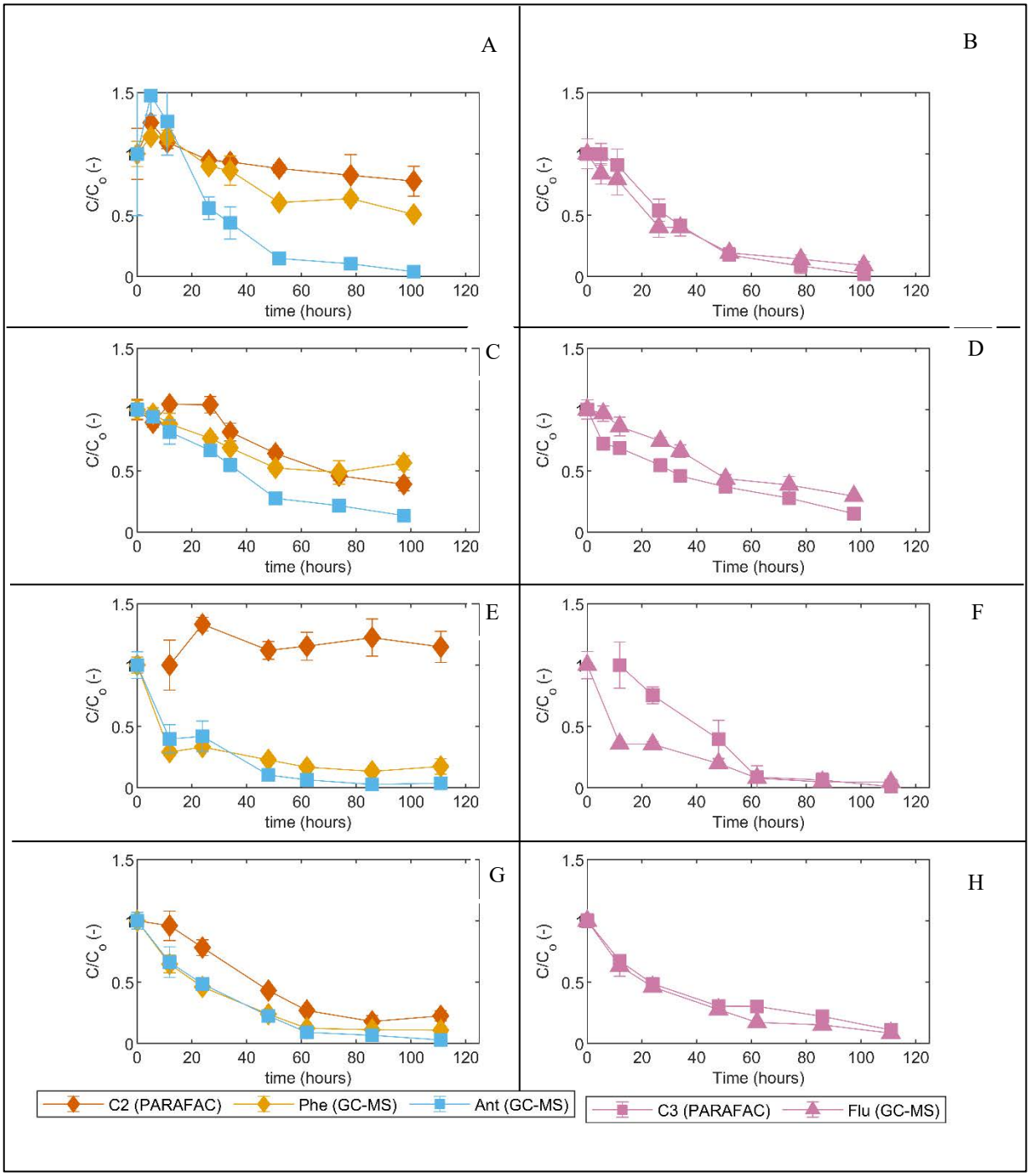

Figure D7. Comparison of PARAFAC and GC-MS results for C2/Ant/Phe and C3/Flu for batch set 1 (A,B), 2 (C,D), 3 (E,F), and 4 (G,H).

Compound Identification Confidence Levels

Library hits were selected for further screening based on the following criteria: peak area > 1000 units, active/blank peak area ratio > 10, mass error ≤ 2 mDa, and compound present in at least 2/3 technical replicates.

Table D9. Confidence level descriptions adapted from Hollender et al. (2023).

Confidence Level	Description	Requirements
1	Confirmed structure via reference standard	MS, MS2, RT, Reference standard
2a	Probable structure via library match	MS, MS2, library/literature MS2
2b	Probable structure via diagnostic evidence	MS, MS2, context
3	Tentative compounds	MS, MS2, context
4	Molecular formula	MS isotope/adduct
5	Exact mass match	MS

Percent Loss and Pseudo-First Order Degradation Rates

Table D10. Percent loss and pseudo-first order rate derived from total and apparent biotic losses. This data is illustrated in Figures V-3 and V-4 in the main text.

			Fluorene		Phenanthrene		Anthracene		Pyrene	
			Value	Standard Deviation	Value	Standard Deviation	Value	Standard Deviation	Value	Standard Deviation
Set 1	Total	% Loss	90.9	5.2	49.5	5.0	96.1	2.9	6.5	5.7
		Rate (hour^{-1})	2.4E-02	1.7E-03	8.5E-03	7.3E-04	3.6E-02	2.8E-03	N/A	N/A
	Biotic	% Loss	66.2	5.3	41.0	5.1	84.5	4.3	6.3	9.8
		Rate (hour^{-1})	2.2E-02	7.0E-03	6.5E-03	4.2E-04	3.7E-02	6.0E-03	N/A	N/A
Set 2	Total	% Loss	70.5	1.2	43.5	7.7	86.3	1.2	22.0	9.7
		Rate (hour^{-1})	1.3E-02	1.5E-03	1.1E-02	1.4E-03	2.0E-02	2.4E-03	7.3E-03	1.1E-03
	Biotic	% Loss	50.6	9.4	31.1	7.8	65.5	18.9	20.7	9.7
		Rate (hour^{-1})	1.1E-02	2.9E-03	7.9E-03	4.1E-03	2.0E-02	1.3E-03	5.9E-03	2.5E-03
Set 3	Total	% Loss	95.4	2.0	82.7	5.1	96.4	1.9	52.7	12.6
		Rate (hour^{-1})	3.4E-02	2.6E-03	1.9E-02	3.0E-03	4.4E-02	4.0E-03	N/A	N/A
	Biotic	% Loss	37.4	8.7	40.8	7.0	35.4	5.5	21.7	13.2

		Rate (hour^{-1})	2.3E-02	5.2E-03	9.5E-03	8.2E-04	3.5E-02	6.3E-03	N/A	N/A
Set 4	Total	% Loss	91.5	2.0	89.3	5.1	97.1	1.9	78.3	12.6
		Rate (hour^{-1})	2.2E-02	1.1E-03	2.7E-02	1.6E-03	3.3E-02	1.5E-03	1.8E-02	1.4E-03
	Biotic	% Loss	72.5	2.1	73.7	5.2	68.2	6.6	68.5	13.0
		Rate (hour^{-1})	1.9E-02	1.4E-03	1.9E-02	6.3E-04	3.0E-02	2.0E-03	1.3E-02	1.2E-03

Table D11. Initial concentrations of PAHs in remediation batch sets. Normalized data shown in Figure V-2.

Batch Set	Fluorene (mg/L)	Phenanthrene (mg/L)	Anthracene (mg/L)	Pyrene (mg/L)
Set 1	0.73 ± 0.06	0.73 ± 0.01	0.42 ± 0.05	0.14 ± 0.002
Set 2	0.96 ± 0.08	1.02 ± 0.08	0.37 ± 0.02	0.15 ± 0.01
Set 3	0.88 ± 0.1	0.74 ± 0.05	0.34 ± 0.04	0.08 ± 0.02
Set 4	1.00 ± 0.06	1.06 ± 0.04	0.52 ± 0.04	0.13 ± 0.01

Toxicity Concentration Calculations

Because the full composition of the post-remediation material is not known, we cannot use concentrations in terms of mass per volume. Rather, we can relate the concentration of the DMSO extracts to the volume of sample that was extracted, giving us units of volume of sample per volume of extract (equation 1). Similarly, the concentration of post-remediation material in each microwell can be expressed as the volume of extract added to the microwell (equation 2). To express the well concentration in terms of the volume of sample extracted, [1] * [2] gives us equation 3. C_{well} in terms of (mL sample/ µL EM) is henceforth used to express exposure concentrations.

[1] $C_{extract}$ (mL sample/µL DMSO) $= \frac{V_{sample\ extracted}\ (mL\ Sample)}{100\ \mu L\ DMSO}$

[2] C_{well} (µL DMSO /µL EM) $= \frac{V_{DMSO\ Added}\ (\mu L\ DMSO)}{V_{well}\ (\mu L\ EM)}$

Where $V_{DMSO\ Added}$ (µL DMSO) $= \frac{C_{well\ (reported)}\ (\mu M) * V_{well}\ (\mu L\ EM)}{C_{extract\ (reported)}\ (mM) * 10^3 (\frac{\mu M}{mM})}$

Multiplying [2] by [1] gives:

[3] C_{well} (mL sample/µL EM) $= \frac{V_{sample\ extracted}\ (mL)}{V_{well}\ (\mu L\ EM)}$